Institut für Hochfrequenztechnik
und Radarsysteme

Microwaves and Radar Institute

Status Report
2000 - 2005

Research Results and Projects

DLR

Published by German Aerospace Center
A member of the Helmholtz Society

Microwaves and Radar Institute

Director of the Institute Prof. Dr.-Ing. Alberto Moreira

Address Oberpfaffenhofen
D-82234 Weßling
www.dlr.de/hr

Layout ziller design, Mülheim an der Ruhr

Printed by Buch- und Offsetdruckerei Richard Thierbach GmbH,
Mülheim an der Ruhr

First impression Oberpfaffenhofen, April 2006

Microwaves and Radar Institute

Status Report
2000 - 2005

Research Results

DLR

Preface

This report summarises the research activities and projects of the Microwaves and Radar Institute (HR) of the German Aerospace Center (DLR) in the timeframe between 2000 and 2005. It has been written for the Institute's evaluation in spring 2006, but it also gives an inside perspective into the Institute's activities for partners in science, politics and private enterprises as well as for interested readers.

Since 2000 we have had a challenging time at the Institute. In 2000 we were proud to participate in the SRTM mission with the leadership for the X-SAR project. The mission was a success in all senses, from the completeness of the data acquisition during the eleven-day mission up to the excellent accuracy of the derived Digital Elevation Models. One year later a positive decision was given for the start of the SAR-Lupe project. SAR-Lupe consists of a constellation of five high resolution SAR satellites operating in X-band and will be the first satellite-based reconnaissance system of the German Ministry of Defence. The Institute supports this project with technical consultancy in a number of system aspects, like mission planning, sensor performance estimation and simulation.

A few months later we obtained the approval for the realisation of TerraSAR-X, which will be the first German radar satellite. It will deliver radar images with a resolution up to one meter and is being realised under a Public Private Partnership between DLR and EADS Astrium GmbH. While DLR provides the satellite and instrument operations, data processing, calibration and data distribution to the scientific community, Infoterra will be responsible for the commercial data exploitation. Within the TerraSAR-X project the Institute is delivering system engineering support, holding the mission manager position and developing the Instrument Operations and Calibration System.

Building on the experience gained in more than 25 years with the successful participation in NASA's Shuttle Radar Programme and the TerraSAR-X mission, the Institute submitted in November 2003 the TanDEM-X mission proposal in response to a national call for future Earth observation missions. TanDEM-X represents a further highlight in the scope of the German spaceborne radar programme. The mission proposal profits from the same partners as for TerraSAR-X and has been accepted for realisation in March 2006 following a successful demonstration of its feasibility during the phase A study. TanDEM-X is a challenging mission in many aspects. It has the objective to generate a consistent, global Digital Elevation Model with an unprecedented accuracy. This goal will be achieved by means of a second slightly modified TerraSAR-X satellite (TanDEM-X) flying in a close orbit formation with TerraSAR-X. It will be the first spaceborne bistatic radar system and the first operational close formation flying system in space. In addition to across-track interferometry, TanDEM-X will allow the demonstration of several new techniques and modes like digital beamforming, super resolution, single-pass polarimetric SAR interferometry, four phase-center along-track interferometry and others.

The Institute participated in the last years in a number of ESA projects and has developed a close cooperation with the German space industry. It contributes actively to several new satellite programmes such as Sentinel-1, SMOS, MAPSAR, ALOS/PALSAR and the next generation of reconnaissance satellites. Furthermore, the Institute carried out many innovative projects using passive microwave for anti-personnel land-mine detection, soil moisture retrieval and for security applications.

Several major airborne SAR campaigns have been carried out with the Institute's E-SAR system in Europe, Asia and Africa. Innovative data acquisition modes of the E-SAR system allowed us to demonstrate for the first time the potential of polarimetric SAR interferometry (Pol-InSAR) for forest height retrieval in tropical areas. Pol-InSAR and tomographic data acquisitions over ice and agricultural fields promise a breakthrough for quantitative parameter retrieval. An airborne bistatic SAR experiment using E-SAR and ONERA's airborne SAR system RAMSES was also successfully performed in 2003, producing the first airborne bistatic SAR data in Europe.

I am proud to lead and work together with a first-class team of highly motivated colleagues and to be guiding the Institute towards new challenges. I hope you enjoy reading this report and sharing the excitement of the challenges to come.

Oberpfaffenhofen, April 2006

Prof. Dr.-Ing. habil. Alberto Moreira

Content

1 Overview

This report summarises the research activities and projects of the Microwaves and Radar Institute of the German Aerospace Center in the timeframe between 2000 and 2005. The Institute is located in Oberpfaffenhofen near Munich and has a long history dating back to the beginning of the last century. Today the Institute focuses its research on active and passive microwave techniques, sensors and applications related to remote sensing, environmental monitoring, reconnaissance and surveillance as well as road traffic monitoring. The Institute has about 90 researchers, engineers and technicians and has become the driving force of the SAR Center of Excellence at DLR. It is a leading institution in SAR remote sensing in Europe and worldwide.

1.1 Microwaves and Radar Institute

Mission and Profile

The Institute contributes with its know-how and expertise in passive and active microwaves to the development and advancement of ground-based, airborne and spaceborne sensors, concentrating its research work on the concept and development of new microwave techniques and systems as well as sensor-specific applications. The Institute's strength is the execution of long-term research programmes with applications in aeronautics, air- and spaceborne remote sensing, traffic monitoring as well as reconnaissance and security. In line with the German Space Programme, the Institute works in close collaboration with the national space agency, ESA, German industries, and the responsible ministries. Education of young scientists in the scope of internships and diploma or doctoral theses is also an important part of the Institute's mission.

Expertise and Facilities

The Institute's expertise encompasses the whole end-to-end system know-how in microwave sensors. This allows us to play a key role in the conception and specification of new sensors, including the development of new technologies and techniques.

The Institute's experience in SAR systems goes back more than 25 years. Examples of SAR missions in which the Institute has been involved are ERS-1, SIR-C/X-SAR, SRTM, ENVISAT/ASAR, SAR-Lupe, TerraSAR-X, ALOS/PALSAR and TanDEM-X.

The Institute operates a number of research and measurement facilities to support the development and validation of new sensors and techniques:

- *Experimental-SAR (E-SAR)* – a high resolution airborne SAR system in P-, L-, C- and X-band for the demonstration of new techniques and technologies, for the development of new applications as well as for the simulation of future spaceborne SAR systems. E-SAR has attained a leading position among the airborne SAR sensors for civil applications in Europe (section 2.2).
- *Large Scale Anechoic Chamber* – an indoor chamber (ca. 10 x 5 x 5 m) for mono- and bistatic radar signature measurements operating from 88 to 96 GHz. The target size is up to 60 mm and measurements of the complex co-polar and cross-polar scattered field are possible. Operation is performed via a PC-based Graphical User Interface with automatic real-time data acquisition and visualisation (section 2.3.9).
- *Small Scale Anechoic Chamber* – an indoor chamber (ca. 5 x 4 x 3 m) for free space reflection measurements from 8 to 12 GHz for the determination of the complex material constant. Material samples can be flat or rough plates with typical sizes of 25 cm x 25 cm. Operation is performed via a PC-based Graphical User Interface with automatic real-time data acquisition and visualisation as well as controlled height adjustment and rotation of the probe (section 2.3.9).
- *Antenna Measurement Facility (AMA)* – long-range open-air antenna measurement facility from 10 MHz to 40 GHz (shared with the Institute for Communication and Navigation). It has a measurement range of up to 180 m and a fully automated measurement procedure. Antenna sizes of up to 5 m x 4 m and 200 kg for the turn-table assembly and up to 2 t for installation on the top of the main tower are possible (although a crane is required in the latter case).
- *Polarisation Diversity Radar* (*POLDIRAD)* – a coherent fully polarimetric C-band weather radar (jointly operated with the Institute of Atmospheric Physics and located on the roof of its building), has a 5 m antenna aperture diameter without a radome (1° resolution in elevation and azimuth), 250 kW transmitter peak power, PRF up to 2400 Hz and 300 km maximum range.

- *Microwave Research Laboratories* – two research laboratories specially equipped for development, optimisation, integration, testing and calibration of radar (300 MHz - 18 GHz) and radiometer (1 GHz – 150 GHz) systems. It also includes an Inverse SAR facility for the RCS measurement (1 GHz – 18 GHz) of smaller objects and a ground-based passive radiometric imager (9.6, 37, and 90 GHz).
- *Mechanical Workshop* – to support the developments and integration of ground-based or airborne microwave sensors. Design and manufacturing of high-precision mechanical drives, positioning systems, mechanical millimeter-wave and microwave components in machining and electroforming techniques, and various racks and housings.
- *Calibration Facility (CALIF)* – passive and active radar calibrators as well as various analysis software tools for the derivation of different calibration parameters and for image quality analysis, verification and validation. Depending on the satellite mission, corner reflectors, ground receivers as well as transponders can be deployed over an extension of more than 450 km.
- *Reconnaissance Mission Simulator* – a modular simulation tool for modelling the end-to-end system chain of a space- or airborne reconnaissance mission for planning, analysis, and optimisation purposes. The main functions are mission analysis and planning, satellite simulation, coverage and revisit time analysis, design and modelling of a realistic target scenario, modelling of the radar sensor characteristics, generation and processing of SAR raw data, and image quality analysis.

The above-mentioned facilities are an integral part of the research activities and projects of the Institute. A proposal for a new lab building annexed to the Institute's main location has been submitted to the Helmholtz Association of the German Research Centers (HGF). It is described in the second volume of this report. The main requirement for the new building arises from the need to integrate the laboratories, hardware developments and measurement facilities into a dedicated building. A further requirement arises from the need to expand the existing anechoic chamber to a compact range facility.

Organisation

The Institute has 4 departments working in well established research programmes, projects and external contracts. In each department the research field is focused on a particular area as described below (Table 1.1).

For many years the Institute has established a matrix structure to allow the use of the expertise and personnel from different departments for the execution of large projects and research activities. The TerraSAR-X project is a notable example. The project leadership for the Institute's contributions is under the responsibility of the Satellite SAR Systems department. In this department, approx. 65% of the personnel are allocated to the project, including the project leader; the remaining 35% are coming from two other departments in the Institute.

Table 1.1 Institute's departments and their respective research fields.

Department	Competence	Research fields
SAR Technology	*Airborne SAR*	Radar technology and development, antennas, signal processing, polarimetric SAR interferometry, airborne campaigns
Microwave Systems	*Microwave techniques*	Calibration, transponders, mono- and bistatic signatures, propagation, material constant determination, traffic monitoring with radar
Satellite SAR Systems	*Spaceborne SAR*	Spaceborne SAR techniques, system concepts, SAR missions and operations, system engineering and performance, digital beamforming, bistatic systems
Reconnaissance and Security	*Active and passive microwave sensors for reconnaissance and security applications*	SAR data and mission simulator, mission planning, analysis and optimisation, Inverse SAR, radiometry, synthetic aperture radiometry

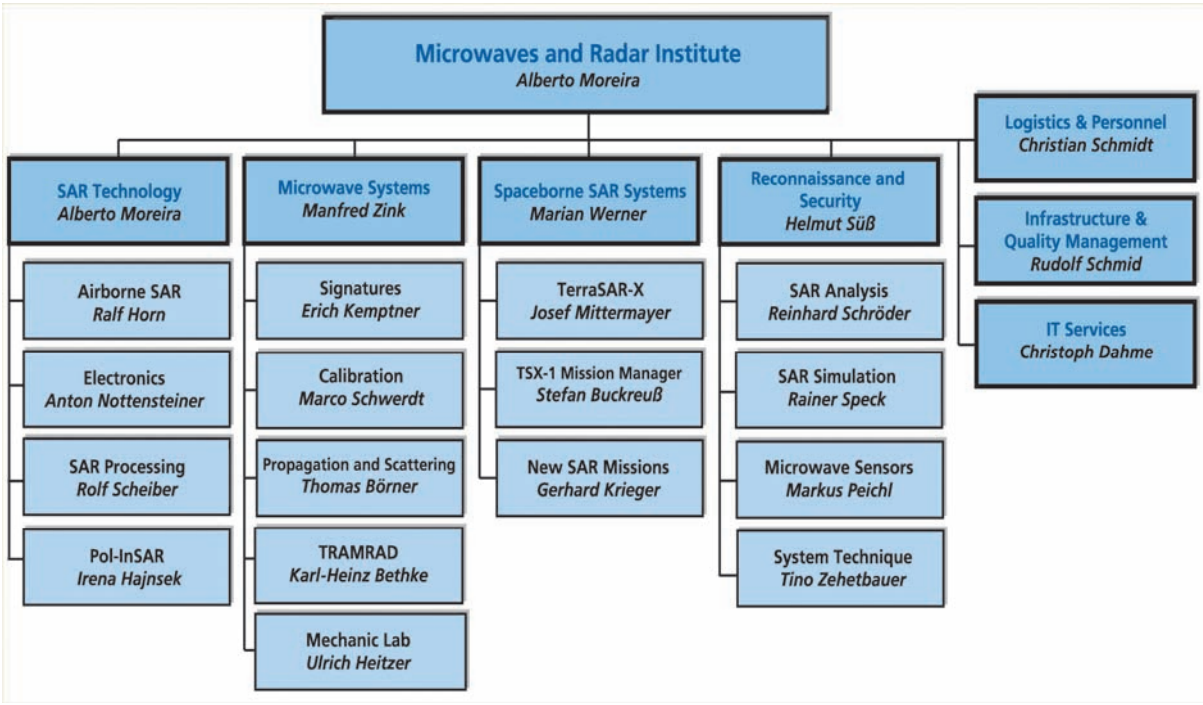

Figure 1.1 Organisation of the Microwaves and Radar Institute.
From 1996 to 2005, the Microwave Systems Department has been led by David Hounam who is retiring in spring 2006. Manfred Zink took over the leadership of this department at the beginning of 2006.

Figure 1.1 shows the organisation of the Institute with its research departments and associated infrastructure. The Institute forms also a cluster with the Institute for Communication and Navigation (IKN). The Antenna Measurement Facility (AMA) and the mechanical workshop are shared within the cluster activities. Furthermore, the Institute works very closely together with three other DLR Institutes at Oberpfaffenhofen within the framework of the TerraSAR-X project: German Space Operation Center (GSOC), German Remote Sensing Data Center (DFD) and Remote Sensing Technology Institute (IMF). Through the airborne SAR campaigns we are in close collaboration with DLR's Flight Operations Department (FB).

The directorship of the Institute is linked to a full professorship at the University of Karlsruhe (Institut für Höchstfrequenztechnik und Elektronik – IHE). Several joint projects are being carried out in cooperation with the University of Karlsruhe in the fields of digital beamforming, calibration transponders for TerraSAR-X and antenna developments.

1.2 Summary of Major Achievements

The last five years in the Institute were characterised by several highlights, particularly in the SAR field. In 2000, following a peer review by an external board of examiners, the Institute was recognised as a **DLR Center of Excellence for SAR**, due to its expertise in SAR technology, techniques, and missions. The German Remote Sensing Data Center (DFD) and the Remote Sensing Technology Institute (IMF) are partners of the Institute in this recognition. We also collaborate closely with these institutes in the TerraSAR-X and TanDEM-X projects.

With the continuity of successful work in SAR over 25 years it has been possible to channel the experience gained from the planning and implementation of international space missions into a national SAR programme. Due to the end-to-end system know-how from data acquisition (including the Institute's airborne SAR) through data interpretation and research into new applications, the SAR Center of Excellence has become one of the leading international research facilities in SAR.

In the following a brief summary of the major achievements and projects will be given. Section 2 complements this summary with a description of the research activities and projects.

In February 2000, the 11-day **Shuttle Radar Topography Mission (SRTM)** was successfully carried out in partnership with NASA/JPL (section 2.1.1). On-board were a German X-band imaging radar (X-SAR) and a NASA/JPL C-band radar (SIR-C) augmented by a deployable 60-meter mast on which secondary receive antennas were installed. The Shuttle Endeavour orbited the Earth 176 times at a height of 240 kilometers above the Earth's surface. The ambitious goal of generating the first, almost global, homogeneous Digital Elevation Model of the Earth's surface with an unsurpassed relative height accuracy of ca. 6-10 m was achieved. Around 120 million km^2 in C-band radar and 64 million km^2 in X-band radar have been processed and are available as maps. One major challenge was the continuous measurement of the relative positions of the radar antennas which determined the interferometric baseline. The success of the SRTM mission and the experience gained was a prime factor in achieving approval for the German TerraSAR-X project.

The Institute has supported with its research work for a long time period the development of very high resolution spaceborne imaging radar systems in recognition of their usefulness for a wide variety of applications for **reconnaissance and security** (sections 2.1.10, 2.3.3, 2.3.5, 2.3.9 and 2.3.10). Since 1989, it has participated in the European EUCLID programme, particularly in the SAR priority areas. Its research work contributed to the recognition of the potential of such systems, culminating in the realisation of the German **SAR-Lupe** programme in 2001. The first satellites will soon be launched and will provide valuable data for reconnaissance and security related applications. The potential of SAR as a source of information for reconnaissance and security purposes has always been an important topic in the Institute. In the interests of both political and military decision-making, the Federal Armed Forces need to be able to contribute towards the early recognition of crisis situations and be capable of providing comprehensive information for post crisis situations. The SAR-Lupe satellite system, as an information system, is intended for use exclusively in meeting core military requirements for unrestricted access, rapid image delivery time, the highest possible resolution, geographical accuracy, worldwide imaging capability and confidentiality.

In 2002, a small but programmatically important study was awarded to EADS Astrium GmbH and the Institute, namely **SAFARI** (Strategische Ausrichtung für raumgestützte Radarinstrumente). The aim was to develop a long-term strategy for spaceborne SAR development. The study identified the need for companion satellites, an example being TanDEM-X (section 2.1.3), the need for **bistatic and multistatic SAR** (sections 2.1.4 and 2.3.1), **digital beamforming** technology (section 2.3.2) and **SAR constellations** required for traffic monitoring with radar (section 2.3.4). Hence, SAFARI paved the way for developments, which are now being realised, giving German radar science a decisive lead.

In the same year, the **TerraSAR-X** project was approved. It is currently the DLR's largest space project and is being carried out within the framework of a Public Private Partnership between DLR and EADS Astrium GmbH (section 2.1.2). TerraSAR-X is the fruit of the consistent development of German radar technology over many years and is an example of successful cooperation with the German aerospace industry. TerraSAR-X is part of the newest generation of high resolution radar satellites for observing the Earth with a resolution down to one meter. Its launch is scheduled for 2006. The project has enormous potential for the commercial and scientific exploitation of radar data. TerraSAR-X is poised to achieve a leading world-wide market position.

The Institute has cooperated with ONERA in microwave research for a number of years. The joint interest in **bistatic SAR** imaging was leading to a first notable bistatic SAR campaign in 2003 (section 2.3.1) with ONERA's airborne SAR system RAMSES and the Institute's E-SAR. The campaign generated new bistatic SAR products, opening up new applications, and tested the techniques for the TanDEM-X configuration, like the tandem geometry and the method of synchronizing the sensors.

In the same year, the **TRAMRAD** project (Traffic Monitoring with Radar) commenced with the aim of paving the way for radar systems to monitor road traffic over wide areas (section 2.3.4). The Institute had been following the developments in radar systems for moving target detection for several years, recognizing the need for non-cooperative means of remotely locating vehicles. TerraSAR-X will have a mode to detect moving targets and will generate experimental products for traffic monitoring from space for the first time, and it can be expected that future SAR sensors will follow.

The research into microwave imaging radiometers is a traditional field in the Institute and the work on aperture synthesis techniques for high resolution were successfully demonstrated (section 2.3.10). The expertise gained led to the invitation to advise ESA on the L-band **SMOS** (Soil Moisture and Ocean Salinity) sensor, which uses this technique. Development started in 2003 and the launch is planned for 2007. The sensor promises to set new standards in passive microwave remote sensing.

The **experimental airborne SAR system (E-SAR)** has attained a high degree of capability with respect to resolution and to the number of frequencies, polarisation modes, etc., with the consequence that it has become the sensor of choice in Europe for scientific SAR investigations (sections 2.2.1 and 2.2.2). Several major campaigns in Europe, Africa and Asia have been carried out in the last few years (section 2.2.3), demonstrating the high degree of maturity of the system and its world-wide deployment. The Institute is currently developing the **F-SAR** airborne sensor to further improve the quality of the SAR products and to provide new measurement modes (section 2.2.6 and 2.3.8). F-SAR should guarantee airborne SAR services well into the future.

Polarimetric SAR interferometry (Pol-InSAR) is today an established remote sensing technique that allows the investigation of the 3-D structure of natural volume scatterers (section 2.2.4). From the very beginning the Institute developed this new technique, leading to expertise in sensor technology, system and instrument design, performance analysis as well as processing, modelling and inversion techniques. With the E-SAR sensor, the Institute demonstrated for the first time airborne polarimetric repeat-pass interferometry and tomography (sections 2.2.2, 2.2.4 and 2.2.5). Pol-InSAR techniques will be faced with the potential and the challenges arising from an extended observation space provided from multi-baseline, multi-frequency, bi- and multistatic sensor configurations forcing the evolution of quantitative measurement and information product generation in SAR remote sensing.

Radar calibration has long been an important field of the Institute, in accordance with the goal to optimise the performance of radar sensors (section 2.3.7). The expertise gained from the national X-SAR and SRTM projects and the European ERS-1/2 and ENVISAT/ASAR sensors was recognised when ESA appointed the Institute to establish a calibration concept for the L-band SAR on **TerraSAR-L** (section 2.1.5) in 2004 and the C-band **Sentinel-1** (section 2.1.6) in 2005. Sentinel-1 is currently ESA's first contribution to the EU's GMES (Global Monitoring for Environment and Security) programme, and Germany has pledged its support to lead the project.

TanDEM-X (TerraSAR-X **a**dd-o**n** for **D**igital **E**levation **M**easurement) is a mission proposed by the Institute with the aim to generate from space a global, Digital Elevation Model with an unprecedented accuracy (section 2.1.3). The mission proposal has been approved for the realisation phase. The aim of the mission will be achieved by supplementing the TerraSAR-X satellite (with planned start for 2006) with an additional X-band SAR satellite (TanDEM-X) in a tandem orbit configuration. The scientific utilisation spectrum can be divided up into high-precision digital elevation models, along-track interferometry (e.g. measurements of the ocean currents and road traffic monitoring) and innovative bistatic applications (e.g. polarimetric SAR interferometry, digital beamforming). TanDEM-X represents an important step towards a system of radar satellites and will provide sustained support for Germany's leading role in the sector of SAR technology in X-band.

1.3 Future Research Activities and Projects

Looking ahead to the next 5 years the Institute will continue to initiate and contribute to several projects that will be decisive for its long-term strategy. Examples are TerraSAR-X, TanDEM-X, as well as the demonstrator for future reconnaissance systems, the new airborne SAR system, ALOS/PALSAR, MAPSAR, SMOS, TRAMRAD, Sentinel-1[1], HABITAT[2] and others. Section 2 describes the projects and achievements in the past 5 years and provides an outlook on the future activities. These projects are accompanied by several research programmes that allow the Institute to keep a step ahead in the development of new research fields. Examples of research programmes are bistatic and multistatic SAR systems, digital beamforming, Inverse SAR, polarimetric SAR interferometry and tomography, calibration, signatures, propagation, antennas, and imaging techniques for radiometry. The research programmes are closely inter-connected to the project activities. As a matter of fact most of the current projects in the Institute have

[1] Participation of the Institute is being consolidated at the time of the report compilation.

[2] Depending on a positive selection for a phase A study of the next ESA Earth Explorer Core Mission.

started as research programmes with typical durations of ca. 2 to 5 years. Today, the Institute has more than 50% of its resources allocated to projects and external contracts. Due to the success in the approval of the new mid-term and long-term projects, this percentage will increase to approx. 60-70% in the next 5 years.

In a changing world high-resolution and timely geo-spatial information with global access and coverage becomes increasingly important. For example, a constellation of SAR satellites will play a major role in this task since SAR is the only spaceborne sensor that has an all-weather and day-and-night high-resolution imaging capability. Examples of applications for such a constellation are environmental remote sensing and protection, road traffic, hazard and disaster monitoring as well as security related applications.

One challenge for future spaceborne SAR systems is to optimise the performance/cost ratio as much as possible so that a constellation of satellites becomes affordable. Innovative concepts with bistatic and multistatic system configurations represent an attractive solution that exploits the use of small receiver satellites acquiring the backscattered signal of active MEO or GEO satellites. Utilisation of the same transmit signal for different applications can also be explored, as in the case of GPS reflectrometry for ocean and land remote sensing. Digital beamforming for transmit and/or receive will solve the contradiction posed by the antenna size in traditional SAR systems that prohibits the SAR sensor from having high azimuth resolution and a large swath width at the same time. Digital beamforming is a clear trend for future systems, allowing enormous flexibility in the sensor imaging mode, sensor calibration, interference removal and ambiguity suppression. These concepts will allow the implementation of a flexible SAR sensor network with a faster access time and almost continuous imaging capability which is necessary for time critical applications. High-flying platforms and unmanned vehicles will certainly act as a complementary platform for this network of sensors. Furthermore, radar satellites flying in close-formation will allow the construction of sparse arrays with enhanced imaging capabilities.

Another important aspect for actual and future microwave sensors is the ability to provide quantitative and reliable measurements of the required information to the user community. In the past, information was based on a more qualitative, less reliable basis. Today, the sensor information becomes multi-dimensional as different sensor sources, polarisations, temporal and spatial baselines, aspect angles and frequencies are used for reliable parameter retrieval. The Institute will further concentrate its activities in system calibration and in the development of algorithms for sensor-specific parameter retrieval, as in the case of multibaseline polarimetric SAR interferometry. Besides SAR systems the Institute also aims to increase its participation in the concept and development of future spaceborne microwave missions such as range-Doppler and interferometric altimeters, radar sounders and advanced radiometers.

The vision of a sensor network is in some aspects not too far away. The Institute is committed to increasing its participation to the development of future microwave satellites for remote sensing and reconnaissance. It aims to expand its expertise and leadership in strategically important projects and research areas. Together with its cooperation partners in DLR, industry and science the Institute will play a key role in the realisation of this vision.

2 Research and Project Results

2.1 Spaceborne SAR

2.1.1 Shuttle Radar Topography Mission - SRTM

Figure 2.1 X-SAR-SRTM mission patch.

On February 22, 2000 one of the most complex Space Shuttle missions was successfully completed, the Shuttle Radar Topography Mission (SRTM). The main objective of this mission was to collect interferometric radar data for the generation of a near global Digital Elevation Model (DEM), covering the Earth's surface between -56° and +60° latitude.

Figure 2.2 View into Endeavours cargo bay with the deployed SRTM mast (Photo NASA).

The SRTM mission was a follow-on to the Shuttle Imaging Radar-C/X-band Synthetic Aperture Radar (SIR-C/X-SAR) missions that were successfully conducted twice in April and October 1994 [58]. For SRTM, the SIR-C (5.6 cm wavelength) and X-SAR (3 cm wavelength) radar instruments had each to be supplemented by a second receive channel, as well as a second receive only antenna at the end of a 60 m long deployable mast (Figure 2.2) forming the first spaceborne single-pass interferometer.

SRTM was a cooperative project between NASA, NGA (National Geospacial-Intelligence Agency) and DLR. NASA's Jet Propulsion Laboratory (JPL) was responsible for the C-band radar system, the mast and the Attitude and Orbit Determination Avionics (AODA). DLR was responsible for the X-band radar system (X-SAR). The Institute had the project lead and was responsible for the specification, system engineering, mission operations (with support from DLR-GSOC), calibration and the scientific exploitation. Data processing, archiving and data distribution was the task of DLR-CAF. EADS Astrium GmbH was the main contractor for the X-SAR flight hardware development, integration and test.

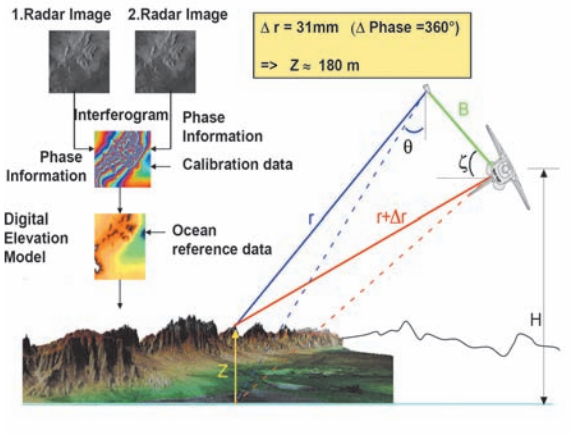

Figure 2.3 Single-pass SAR interferometry principle.

Single-Pass SAR Interferometry

Building a single-pass SAR interferometer requires at least one transmitter and two receivers with antennas separated by a so-called interferometric baseline (Figure 2.3). For SRTM, the baseline was formed by the 60 m long deployable mast structure reaching out of the orbiter cargo bay and carrying the secondary antennas at its end. The same reflected radar signal from points on the ground is received by both antennas, inboard and outboard, but at slightly different times, or as we call it with a phase difference, due to the tiny difference in distance. This phase difference can be accurately estimated, because single-pass interferometers do not suffer from problems with atmospheric disturbance and temporal decorrelation of the target backscatter encountered with repeat-pass interferometry.

With the precise knowledge of the shuttle's position and the baseline vector in space relative to the spot on the ground at any time, the height of the target can be processed. Orbit and baseline were measured with the AODA system: a set of GPS receivers, gyros, electronic distance me-

ters and star trackers. The position of the interferometer was measured by GPS with an accuracy of 1 m. The baseline angle was measured with an accuracy of about 2 arcseconds (short-time) and 7 arcseconds (mission). The baseline length was determined to millimeter accuracy.

The Mission

Seven hours after launch the mast had been successfully extracted and soon the first test data take was acquired over New Mexico / USA and processed by DLR. Figure 2.4 shows the first interferogram with the oscillations of the mast still uncompensated and without calibration.

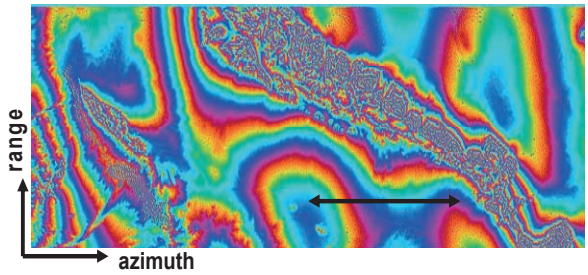

Figure 2.4 First X-SAR interferogram of the Shuttle Radar Topography Mission. The arrow shows the effects of uncompensated mast oscillations.

The mapping of the continents was performed by operating the radar only over land with 5 to 15 seconds coverage over the ocean before and after the land. These aquisitions served as an absolute height reference using the well known ocean heights. More than 700 data takes were performed to map the earth in 11 days. Additionally, several long data takes only over ocean have been acquired to support the calibration and verification of the system [420].

The only problem during the mission was the malfunctioning of a cold gas valve. In consequence, the baseline orientation had to be maintained by corrective firings of the attitude control thrusters about every 90 seconds. These firings lead to increased oscillations of the mast and in consequence, to increased processing complexity and DEM errors [424]. Nevertheless, after 159 orbital revolutions the C-band system with its 225 km wide swath had managed to cover the required surface. The X-band coverage, limited due to a swath width of 50 km, still comprises more than 60 million square kilometers.

Data Analysis and Results

The mission analysis revealed an excellent stability of the radar systems and a homogenous data quality with respect to the basic radar parameters, like received echo level, antenna azimuth beam alignment, interferometric coherence and Doppler centroid frequency. During a collaborative calibration phase after the mission that lasted more than one year, the processing teams calibrated all the timings, offsets and dynamic behaviour of the instruments [427].

The relative height error was specified to be 6 meters (90%). This accuracy was generally confirmed by DLR investigations, e.g. by comparison with navigation points as shown in Table 2.1. Several other investigators confirmed this accuracy, e.g. an independent quality assessment at a 70 km by 70 km test site south of Hanover, Germany, using trigonometric points and the Digital Terrain Model ATKIS DGM5 concludes with a mean value of the height differences μ of 2.6 m and a standard deviation σ of 3.4 m.

Table 2.1 SRTM DEM validation with navigation points in the western part of Germany.

flat terrain			
	number	**μ [m]**	**σ [m]**
forested areas	2329	-6.20	6.74
urban areas	1683	-2.63	4.10
open landscape	20786	-0.94	4.31
Σ	24798	-1.55	4.84
moderate relief			
	number	**μ [m]**	**σ [m]**
forested areas	1970	-1.98	7.60
urban areas	725	-1.14	4.86
open landscape	8000	+0.15	4.54
Σ	10695	-0.33	5.33
highlands			
	number	**μ [m]**	**σ [m]**
forested areas	2272	-4.43	8.62
urban areas	766	-1.04	5.29
open landscape	7693	-0.74	5.36
Σ	10731	-1.54	6.37

The achieved height errors of ±2.5 m correspond to a line-of-sight mast motion compensation accuracy of 0.44 mm, which was an incredible achievement. Nevertheless, residual, uncompensated 1st order oscillations of the mast translate to this measurable error on an 8 km scale in flight direction.

The long term variations in the 10 to 20 minute scale are of little relevance for the user, as they represent only a small height offset within a DEM product. These slow drift errors are within specification and entirely handled by the ocean calibration and bundle adjustment approach.

With SAR interferometry, the location or height of a representative phase center of the backscattering resolution cell is measured. In principle C-band radar waves should have a higher penetration into the vegetation than X-band waves leading to differences in the interferometric height measured in the two systems over forested areas. To compare the penetration between C- and X-band for example into rain

forest, several areas in Brazil and Kongo (Figure 2.5) have been investigated. A relatively flat terrain and visible clear-cuts along roads have been selected to remove any offset between C- and X-band not due to penetration effects.

The resulting height differences of about 1 m are not very significant and well within the height error boundaries of both systems.

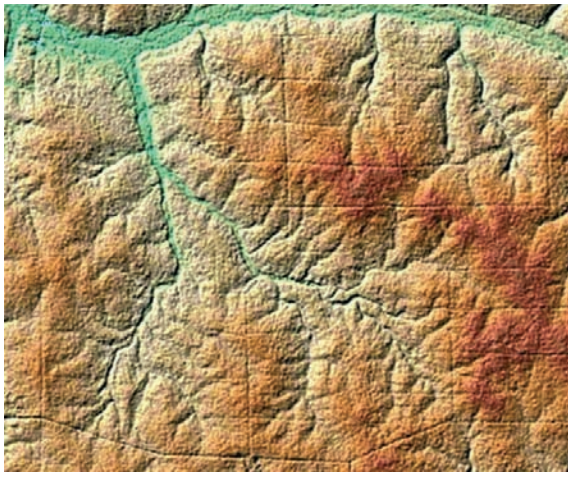

Figure 2.5 SRTM X-band digital elevation model shows topography plus vegetation heights, rivers and clear cuts in the Kongo rain forest.

In response to the announcement of opportunity (AO) 102 proposals have been accepted [423] and more than 1200 DEM and radar products for scientific evaluation with regard to validation, calibration and geoscience applications have been ordered. Hundreds of papers have been written using SRTM data for their investigations.

Though the X-band data from SRTM have a better performance than the C-band data, the gaps in the coverage and the cost for the data access have reduced the worldwide use considerably.

For many applications, the 1 arcsec posting and the accuracy of the SRTM dataset is still not sufficient and the area north and south of 60 degrees latitude is still only available with 30 arcsec resolution. A satellite mission like TanDEM-X (section 2.1.3) will provide DEM performance of the next higher quality level and fill the gaps.

2.1.2 TerraSAR-X

The German national SAR mission TerraSAR-X is based on a public-private-partnership agreement between DLR and EADS Astrium GmbH. It is the successor of the scientifically and technologically successful radar missions X-SAR (1994) and SRTM (2000) and is designed for scientific and commercial applications.

EADS Astrium GmbH is developing the TerraSAR-X satellite (Figure 2.6), whereas DLR is responsible for the overall mission and will provide the necessary ground segment infrastructure.

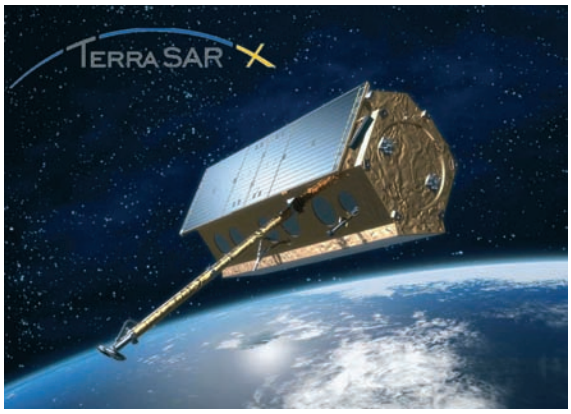

Figure 2.6 Artist's view of the TerraSAR-X spacecraft.

The Microwaves and Radar Institute is responsible for SAR system engineering, including support to the DLR project management, performance control, calibration and verification and the design and implementation of the Instrument Operations and Calibration Segment (IOCS). Ground segment integration and mission management are also carried out by the Institute.

The commercial and scientific exploitation of the TerraSAR-X mission is covered by Infoterra GmbH (a subsidiary of EADS Astrium) and DLR, respectively.

Mission and System

The TerraSAR-X satellite will be launched in summer 2006 on a Russian DNEPR-1 with a 1.5 m long fairing extension. All launch vehicle elements except for the fairing inter-stage are unmodified components of the original SS-18 intercontinental ballistic missile. The lift capability into the selected orbit is 1350 kg.

For the orbit selection, an altitude range between 475 km and 525 km has been investigated. The sun-synchronous dawn-dusk orbit with an 11 day repeat period defined in Table 2.2 showed the best performance with respect to order-to-acquisition and revisit times.

Once in orbit, the satellite will be operated from the German Space Operation Center (GSOC) in Oberpfaffenhofen. In the system baseline, two ground stations in Germany are foreseen. Weilheim is used as the telemetry and telecommand station and Neustrelitz serves as the central receiving station for the X-band downlink (Figure 2.7). Beyond that, additional Direct Access Stations - commercial partners of Infoterra GmbH - are foreseen to extend the baseline receiving station concept [124].

Table 2.2 TerraSAR-X Orbit Parameters.

Parameter	Mission Orbit
Orbit Type	Sun-synchronous repeat orbit
Repeat Period	11 days
Repeat Cycle	167 orbits in the repeat
Orbits per Day	15 2/11
Equatorial Crossing Time	18.00 h ±0.25 h ascending pass
Eccentricity	0.0011 – 0.0012
Inclination	97.443823°
Argument of Perigee	90°
Altitude at Equator	514.8 km
Ground Track Repeatability	within ±250 m per repeat cycle

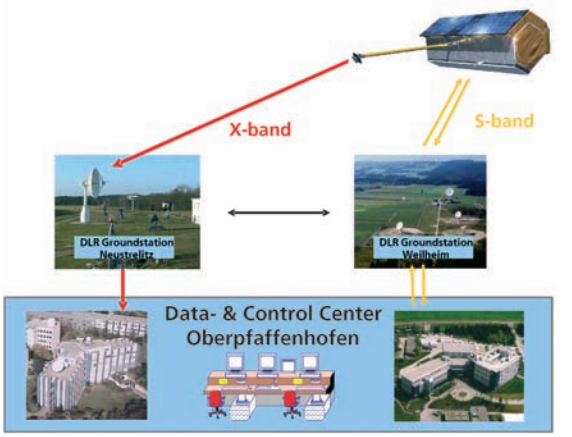

Figure 2.7 TerraSAR-X data flow concept.

TerraSAR-X carries an advanced high resolution X-band Synthetic Aperture Radar (SAR) based on active phased array technology which allows the operation in Spotlight-, Stripmap- and ScanSAR Mode (Figure 2.8) in various polarisations. It provides the ability to acquire high resolution images for detailed analysis, as well as wide swath images for overview applications.

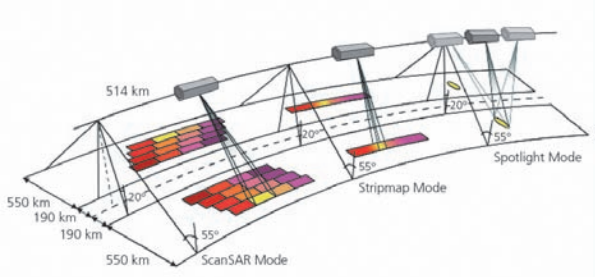

Figure 2.8 TerraSAR-X modes of operation.

The X-band SAR instrument operates at a center frequency of 9.65 GHz and with a maximum bandwidth of 300 MHz [259]. The antenna is capable to operate in two polarisations; H and V on transmit as well as on receive and consists of 12 panels with 32 dual polarised slotted waveguide subarrays stacked in elevation. Each subarray is fed by a dedicated Transmit/Receive Module (TRM). The SAR antenna's approximate dimensions are 4800 mm in length, 800 mm in width and 150 mm in depth. It features electronic beam steering in azimuth (±0.75°) and elevation (±20°). The acquired SAR data are stored in a Solid State Mass Memory Unit (SSMM) of 256 Gbit end-of-life capacity before they are transmitted to ground via a 300 Mbit/s X-band System.

All payload sub-systems are fully redundant, i.e. main and redundant functional chains exist. This allows the utilisation of a new concept that involves activation of both functional chains at the same time, one being the master for timing purposes. As a result operation in an experimental Dual Receive Antenna (DRA) Mode, where the echoes from the azimuth antenna halves can be received separately, becomes possible. This new experimental mode enables the interesting new features like Along-Track Interferometry (ATI), fully polarimetric data acquisition and the enhancement of the azimuth resolution.

Ground Segment

The TerraSAR-X Ground Segment is the central facility for controlling and operating the TerraSAR-X satellite, for calibrating the SAR instrument, archiving the SAR-data and generating and distributing the basic data products. The overall TerraSAR-X Ground Segment and Service Segment (Figure 2.9) consist of three major parts:

- Ground Segment which is provided by DLR,
- TerraSAR-X Exploitation Infrastructure (TSXX) under the responsibility of Infoterra and
- Science Service Segment coordinated by DLR.

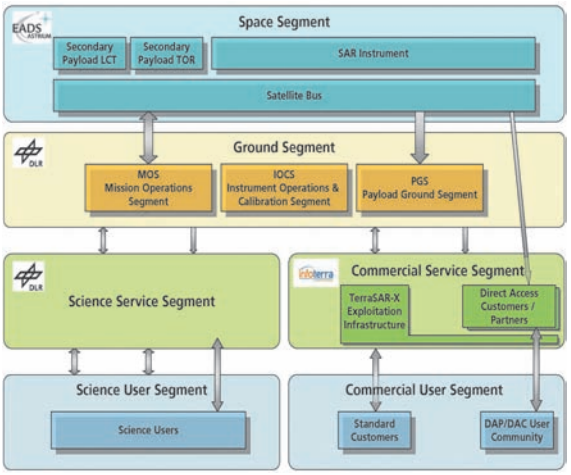

Figure 2.9 TerraSAR-X system overview: the space segment comprising the TerraSAR-X instrument and two secondary payloads, the ground segment with its three sub-segment, and the scientific and commercial service and user segments.

SAR System Engineering

The SAR System Engineering provides the SAR know-how to operate the instrument within the required specifications and to monitor the payload hardware. It also provides support to the ground segment integration and the overall project management.

Examples for major tasks of SAR System Engineering are:

- Specification of TerraSAR-X modes and imaging beams
- Overall SAR system performance control
- Instrument shadow engineering
- Support in instrument acceptance tests
- Technical support for project management decisions
- Algorithm development for Spotlight SAR processing
- Attitude steering definition law for Doppler centroid minimisation

In the following, examples of three SAR System Engineering tasks are presented in more detail: the development of Spotlight processing algorithms, the zero-Doppler attitude steering law and the selection of swath positions and corresponding beam patterns.

Spotlight Processing Algorithms

The Extended Chirp Scaling Algorithm for Steering Spotlight [38] has been enhanced for the processing of TerraSAR-X sliding Spotlight raw data. The enhancement consists more of a detailed analysis of the sliding Spotlight geometry and raw data signal and does not introduce fundamental new processing steps. The basic structural formulation of the algorithm and the Range compression is explained in detail in [258], while azimuth compression and the subaperture method are accurately derived in [38]. Figure 2.10 gives an overview of the algorithm.

Raw data of a point target are shown in the upper plot on the left. Processing starts with an azimuth sub-aperture formation in order to avoid up-sampling of the raw data in azimuth. The formation of the sub-apertures is indicated in the upper plot on the right by vertical lines. The subaperture approach allows a non-ambiguous azimuth frequency representation, the use of short azimuth FFTs, and the azimuth dependent update of processing parameters, e.g. the processing velocity.

In the next steps, range cell migration correction and range compression are performed by chirp scaling. The result of the range processing is shown in the middle left plot. The signal is range compressed and without range cell migration.

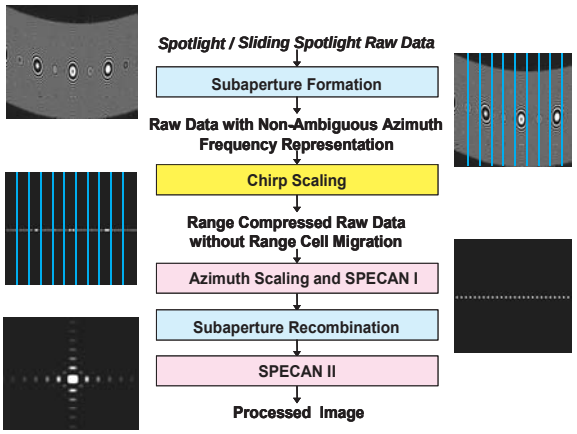

Figure 2.10 Algorithmic steps of Extended Chirp Scaling processor for Sliding Spotlight Mode products.

After range processing, azimuth compression is performed by SPECtral ANalysis (SPECAN) combined with azimuth scaling. The two stages of the SPECAN processing are deramping (SPECAN I in Figure 2.10) and final azimuth FFT (SPECAN II). The effect of the deramping operation on the point target signal can be seen in the lower plot on the right. The azimuth signal modulation is no longer a linear frequency modulation but has changed to a constant frequency, observable in this plot by the regular alternation of bright and dark sections of the range compressed signal. This plot shows the signal after the recombination of the sub-apertures, i.e. there are no more vertical lines visible.

Finally, the last step in the Sliding Spotlight SAR processing is an azimuth FFT (SPECAN II) which compresses the signal in azimuth. The final result is the impulse response function in the lower left plot in Figure 2.10.

Zero-Doppler Attitude Steering

The Total Zero Doppler Steering developed for TerraSAR-X enables SAR data acquisition with Doppler centroids close to zero independent of incidence angle and terrain height variation [11]. This is achieved by introducing a slight pitch steering on top of the standard yaw steering to align the satellite attitude to its velocity vector.

The implementation in TerraSAR-X is based on a look-up table with a step width of two degrees in argument of latitude and linear interpolation in-between. The look-up table implementation and satellite pointing errors result in a residual Doppler centroid below 120 Hz for left and right looking geometries.

Figure 2.11 shows the applied TerraSAR-X attitude steering law. Yaw and pitch angles are shown in red and green colours, respectively.

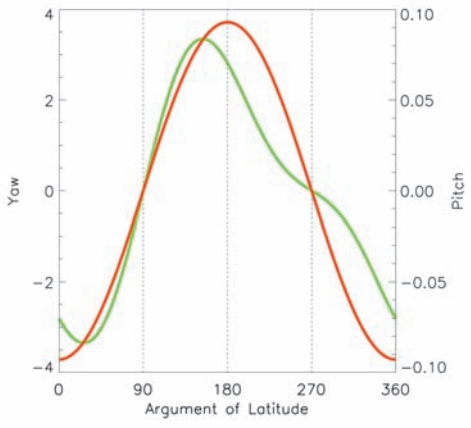

Figure 2.11 Attitude steering law for TerraSAR-X: yaw (red) and pitch (green) angles in degree versus latitude in degrees.

Selection of Swath Positions and Definition of Beam Patterns

In selecting the swath position for TerraSAR-X the timing is challenging due to the high pulse repetition frequency (PRF) between 3000 and 6500 Hz and the strategy of alternating pulses for dual and full polarisation modes.

Figure 2.12 shows, as an example, the timing diagram for the Stripmap Near and Stripmap Far beams, which are used for Dual and Full Polarisation modes. The principle strategy is to define the look angles for a minimum orbit height and to keep the look angles constant during the mission. In the figure, the red colours show the allowed PRFs for the compressed Stripmap near echo signal and the red and yellow colours together correspond to the non-compressed signal. The Stripmap far beams are shown in blue and grey colour.

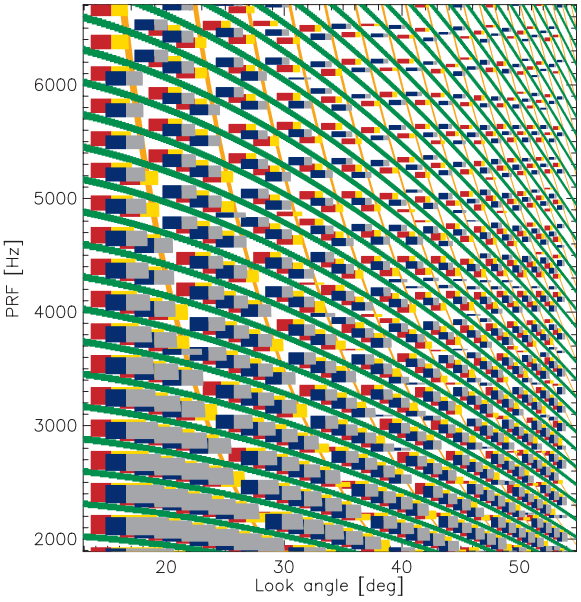

Figure 2.12 Timing diagram used for defining Stripmap near and far beams.

After selection of the swath positions (i.e. look angles) and swath widths, the beam coefficients for the required antenna patterns are determined using the antenna pattern optimisation tool described in 2.3.7. Further constraints, like side-lobe suppression levels are also taken into account.

Beyond these specification tasks, SAR System Engineering accompanies and influences the development process of the SAR instrument. Knowledge about the instrument, acquired in this process, is transferred into the ground segment.

The Instrument Operations and Calibration Segment

TerraSAR-X is the first mission to implement the novel concept of a dedicated ground segment facility comprising all the tools for instrument operations, performance monitoring as well as system and product calibration and verification. The block diagram in Figure 2.13 shows three sub-sections of the IOCS and their components.

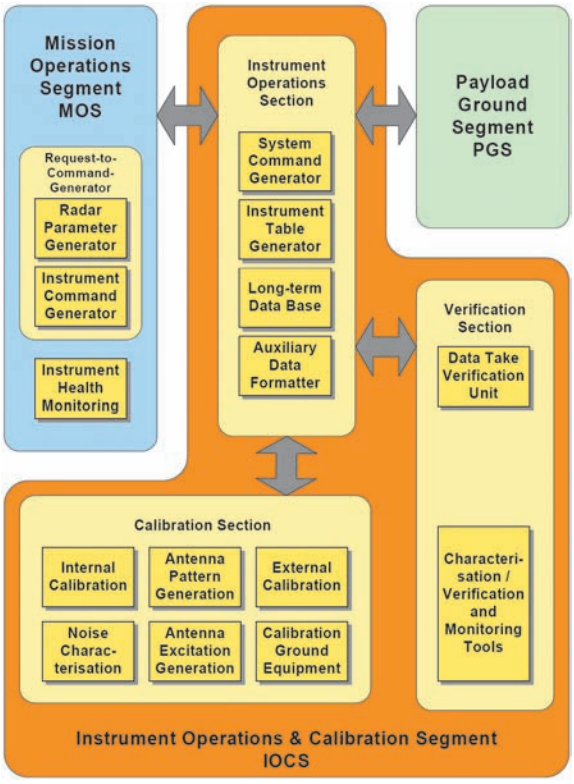

Figure 2.13 Overview of the TerraSAR-X IOCS.

The Instrument Operations Section has the function to operate the SAR instrument in its different operational SAR modes Stripmap, ScanSAR, Spotlight and in the experimental modes. The main tasks are to:

- generate, maintain, archive and distribute all required instrument tables for use on-board

and on-ground, generate radar parameters and command information for each SAR data acquisition,
- generate flight procedures with respect to the SAR instrument for nominal and contingency operations,
- provide and maintain a Long Term Data Base (LTDB) for archiving all relevant instrument information throughout the whole mission,
- provide auxiliary products with all calibration and instrument information required in the SAR data processing.

A key element of the IOCS is the LTDB. The central role of this archive is to provide all required data for system performance prediction and execution of corrective measures throughout the whole mission lifetime. In previous SAR missions, this information was often distributed over different locations. With the LTDB architecture, all mission data relevant for SAR system performance assessment are brought together and can be accessed by calibration, characterisation, monitoring, and verification tools. These tools are able to quickly provide a more complete picture of the whole TerraSAR-X system and its performance in shorter time. The effort for contingency analysis and the identification of countermeasures can be reduced. Under long term system monitoring aspects, it is possible to detect performance degradations with more anticipation and to provide more room for degradation mitigation.

The Verification Section ensures the correct in-orbit operation of the entire SAR system from data take instrument command generation to ground processing and has to technically release the SAR products. The complete SAR system verification is performed during the commissioning phase and at regular intervals during the mission. Specific verification activities can be triggered by faults and failures for trouble shooting. Typical tasks performed by this section are: data take verification, long-term SAR system monitoring, and instrument health monitoring.

The Calibration Section comprises all the analysis tools necessary for the internal and external calibration, antenna pattern determination including optimisation of beam coefficients, control of ground equipment, and noise characterisation. Further details on the TerraSAR-X calibration concept and its implementation are described in 2.3.7.

In the process of building up the TerraSAR-X ground segment, it turned out that the combination of SAR System Engineering, Calibration and Verification, and the development of the IOCS, which integrates all the required tools and facilities and provides a central archive for all performance relevant information, was a logical and very successful approach.

2.1.3 TanDEM-X

After the successful participation in the Shuttle missions SIR-C/X-SAR and SRTM, the first national SAR mission TerraSAR-X opened a new era in the German Space Programme and provided a major push for our R&D activities on high resolution X-band SAR. In this spirit, the proposal to add a second, almost identical spacecraft (TDX), to TerraSAR-X (TSX-1) and to fly the two satellites in a closely controlled tandem formation was born.

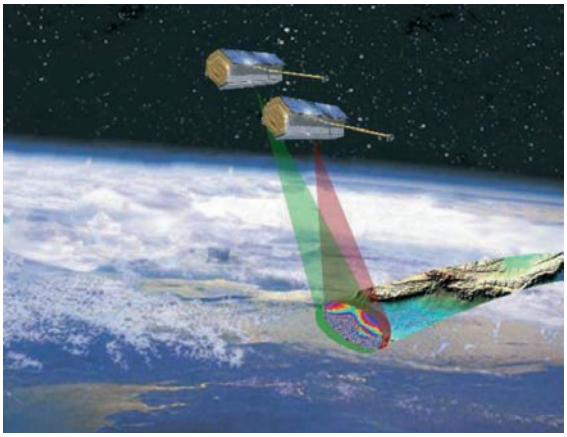

Figure 2.14 TSX-1 and TDX in tandem formation flight.

The TanDEM-X (TerraSAR-X add-on for Digital Elevation Measurement) Mission has the primary objective of generating a consistent, global DEM with an unprecedented accuracy according to the HRTI-3[1] specifications. Beyond that, TanDEM-X provides a configurable SAR interferometry platform for demonstrating new SAR techniques and applications [214]. TDX has SAR system parameters which are fully compatible with TSX-1, allowing not only independent operation from TSX-1 in a monostatic mode, but also synchronised operation (e.g. in a bistatic mode). The main differences to the TerraSAR-X satellite are the more sophisticated propulsion system to allow for constellation control, the additional S-band receiver to enable for reception of status and GPS position information broadcast by TerraSAR-X and the X-band inter-satellite link for phase referencing between the TSX and TDX radars (the required modifications on the TSX spacecraft have already been implemented). The TDX satellite is designed for five years of nominal

[1] HRTI-3 specification: relative vertical accuracy 2 m (90% linear point-to-point error over 1°x1° cell), absolute vertical accuracy 10 m (90% linear error), absolute horizontal accuracy 10 m (90% circular error), post spacing 12 m x 12 m.

operation. 3 years of joint operation with TSX-1 will be sufficient to fulfil the TanDEM-X user requirements.

User Requirements

The collection of scientific and commercial user requirements for the TanDEM-X mission clearly demonstrates the need of a HRTI-3 DEM data set with global access (see comparison with existing DEM products in Figure 2.15) for both scientific and commercial users [265], [490]. The majority of the geoscience areas like hydrology, glaciology, forestry, geology, oceanography, and land environment require precise and up-to-date information about the Earth's surface and its topography. Digital topographic maps are also a prerequisite for reliable navigation, and the improvements in their precision needs to keep step with advances in the performance of global positioning systems. Hence, TanDEM-X is fortuously timed to augment the exploitation of the GALILEO programme. From the commercial point of view, DEMs and ortho-rectified images are the most important products for a growing earth observation market.

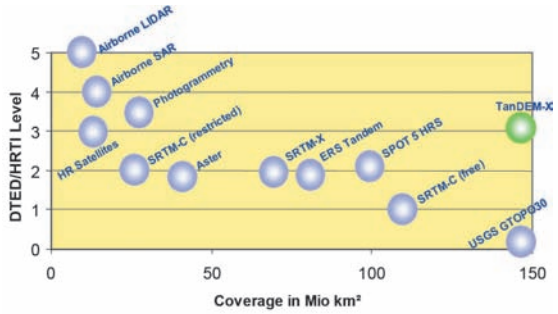

Figure 2.15 HRTI-level versus coverage indicating the uniqueness of the global TanDEM-X HRTI-3 DEM.

From a comprehensive user survey, three standard data products have been derived: standard HRTI-3 DEMs, Customised DEMs (CDEM) with even higher height resolution or improved horizontal spacing and Radar Data Products (RDP) acquired by along-track interferometry or new SAR techniques. Both scientific and commercial user requirements can be satisfied by these products and by the formation and coverage concept.

The Helix Orbit Concept

The TanDEM-X mission concept is based on a coordinated operation of two spacecraft flying in close formation [151]. Using two spacecraft provides the highly flexible and reconfigurable imaging geometry required for the different mission objectives. For example, the primary goal of generating a highly precise HRTI-3 DEM requires variable cross-track baselines in the order of 300 to 500 m.

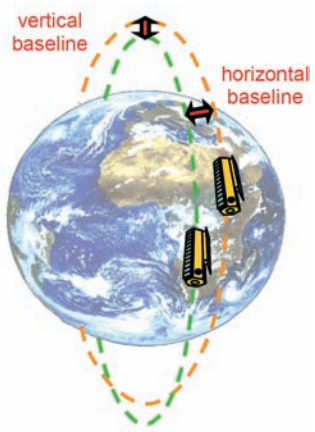

Figure 2.16 Artist's view of the Helix orbit concept used for the TanDEM-X mission.

In this close formation flight collision avoidance becomes a major factor and a minimum safety separation of 150 m perpendicular to the flight direction is to be observed around the orbit at any time. A formation, which fulfils these requirements, is the Helix formation shown in Figure 2.16. By an adequate eccentricity/inclination-vector separation, the two satellite orbits can be controlled accurately enough to ensure the minimum safety distance with negligible low risk. Although ground control is the baseline for manoeuvring the satellite, TDX will be able to receive GPS position information of TSX-1 via a dedicated intersatellite S-band link and to react autonomously in a contingency case.

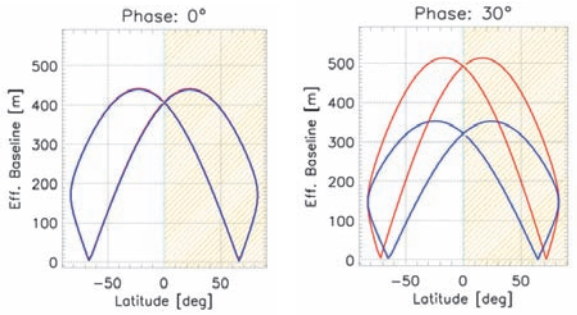

Figure 2.17 Effective baselines for different phases of libration, (blue) right-looking, (red) left-looking; in the left plot the blue curve is on top of the red one.

Exposed to the forces of the Earth's geoid, the two satellites start to move around the frozen eccentricity, resulting in a motion of libration. This effect can be advantageously used to achieve the desired baselines (Figure 2.17). The phase of libration can be adjusted by orbit manoeuvres, keeping the satellites at any desired phase with low fuel costs.

TanDEM-X Operational Modes

Interferometric data acquisition with the TanDEM-X satellite formation can be achieved in

three different operational modes: Bistatic, Monostatic, and Alternating Bistatic Mode [213].

Operational DEM generation is planned to be performed using bistatic interferometry (Bistatic Mode), which is characterised by the illumination of a scene by one transmitter and the simultaneous measurement of the same scene with two receivers (Figure 2.18), thereby avoiding temporal decorrelation. To provide sufficient overlap of the Doppler spectra, less than 2 km along-track baselines are required while the effective across-track baselines for high resolution DEMs have to be in the order of 300 m. Over moderate terrain one complete coverage with such across-track baselines will be sufficient, but for mountainous areas (about 10% of the Earth land surface) additional data acquisitions with different baselines and viewing geometry are required. Phase unwrapping problems over rough terrain can be solved step-by-step acquiring two or more data sets with decreasing baseline (increasing height of ambiguity), see also section 2.1.4.

Because of the slight differences in the Ultra Stable Oscillator (USO) characteristics of the two instruments PRF synchronisation and relative phase referencing between the satellites (exchange of USO signals via a dedicated X-band inter-satellite link) are mandatory in this mode.

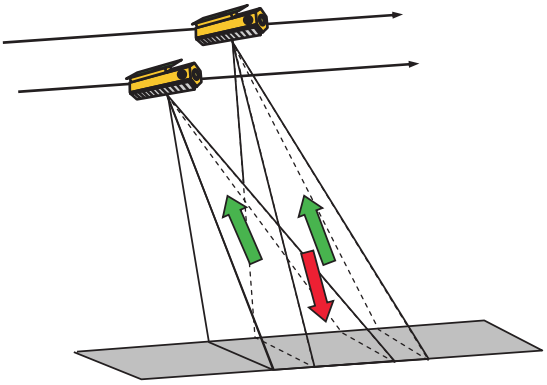

Figure 2.18 TanDEM-X in bistatic mode: one satellite transmits and both receive the echoes simultaneously.

The Radar Data Mode has been introduced as a synonym for the demonstration of innovative SAR modes and applications, offering a large variety of geometric constellations and of radar instrument settings (all SAR modes including 2 + 2 receive phase centers). The instruments are commanded according to the parameters selected by the scientists for Along-Track Interferometry (ATI) applications and for demonstration of new SAR techniques.

Synchronisation

In Bistatic Mode the TanDEM-X interferometer is operated with two independent oscillators. Uncompensated oscillator noise will cause a slight deterioration of the bistatic impulse response, a significant shift of the bistatic SAR impulse response, and substantial interferometric phase errors in case of bistatic interferometric operation [215]. To correct for these phase errors and also to enable pulse repetition interval (PRI) synchronisation, the TanDEM-specific SAR instrument features provide a scheme for transmission and reception of USO phase information between the SARs with adequate SNR. On both the TDX and TSX-1 spacecraft six synchronisation horn antennas are added at selected positions shown in Figure 2.19 to ensure full solid-angle coverage with low phase disturbance.

The required precise phase referencing for DEM generation in bistatic interferometry mode can be achieved using synchronisation pulses with a PRF in the order of 10-20 Hz. For a SNR of 30 dB (a reasonable assumption for along-track displacements up to 1 km) the residual interferometric phase error can be reduced to below 1°.

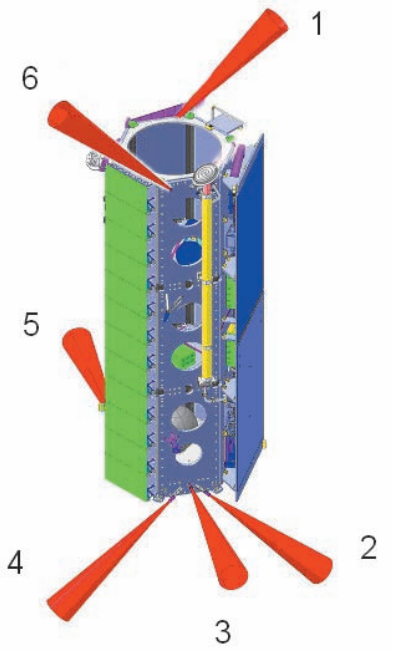

Figure 2.19 Accommodation of synchronisation horn antennas with the beams shown in red.

Predicted DEM Generation Performance

A detailed height performance model has been developed for the Bistatic Mode covering the relative height error estimates, the calibration concept and the absolute error predictions [505].

Relative Height Error Estimation

The performance prediction for the relative height error is based on the following random error contributions:

- Noise due to the limited SNR during SAR data acquisition and interferogram generation, quantisation errors from block adaptive quantisation, limited co-registration accuracy and processing errors, as well as range and azimuth ambiguities. Decorrelation due to thermal noise in the instruments dominates this error contribution. The achievable error reduction is mainly limited by the maximum baseline (minimum height of ambiguity) that can be handled in the phase unwrapping process. Heights of ambiguity below 40 m and corresponding perpendicular baselines between 150 m and 400 m are required to reduce this error contribution to a relative height error below 2 m.
- Interferometric phase errors caused by the residual errors in the phase referencing via the noisy synchronisation link.
- Random contributions from the TSX-1 and TDX internal calibrations and uncompensated phase drifts along a data take also affecting the synchronisation link.
- 3-D baseline estimation errors causing primarily a systematic phase/height ramp in the cross-track direction (~0.3 cm/km for a height of ambiguity of 35 m and a baseline estimation error in line of sight of 1 mm).

A combination of all these error sources yields the predicted relative height accuracy as shown in Figure 2.20. The predicted point-to-point height errors are below 2 m for the full performance range of TSX-1 (and TDX) which ranges from 20° incidence angle up to 45° incidence angle.

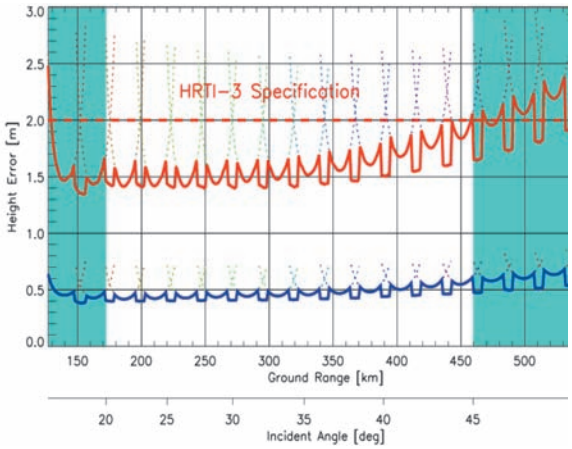

Figure 2.20 Predicted relative height errors for a height of ambiguity of 35 m. The red curve shows the predicted point-to-point height errors at a 90% confidence level. The blue curve represents the predicted standard deviation of the relative height errors.

Height Calibration Concept

The absolute height accuracy is mainly driven by the distribution and accuracy of reference height information, the calibration and mosaicking concept and the data acquisition strategy. Long continuous data takes up to 1000 km length are preferred to avoid additional errors from scene concatenation. The current calibration concept foresees the following steps:

- The generation of "raw" DEMs using SRTM heights or even lower-resolution DEMs as reference (absolute accuracy of the reference data has to be sufficient to resolve the height of ambiguity interval).
- Evaluation of swath overlaps in these raw DEMs (6 km overlap between the currently used TerraSAR-X swaths) for consistency checks between acquisitions, along-track error reduction and across-track tilt correction.
- A bundle adjustment based on the analysis of relative deviations between raw DEMs and absolute calibration references over large areas, up to continental size. Relative references can be derived from overlap areas with crossing tracks and from the previously mentioned swath overlaps. Adequate crossing tracks have to be included in the reference mission scenario. Additionally, absolute references like highly accurate DEMs from airborne LIDAR, photogrammetry, other SAR systems, GPS tracks, spaceborne laser and radar altimeters are required. Ocean surfaces might be used as well, if their reflectivity is high enough and if they are imaged with a short along-track baseline to minimise decorrelation. The output of this step, which depending on the amount of errors might require iterations of the raw DEM generation step, is the final DEM.

Absolute Height Error Estimation

The HRTI-3 standard requires for the absolute height accuracy a value of 10 m at a 90% confidence level. On top of the above presented relative height errors, which contribute as a random component, the following error sources have to be considered in predicting the absolute height error:

- Accuracy of the interferometric baseline (between the SAR antenna phase centers) with contributions from the GPS differential carrier phase measurements. GSOC and GFZ independently confirmed that the relative vector between the spacecraft's center of mass can be determined to within 1 mm.
- The knowledge of the satellite's attitude and the SAR antenna phase center, and the accuracy of the transformation from the spacecraft to the Earth fixed coordinate systems.

- Uncompensated long-term instrument phase errors due to temperature drift in the internal calibration network and the synchronisation link.
- Residual errors in the bundle adjustment process and quality of the reference height information.

The Phase A estimate of the various error contributions results in an absolute height accuracy of 6.6 m demonstrating that TanDEM-X allows for the derivation of highly accurate digital elevation models according to the emerging HRTI level 3 standard and even beyond in Stripmap mode. DEMs with 2 m relative height accuracy (point-to-point errors at 90% occurrence level according to the HRTI-3 standard) will require a height of ambiguity which is in the order of 30-40 m. This height of ambiguity corresponds to perpendicular baselines of 150 m to 400 m for incidence angles of 20° and 45°, respectively.

Radar Data Mode

The Radar Data Mode stands for any acquisition of TanDEM-X data products which are not covered by the DEM class. Examples are along-track interferometry, polarimetric SAR interferometry, four phase center moving target indication, bistatic SAR imaging, and digital beamforming.

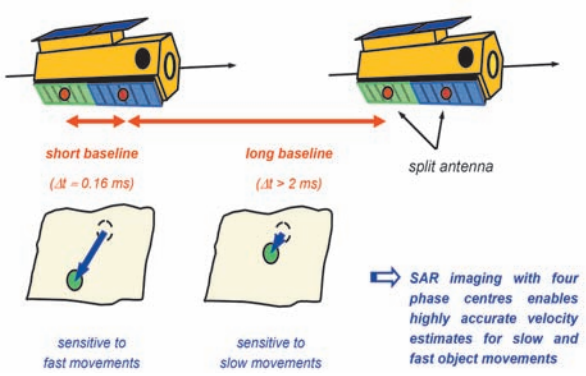

Figure 2.21 Along-track interferometry modes in TanDEM-X.

Along-track SAR interferometry can either be performed by the so-called dual receive antenna mode with a baseline of 2.4 m from each of the satellites or by adjusting the along-track distance of the two satellites to the desired size (Figure 2.21). The newly developed orbit concept allows this distance (called along-track baseline) to be adjusted from zero to several kilometers. This technical feature is essential as this application requires velocity measurements of different fast and slow objects. Mainly four scientific application areas are identified to explore the innovative along-track mode: oceanography, traffic monitoring, glaciology and hydrology. Of scientific interest is the identification of moving objects as well as the estimation and the validation of different velocity estimates. In all three application areas the knowledge of the velocity will improve model predictions for environmental, economical, as well as social aspects.

With TanDEM-X, innovative SAR techniques will be demonstrated and exploited, which open up new perspectives for future SAR systems. The focus will be on the research areas:

- Bistatic and multistatic SAR imaging enabling enhanced scene feature extraction by combination of monostatic and bistatic signatures. This is due to the substantially increased observation space in bistatic SAR.
- Polarimetric SAR interferometry allows for precise measurements of important vegetation parameters like vegetation height and density (sections 2.1.8 and 2.2.4). Figure 2.22 shows the predicted performance in estimating the height of sun flower plants.
- Digital beamforming and superresolution.

The main interest for these research areas lies in the understanding and the development of new algorithms.

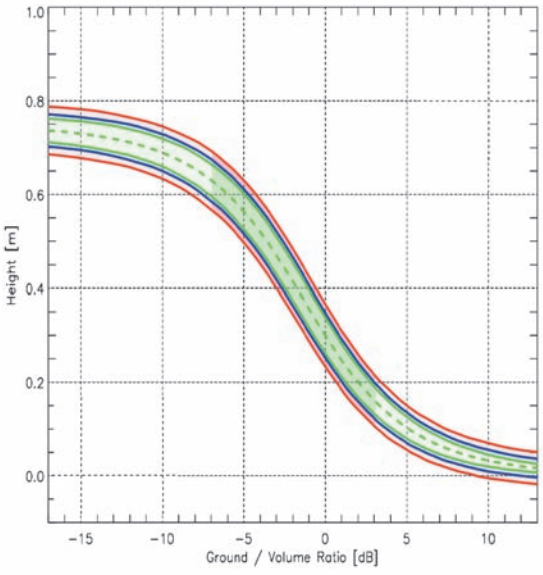

Figure 2.22 TanDEM-X height estimation performance for sun flower plants based on the Random Volume over Ground model. The dashed green line indicates the height variation of the interferometric phase center with different polarisations (corresponding to a variation of the ground-to-volume ratio on the abscissa). The green tube shows the height errors due to volume decorrelation for different effective baselines and an independent post spacing of 30 m x 30 m. The blue and red tubes show additional errors due to the limited system accuracy for scattering coefficients of -10 dB and -15 dB, respectively. The dark areas of the phase tubes indicate those ground to volume ratios which are addressable by the different polarisations.

Mission Scenario

Contrary to conventional Earth Observation missions, the TanDEM-X global mapping strategy has also to account for the formation geometry, as for given HELIX parameters, DEM acquisitions are only possible for a certain latitude range. Furthermore, in the parallel operation of the TanDEM-X and TerraSAR-X missions, the latter should not be disturbed and the TanDEM-X acquisitions have to be planned as a quasi background mission.

With these constraints and the assumption of a three year tandem phase (joint operation of TSX-1 and TDX) and the use of the TerraSAR-X standard Stripmap beams covering incidence angles from 20° to 45°, a reference mission scenario [151] has been developed including sufficient time slots for the acquisition of CDEMs and RDPs.

In a first phase after commissioning and first formation set-up, a global DEM is derived by monitoring the Earth at the northern hemisphere with ascending orbits and the southern hemisphere with descending orbits. The respective formations are adopted such that the required height of ambiguity fits to the respective mapping region. In the next mission phase, the formation will be shifted by 180° in phase (which corresponds to an 'exchange' of the satellites) and the resulting formation acquires "crossing tracks" on descending orbits on the northern, and ascending orbits on the southern hemisphere. Then DEM generation is performed for terrain which requires additional data. In the next mission phase, the satellites will be separated in along-track e.g. for bistatic monitoring and ATI experiments. Finally, the satellites will be separated at the end of the mission to a distance, where the ground track separation in the Earth fixed frame is one day, to perform further ATI experiments. In any phase, orbital periods, which are not required for deriving the global DEM, will be used for generation of CDEMs or RDPs.

The TanDEM-X mission encompasses scientific and technological excellence in a number of aspects, including the first demonstration of a bistatic interferometric satellite formation in space, as well as the first demonstration of close formation flying in operational mode. Several new SAR techniques will also be demonstrated for the first time, such as digital beamforming with two satellites, single-pass polarimetric SAR interferometry, as well as single-pass along-track interferometry with varying baseline. TanDEM-X takes advantage of the heritage from the SRTM and SIR-C/X-SAR missions, as well as more than 25 years of experience in radar technology.

2.1.4 Microsatellite SAR Formations

Currently available interferometric data from spaceborne SAR sensors suffer either from temporal and atmospheric disturbances (repeat pass interferometry) or from a limited interferometric baseline (60 m on SRTM). To overcome these limitations, several suggestions have been made to acquire interferometric data in a single pass by using two (like TanDEM-X) or more independent radar satellites operating in a fully or semi-active SAR mode.

An efficient realisation of such systems may be achieved by a set of passive receivers on board a constellation of microsatellites which simultaneously record the backscattered signals transmitted by a conventional spaceborne radar. Such a configuration represents a cost-efficient implementation of a highly capable interferometric single-pass SAR system in space and enables not only the cost-efficient acquisition of high quality DEMs on a global scale, but also along-track interferometric applications, like mapping of ocean currents, reduction of ambiguities, and/or superresolution in both azimuth and range.

It is an important design goal for multistatic interferometric SAR formations to achieve an almost constant baseline between the spacecraft [25]. For along-track interferometry such a constant separation is easily obtained by inducing an along-track displacement between the individual satellites. However, such a simple solution is not possible for cross-track interferometry, since neither the vertical nor the horizontal cross-track separations remain constant for freely orbiting satellites on natural orbits, which are necessary to keep the fuel consumption within reasonable limits.

One of the first formations of microsatellites, proposed by CNES in the late 90s, is the Interferometric Cartwheel. An inherent property of the Interferometric Cartwheel is the close coupling between radial separation and along-track displacement with the consequence that the common azimuth bandwidth for cross-track interferometry is reduced and the temporal delay between the iso-Doppler data acquisitions might exceed the decorrelation time over ocean surfaces.

The so-called Cross-Track Pendulum configuration [25] consists of three microsatellites but, for forming the desired baselines, a different approach is made: all satellites have frozen orbits and equal velocities. This leads to a constant along-track separation. The interferometric cross-track baselines are then provided by selecting orbits in different orbital planes with distinct ascending nodes and/or inclinations. This implies a horizontal cross-track separation of the satel-

lites as shown in Figure 2.23. Since the along-track and cross-track components are completely decoupled in the Pendulum configuration, the along-track displacements may be optimised independently. A small drawback of the Pendulum configuration is the additional fuel (about 1 kg per year per km baseline for a microsatellite) required for keeping the formation stable [25].

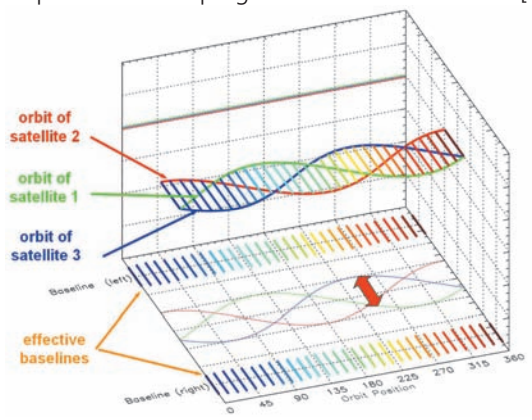

Figure 2.23 Orbits and interferometric baselines for the Cross-Track Pendulum.

Another configuration proposed is a combination of the Cartwheel and the Cross-Track Pendulum. The 'CarPe' configuration [25] consists of two satellites forming a Cross-Track Pendulum with different ascending nodes and one satellite with a slightly eccentric orbit. Since all orbits have the same inclination, no additional fuel is required for a compensation of differential nodal drifts. The advantage of the CarPe configuration is the availability of a constant along-track baseline for along-track interferometry which is accompanied by the very stable cross-track baselines [25].

Microsatellite Formation with TerraSAR-L

After attempts to fly an Interferometric Cartwheel with ENVISAT and ALOS, ESA initiated and supported a joint CNES/DLR study to analyse the option of adding such an interferometric formation of passive receiver satellites to the TerraSAR-L mission (section 2.1.5). The primary objective was the generation of a global DEM of HRTI level-3 quality (section 2.1.3). ATI applications like ocean current monitoring and sea ice dynamics were further important objectives. With TerraSAR-L being designed for fully polarimetric operation the capabilities of Polarimetric SAR Interferometry for forest monitoring have been investigated as well (section 2.1.8).

Different to earlier proposals, the formation was considered an integral element of TerraSAR-L, i.e. special modes exploiting the full capabilities of the main spacecraft would allow for an improved performance. Furthermore, inter-satellite links to synchronise the data recording and to provide telemetry and telecommand communication and science data downlink via TerraSAR-L and, hence, simplify the micro satellite architecture have been considered. In the study, several orbital configurations have been investigated in detail and compared with each other.

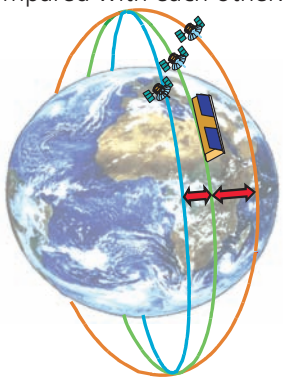

Figure 2.24 Trinodal Pendulum configuration proposed for a TerraSAR-L formation.

One of the favourite candidates, the Trinodal Pendulum (Figure 2.24, Figure 2.25), consists in its original configuration of three microsatellites, orbiting with the same inclination, eccentricity, argument of perigee and semi-major axis as the illumination master satellite [361]. The right ascensions of the ascending node of each of the three microsatellites are chosen in such a way that the horizontal cross-track displacements correspond to the desired effective baselines for interferometric data acquisition. Additionally, the along-track displacements between the single microsatellites are chosen such that the microsatellites monitor the requested scene on the Earth's surface with minimum relative time lags under the constraint that small along-track displacements will be required to avoid a collision within the formation at the northern and southern turns.

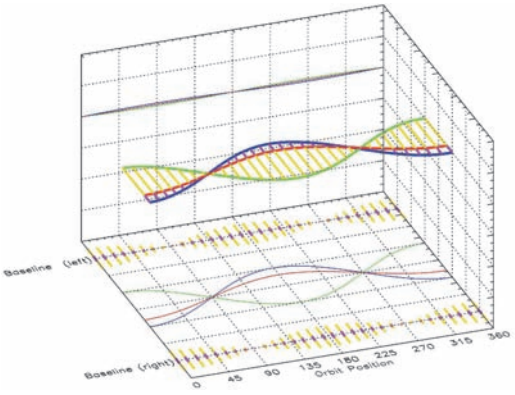

Figure 2.25 Orbits and interferometric baselines for the Trinodal Pendulum.

The Trinodal Pendulum offers the opportunity to acquire short and long baselines simultaneously during one single pass, facilitating phase unwrapping for the small heights of ambiguities required to achieve HRTI-3 level DEMs. This way, it makes effective use of the available resources from the transmitter (e.g. signal power, illumination time, etc.). Furthermore, possible errors due to temporal changes between subsequent scene acquisitions are avoided. An alternative configuration proposed by CNES is the Two-Scale Cartwheel, an evolution of the original Cartwheel.

The study concluded that there is almost no collision risk between the master satellite and the microsatellites. In case of a failure (no orbit control) of a microsatellite, it will decrease its semi-major axis, thus increasing its along-track distance to TerraSAR-L flying behind the microsatellites. Inside the formations a low probability of collision might exist, which can be avoided with the Helix concept [148]. The transfer from one constellation to another is possible and achievable with reasonable fuel consumption and time.

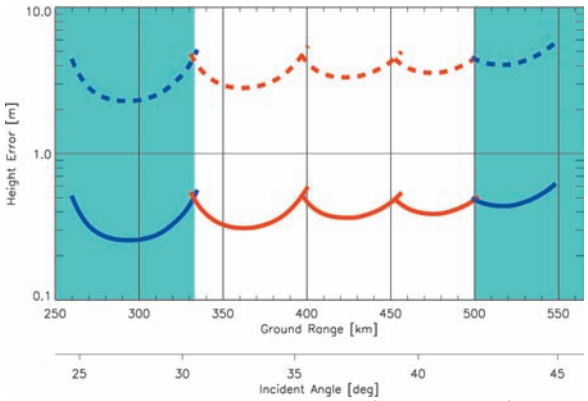

Figure 2.26 Predicted height error for a height of ambiguity of 100 m (dashed) and 10 m (solid).

A detailed performance model has been developed including the phase noise caused by limited signal-to-noise ratio (SNR), range and azimuth ambiguities, quantisation errors, local slopes, and volume decorrelation. With a given horizontal posting of the final DEM products (i.e. 12 m for HRTI-3 data), the achievable height accuracy can be estimated. Figure 2.26 shows the predicted height error for a height of ambiguity of 100 m (dashed) and 10 m (solid). It is obvious, that the height accuracy increases with a decreasing height of ambiguity. On the other hand, a small height of ambiguity is likely to cause phase unwrapping problems, especially in mountainous areas. Note, that the baseline ratio of the example in Figure 2.26 has been chosen such that the height errors from the DEM acquisition with the small baseline stay below the height of ambiguity for the large baseline. It would, hence, be possible to use the interferometric data from the small baseline to assist phase unwrapping in the highly sensitive large baseline interferogram (section 2.3.1.

The analyses have shown that the TerraSAR-L microsatellite formation would be an excellent means of acquiring a global DEM according to the HRTI level-3 specification. The required mission time for a global DEM acquisition has been estimated to be in the order of 1 year, assuming an average data collection of 3 minutes per orbit. In a later mission phase, the performance might even be improved beyond the HRTI level-3 specification by increasing the length of the interferometric baselines.

2.1.5 TerraSAR-L

TerraSAR-L was originally planned to complement TerraSAR-X under the Infoterra/TerraSAR initiative of EADS Astrium Ltd., BNSC, and DLR. While TerraSAR-X is being implemented as a German national mission (section 2.1.2), TerraSAR-L was proposed as an element of ESA's Earth Watch Programme, where the system definition was developed up to Phase B level concluding in a Preliminary Design Review (PDR). The Institute contributed to the Phase B study with the definition of the System Calibration and Verification Plan [466] and the specification of the Instrument Calibration Segment [468]. Furthermore, jointly with CNES the option of a microsatellite constellation flying in formation with TerraSAR-L (section 2.1.4) was studied.

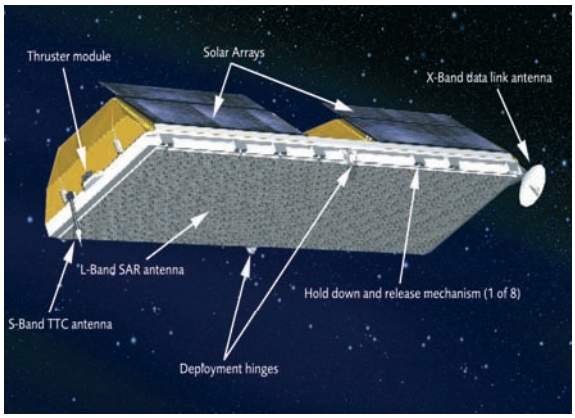

Figure 2.27 Artist's view of TerraSAR-L (© Astrium Ltd.).

The snapdragon platform is optimised for and built around the active phased array antenna of the L-band Synthetic Aperture Radar (L-SAR). The L-SAR instrument is based on an 11 m x 2.9 m active phased array antenna build up of 160 transmit/receive modules (TRMs). This instrument features on top of standard Stripmap and ScanSAR operations, full-polarimetric capabilities, repeat-pass ScanSAR interferometry and a Wave Mode.

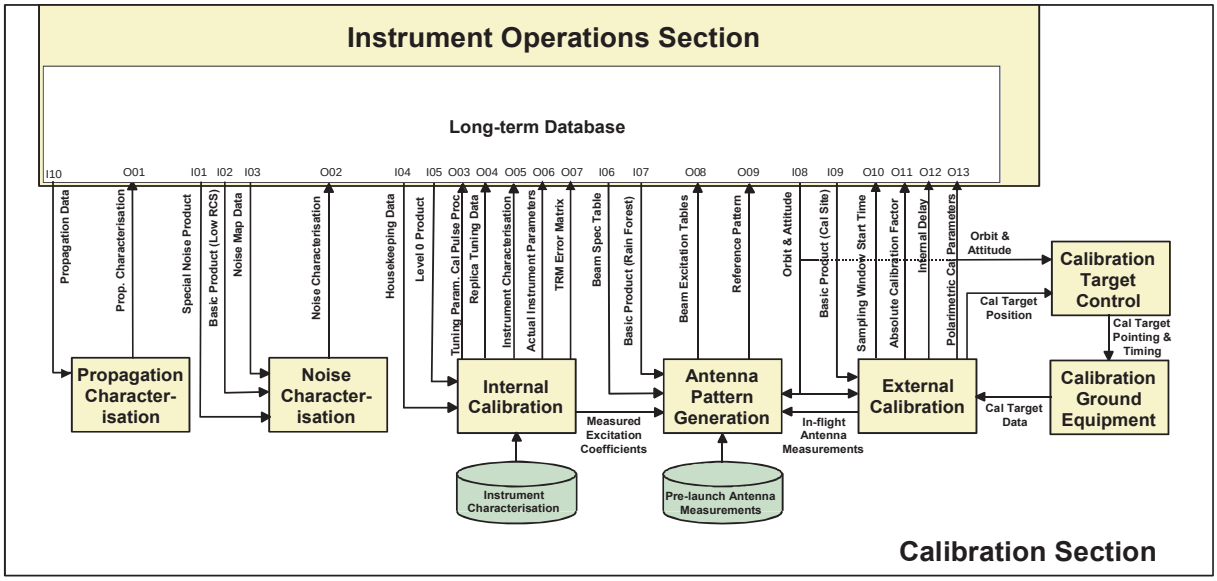

Figure 2.28 Block diagram of the calibration section including interfaces to the long-term data base.

As for TerraSAR-X the calibration and verification of a multi-mode, multi-beam instrument in a short commissioning phase (in the case of TerraSAR-L only 3 months) is a major challenge requiring new concepts and strategies. Dynamic recalibration of the antenna due to graceful degradation of the TRMs throughout the mission lifetime, polarimetric calibration, and ionospheric propagation effects (most importantly Faraday rotation) are further issues that had to be covered.

Therefore, the methodology developed for TerraSAR-X has also been applied for the TerraSAR-L calibration concept [466]. The active antenna has the advantage of the ability to be mathematically modelled, enabling the antenna patterns to be accurately computed from the commanded excitation values, pre-launch antenna and in-orbit TRM characterisation data. This antenna-model approach puts special emphasis on precise pre-launch characterisation and allows replacing traditional beam-to-beam calibration reducing the in-flight effort to the verification of the antenna model and absolute calibration measurements (section 2.3.7).

For in-flight TRM characterisation, a coding technique like PN-gating for TerraSAR-X has been designed, that allows taking measurements in a realistic operational scenario and power supply load conditions, i.e. all modules are on. Algorithms for polarimetric calibration of different product levels have been developed including a combined correction of Faraday rotation in the case of quad-pol data. For non quad-pol data, a strategy to detect potential propagation effects via externally provided TEC maps has been conceived. In the PDR, the robust design of the calibration concept has been confirmed.

Again, in following the TerraSAR-X model for TerraSAR-L, a dedicated Instrument Calibration Segment [468] was specified including all the tools required for instrument and product calibration and verification, the generation of auxiliary products required in the ground processor, as well as for the update of instrument parameter tables on-board and in the ground segment.

After a successful PDR the TerraSAR-L programme has been halted for the time being. However, enough interest in a European L-band mission has been created and options for implementing this mission have been actively sought, our HABITAT (section 2.1.8) proposal in response to ESA's last call for new Earth Explorer missions being the most promising one.

2.1.6 Sentinel-1 and GMES

As part of the Global Monitoring for Environment and Security Programme (GMES), ESA is undertaking the development of Sentinel-1, a European polar orbit satellite system for the continuation of SAR operational applications in C-band after the ENVISAT/ASAR is decommissioned. The Sentinel-1 mission requirements have been optimised to enhance the performance and operational capabilities of the GMES Service Element.

As a member of the industrial consortium the Institute is contributing the concept for the calibration and verification [465] of the Sentinel-1 SAR system to ESA's Phase B1 study. The concept identifies and describes all facilities and activities necessary to deliver verified and calibrated SAR

products. It specifies the associated algorithms and tools and plans the relevant activities. The Sentinel-1 calibration concept is based on the methodology developed for TerraSAR-L (section 2.1.5), which is in turn based on the Institute's heritage from calibration work on ERS-1, SIR-C/X-SAR, SRTM, ENVISAT/ASAR, as well as TerraSAR-X. Consequently, Sentinel 1 will profit from new, innovative methods shortly to be validated on TerraSAR-X and briefly described in the following.

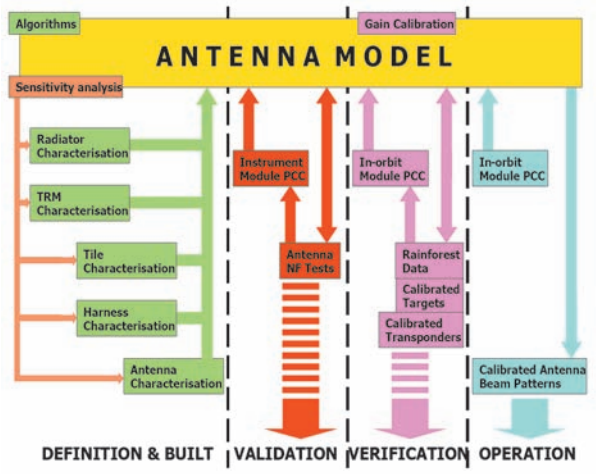

Figure 2.29 Life cycle of the antenna model, the key element in the Sentinel-1 calibration concept.

Antenna Model Approach

Sentinel-1 is also an advanced multi-mode synthetic aperture radar system providing Stripmap operation with adjustable swath positions or Wide Swath modes (both in dual polarisation) and the Wave mode (single polarisation). This results in a multitude of beams with different antenna patterns.

Following the developments for TerraSAR-X and TerraSAR-L, the Sentinel-1 calibration concept is also built around an antenna model, which enables the antenna pattern to be accurately derived from the applied excitation coefficients.

The life cycle of this antenna model is shown in Figure 2.29. It will commence with a definition of requirements and will then be produced and validated prior to launch by using ground based measurements. This activity may involve some levels of iteration of the model once the validation has commenced. The validated model will be available prior to launch, will be verified in orbit in the commissioning phase and will be used from commissioning onwards. Input data from ground based characterisation and in-orbit internal characterisation will be used to provide the beam patterns which will be required during data analysis and image processing.

With the aid of the antenna model, system calibration can be achieved by a limited number of in-orbit verification measurements using suitable ground targets. In this way the commissioning phase can be significantly reduced compared to the traditional (e.g. ASAR) approach based on the calibration of individual beams.

Pulse Coded Calibration (PCC)

The pulse coded calibration is a means of characterising individual rows or modules of an active antenna while all are operating. The Sentinel-1 instrument is capable of calibrating during each imaging mode thanks to PCC. The measured excitation coefficients directly feed into the antenna model for dynamic re-calibration. The PCC or PN-Gating method (section 2.3.7) was developed in the Institute [176] and is to be implemented for the first time on TerraSAR-X.

Noise Characterisation

In an imaging radar system noise not only impacts on the image contrast (radiometric resolution) but can lead to radiometric errors and image impairment due to noise artefacts.

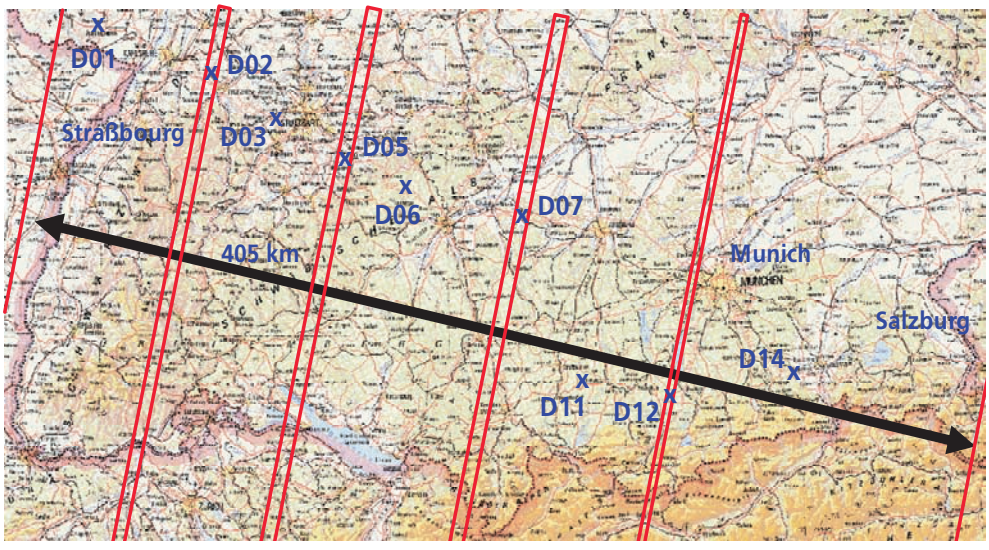

Figure 2.30 Oberpfaffenhofen calibration facility as a potential contribution to Sentinel-1: Example set-up for ENVISAT/ASAR ScanSAR calibration, indicating ground target locations deployed in South Germany.

Although the resolution cannot be restored in the data processing, the radiometric bias errors due to noise can be corrected. A prerequisite is the characterisation of the system noise level, which is achieved by collecting data with the radar transmitter switched off, the so-called receive only mode. The noise measurements obtained are adjusted for the system gain and annotated to each product to allow the user to correct the radiometric bias if required.

Last December's approval of the first phase of the GMES programme includes the continuation of the preparatory activities and in the case of Sentinel-1 the full implementation of the mission. With our current contribution to the Phase B1 study and our long-term experience in SAR calibration we are well prepared to take over responsibility for the detailed Sentinel-1 system calibration and verification plans, design and development of the required tools and facilities but also for the planning and execution of the campaigns in the commissioning phase. For the latter the Institute is well equipped [328] with calibration targets and operates and maintains a large calibration site in Southern Germany (Figure 2.30).

2.1.7 Advanced Land Observing Satellite - ALOS

ALOS, an enhanced successor of the Japanese Earth Resources Satellite 1 (JERS-1), was launched from JAXA's Tanegashima Space Center in January 2006. ALOS operates from a sun-synchronous orbit at 691 km, with a 46-day recurrence cycle carrying a payload of three remote sensing instruments: the Panchromatic Remote Sensing Instrument for Stereo Mapping (PRISM), the Advanced Visible and Near-Infrared Radiometer type 2 (AVNIR-2) and the polarimetric Phased Array L-band Synthetic Aperture Radar (PALSAR).

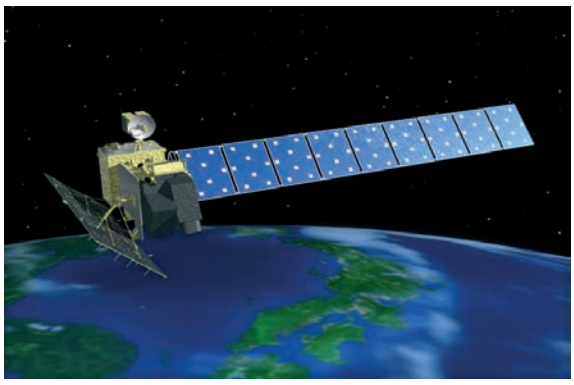

Figure 2.31 The Advanced Land Observing Satellite - ALOS (© JAXA).

The PALSAR sensor has the capacity to operate with a wide range of off-nadir angles and resolutions in a single-, dual-, and quad-pol mode. However, four modi have been prioritised for a simplified observation scenario:

- Single-polarisation (HH), @ 34.3 deg. and 10 m resolution;
- Dual-polarisation (HH-VH or VV-HV), @ 34.3 deg. and 20 m resolution;
- Quad-polarisation (HH-HV-VH-VV), @ 21.5 deg. and 20 m resolution;
- ScanSAR single-polarisation (HH) and 100 m resolution.

The main characteristics of the quad-pol mode are summarised in Table 2.3.

Table 2.3 Parameters of the PALSAR quad-pol mode.

RF-center frequency	1.270 GHz (L-band)
System bandwidth	14 MHz
Sampling Frequency	16 MHz
PRF	1500-2500 Hz
Transmit Peak Power	2 kW
Incidence Angle	21.5° (selective on 18.5°)
NESZ	< - 31dB
Observation Swath	30.6 Km (@ 21.5°)
Range Resolution	31.2 m (ground range @ 21.5°)
Azimuth Resolution	20 m (4 looks)
A/D Convertion	5 bit
Data Rate	249 Mbps

The Institute is involved in science, calibration and validation activities of the ALOS project. It is part of the international science team of JAXA's Kyoto &Carbon (K&C) Initiative. A MoU signed between JAXA and DLR establishes the framework of the K&C cooperation. Furthermore, the Institute is a member of JAXA's international Calibration and Validation team and supports ESA's calibration and validation activities of ALOS-PALSAR products distributed by the European ADEN node.

The Kyoto & Carbon Initiative

The Kyoto & Carbon Initiative is an international collaborative project and forms the continuation of JAXA's JERS-1 SAR Global Rain Forest and Global Boreal Forest Mapping project (GRFM/GBFM) into the era of ALOS. The initiative is set out to support explicit and implicit data and information needs raised by international environmental Conventions, Carbon Cycle Science and Conservation of the environment (CCCs). This Initiative is led by JAXA which is responsible for management, data acquisition, processing and distribution. Product development is undertaken jointly by JAXA and an international science team that involves academic and research organisations from 13 countries. The initiative is structured around three main thematic areas

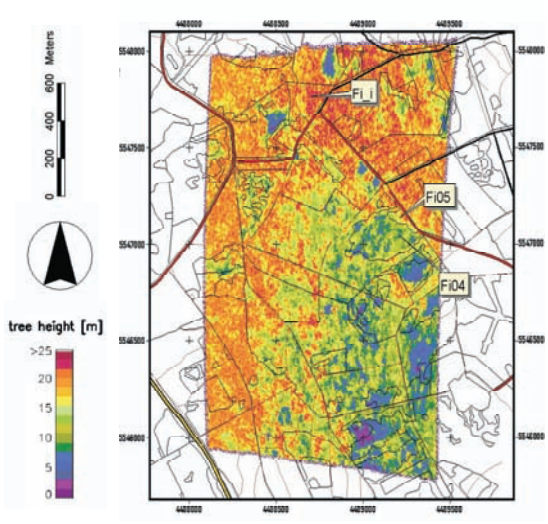

Figure 2.32 Forest height map (Fichtelgebirge/Germany) derived from E-SAR data using Pol-InSAR techniques.

(Forests, Wetlands and Desert & Water). The Forest Theme is focused on supporting the UNFCCC Kyoto Protocol and the part of the carbon research community concerned with CO_2 fluxes from terrestrial sinks and sources. Key areas considered include the mapping of land cover (forest), forest change, biomass and structure. Within the Forest Theme the Institute is leading the scientific activities on Polarimetric SAR Interferometry (Pol-InSAR) techniques [368] and coordinating the Forest Height Map Product (Figure 2.32), i.e. the demonstration of pre-operational forest height map generation in ALOS terms.

The Forest Height Map Product

Based on repeat-pass quad-pol interferometric SAR data acquired by the ALOS/PALSAR sensor - during its early calibration/validation phase - model based estimation of forest height is proposed. In order to improve the estimation accuracy, the observation vector is planned to be extended, including the two dual-pol single-baseline data sets acquired in the later ALOS/PALSAR operation phase.

The expected temporal decorrelation effects will reduce the estimation performance of forest height significantly. Nevertheless, ALOS provides, for the first time, the possibility to demonstrate and evaluate the new methodology of Pol-InSAR on a global scale. For this, 60 study sites worldwide have been selected covering a wide range of forest structural types, ranging from tropical rainforest to low open woodlands. The main tasks in the K&C frame are:

- Inversion methodology development adapted /optimised to the actual ALOS data acquisition scenario.
- Product generation and validation (in cooperation with local investigators) for a number of selected study sites world-wide.

In case of a successful demonstration, it is planned to carry out a dedicated Pol-InSAR experiment in a later phase of the ALOS mission. If the inversion performance does not justify a dedicated Pol-InSAR, experiment the focus will be on the evaluation of the selected test sites with the goal to define the system requirements for a dedicated, mission as proposed with HABITAT (section 2.1.9) in response to ESA's call for ideas for the Next Earth Explorer Missions.

Pol-InSAR Product Calibration and Validation

Within the framework of the international JAXA calibration/validation group the Institute is responsible for calibration and validation of Pol-InSAR data and products. The main challenge faced in calibration of the interferometric coherence is the separation of system, propagation, processing, and calibration induced decorrelation contributions from decorrelation, due to the structure and temporal instability of the scatterer. The estimation of these decorrelation contributions is essential for isolating the volume (i.e. vertical spectral) and temporal decorrelation contributions that contain the physical information used in parameter inversion and classification algorithms.

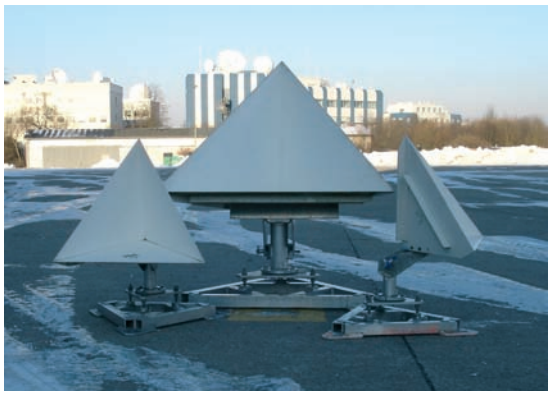

Figure 2.33 Corner reflectors of this type with 1.5 and 3 m side length will be used for PALSAR product verification.

Verification of PALSAR products distributed by the European ADEN Node

Another important contribution to the ALOS mission is the verification and validation of PALSAR products distributed by the European ADEN node. Under a contract with ESA/ESRIN, the Institute has to assess ALOS/PALSAR data quality during the commissioning phase of the instrument and to provide a set of algorithms for quality control throughout the mission lifetime.

Software tools to be developed and implemented include point target analysis, distributed target analysis, geometric analysis, antenna pattern estimation, polarimetric analysis and the estimation and analysis of propagation effects. The framework for this tool set is the in-house developed CALIX software (also section 2.3.7), which is our standard calibration and verification environment also being used within the IOCS for TerraSAR-X.

During calibration and verification campaigns, active and passive calibrators (transponders, dihedral and trihedral reflectors, Figure 2.33) will be deployed as external references, providing well-defined point target responses for product quality assessment.

Since PALSAR is the first fully polarimetric spaceborne L-band sensor, propagation effects are important new issues to be addressed. The main challenge is to assess the influence of the ionosphere on the polarisation, known as Faraday rotation. This effect depends on the Total Electron Content (TEC) in the ionospheric layer below the ALOS spacecraft and is proportional to the wavelength squared. Being negligible for X-band sensors, Faraday rotation is significant in L-band and can reach up to 100° with a pronounced diurnal variation and a strong dependence on solar activity during the 11-year solar cycle.

After the successful launch JAXA is currently performing early functional check-outs. First acquisitions over our Pol-InSAR and calibration test sites are envisaged for April and the detailed planning of the campaigns has started. First results are expected in summer 2006. The PALSAR product verification activity for ESA will be finished early 2007.

2.1.8 Multi-Application Purpose SAR - MAPSAR

The Brazilian-German MAPSAR mission is a proposal for a light (500 kg class satellite) and innovative L-band SAR sensor, based on INPE´s Multi-Mission Platform (MMP). The main mission objectives are the assessment, management and monitoring of natural resources. The mission is currently being investigated by INPE and DLR in a Phase A study as a follow up on a preceding successful pre-phase A study [55]. The initiative of the joint study of a small spaceborne SAR is a consequence of a long term Brazilian-German scientific and technical cooperation that was initiated between INPE and DLR in the seventies.

User Requirements

The MAPSAR mission is tailored to optimally support the potential user groups in both countries, taking into account distinct aspects of specific applications. A first workshop with potential end users of MAPSAR in Brazil was conducted to develop requirements and recommendations aiming at a joint DLR - INPE spaceborne SAR programme. The consensus of the Brazilian working group was that a spaceborne SAR mission will provide a powerful new tool to acquire data and to derive important and unique information of vegetated terrain of the Amazon region. Due to the enormous scarcity of up-to-date information, which is fundamental for planning and strategic decision-making about environmental assessment, management and monitoring of natural resources in the Brazilian Amazon, the proposed light spaceborne SAR initiative should be strongly oriented to a quasi-operational ("application-oriented") system. This is dedicated to thematic mapping purposes for topography, vegetation and deforestation, geology, hydrology, etc.

A second workshop of potential MAPSAR end users was conducted in Germany to merge the final user requirements of both countries as the basis for the sensor and satellite design within the Phase A study. The workshop revealed that the Brazilian applications are also of high interest to the German potential user community. Additional applications, which are of specific importance for the German user side, such as biomass estimation, disaster monitoring and security, complement the Brazilian disciplines. The common aim is a global biomass mapping mission covering major forest biomes of the globe (tropical and boreal regions). This requires the capability of polarimetry and interferometry SAR (Pol-InSAR) for forest height estimation, which is directly related to forest biomass using allometry.

Due to the INPE´s Multi-Mission Platform performance (mass, power generation, geometric envelope and data rate), main limitations were imposed upon the satellite configuration: use of a single frequency and a light weight antenna. The resulting reflector antenna concept limits the maximum instantaneous swath width to approximately 55 km (Table 2.4).

Table 2.4 MAPSAR mission parameters taking into account user requirements and Multi-Mission Platform constraints.

Frequency	L-band
Polarisation	Single, dual and quad
Incidence Interval	20° - 45°
Spatial Resolution	3 – 20 m
Swath	20 – 55 km
Orbit Inclination	Sun-synchronous
Coverage	Global
Look Direction	Ascending/descending
Revisit	Weekly
Data Access	Near real time
Additional Requirement	Stereoscopy & Interferometry

Mission Design

The wide spread applications require different radar polarisations and different spatial resolutions. Furthermore, stereoscopy and interferometry require different orbit repetition cycles and coverage sequences. Nevertheless, the disciplines can be optimised for two different orbit heights in order to get appropriate coverages. In both cases, sun-synchronous orbits are recommended for technical reasons. Considering the requirements of the Brazilian Multi-Mission Platform and the SAR sensor, it was concluded to concentrate the investigations on orbits heights between 600 and 620 km.

MAPSAR Satellite

The L-band SAR sensor is based on a reflector antenna concept. The main advantage is the possibility to realise full polarisation and high bandwidth with low technological risk at low cost. The MAPSAR satellite utilizes a modular concept, consisting of a payload module on top of a Multi-Mission Platform. Figure 2.34 shows an artist's view of the satellite configuration without the foldable main reflector.

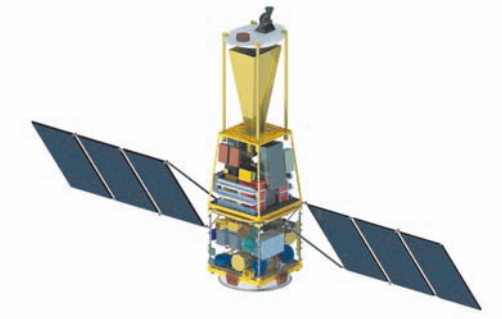

Figure 2.34 MAPSAR in-orbit satellite configuration.

A key problem for an L-band SAR is the large antenna size compared to higher radar frequencies. Reducing the antenna dimensions as far as possible is mandatory under the launcher and platform constraints. A Cassegrain configuration with an elliptical foldable parabolic main reflector with 7.5 m length in azimuth and 5 m width in elevation was considered. Neither the subreflector mounting, nor the horn type prime radiator need to be folded. The resulting antenna gain in combination with a low orbit allows very good sensitivity with a reasonable power budget.

The mechanical concept for the antenna main reflector was identified as one of the critical technologies. It was developed in a co-operation with the Institute of Lightweight Structures of the Technical University of Munich. The reflecting surface is a triaxially woven fabric of carbon fibre reinforced silicone (CFRS). The material is extremely light and fully space qualified. The support structure consists of CFRS rib membranes, which are deployed and stiffened with a pantograph mechanism. Figure 2.35 shows the principal of the deployment mechanism.

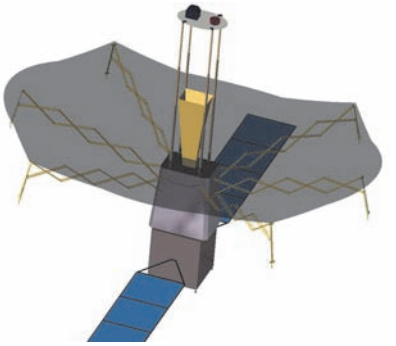

Figure 2.35 Pantograph supported deployment mechanism for the MAPSAR antenna main reflector.

The high power amplifier for generation of the radar pulses was identified to be the second critical technology for the overall concept. A space qualified amplifier in the class of 1 kW is not yet available on the market. A new design was developed based on combining the power of four space qualified travelling wave tube (TWT) amplifiers with 250 W output power each (Figure 2.36). The power combining is done in wave guide technology where the second stage is directly performed in the orthomode transducer of the L-band horn. The power combining is controlled by low power phase shifters driving the TWTs. This concept also avoids high power switching mechanisms by using polarisation synthesis. The phase of one channel is switched between 0° and 180° for alternating radar pulses. This results in two independent polarisations which are tilted 45° against the horizontal plane. In the receive path of the instrument the phase switching is compensated and the final rotation of the polarisation matrix will be done in the SAR processor. The preliminary integration concept of the radar hardware in the payload module is depicted in Figure 2.37.

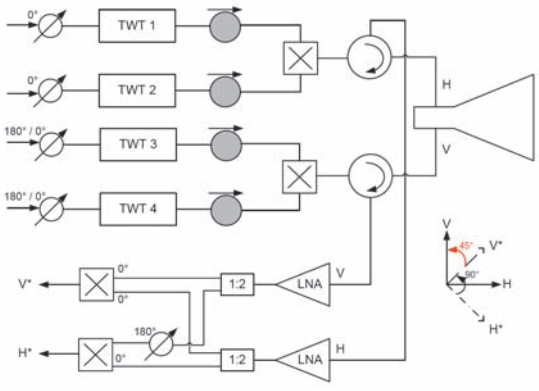

Figure 2.36 Power combining and polarisation synthesis in the MAPSAR radar payload.

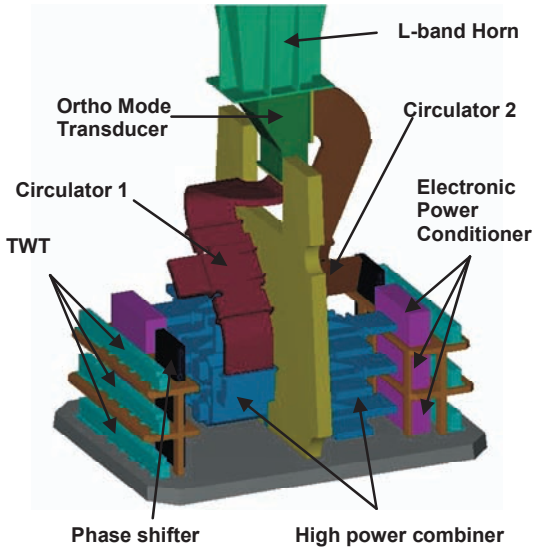

Figure 2.37 Concept for the integration of the key components of the radar instrument in the payload module.

Table 2.5 presents a summary of the estimated mass budget for the MAPSAR payload. The total mass of 282 kg is just compatible with the specified value of the Multi-Mission Platform. The total mass of the satellite is estimated to be 532 kg. In terms of dimensions, the payload layout is compatible with the majority of MMP considered standard launcher family.

Table 2.5 MAPSAR payload estimated mass budget.

Sub-System	Mass [kg]
Mechanical Structure	30
Thermal Control	4
Antenna Reflectors & Feed	85
Radar instrument incl. harness	121
Data Storage & Transmitter	42
Total Mass	282

MAPSAR represents an innovative small L-band SAR mission with a high degree of innovation in the design of the small SAR payload, the reflector antenna, and with remarkable sensor performance. The applications will take advantage of high spatial resolution L-band SAR with enhanced capabilities (polarimetry, stereoscopy, interferometry), particularly suitable for the Amazon region and boreal forest operations. The MAPSAR initiative aims at providing a "public good" service, not excluding commercial aspects. System deployment after phase A completion is estimated to be in five years, which leads to a possible system operation in 2011. The Phase A study is planned to be finished by mid 2006 and options for a continuation into follow-on phases are being investigated.

2.1.9 HABITAT Earth Explorer Mission

In response to ESA's Call for Ideas for the Next Earth Explorer Core Missions in March 2005 the Institute, together with nine European academic partners, supported by an international team of associated scientist and in close cooperation with European industrial partners proposed HABITAT (Hazard & Biomass Interferometric SAR Observatory [562]): a mission to contribute to the study of forest ground cover and ground motion.

HABITAT will use an innovative bistatic radar configuration consisting of a dual-polarised L-band SAR illuminator accompanied by three passive microsatellites operating in single-pass interferometric mode, quad-polarisation, and with two spatial baselines. HABITAT will establish a significant contribution to the understanding of the carbon cycle by mapping above ground forest biomass stock and the dynamics of all key forest biomes globally. HABITAT is also optimised with respect to wetland mapping and measuring the ground motion caused by earthquakes and volcanoes on a global scale, even in the presence of vegetation. Thus, within HABITAT, three scientific objectives are enabled by the same technology.

The Institute is responsible for the coordination and development of the Pol-InSAR component within the forest biomass estimation theme and supports mission design and operation activities.

Forest Biomass Estimation

The estimation of above ground forest biomass in terms of HABITAT is a two step procedure:

- Model based estimation of forest height and basal area from InSAR coherence.
- Biomass estimation from the obtained forest height and basal area estimates.

Biomass Estimation: Forest (stand) biomass is given by the product of basal area (i.e. the cross-section area of all trees per unit area), basal area weighted forest height, and density. This biomass measure conforms with the stem volume standard in the forestry applications and compatible with most national and international forest inventories. Total above-ground forest biomass which also includes branches, leaves, and depending on the definition, standing dead trunks and undergrowth, is typically calculated from stem biomass estimates through the use of biomass expansion factors. Accordingly, the estimation of forest height and basal area allows a direct estimation of above ground forest biomass.

Estimation of Forest Height & Basal Area: The estimation of both forest height and basal area from the individual interferometric coherence components is based on the inversion of the Random Volume over Ground (RVoG) scattering model. Accordingly, forest height can be estimated with an accuracy of 10-20% largely independent of terrain and/or forest conditions and does not rely on any a-priori information (section 2.2.4).

Via discontinuities in the horizontal structure of the canopy layer of the RVoG model it is possible to introduce an "area fill factor" in the model, which, in open canopy forests, is directly related to forest basal area. Due to the different temporal stability of bare and forested ground it is now possible to relate temporal decorrelation to the ratio of stable/non-stable, i.e.bare/forested contributions, by using this discontinuous RVoG model. This allows, in the case of a repeat-pass interferometric system and in the absence of any volume decorrelation effects arising from non-zero spatial baseline components, to estimate basal area from interferometric measurements. Model-based estimation of the "area fill factor"/basal area and its relation to forest stem volume and forest biomass have been demonstrated with an accuracy of 10-30% in several studies on boreal forest at C-, and L-band by means of ERS-1, ERS-2 and JERS-1.

Earth Quakes and Volcanoes

L-band SAR interferometry is also ideal for large scale high resolution ground motion measurements. To realise this potential, HABITAT will provide global coverage and a dense time series of measurements, a narrow orbital tube to minimize topographic noise and spatial decorrelation, a wide bandwidth to reduce ionospheric noise by split-channel processing, precise orbital knowledge from on-board GPS, and left- and right-looking capability to improve 3-D motion reconstruction.

2-D motion retrieval of the ground surface requires ascending and descending right-looking image acquisitions for all targets. The North-South (NS) component of the motion will be recovered by either combining left and right looking acquisitions or by using incoherent speckle tracking, if possible in connection with a spot mode to improve the azimuthal resolution of the system. Using temporal stacking, about 3 years are required to reduce the atmospheric noise level to 1 mm/10 km/year. This contribution could alternatively be estimated and removed using stable reference points.

Wetlands

The diversity of wetland environments presents significant challenges for an observation strategy. HABITAT's multi-temporal L-band Pol-InSAR data acquisitions provide optimal opportunities for wetland characterisation, mapping and monitoring, and represent a complement to other data sources (e.g., optical data). Key elements of the wetlands science plan include

- detection of open water, inundated forest and macrophytic vegetation,
- retrieval of vegetation biomass (up to ~60-80 t/ha) through empirical relationships or using inversion modeling,
- retrieval of structure (incl.vegetation height) using backscatter and interferometric data,
- detection of change (e.g., seasonal inundation, deforestation, rice cultivation, freeze-thaw cycles, flooding) through comparison of multi-date imagery.

By integrating the information provided by HABITAT, the process of characterising and mapping wetlands will be refined.

Technical Concept

The HABITAT space segment is built on TerraSAR-L for the main spacecraft and the Cartwheel micro satellites for the bistatic receivers. Both systems have been studied up to PDR level and different concepts for close formation flying have been investigated (section 2.1.4). The formation will be operated at a mean altitude of 648 km in a near-polar, sun-synchronous, dawn-dusk orbit with an 18-day repeat cycle. Orbit maintenance is required to ensure repeat passes within a 250 m orbital tube.

The TerraSAR-L snapdragon platform is built around the 11 m x 2.86 m active phased array antenna of the L-SAR operating in standard Stripmap and interferometric ScanSAR modes at up to 85 MHz bandwidth. At least three microsatellites flying in formation (along-track distance 20-100 km) with the main transmitter and acting as bistatic receivers enable single-pass interferometric acquisitions unaffected by temporal decorrelation effects. The TerraSAR-L Cartwheel study revealed the importance of formations providing simultaneously multiple baselines, which are also necessary to achieve the required performance in forest biomass retrieval from Pol-InSAR. Elegant solutions for the acquisition of such a second baseline are the Trinodal Pendulum or the Two-Scale Cartwheel.

Mission Operation Scenario

The HABITAT system is capable of achieving the primary mission objectives in 5 years of nominal mission duration. The basic approach dedicates distinct repeat cycles to either one or the other objective, i.e. for most (up to 14) of the 20 yearly repeat cycles monitoring of seismically active zones or volcanoes is carried out using only the main satellite in D-InSAR mode, whereas the biomass mapping requires 6 repeat cycles per year in bistatic quad pol operation for bi-annual coverage of all forest areas. Wetlands will be covered by both: quad-pol mode for detailed characterisation and D-InSAR mode in its dual-pol option for monitoring.

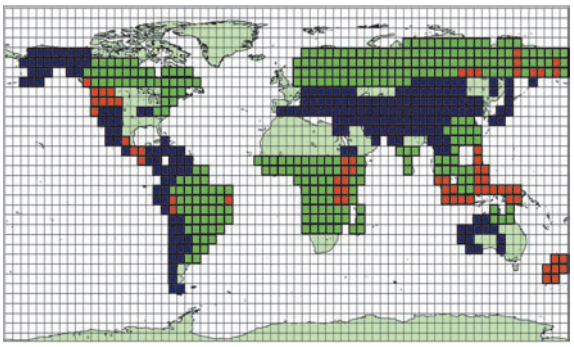

Figure 2.38 HABITAT areas of interest: green: biomass – blue: earthquakes & volcanoes – red: combined.

A sustainable data reception and distribution scenario can be established assuming the TerraSAR-L baseline of three ground stations providing an average contact time of 20 min/orbit. Serving the different mission objectives with distinct operation modes in separate acquisition cycles and over separate areas of interest (Figure 2.38) guarantees an observation strategy that completely safeguards the multiple objectives. The main products expected from HABITAT are summarised in Table 2.6.

Table 2.6 Potential HABITAT products; the observation interval (i.e. mission duration) is 5 years.

Products	Accuracy	Resolution [m²]	Observation Frequency
Forest Height	10 – 20%	50 x 50	6 months
Basal Area	20 - 40%	50 x 50	6 months
Biomass	10 – 20%	50 x 50	6 months
Carbon	10 - 20%	50 x 50	6 months
Forest Change	5%	50 x 50	18 days
Ground Motion	mm	50 x 50	18 days
3-D Motion	mm	5 x 5	18 days

ESA's evaluation process and final endorsement of missions for assessment study by the Earth Observation Programme Board will be completed in late spring 2006. Up to six mission concepts will be selected to go into a Phase A study.

2.1.10 Reconnaissance Systems

The information demand for future spaceborne reconnaissance systems can only be covered by multi-sensor systems on different satellite platforms. Current spaceborne reconnaissance systems are optimised only to a limited number of selected parameters, e.g. type of the sensor, revisit time, incidence angle, etc. Future reconnaissance missions have to be provided with imaging capabilities independent of weather and time (SAR), capabilities for heat detection (IR) and material determination (hyper-spectral). Multi-sensor systems with very high spatial and radiometric resolution cannot efficiently be integrated on a single platform, because of different image acquisition geometries, platform size and resources. Figure 2.39 shows a possible generic scenario for such a multi-platform system consisting of image (IMINT), signal (SIGINT) and human (HUMINT) intelligence sensors on different ground, air and space based platforms.

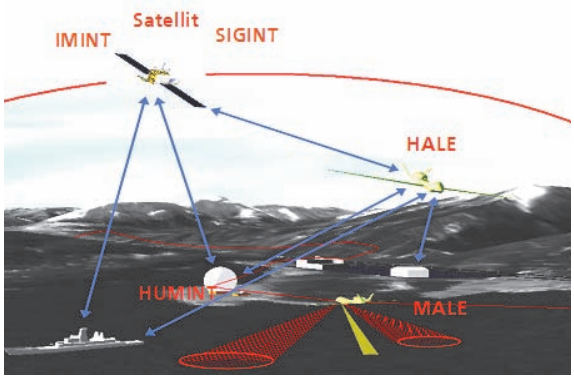

Figure 2.39 Multi-platform reconnaissance system consisting of different information sources (IMINT, SIGINT and HUMINT) and data links to dislocated ground stations.

For analysing and increasing the efficiency of existing and future reconnaissance systems (also valid for civil earth observation), the design and development of tools to simulate the interactions between the single elements of the complete system is necessary. An end-to-end simulation concept was realised with the main focus on the principal user needs (Figure 2.40). The modular simulation concept guarantees the necessary continuous flexibility. It can presently handle nearly all possible platforms e.g. cars, trucks, airplanes, UAVs, ships, and spacecraft in a wide variety of scenarios.

The two major parts of this tool are the mission simulator and the SAR end-to-end simulator. With respect to given user requests the tasks of the mission simulator are to plan and analyse the geographical or time dependent coverage of the regions of interest and to optimize the mission with regard to major aspects, like platform resources, and sensor characteristics.

The SAR end-to-end simulator has the task of generating a simulated SAR image from an optical image, another radar image or a map. The simulator consists of modules for target and scenario generation, modelling the platform and sensor behaviour, processing of the simulated raw data, and analysing the simulated image quality. Further tools for assistance of the simulator are the parameter generator, which is suited for a very first design of a spaceborne SAR system, and the performance estimator, which can predict the image quality parameters to be expected very exactly without processing the raw data. The block diagram of the complete end-to-end simulation concept is displayed in Figure 2.40. The SAR end-to-end simulator is described in more detail in section 2.3.5.

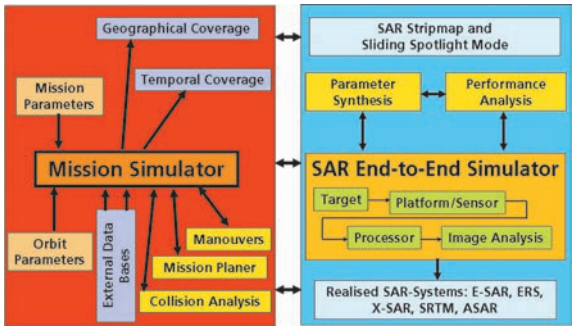

Figure 2.40 Generic reconnaissance system simulation concept; the mission simulator generates the principal geometry for the SAR end-to-end simulator according to the user requirements.

Mission Simulator

The mission simulator is a tool to simulate a complete multi-platform reconnaissance system considering multi-user aspects. The user can define different multi-mission scenarios and system constraints. The tool allows geographical coverage analyses, field of view analyses, global coverage and contact calculations, as well as time dependant coverage analyses, like the calculation of response time, revisit times and image information age. These results can be used for subsequent mission optimisations. Finally, the mission planning capability can be used to optimize multi-user driven imaging requests for different parameters, like number of images or short time intervals between image acquisition and image delivery to the user's ground segment. The analyses are supported by external data bases, which can communicate with the mission simulation via existent interfaces. It is also possible to carry out collision analyses with space debris using the NORAD data base or predicting shadowing effects, if a digital elevation model of the area of interest with sufficient resolution and quality is available. The functions are shown in Figure 2.41.

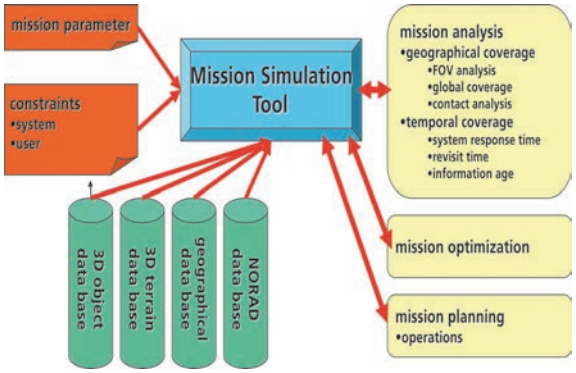

Figure 2.41 Scheme of mission simulator displaying the data flow from user inputs to different simulation results supported by external data bases.

As shown in Figure 2.42, the mission simulator consists of the four core modules: the mission analyser, the mission planner, the satellite simulator, and the coverage analysis tool, which is supported by commercial orbit propagators. To analyse external scenarios, the mission simulator provides an interface to two commercial software tools, the Satellite Tool Kit (STK) and the FreeFlyer.

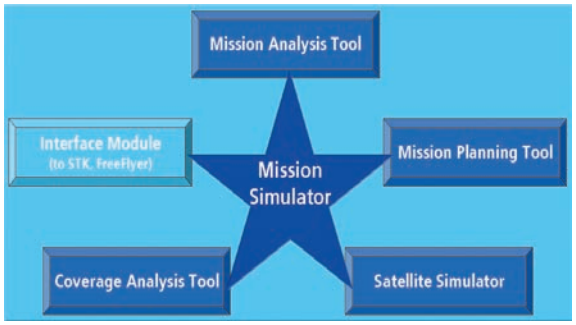

Figure 2.42 Modular design of the mission simulator with the four core modules: mission analysis tool, mission planning tool, satellite simulator, Coverage Analysis Tool (CAT) and interfaces to COTS software products.

Mission Analysis Tool

Using the mission analysis tool all parameters of a simulated mission can be calculated and analysed. For example it is possible to make a coverage analysis of an area of interest to determine the revisit time of the system. Figure 2.43 shows a coverage analysis for Brazil produced for the MAPSAR project [183], [202] (section 2.1.8).

Further analysis examples are the determination of the system response time, the image information age, and the field of view analysis of moving or stationary sensors. Figure 2.44 shows the result of the contact analysis of a satellite ground segment considering local terrain aspects.

Figure 2.43 Coverage analysis for the MAPSAR mission. The colour scale indicates the different region-dependent revisit times for Brazil.

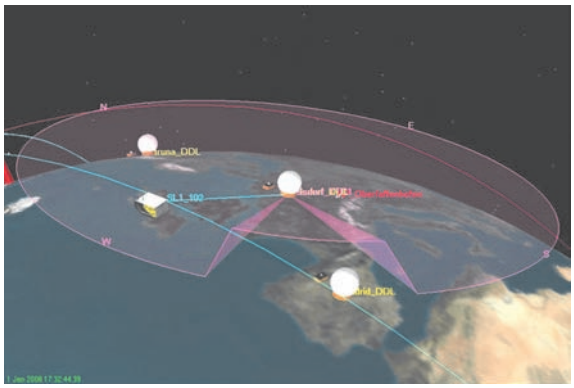

Figure 2.44 Ground station contact analysis with a limited field of view caused by high trees in the ground station area.

In addition, the mission analysis tool is able to calculate the necessary input parameters for the mission planning tool, like ground station contacts, inter-satellite data link contacts and contacts to other platforms mentioned above. If a DEM is available, the calculation of the contact times also considers the three dimensional geographical coordinates. For better visualisation, the overlay or registration of the scene with a satellite image is possible.

Mission Planning Tool

The mission planning tool can be used for the definition, design and analysis of multi-user driven multi-mission and multi-platform scenarios. Starting with a list of orders generated by the user, the coordinates of all targets on the order list will be converted by a target generator to a special format readable by the mission planning tool. In a second step, all possible contacts of the satellites to one or more ground stations and to all targets are calculated. Considering the constraints given on the resources of the system (e.g. power, data storage, priority of orders, etc.), the mission scheduler creates an optimised scheduling and shows it within a result list. The results are displayed graphically. A further feature is the option to prioritize particular orders. The mission plan can be optimised by iterations (Figure 2.45).

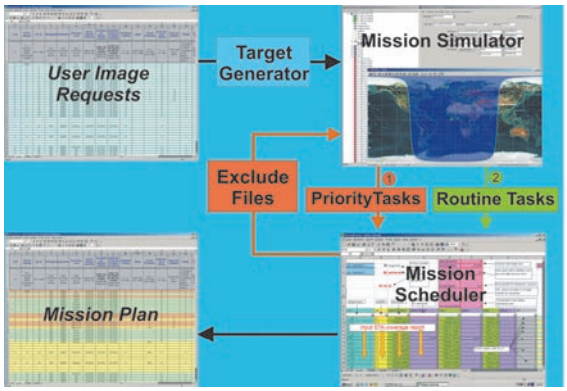

Figure 2.45 Work-flow of the mission planning tool: satellite images with different priorities requested by the user, are pre-calculated by the mission simulator (access times, commanding and download times) and then optimised by the mission scheduler by time to get the best mission plan.

Satellite Simulator

The satellite simulator models the most important satellite sub-systems and can be used to calculate the satellite system driven constrains of the reconnaissance system required for the mission analysis, optimisation and planning activities. Presently, five of the satellite subsystems are modelled: the SAR sensor imaging geometry and field of view aspects, the orbit control system, the power system, the attitude control system, and the data storage system. These five systems significantly influence the capability of the reconnaissance system regarding the feasibility and number of orders, geographical location of the targets, and system response time. As an example Figure 2.46 depicts an image acquisition manoeuvre of a SAR reconnaissance system, showing the important coordinate systems. The satellite has to be manoeuvred from its nominal mode to the image acquisition location by pre-defined quaternion files considering the speed and acceleration constraints. The simulation of the manoeuvre allows the analysis, if the image coordinates have been hit by the SAR beam within the required constraints. These aspects are very important for platforms with reflector antennas and mechanical beam steering.

Coverage Analysis Tools (CAT)

The coverage analysis tool contains several modules for the valuation of alternative mission concepts concerning complete sensor coverage aspects. The CAT was developed by the Institute and is based on the Microsoft Excel environment

for the graphic user interface (GUI) in combination with interfaces to the mission simulator. The current version includes capabilities for analysis of orbit nodal drift aspects, latitude dependent coverage and especially, investigation of information age and the system response time which can be achieved for the image products from reconnaissance satellites [610]. It is important for the validity of the calculated results that as much as possible operational constraints are considered, such as available satellite data storage, minimum time between two satellite target accesses and other user or satellite defined access restrictions.

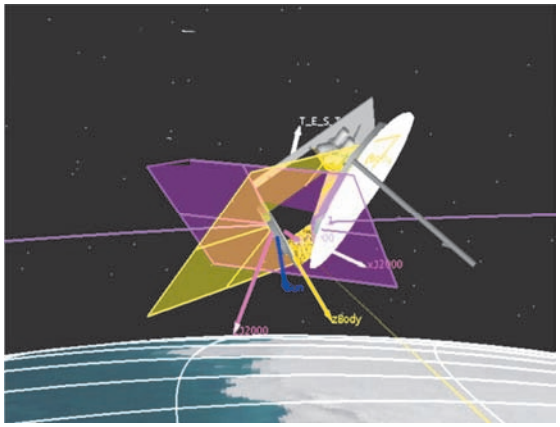

Figure 2.46 Image acquisition manoeuvre of a SAR reconnaissance satellite with a reflector antenna simulated and analysed with the satellite simulator using a pre-calculated quaternion file.

Simulation Example of a Multi-Platform Reconnaissance System

The following example demonstrates the simulation of a multi-platform reconnaissance mission consisting of two satellite platforms with a SAR payload on each [445]. In Figure 2.47 for example, the Canadian Radarsat-2 with a moderate spatial resolution detects an unknown ship near the coastline. The acquired image is transferred via a geostationary communication satellite to the ground station, where a SAR image is generated. The position and the velocity vector of the ship can be determined. A short time later after the analysis of the data, a high resolution reconnaissance system is commanded to acquire an image with sufficient resolution for the identification of the ship, the determination of the technical characteristics and activities.

One of the main objectives of the ongoing developments of the mission simulator is to provide an automated, optimised mission planning and design tool for future multi-sensor reconnaissance missions and satellite constellations [441].

The developments will focus on a corresponding simulation tool and an operations plan optimizer. The corresponding boxes of the work-flow are marked blue in Figure 2.48.

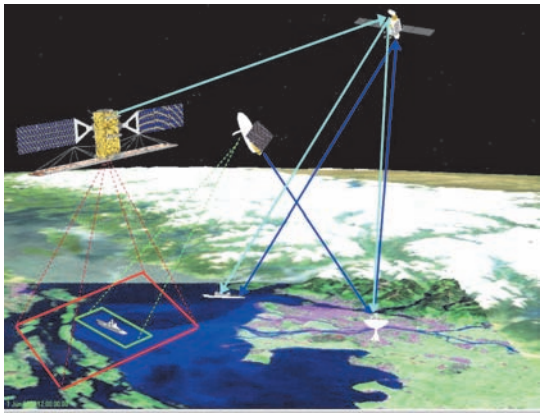

Figure 2.47 Multi-mission reconnaissance system consisting of Radarsat-2 and an additional high resolution imaging system.

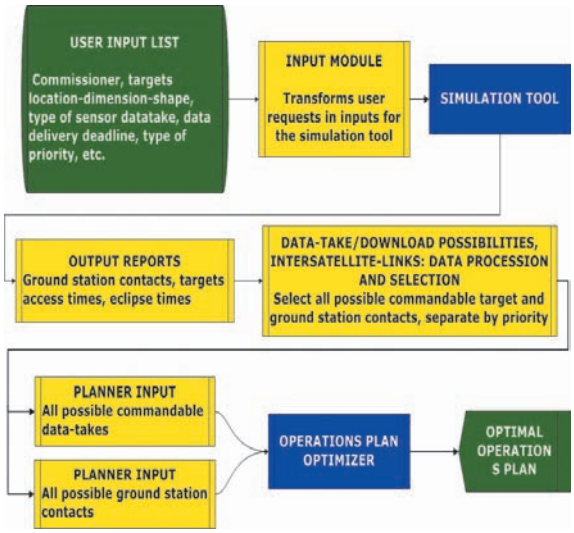

Figure 2.48 Work-flow of the next generation mission planning tool.

This simulation module will contain new features, like an integrated sensor performance analysis tool with different constellation configurations, different target and mission scenarios and with the possibility to consider inter-satellite links for commanding, as well as for data transmission.

The operations plan optimizer will be a completely new developed module that extends the presently used first-in first-out (FIFO) planning method. It will allow the optimisation of multiple mission objectives and calculates optimal solutions driven by specific performance figures of merit e. g. the minimisation of system time response, the minimisation of the information age, the maximisation of the number of data-takes in a given time span, etc.

These goals will be realised by modification and development of existing constraint satisfaction techniques to fit them to space operations planning and scheduling problems. Different optimisation techniques for constraint satisfaction optimisation problems will be compared, such as combinatorial optimisation approaches, deterministic and heuristic approaches and genetic algorithms. They will be realised in the operations plan optimizer module.

The final version of the mission simulator will be an end-to-end simulation environment for reconnaissance systems, to be used during system studies and development phases, system analyses and realisation, and finally to support the system operations.

2.2 Airborne SAR

2.2.1 Experimental SAR - E-SAR

E-SAR identifies the DLR airborne Experimental Synthetic Aperture Radar system which is operated by the Microwaves and Radar Institute in cooperation with the DLR flight facilities on-board a Dornier DO228-212 aircraft (Figure 2.49 and Figure 2.50). Being developed in the Institute, E-SAR delivered first images in 1988 in its basic system configuration. Since then the system has been continuously upgraded to become what it is today: a versatile and reliable workhorse in airborne Earth observation with applications worldwide.

Figure 2.49 E-SAR onboard DLR's Dornier DO228-212 aircraft touching down after a successful measurement flight.

The DO228 is a twin-engined short take-off and landing aircraft. The landing strip must have a minimum length of about 900 m. The cabin is not pressurised. It can carry up to 1000 kg of payload. Special modifications (28 VDC and 220 VAC instrumentation power supply, hardpoints, bubble windows, circular mounts in the roof, and a floor bay with a roller door) make it ideal for scientific instrumentation. The operational cost is comparatively low.

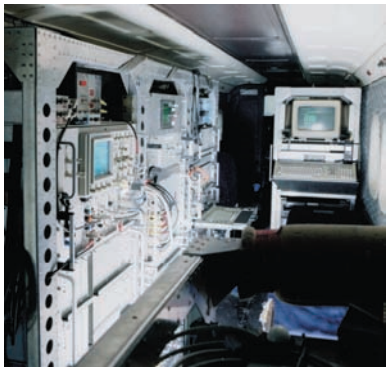

Figure 2.50 View inside the cabin of the DO228 aircraft. The racks are approx. 1.2 m high.

The maximum operating altitude with E-SAR onboard is about 6000 m above sea level. For SAR operation the ground speed ranges from 140 kt to 200 kt. Depending on the SAR configuration the endurance varies between 2.5 and 4 hours.

E-SAR operates in 4 frequency bands (X-, C-, L- and P-band), hence it covers a range of wavelengths from 3 to 85 cm. The polarisation of the radar signal is selectable, horizontal as well as vertical. In polarimetric mode the polarisation is switched from pulse to pulse in (HH-HV-VV-VH) sequence. E-SAR technical parameters are listed in Table 2.7.

Table 2.7 E-SAR technical parameters.

	X	C	L	P
RF [MHz]	9600	5300	1300	350
Bw [MHz]	100 or 50 (selectable)			
Sampling	6 or 8 bits, complex (I and Q)			
Data rates	8 or 16 MByte/s (selectable)			
Rg res. [m]	2 or 4 (selectable)			
Az res. [m]	0.25	0.3	0.4	1.5
Rg cov. [km]	3 or 5 (selectable)			

E-SAR offers high operational flexibility. The measurement modes include single channel operation, i.e. one wavelength and polarisation at a time, and the modes of SAR Interferometry and SAR Polarimetry. The system is polarimetrically calibrated in L- and P-band. SAR Interferometry is operational in X-band (XTI and ATI). Repeat-Pass SAR Interferometry in combination with polarimetry is operational in L- and P-band.

A real-time D-GPS/INS System (IGI CCNS4/ Aerocontrol IId) combined with a FUGRO OmniStar 3000L D-GPS receiver allows most precise navigation and positioning. E-SAR is hence able to generate geocoded image products of very high geographical precision. Repeat-Pass SAR Interferometry at baselines of less than 10 m is possible, allowing the realisation of advanced and innovative techniques like Pol-InSAR and tomography as well as coherent change detection. An example for the precision in flight track maintenance is shown in Figure 2.51. Three consecutive passes of about 6 minutes duration each were flown with a nominal baseline of 5 m.

Part of the sensor system is an operational E-SAR ground segment. After transcription from HDDC (SONY SD-1) to hard disk drive the E-SAR Extended Chirp Scaling (ECS) processor converts the SAR data to calibrated image data products (refer to section 2.2.2 for details). To increase the product quality level to CEOS level 1b, radiometric and polarimetric calibration, DEM generation and geocoding are operationally implemented.

For calibration trihedral radar corner reflectors are set up on the Oberpfaffenhofen airfield, the premises of DLR and in the neighborhood. Their size varies between 0.9 m and 3 m leg length. The geographical positions are precisely known.

Finally, the ground segment is completed by DLR's DIMS archiving system and the EOWEB internet portal, which provides a user access point.

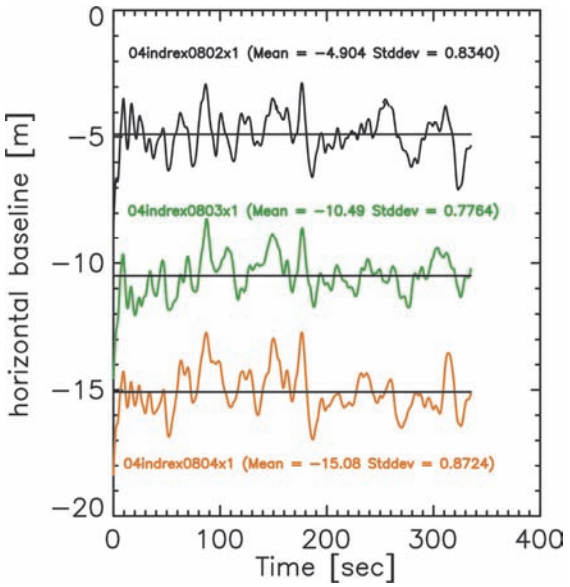

Figure 2.51 Repeat-pass SAR interferometry baselines achieved during INDREX-II campaign in Indonesia. Deviations are less than 1 m (rms) for each of the 3 passes with a nominal horizontal baseline of 5 m.

E-SAR System Upgrades

New P-band (300 to 400 MHz) – Wideband low frequency SAR is highly susceptible to radio frequency interference. Such interference was discovered in P-band in the range from 400 to 500 MHz, which in Europe is fairly crowded with TV broadcasting stations. To achieve better image quality the center frequency was shifted to 350 MHz.

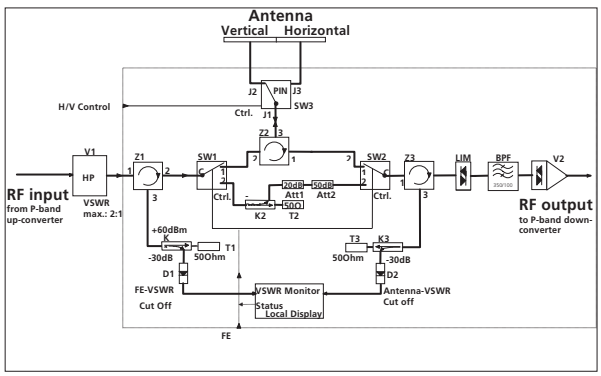

Figure 2.52 The new E-SAR P-band front-end block diagram.

A new P-band subsystem was built, including antenna, IF converter and front-end sections (Figure 2.52). The P-band antenna is described in section 2.3.8 [223][225]. In 2003 the first flight tests were executed. The image quality proved to be very good in terms of geometric and radiometric resolution as well as SNR and RF interference level. An image example is shown in Figure 2.53 with a single-look resolution of about 2.2 m x 2 m (range x azimuth).

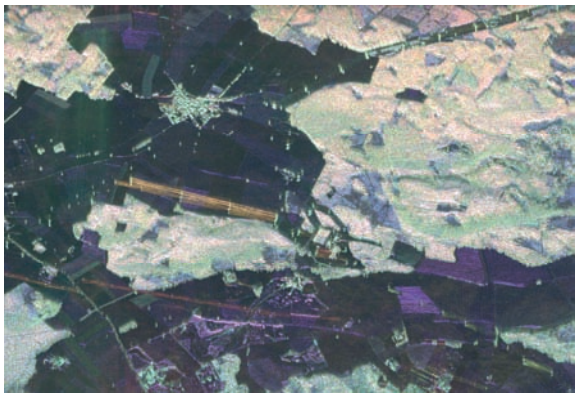

Figure 2.53 E-SAR P-band image (300 to 400 MHz) of a calibration test site. Scene size is about 3.2 km x 7 km, illumination direction from the bottom.

Step Frequency – Technology still imposes some limits on radar chirp bandwidth, mainly if a reconfigurable signal generation is necessary, as for the E-SAR system. To meet user requirements for very high resolution, alternative methods to synthe the size bandwidths up to 1 GHz are needed. One attractive method is the Step Frequency approach that was adopted for the E-SAR system. For experimental purposes a Step Frequency converter unit was developed and tested with E-SAR.

The unit provides 200 MHz maximum bandwidth and spectrum overlap ranging from 0 to 100 % alternating the normal 100 MHz-chirp pulse-to-pulse (Figure 2.54). Flight tests were conducted with different degrees of overlap (10 %, 20 % and 50 %).

For processing of the data, a dedicated software package had to be developed. The work was completed successfully and the improvement in range resolution has been demonstrated (Figure 2.55 and Figure 2.56).

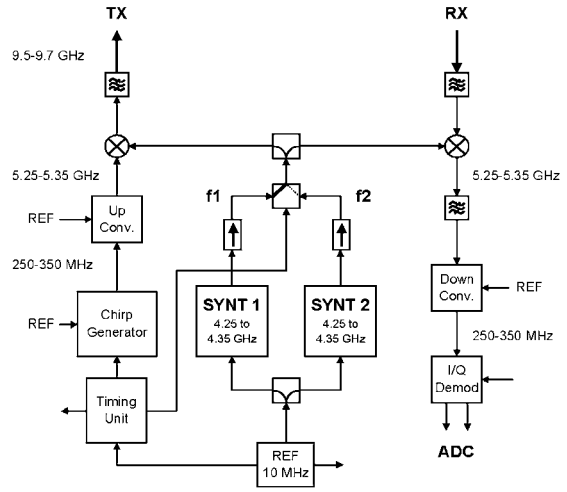

Figure 2.54 E-SAR Step Frequency converter block diagram.

Table 2.8 shows the results of the achieved geometrical resolution for a point target at 160 MHz bandwidth and 20% overlap in Step Frequency mode in comparison to the normal chirp bandwidth (100 MHz, standard). The selected point target in Figure 2.56 is a 1.5 m radar trihedral reflector located on the airfield. The black lines indicate the normal resolution case.

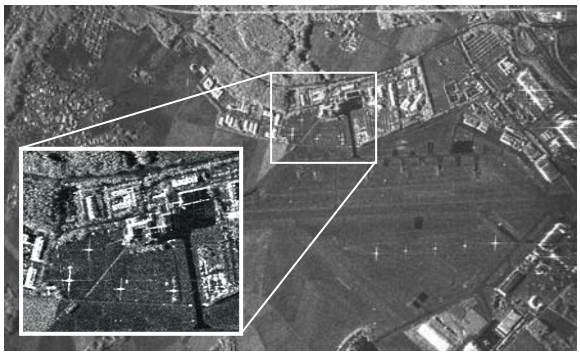

Figure 2.55 The Oberpfaffenhofen airfield and DLR research center – X-band Step Frequency image at 160 MHz total range bandwidth (20% spectrum overlap).

Table 2.8 Comparison of the point target resolution with 100 MHz (standard mode) and with 160 MHz (Step Frequency mode).

	Theoretical		Measured	
	Rg [m]	Az [m]	Rg [m]	Az [m]
standard	1.35	0.80	1.36	0.90
Step Freq.	0.79	0.80	0.80	0.90

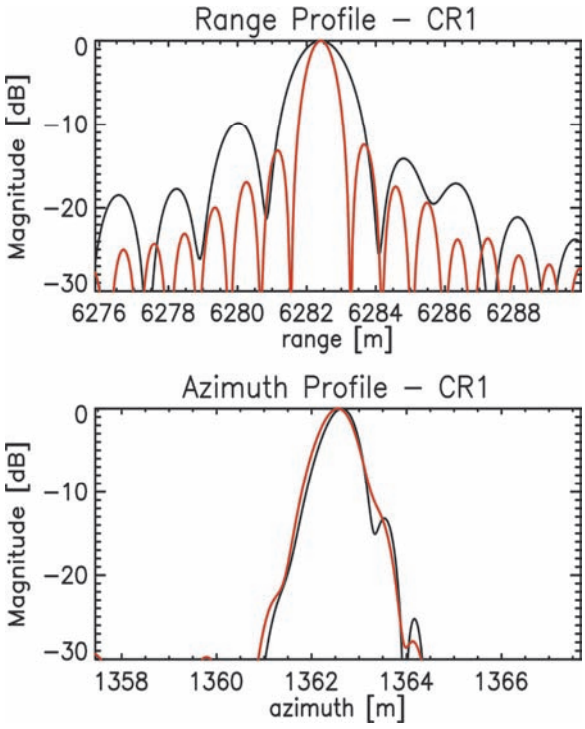

Figure 2.56 Improved range resolution demonstrated by a cut through the impulse response of a radar reflector. Black line: original impulse response function (IRF), red line: Step Frequency IRF. Hamming weighting was applied only in azimuth.

Since many years, E-SAR has been heavily used for SAR experiments and measurement campaigns. It has evolved to be an important tool for SAR research and applications in Europe. Section 2.2.3 summarizes a number of scientifically and technically important SAR missions and projects which were executed in recent years with great success.

However, while many questions could be answered in the past, new challenges have come up requiring new solutions. The Institute is developing a new airborne SAR facility identified as F-SAR (section 2.2.6). F-SAR will have enhanced measurement capabilities, such as simultaneous full-polarimetric measurements at four wavelengths (X-, C-, L- and P-band). It will also offer simultaneous X- and S-band single-pass polarimetric interferometry.

While F-SAR is in the building phase, E-SAR is still maintained and used for campaigns. Minor upgrades are implemented to cover immediate scientific needs such as those for TerraSAR-X.

2.2.2 Processing Algorithms

Synthetic Aperture Radar systems, in particular airborne SAR, require sophisticated signal processing in order to obtain the desired information from the data. Spatial resolution as well as radiometric and interferometric calibration accuracy have direct influence on the potential to measure

or infer physical parameters. As the E-SAR system is often employed to experiment with innovative operating modes to establish new applications, the development of new algorithms to provide the new information and to improve the quality of the associated data products is an ongoing process.

In addition, the increasing amount of acquired and processed E-SAR data poses strong requirements on efficient algorithm implementation. About 300-400 data takes per year were acquired during the last 4 years, corresponding in average to ca. 300-400 GB of raw data per year and the same amount of processed data product.

The E-SAR processor is based on an advanced SAR processing algorithm that was developed at the Institute. The Extended Chirp Scaling (ECS) algorithm is able to accommodate the requirements posed by the high resolution, phase preserving data processing and at the same time allows accurate motion error correction. All processing steps are performed without interpolation, as in the original version of the Chirp Scaling algorithm. The ECS processor has also been extended for the processing of ScanSAR and Spotlight mode data [560]. This extension has been adopted for the operational processing of the TerraSAR-X satellite [558].

Linked to the requirements of high resolution and precise motion compensation together with the high number of flight campaigns abroad, the E-SAR processing software has been extensively adapted to run on individual LINUX-PCs while accessing common data storage for the raw and processed data. During campaigns outside of Europe (India, Indonesia, and Tunisia) this concept allowed on-site data processing and quality checks. As a consequence, the installation of a temporary license of the E-SAR processor at the Space Applications Centre of ISRO in Ahmedabad, India also became feasible, which enabled the ISRO scientists (after proper training) to process and evaluate the E-SAR data of the 2004 INDSAR campaign by themselves.

The E-SAR processor provides the following operational products:

- Slant range polarimetric multilook and SLC data (Radar Geometry Images – RGI product). The C-band image of Oberpfaffenhofen shown in Figure 2.57 is derived from two dual-polarised data takes, thus providing quasi full polarimetric information.
- Geocoded Terrain Corrected Data (GTC product).
- Digital Elevation Models (DEM product).
- Repeat-Pass Interferometric Data (RP-InSAR product)

Dedicated software has been developed to segment long data takes as acquired during INDREX and SVALEX campaigns and to allow perfectly overlapping data products for a specific area (e.g. areas acquired at different frequency bands). For archiving purposes, each data product is ingested into the Data Ingestion and Management System (DIMS) of the German Remote Sensing Data Center (DLR-DFD) allowing a world-wide access via EOWEB (eoweb.dlr.de).

In the last 5 years the algorithm development activities for the airborne SAR processor focused on the needs imposed by the Pol-InSAR and tomographic imaging modes as well as by differential and along-track airborne SAR interferometry. In the following sections some of the most important developments are described.

Figure 2.57 Fully polarimetric E-SAR image of Oberpfaffenhofen, incl. DLR facilities in image center; composite obtained from 2 dual-polarized data takes in C-band (HH-green, HV-red, VV-blue).

DEM Generation

Digital Elevation Models are one of the standard E-SAR products. However, large scale mapping is a challenge due to the small E-SAR swath width of only 3.5 km. Therefore, a mosaic procedure is used to generate large area DEMs. With the opportunity of data acquisition near Lago Maggiore (Italy), the mosaic procedure was extended to incorporate iterative topography adaptive compensation of residual motion errors [3][97]. An elevation model covering an area of 15 km x 15 km was generated from 15 different tracks. It is depicted in Figure 2.58. Horizontal posting is 2 m and height accuracy is better 2 m rms (>5 m rms on steep slopes). Total height variation is about 1500 m. Black areas correspond to areas where no signal information is available (e.g. lakes).

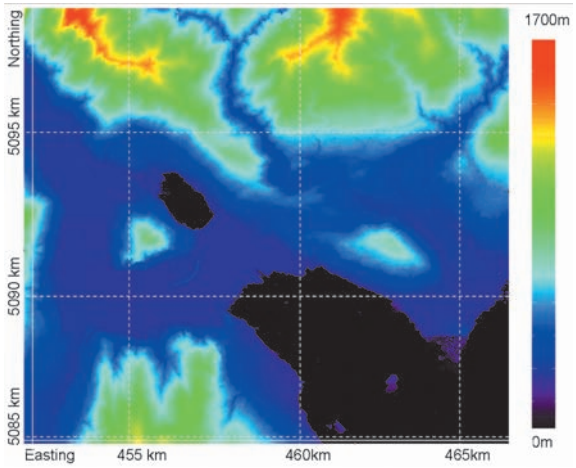

Figure 2.58 Digital elevation model of Lago Maggiore area obtained from single-pass interferometric E-SAR data in X-band of 15 km x 15 km (WGS-84, UTM zone 32).

Airborne Repeat-Pass SAR Interferometry

A dedicated processing chain for repeat-pass SAR interferometry was implemented demanding high complexity in the algorithm developments. Accurate processing is a precondition to obtain high quality Pol-InSAR data products as input to the model-based inversion approaches (section 2.2.4). The performance of standard airborne SAR processing is limited by the accuracy of the navigation data available to perform the motion compensation (state-of–the-art is a combination of inertial and GPS sensors). Although the relative accuracy is very good, enabling well focused data, the absolute performance is limited by the absolute precision of the differential GPS signal, which is in the order of 5-10 cm (ca. one interferometric phase cycle assuming SAR data at L-band and the two-way propagation delay). It is obvious that this accuracy is insufficient for repeat-pass interferometry.

A robust error estimation approach was developed based on the so-called multi-squint technique. Residual errors (in horizontal and vertical directions) between the two tracks of the interferometric acquisitions are iteratively estimated from the processed interferometric SAR data using special algorithms. An example is depicted in Figure 2.59.

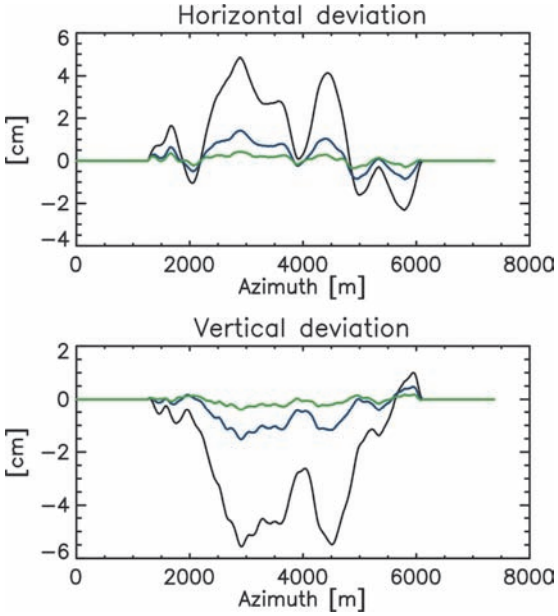

Figure 2.59 Residual track errors measured and corrected by the repeat-pass processing approach. Almost perfect compensation is reached after 3 iterations, corresponding to a correction of residual motions errors to millimeter accuracy.

The original residual track errors are on the order of 3-5 cm and are in accordance with the accuracy of the navigation system based on differential GPS and INS. Without this compensation approach, phase errors and coherence degradations would occur which have strong impact on the interferometric data quality [48][51][232].

Topographic Motion Compensation

During the development and refinement of the airborne repeat-pass processing strategy it was recognized that the usual approximations for motion compensation are not sufficient and that topography needs to be taken into account very precisely. This led to the development of a new algorithm, the so-called Precise Topography and Aperture (PTA) dependent motion compensation approach [36]. It is based on short time FFT codes and thus makes effective use of the quasi-linear azimuth time-frequency correspondence of the SAR signal. Its application is imperative, not only for processing airborne data in differential SAR interferometric mode, but also for repeat-pass SAR applications in hilly and mountainous areas in general.

Traffic Monitoring

The E-SAR system uses small antennas in order to avoid a gimble-based antenna steering configuration. This leads to an azimuth signal with a very high bandwidth required with a correspondingly high PRF value.

During processing, usually only a small portion of the azimuth bandwidth (ca.150 Hz) is needed to obtain comparable resolutions in azimuth and range directions. The availability of a very high azimuth bandwidth (ca.900 Hz in X-band) of the E-SAR system is beneficial for monitoring moving targets in the along-track interferometric mode, as the signal energy might be shifted outside the azimuth bandwidth used in the conventional processing. Therefore, full azimuth bandwidth processing is required to allow MTI with sufficient accuracy. For this purpose, the E-SAR processor was extended to efficiently allow the allocation of enough memory and the generation of the corresponding phase filter functions. Result is a very high resolution image (up to 10 cm in azimuth) and the associated along-track interferogram.

Figure 2.60 presents a part of such an image and the interferometric phase with a first indication of moving targets. Note that the resolution in range is limited by the bandwidth of the radar system of 100 MHz and is by a factor of 15 worse than the resolution in azimuth. Further evaluation of these data sets is presented in section 2.3.4 and is supporting the TerraSAR-X GMTI processor development [340][417].

Future work in the next two years will be focused on the adaptation and extension of all the developed specific algorithms for the new airborne system F-SAR. Challenging scientific topics currently being investigated are related to airborne differential SAR interferometry and airborne SAR tomography. In addition, signal processing techniques for interferometric radar sounding applications in P-band will be developed. Finally, developments in the processing algorithms are planned for the next years to enhance moving target indication with digital beamforming on receive which will be provided by the new airborne F-SAR system.

2.2.3 Major Campaigns

In the period from 1998 to 2005 about 70 E-SAR airborne SAR campaigns were performed, leading to an average of approx. 10 campaigns per year. About one third of the campaigns was dedicated to research topics (e.g. new operation modes and/or applications), another third to system tests and ardware developments. The remaining third was performed in standard operation modes.

The main objectives of the airborne flight campaigns are:

- Development of innovative SAR modes or operation configurations
- Development and demonstration of novel techniques and new applications

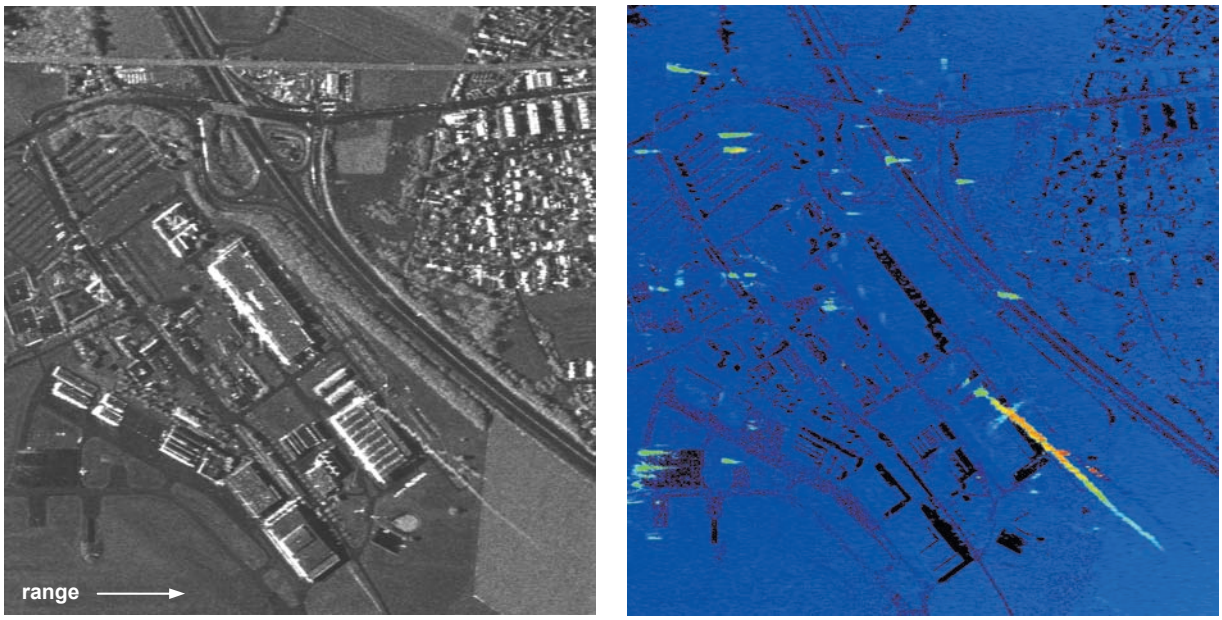

Figure 2.60 Full azimuth bandwidth E-SAR image in X-band (left) and corresponding along-track interferometric phase. Blue colour corresponds to zero phase and represents the stationary targets. The moving targets are shown in green, yellow and orange colours.

- Preparatory experiments for future SAR satellite systems, supporting the data product development as well as system specification

Although the E-SAR was originally intended to be an experimental system, today it has a high degree of operationalization and is a reliable source of high-quality radar data for a large user community world-wide.

The E-SAR campaigns are performed for different interested parties, for SME companies, universities, research institutes, as well as for European and international agencies. Approximately 70% of the campaigns performed during a year are financed through external contracts and 30% through internal DLR research funds.

With the large amount of flight campaigns, a wide range of applications is covered, from areas being cartographically imaged with standard high resolution X-band modes (with the radiometry being corrected for the terrain topography using digital surface model information), to higher quality environmental application products, for example forest height being derived from L-band polarimetric SAR interferometry.

The main application areas up to now are cartography, geology, forestry, agriculture, snow studies, glaciology (land and sea ice), urban areas, bathymetry, monitoring, and surveillance. The geographical distribution of the executed campaigns ranges from Germany to European countries as well as to South and South-East Asia and Africa. Examples of campaigns performed outside central Europe in the last 3 years are India, Indonesia, Svalbard, and Tunisia. In these cases the flight range of the aircraft has been a limiting factor, such that for India and Indonesia the E-SAR system had to be transported separately and installed in the aircraft just prior to the flight campaign.

All calibration and system test flights are performed close to the DLR location at Oberpfaffenhofen. Since 2001 the Institute is following a strategy in which the data acquisitions each year are dedicated to a specific thematic research topic associated with one extensive flight campaign in order to be able to answer urgent scientific questions. A few major campaigns of the E-SAR system, their objectives and particularities as well as first results are presented in the following.

E-SAR Mission Highlights

1998 – The first demonstration of SAR tomography has been carried out in L-band [47]. E-SAR recorded data on 14 parallel tracks over the Oberpfaffenhofen test area. As a result of the tomographic processing a spatial resolution of 3 m was achieved. Section 2.2.5 describes the developed approach and experiment in detail. Figure 2.61 shows a slice of the tomographic data with the different backscattering mechanisms that can be separated using the Pauli decomposition. The strong contributions from volume scatterers from the tree crown are clearly visible in green, while the dihedral scattering is in red and the surface contribution in blue [47][623].

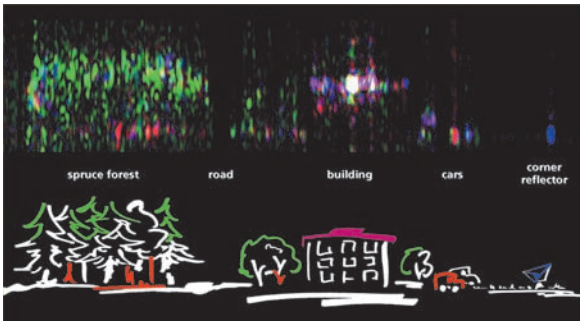

Figure 2.61 First demonstration of airborne polarimetric SAR tomography, where the colours represent different scattering mechanisms (red - dihedral, green - volume, blue - surface scattering). The upper plot represents the tomographic signal intensity as a function of height. The lower plot shows an artist's view of the imaged area.

1999 – 2002 – European aerospace industry as well as the European Space Agency required SAR data to simulate future TerraSAR-X and TerraSAR-L data products. In the projects PROSMART, ISOCROP, TerraDEW, and Dual-band SAR Simulation DLR's E-SAR was the source of multi-frequency, multi-polarization data for a number of different product developments. Operating in various European countries (Figure 2.62), E-SAR collected data for applications in agriculture, forestry and urban planning, areas which were identified as promising. Using E-SAR data high resolution TerraSAR simulated data products have been produced and delivered to the customers for further analysis. In this context the Institute holds a leading position amongst all airborne SAR system operators in Europe.

2003 – The first demonstration of airborne bistatic SAR imaging has been carried out in Europe. As part of a cooperation agreement between the Institute and ONERA a bistatic SAR experiment employing the E-SAR and RAMSES airborne SAR systems was conducted [10]. Technical issues such as time and frequency synchronisation of both systems were solved and the experiments were successfully executed (section 2.3.1) [215][313].

Figure 2.62 E-SAR test site locations across Europe. Black stars: E-SAR campaigns for TerraSAR-X and TerraSAR-L simulation. Orange circles: other campaigns.

In May of the same year, X-band single-pass interferometric data were acquired in support of an EU project for development of an operational monitoring system for glaciers (OMEGA). The objective was to generate a 10 km x 10 km digital elevation model of the Engabreen glacier in Norway, which was compared later with laser and GPS data. Although the radar backscatter and thus the SNR was relatively low due to temperatures much above the melting point, successful computation of the DEM was possible, including the mosaic of several swaths (Figure 2.63). Subsequent comparison with the laser data (obtained 4 weeks later due to continuous cloud cover) revealed an accuracy of approx. 2 m (rms value, peak-to-peak value of 4.2 m with an offset of +0.1 m) considering the complete area of interest.

Figure 2.63 Digital Elevation Model of the Engabreen Glacier in Svartisen, Norway acquired in X-band single-pass SAR interferometry. The height varies by approx. 1500 meters in this sub-image of ca. 2 km x 2 km.

2004 – From July to December 2004 the first two E-SAR campaigns in Asia, namely in India and Indonesia, were executed. The first campaign was conducted by the Institute and the Indian Space Research Organisation (ISRO) during the post-monsoon season. E-SAR was successfully flown over arid regions, flooded, agricultural and open coal mining areas as well as sub-tropical forest regions across the Indian sub-continent. The data were processed and archived by ISRO/SAC, the Space Application Center in Ahmedabad and are still under the authority of the Indian government. Extensive ground measurements were performed during the 2 months of data acquisition in P-, L-, C-, and X-band.

Following India the next campaign was performed in Indonesia, on Kalimantan [392]. The objective of the INDREX-II campaign was to build up a SAR database over different tropical forest types with focus on L- and P-band polarimetry and interferometry data. The initiative to this campaign originated from the Pol-InSAR Workshop held at ESA/ESRIN in 2003 [277] [283] [241] [242] [244] [245]. During this workshop the participating scientists identified gaps in the knowledge of the SAR imaging behaviour in tropical forests. The main scientific question was to determine if L-band radar signal penetrates the dense tropical forest down to the ground and if the Random-Volume-over-Ground model is applicable in this case for the retrieval of tropical forest height measures.

Figure 2.64 A 15 km long wooden bridge installed for collecting ground measurements in the Mawas Peat forest test site (Kalimantan, Indonesia, 2004).

Eight different forest types (example in Figure 2.64) were chosen for data acquisition on ground and from the aircraft. More than 200 GB of raw data in 43 flight hours were acquired in polarimetric and interferometric mode and at different frequencies (X-, C-, L-, and P-band). The length of the flight strips varied from 23 to 80 km. The E-SAR radar system was shipped separately from Germany to India and after the campaign in India to Kalimantan. Despite the high logistical effort - the transportation and

integration of the radar into the aircraft, the system tests and system calibration on site in India and Indonesia - no major technical problems occurred during the whole campaign. The overall time schedule could be followed without major delays, thus achieving all campaign objectives. All requested data could be collected with high radiometric quality and high precision in flight navigation.

The INDREX-II data were processed and delivered to ESA in 2005, which is responsible for the distribution to the European scientific community. The scientific questions posed in the beginning could also be answered by the detailed data analysis. Plotting the complex coherence of a selected data set (Figure 2.65) at different polarisations on a unit circle (Figure 2.66) shows that the loci of the coherence values (red points) are distributed along a line. This is an indication that L-band is penetrating the dense volume down to the ground. The different coherence loci would cluster to one point or would not be matched to a line, if this was not the case. The distribution of the points in Figure 2.66 along a line is due to the polarisation diversity of the ground contribution and to the random nature of the forest canopy in L-band [44].

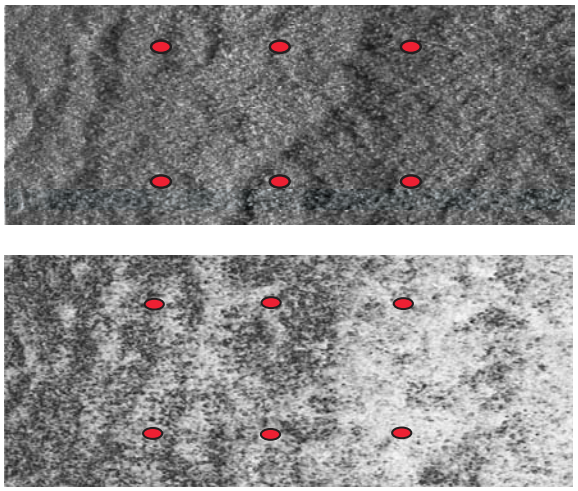

Figure 2.65 Interferometric coherence (bottom) and radar backscatter (top) at L-band in HH polarisation over the hilly dense dipterocarp forest of the Sungai Wain test site. The red dots indicate the sample locations taken for the unit circle plots in Figure 2.66.

In a second step, tropical forest heights were successfully derived from Pol-InSAR data in L- and P-band. A colour composite of the Mawas test site used for the estimation of forest height is shown in Figure 2.67. For both frequencies a similar forest height distribution has been obtained. In a first order analysis the Pol-InSAR derived heights correspond very well to the forest heights estimated on ground. This campaign and the obtained results certainly deliver an important contribution for the future development of SAR satellites in Europe devoted to the monitoring of forested areas and their above-ground biomass (section 2.2.4) [377][393].

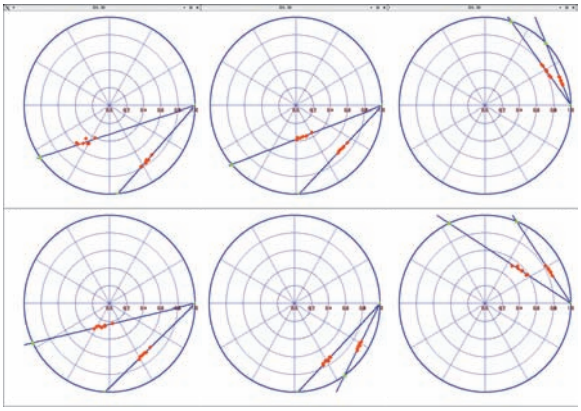

Figure 2.66 Complex coherence in L-band at different polarisations plotted on the unit circle for six sample plots over the Sungai Wain test site.

A first demonstration of the Pol-InSAR technique using spaceborne systems is planned with the PALSAR L-band instrument on-board the Japanese ALOS satellite within the Kyoto & Carbon initiative (section 2.1.7).

Figure 2.67 P/X/L-band polarimetric intensity image of the Mawas test site with a disturbed burned forest area (red) and a natural tropical forest (green). This is a geocoded image with a spatial resolution of 2 m x 2 m.
Colour Composite: red - P-band, (HH+HV+VV)/3; green - X-band, VV; blue - L-band, (HH+HV+VV)/3.

2005 – Major campaigns were carried out in the Arctic and North Africa. Svalbard was selected as the ideal location for a joint DLR and AWI (Alfred Wegener Research Institute) campaign over sea and land ice (SVALEX). Two instruments were flown, the E-SAR on the DLR's DO228 D-CFFU and the meteopod, laser altimeter, line scan camera and surface temperature instrument on AWI's DO228 D-CAWI (Figure 2.68).

Figure 2.68 SVALEX 2005 – The two Do228 research aircraft (right: D-CFFU and left: D-CAWI) at Longyearbyen airport in Svalbard.

The mission objective was to gain knowledge of the land ice volume and the sea ice structure using mainly Pol-InSAR techniques at X-, L- and P-band [52]. In addition, a first ice sounder experiment at P-band with the E-SAR system was performed with different baselines by means of down-looking antenna geometry.

Despite the arctic climate conditions in early April with temperatures below -20°C the campaign could be performed successfully; all planned data were collected and are in the process of being analysed (Figure 2.69). This campaign was funded by DLR in preparation for the polar year in 2007-2008 as well as for the upcoming satellite systems dedicated to Arctic and Antarctic applications (e.g. Cryosat).

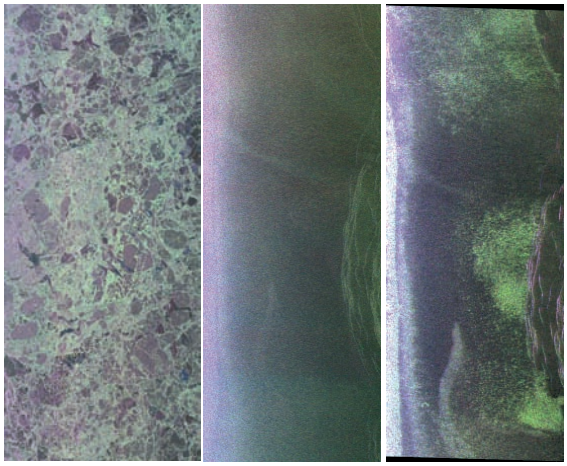

Figure 2.69 Radar backscatter images in RGB colour composite of sea ice (left) and land ice (center) in L-band and land ice (right) in P-band. The center and right images corresponds to the same area. Note the different features in the P-band image showing the very good penetration of the P-band signal in land ice.

AQUIFEREX was an ESA funded campaign that took place in Tunisia in November 2005. The key issues of the project were to support national authorities and international institutions with Earth Observation based technology to better manage internationally shared water resources and aquifers.

E-SAR successfully collected X-, C- and L-band data. At the same time AVIS, an optical system of the Ludwig-Maximilians-Universität of Munich, recorded multispectral images. Synergetic analyses of the collected data are ongoing (Figure 2.70) and are made available for further investigations in ESA's AQUIFER project (an ESA TIGER demonstrator initiative).

2006-2007 – The year 2006 is dedicated to building up a database for agricultural vegetation and surface parameter estimation over a whole vegetation period (planned acquisition time of four months, start: beginning of April). The AGRISAR campaign is funded by ESA to support space segment activities with respect to the GMES/ Sentinel Programme answering open questions concerning system constellations (single, dual, quad polarisation, revisit time, etc.). It supports the scientific community in developing model and inversion algorithms for parameter estimation. The polar year 2007 is dedicated to ice applications. An E-SAR campaign over an arctic region is planned to be performed as part of an ESA supported project in cooperation with AWI.

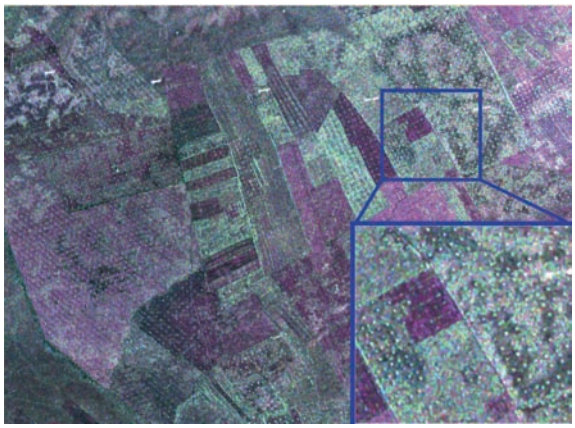

Figure 2.70 Acquired images in C-band (HH-red, HV-green, VV-blue) polarisation over the Ben Gardan test site in South-East Tunisia. Different irrigated fields are visible. The dots on some of the fields are regularly planted olive trees (see zoom).

2.2.4 Polarimetric SAR Interferometry

Polarimetric SAR Interferometry (Pol-InSAR) is today an established remote sensing technique that allows the investigation of the 3-D structure of natural volume scatterers. Interferometric observables are highly sensitive to the spatial variability of vertical structure parameters and allow accurate 3-D localisation of the scattering center. On the other hand, scattering polarimetry is sensitive to the shape, orientation and dielectric properties of scatterers and allows the identification and/or separation of scattering mechanisms of natural media.

In polarimetric interferometry both techniques are coherently combined to provide sensitivity to the vertical distribution of scattering mechanisms. Hence, it becomes possible to investigate the 3-D structure of volume scatterers and to extract information about the underlying scattering processes using only a single frequency polarimetric radar sensor. This promises a breakthrough in solving essential radar remote sensing problems. Indeed, structural parameters of volume scatterers in the biosphere and cryosphere such as vegetation height, structure, biomass and moisture, or snow and ice depth, layering and moisture, are today critical inputs for ecological process modelling and enable monitoring and understanding of ecosystem change. Figure 2.71 shows an example of the estimation of forest height using airborne Pol-InSAR data in L-band.

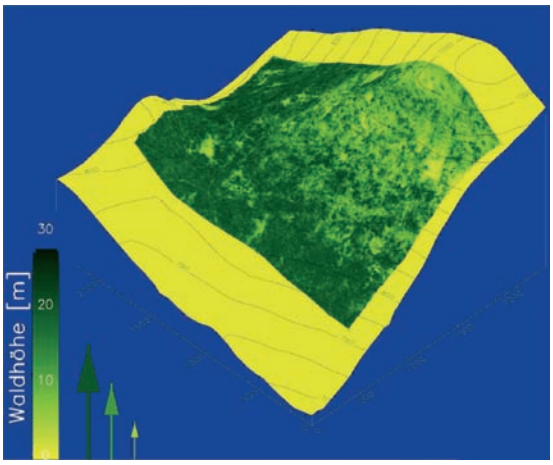

Figure 2.71 Perspective view of forest height and topography variation obtained by means of Pol-InSAR (Test site: Fichtelgebirge, Germany). Validation results are shown in Figure 2.72.

From the very beginning, the Institute developed the new technique of Pol-InSAR leading to expertise in sensor technology, system and instrument design and performance analysis as well as processing, modelling and inversion techniques. The Institute's E-SAR sensor was first to demonstrate airborne polarimetric repeat-pass interferometry at L- and P-band - initiating the development of Pol-InSAR technology in Europe.

In the following, an overview of the activities, advances and achievements in Pol-InSAR techniques and applications developed over the last five years is provided.

Forest Applications

Across the different application fields, the maturity of Pol-InSAR applications is very diverse. Forest applications are by far the most developed and a success story [44][8]. The analysis of the first Pol-InSAR data provided by the SIR-C/X-SAR mission indicated the potential of combining polarimetry with interferometry for forest applications. As a next step, the Institute developed the sensor technology and processing expertise to acquire and process Pol-InSAR data with the E-SAR system in a repeat-pass interferometric mode.

In addition, theory, modelling and inversion techniques have been addressed and advanced in close cooperation with international partners. Early airborne experiments in the late 90s have found their continuation in a series of successful Pol-InSAR demonstration campaigns across Europe performed in cooperation with academic and commercial institutions providing in situ forest expertise. These have culminated in INDREX-II - a large scale airborne experiment sponsored by ESA for the demonstration of Pol-InSAR techniques in tropical forest environments (section 2.2.3)

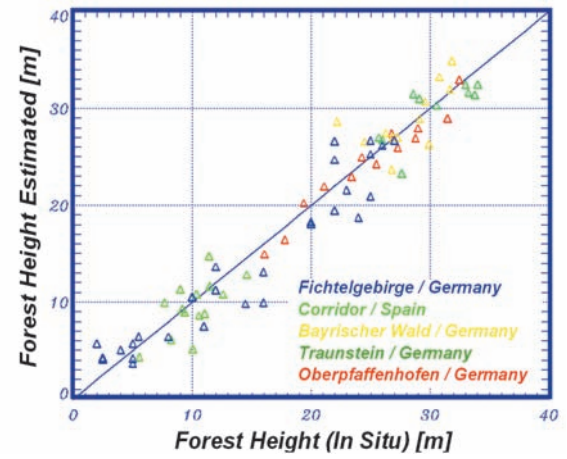

Figure 2.72 The Pol-InSAR forest height validation over 5 European test sites representing a wide range of forest and topographic conditions.

Today, several model based forest parameter inversion approaches, which combine dual or fully polarimetric data with single or multiple baseline interferometric measurements have been proposed, discussed and validated as part of different ESA funded R&D studies (Figure 2.71). The main forest vegetation parameters that can be potentially estimated from polarimetric and interferometric data inversion are described in the following.

Forest height is one of the most important parameters in forestry along with basal area and tree species or species composition. Being a standard parameter in forest inventories, forest height is difficult to measure on the ground and

typical estimation errors are given with 10% accuracy - yet increasing with forest height and density. It describes dynamic forest development, modelling and inventory. Forest height estimation from polarimetric single- and multi-baseline data has been demonstrated in a series of airborne experiments over a variety of natural and commercial as well as temperate and boreal test sites characterized by different stand and terrain conditions [242][243]. The validation indicates an estimation accuracy in the order of 10-20% compared to the forest top height (Figure 2.72). The estimation performance is widely independent of terrain and/or forest conditions. The results from INDREX-II verify the inversion performance at L-band (and at P-band) also for dense tropical forest conditions (Figure 2.73).

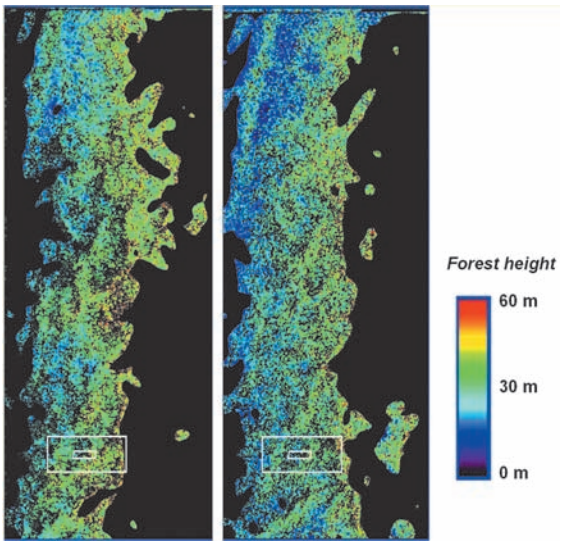

Figure 2.73 Tropical (primary) forest height maps obtained by single baseline Pol-InSAR data inversion at L- (left), P-band (right) in the framework of the INDREX-II experiment in Indonesia.

Forest biomass is the most integrative forest parameter essential for ecological modelling and forest inventory and is today the big unknown in global ecosystem change modelling.

The development of forest height estimation in terms of Pol-InSAR initiated the development and evaluation of allometric biomass estimation schemes in collaboration with academic institutions with forest ecology and modelling expertise.

Indeed, allometric estimation of forest biomass from forest height is robust and does not saturate and is therefore a good candidate for above ground biomass inventory. This is demonstrated in Figure 2.74, where forest height is plotted against forest biomass for 11 of the most common European and North American three species for varying site and thinning conditions.

This very fundamental biological (allometric) relationship between forest height and forest biomass varies only about 10-15% with site conditions and only about 15-20% across species (exceptions are very fast growing pioneer species with very light woods such as poplar and birch). This makes the estimation of forest biomass even in inhomogeneous and natural forest conditions possible by only knowing forest height. The estimation accuracy varies between 20 and 40% up to biomass levels of 450 t/ha. The achieved experimental results are in accordance with general allometric relations for different temperate, boreal and tropical forest ecosystems and with predictions of generalized forest structure models underlying the general character and thus the validity of the height-biomass relationship. However, the largest uncertainties in the height-to-biomass relationship are due to density variations (natural or anthropogenic) especially in low density forest conditions, as present in boreal and savannah forest ecosystems. To reduce the biomass estimation uncertainty and increase the robustness of the methodology, the incorporation of additional information such as basal area becomes important, especially in low density, open canopy forest conditions and is still being investigated.

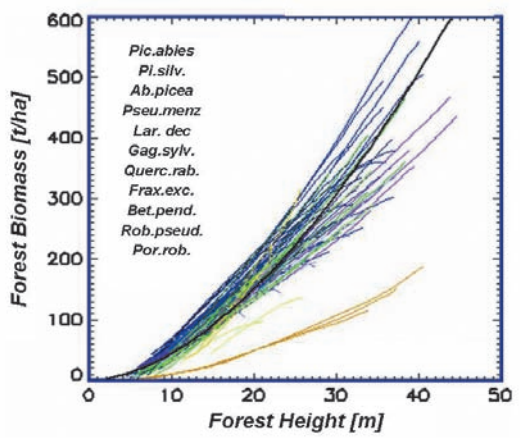

Figure 2.74 Forest height-biomass relationship for 11 different species accounting for varying site and thinning conditions.

Forest canopy structure is a key forest ecosystem parameter. Regarding the estimation of forest biomass, vertical structure information is important as it allows a significant reduction of the biomass estimation error. However, the extraction of forest structure requires besides polarisation also baseline diversity in the observation vector. Dual baseline Pol-InSAR is a very promising configuration for the extraction of structure information and a new research topic in the field of polarimetric interferometry.

Forest parameter (height and biomass) estimation from Pol-InSAR data has today reached a pre-operational stage. As part of ESA's Pol-InSAR Mission and Application Study the actual state of Pol-InSAR techniques and technology has been evaluated and proven with respect to operational information product generation accounting for the technological constraints of actual and/or future satellite missions [562]. Towards a first in-orbit demonstration of the Pol-InSAR technique the Institute is a member of the JAXA's ALOS Carbon & Kyoto Initiative and is responsible for Pol-InSAR forest parameter estimation (section 2.2.2). However, the expected temporal decorrelation will limit the ALOS Pol-InSAR demonstration to favourable datasets only.

Aspiring to global monitoring, the wide spectrum of scientific and technological Pol-InSAR expertise developed within the Institute culminated in HABITAT, an European mission proposal for global above-ground biomass inventory and change monitoring submitted in answer to ESA's Call for Ideas for the Next Earth Explorer Core Missions in 2005 (section 2.1.9).

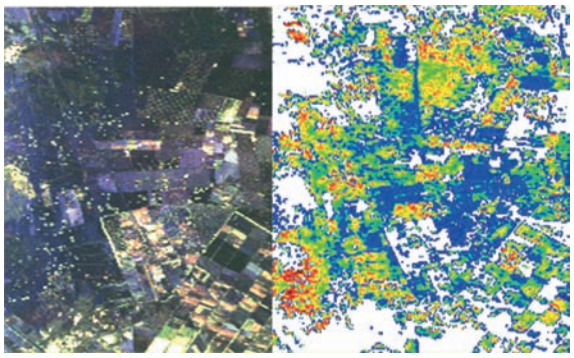

Figure 2.75 Gabes Region in Tunesia (RGB image left – HH+VV (blue), HH-VV (red), HV (green)) and soil moisture map derived from the coherent polarimetric X-Bragg model (right). The soil moisture is ranging between 3 and 30 vol. % from blue to red. The data have been acquired within the AQUIFEREX project. Irrigated fields can be well distinguished.

Agricultural Applications

From the EM scattering point of view, agricultural scatterers can be divided into two categories:

- Bare surfaces are characterised by a direct surface interaction. In this case only the geometric and dielectric properties of the surface affect the scattered wave. Indeed, inversion of soil-moisture and roughness for fully polarimetric data has been further developed and validated while an alternative roughness inversion algorithm from Pol-InSAR data has been proposed [15][16]. In Figure 2.75 the latest inversion result of soil moisture in an arid region is presented. Irrigated and non irrigated fields can be distinguished.
- On vegetated surfaces the waves first propagate through the vegetation layer and then interact with the underlying surface. Vegetation and surface scattering are superimposed. In contrast to forest vegetation applications, quantitative agricultural vegetation Pol-InSAR applications are still in an early phase of development. The significant differences in vegetation height, structure and attenuation values and in the propagation properties through the vegetation layer make the adoption of forest concepts for agricultural applications questionable and ineffective. Opposed to forest applications, where lower frequencies are an advantage agricultural vegetation monitoring is rather a high frequency Pol-InSAR application – a fact that makes airborne repeat-pass demonstration a challenge.

Nevertheless, in the last years first dedicated airborne campaigns and indoor measurements provided the required initialization for the development of dedicated agricultural applications:

Vegetation layer height estimation: The height of agricultural vegetation is an important input parameter for the estimation of crop biomass. Furthermore, monitoring of agricultural plant height at different stages of development allows direct conclusions about crop health and yield. Early results (Figure 2.76) demonstrated the potential of estimating height in the case of large differential extinction crop values.

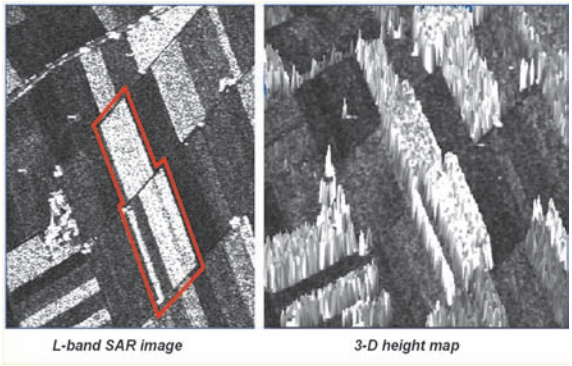

Figure 2.76 SAR image (left) and 3-D height map (right) of a cornfield retrieved from single-baseline Pol-InSAR data inversion (Test site: Küttighoffen, Switzerland).

Extinction of the vegetation layer: Density and water content of the vegetation layer affects the extinction of the forward propagating wave. Different to the forest case, the scatterers within the agriculture vegetation layer are characterized by an orientation correlation introducing anisotropic propagation effects and differential extinction. The extinction coefficient and its variation with polarisation are therefore related to structural attributes such as the leaf area index (LAI) of the vegetation and orientation effects of

vegetation structure. Furthermore, the knowledge of the differential extinction is strongly related to the vegetation moisture content and this, in turn, is an essential parameter for agricultural cultivation management. First positive experimental results point towards a successful development of Pol-InSAR for agricultural applications (Figure 2.77), [375].

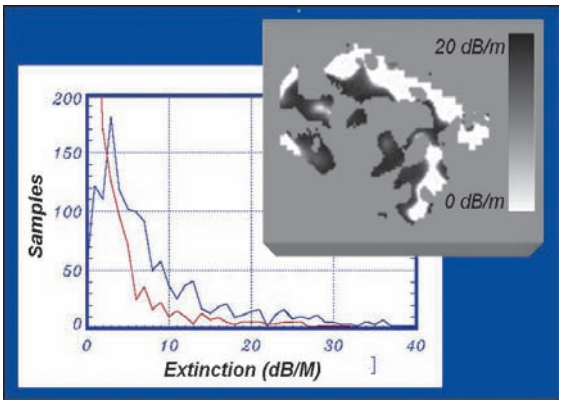

Figure 2.77 Extinction estimates (red HH, blue VV) and spatial differential extinction distribution over a cornfield from Pol-InSAR data inversion (Test site: Alling, Germany).

Moisture Content of the Underlying Surface: Underlying surface moisture is significant for farming optimization and predictive hydrological modelling. This importance - combined with the absence of an alternative remote sensing method for even rough estimation - makes the inversion of the dielectric properties of the underlying surface a challenge. The potential of Pol-InSAR techniques is currently being addressed as part of an ongoing ESA funded R&D study.

Ice and Snow Applications

The cryosphere is dominated by ice and snow scattering volumes. Admittedly, the understanding and development of Pol-InSAR applications with respect to ice and snow is today in a very early stage. First E-SAR airborne campaigns provided appropriate data sets initiating data analysis and leading to first results:

- A multibaseline Pol-InSAR experiment in the Austrian Alps demonstrated that snow acts as a volume scatterer even at L-band and that there is a strong dependence of the interferometric coherence on polarization. This is due to the strong underlying ground scattering component and is similar to the agriculture vegetation case. Local snow depths have been estimated.
- In 2005, an extensive multi-frequency/ multibaseline Pol-InSAR experiment was flown in Svalbard, Norway, and was supported by ground measurements (section 2.2.3). The analysis and interpretation is ongoing.

Urban Areas

One of the most appealing new Pol-InSAR applications recently proposed by the Institute is the identification and characterization of point-like scatterers - so called coherent scatterers - in urban environments [407][408][409]. Urban areas are not volume scatterers in the conventional sense but can be seen as a discrete vertical distribution of scatterers. Coherent scatterers are deterministic scatterers located at different heights within the "urban volume" and can be identified by using spectral correlation of individual or multiple images. Accordingly, their localization can be performed with a limited number of SAR observations, acquired with a short or even without a temporal baseline. The strong polarimetric behaviour of point-scatterers makes polarimetric observation diversity important for achieving large coherent scatterer densities. Figure 2.78 shows the first demonstration of coherent scatterers performed on L-band Pol-InSAR data sets acquired by the E-SAR system over the city of Dresden. The coherent scatterers are colour-coded according to the lexicographic polarimetric basis and are superimposed on the amplitude image.

After localization of coherent scatterers, polarimetry furthermore allows the identification and description of scatterers in terms of canonical scattering processes (e.g. dihedral-, surface-, dipole-type) and enables the characterization of geometric and dielectric properties. There is a wide spectrum of potential applications for coherent scatterers ranging from polarimetric/interferometric calibration and urban DEM generation to information extraction from individual scatterers and change monitoring.

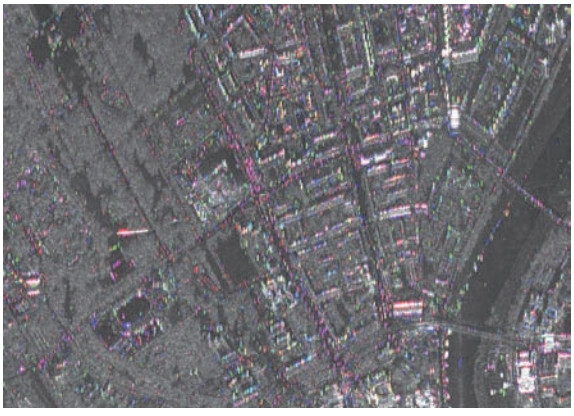

Figure 2.78 Coherent scatterers at different polarizations: HH (red), VV (blue), HV (green) (Test site: Dresden, Germany).

The rapid development of Pol-InSAR techniques combined with ESA's interest in coordinating the European activities and establishing a forum for

scientific exchange finally manifested in the Pol-InSAR 2003 and 2005 workshops organized by ESA at ESRIN (Figure 2.79). The workshops assessed the state of the art in the field, formulated recommendations for algorithm development, new products as well as future missions and applications. The Institute was involved in the scientific organization of the workshops and participated with key contributions.

Figure 2.79 Scientific exchange: European conference on Pol-InSAR topics.

As a direct result of the recommendations made at the first Pol-InSAR Workshop, the Polarimetric SAR Data Processing and Educational Tool has been developed under ESA contract by a consortium comprising the University of Rennes 1, DLR and AEL Consultants. POLSARPRO aims to facilitate the accessibility and exploitation of multi-polarized SAR data sets. A wide-ranging tutorial and comprehensive documentation provide a grounding in polarimetry and polarimetric interferometry necessary to stimulate research and development of scientific applications that exploit polarimetric data and techniques. All results of the POLSARPRO project are distributed by ESA free of charge.

Looking into the future, Pol-InSAR techniques will be faced with the potential and the challenges arising from an extended observation space provided by multi-baseline, multi-frequency, bi- and multistatic sensor configurations forcing the evolution of quantitative measurement and information product generation in SAR remote sensing.

2.2.5 Tomography

As presented in the previous section, polarimetric SAR interferometry is a suitable technique for measuring vegetation height and for inferring biomass via suitable models. However, it is not possible to obtain information about the vertical backscattering structure of the volume without using appropriate models with a-priori information of the volume scatterer distribution. SAR tomography allows a three-dimensional (3-D) imaging of the volume, i.e., it allows a vertical separation of scattering centers at different heights. It is a direct measurement technique in the sense that it does not require a model. The first demonstration of SAR tomography has been carried out at DLR using airborne L-band repeat-pass data showing the imaging of forest areas with a vertical resolution of the order of a few meters [47].

The tomographic imaging technique can be understood as the generation of an additional synthetic aperture perpendicular to the flight track. This synthetic aperture consists of several parallel tracks or orbits with a horizontal or vertical displacement (Figure 2.80). A larger span of this aperture provides better resolution in the third dimension (height), and closer spacing between adjacent tracks influences favourably the unambiguous height range, i.e., the volume height to be imaged. Therefore, it is beneficial to obtain as many tracks as possible at an adequate minimum distance from each other. Typically, the number of images *N* is between 5 and 15 in order to be able to distinguish *N-1* layers in the volume.

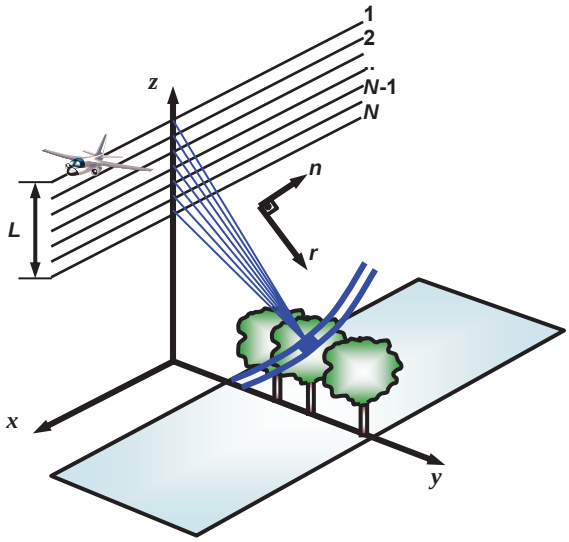

Figure 2.80 Flight geometry for 3-D imaging via SAR tomography using repeat-pass flight acquisition. A bistatic configuration consisting of several microsatellites flying in formation can be used in case of a spaceborne system realisation.

For generating a tomographic image, one first has to process all the SAR images taking into account that subpixel co-registration and precise phase conservation is required. Advanced motion compensation techniques must be used as described in section 2.2.2 for ensuring that the phase accuracy between the series of images is in the order of a few degrees. In a second step the focusing in the third dimension is performed for each resolution cell, corresponding to the generation of the synthetic aperture in the across-track direction. This step can be performed either via time-domain focusing methods like the back-

propagation technique or by Fourier domain approaches. For both cases the irregular track spacing associated with the motion errors and the limitations of the navigation system accuracy turned out to be a challenge in the development of the tomographic processing chain. In several segments in the azimuth direction of the tomographic flight tracks the minimum spacing between the tracks of ca. 20 m required for the unambiguous tomographic imaging was violated due to turbulences and inaccuracies in the maintenance of the nominal flight track by the aircraft pilot. The developed technique to decrease the ambiguities associated with the non-regular track spacing leads to a signal-to-ambiguity reduction greater than 15 dB.

The fully polarimetric L-band mode of the Intstitute's E-SAR system was selected for the tomographic experiment. 14 tracks of full-polarimetric L-band data were acquired by the E-SAR system in 1998 at a nominal spacing of 20 m. Figure 2.81 shows the real horizontal spacing obtained in this experiment, to achieve an unambiguous volume height of 35 m and a height resolution of 3 m in the mid range of the image. The temporal decorrelation between the images was very small, showing a coherence higher than 0.9 even over forested areas.

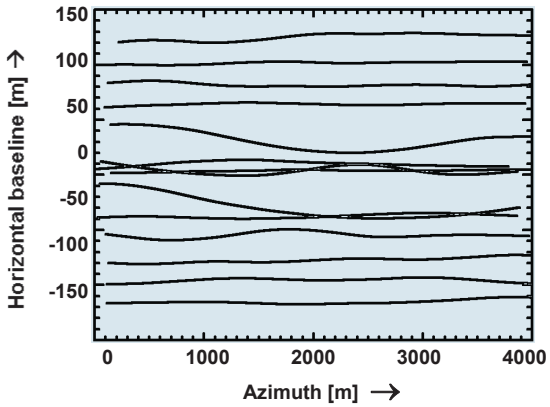

Figure 2.81 Actual flight tracks configuration of the first airborne experiment dedicated to SAR tomography. 14 tracks were flown with a nominal separation of 20 m. One additional track was flown at 0 m baseline to verify the temporal decorrelation between the first and last acquired images (time separation of ca. 3.5 hours).

Investigations of a spruce forest area reveal the potential of SAR tomography, especially in combination with polarimetry. As shown in Figure 2.82 the following contributions can easily be distinguished: 1) dihedrale scattering with a phase center at a height of ca. 5 meters due to the ground and stem interaction (clearly seen in the HH-VV channel of the Pauli decomposition) and 2) random volume scattering in the crowns (dominant in HV-polarisation). The separation of the scattering centers in height between ground and canopy also gives a good indication of forest height (ca. 20 m) and height of crown above ground and indicates no presence of understory for this forest type. Several other tomographic plots of deciduous and mixed forests have shown that the canopy can generally be assumed to be a random volume at L-band, confirming the model used for height retrieval with the polarimetric SAR interferometric technique in the previous section.

The repeat-pass scenario used in this demonstration requires a relatively high effort to acquire a single tomographic data set. Today's research work concentrates on the reduction of the number of acquisitions by means of spectral estimation techniques. Further research has been performed toward the spaceborne implementation of tomography, for example in connection with the mission proposal HABITAT (section 2.1.9). With the selection of proper orbit configurations, 3 or 4 microsatellites in a repeat-pass scenario can acquire suitable tomographic data after 2 to 3 revisit cycles of the satellites. The effect of the temporal decorrelation in this acquisition scenario related to the selection of the optimal baselines is also a research topic that could be verified by a further airborne experiment.

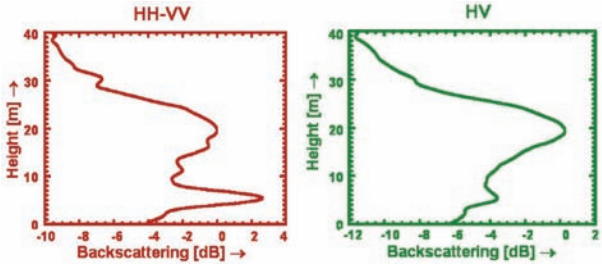

Figure 2.82 Distribution of backscatter intensity vs. height for a spruce forest in different polarisations (HH-VV and HV). The plot on the left shows the strong reflection at ca. 5 m height caused by the double bounce scattering due to the interaction between tree trunk and ground (observed in the HH-VV channel of the Pauli representation). On the right the dominant reflection of the canopy observed in the cross-polarisation channel (HV+VH) is recognised.

2.2.6 New Airborne SAR - F-SAR

F-SAR identifies the successor of the well-known E-SAR system and is under development at the Institute. The development was triggered by the strong demand of E-SAR users and customers for data being simultaneously acquired at different wavelengths and polarisations as well as by the demand for very high range resolution. E-SAR cannot cope with these requirements due to design and technological limitations. F-SAR is a totally new development utilizing most modern hardware and commercial off-the-shelf components. As for E-SAR DLR's Dornier DO228-212

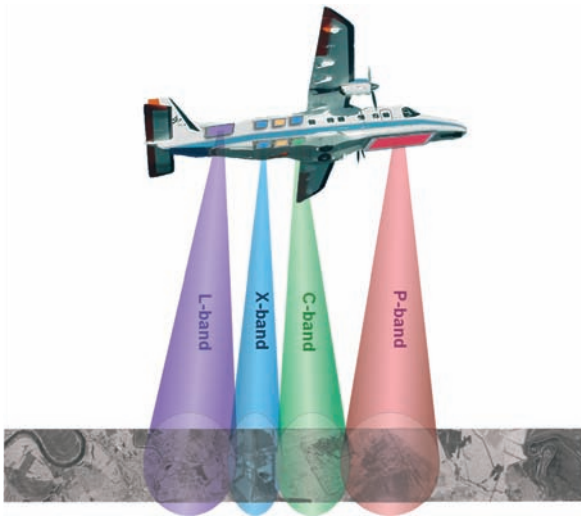

Figure 2.83 Artist's view: F-SAR acquiring data simultaneously in X-, C-, L- and P-band.

aircraft was the first choice as platform for the new system (Figure 2.83).

F-SAR is a fully modular system and will operate in X-, C-, S-, L- and P-bands with

- fully polarimetric capability in all frequencies,
- single-pass polarimetric interferometry capability in X- and S-band,
- four recording channels with data rates of up to 2 Gbit/s per unit,
- precise internal calibration (relative accuracy better than 1 dB) and
- fully reconfigurable operation modes including capability for digital beamforming on receive.

Furthermore, repeat-pass Pol-InSAR will be a standard measurement mode. Range resolution in each frequency band has been defined by specific user requirements. While 100 MHz has been adopted for P-band, a Step Frequency approach is used to achieve up to 800 MHz effective signal bandwidth in X-band to satisfy the requirement for very high resolution.

The F-SAR system comprises a basic system control and data acquisition sub-system to which individual RF subsystem modules are connected (Figure 2.84). System control is based on an extended CAN bus and Ethernet concept. This gives the necessary flexibility and the degrees of freedom to configure the system optimally for carrying out the desired measurements and experiments such as bistatic SAR. Further, the concept makes an extension to any other RF band an easier task.

A new antenna mount designed to fix planar array antennas to the aircraft is under development (Figure 2.85). Fully fledged in multi-frequency configuration it holds 7 right-looking dual polarised antennas: X-band (3), C-band (1), S-band (2) and L-band (1). The P-band antenna is mounted under the nose of the aircraft as indicated in Figure 2.83.

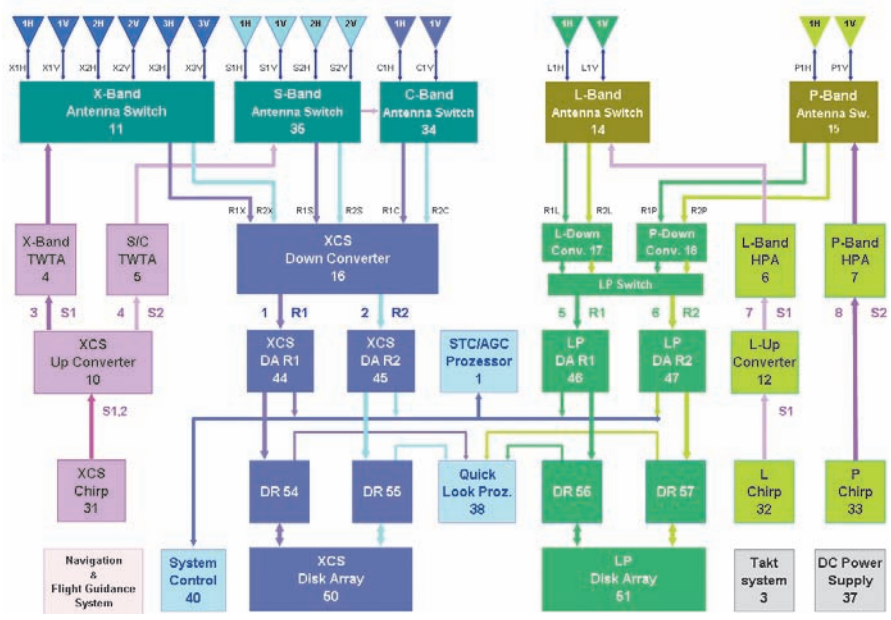

Figure 2.84 F-SAR system configuration for multi-frequency and polarimetric operation in X-, C-, S-, L-, P-band including single-pass interferometric capabilities in X- and S-band.

One important advantage of the antenna mount will be that it makes easier to change the antenna configuration and to mount other antennas avoiding individual airworthiness certification procedures at the same time. Main F-SAR technical parameters are given in Table 2.9. The radar is designed to cover an off-nadir angle range of 25 to 55 degrees at altitudes of up to 6000 m above sea level, which is the maximum operating altitude of the DO228.

Table 2.9 F-SAR technical characteristics.

	X	C	S	L	P
RF [GHz]	9.60	5.30	3.25	1.325	0.35
Bw [MHz]	800	400	300	150	100
PRF [KHz]	5	5	5	10	12
PT [kW]	2.50	2.20	2.20	0.70	0.70
Rg res. [m]	0.3	0.6	0.75	1.5	2.25
Az res. [m]	0.2	0.3	0.35	0.4	1.5
Rg cov. [km]	12.5 (at max. bandwidth)				
Sampling	8 Bit real; 1 Giga sample or 500 Mega samples; max number of samples 64 K per range line; 4 recording channels				
Data rate	247 MByte/s (max. per rec. channel)				

Figure 2.85 New F-SAR antenna mount attached to the right-hand side of the aircraft behind the wing allowing 7 antennas to be integrated.

A central computer unit controls the radar via a CAN bus and Ethernet (Figure 2.86). There are 4 modes of operation:

- System configuration
- System test
- Internal calibration
- Radar operation

The required synchronous timing and clock signals are generated in the main timing unit with less than 6 ps jitter and rise times of less than 80 ps. A 50 MHz ultra-stable quartz oscillator is the reference. The IGI D-GPS/INS based precision navigation system delivers a GPS 1 PPS signal which regularly triggers an absolute time stamp in the raw data header.

In its basic configuration the radar operates with four 1-GS ADC. The timing unit allows for two additional ADC. Each ADC unit has integrated raw data formatting thus the number of recording channels can be easily increased if needed. High-speed data recording units are connected via optical fibre. A second optical fibre links the ADCs to the control computer (monitoring bus) for internal calibration and system monitoring. Quick-look processing will be implemented via dedicated hardware and an optical fibre link to the data recording units. On-line and/or off-line operation is possible.

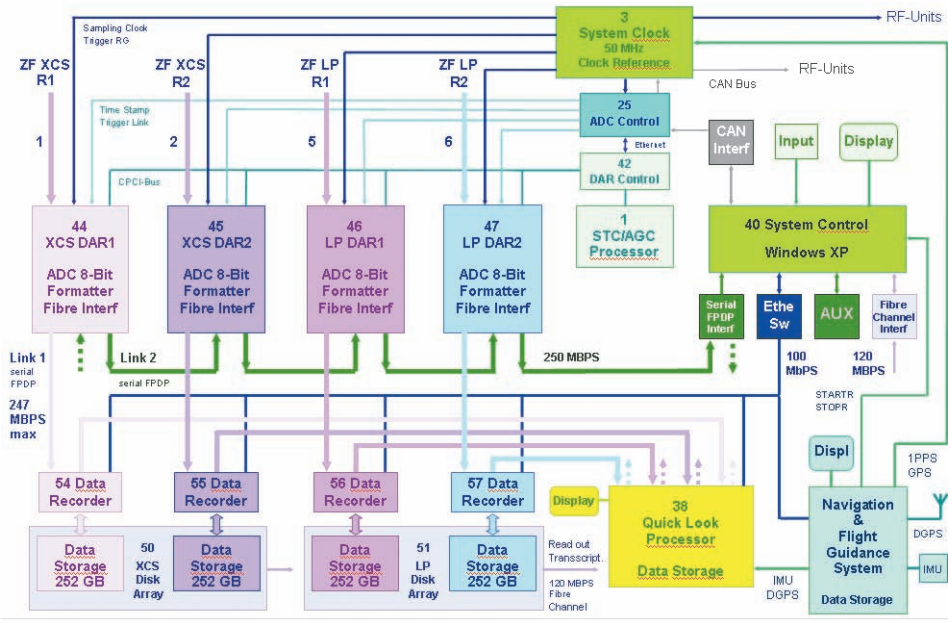

Figure 2.86 Block diagram of the F-SAR system control and data acquisition sub-system.

F-SAR is in the building phase and has successfully passed a series of laboratory tests. The maiden flight of the new radar is planned for late 2006. Alternative solutions for a more suitable aircraft with improved performance in terms of flight range and altitude are being investigated in order to better cope with the requirements of future campaigns and missions.

2.3 Microwave Systems: Research and Technology

2.3.1 Bistatic and Multistatic SAR

Bistatic and multistatic synthetic aperture radar operates with transmit and receive antennas mounted on separate platforms (Figure 2.87). Such a spatial separation has operational advantages, increasing the capability, reliability and flexibility of future SAR missions and generating new, innovative data products.

Interest in such systems has significantly increased in the last few years and bistatic SAR (one transmitter, one receiver) is now a major topic at many international remote sensing conferences. This upsurge goes hand in hand with progress in satellite navigation, communications and miniaturisation, allowing the realisation of concepts, previously regarded as unfeasible. Several proposals for spaceborne missions have been made; e.g. BISSAT (Italy), TerraSAR-L Cartwheel (ESA, section 2.1.4), TechSAT21 (USA), Radarsat-2/3 tandem (Canada), as well as our own TanDEM-X (DLR, section 2.1.3).

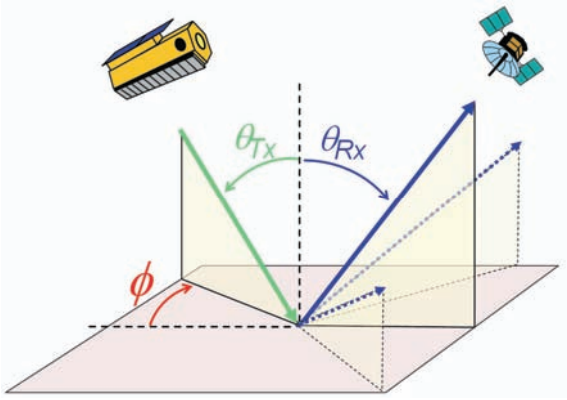

Figure 2.87 Scattering geometry of bistatic and multistatic (dotted) SAR systems with different incidence θ_{Tx} and departure θ_{Rx} angles for the transmit and receive signals. The planes are also offset by ϕ.

Eventually, the capabilities of such systems may cause a paradigm shift in radar remote sensing, replacing conventional large and complex monostatic radar satellites by clusters of small and low-cost microsatellites operating in consort. By distributing the functions, modular and scalable designs are conceivable, reducing the mission risk and enabling a wealth of new imaging modes, which can even be dynamically reconfigured to serve changing tasks [28] [391] [501]. Some capabilities are:

- Single-pass cross-track interferometry for the derivation of global, precision DEMs
- Along-track interferometry for global measurements of ocean currents and sea ice drift
- Polarimetric SAR interferometry for forest mapping and global biomass estimates
- Ambiguity suppression for wide swath SAR imaging with high resolution
- Frequent monitoring for the detection of fast scene changes and timely information
- Multi-baseline SAR tomography for 3-D imaging of semi-transparent volume scatterers
- Multi-aperture ground moving target indication for large area traffic monitoring
- Double differential SAR interferometry for the measurement of vertical scene displacements
- Multi-angle SAR imaging for improved segmentation, classification and object recognition

Mission Definition and Constellation Design

An important parameter in defining a spaceborne SAR mission is the selection of a suitable orbit. This becomes even more important for bistatic and multistatic radar missions, where two or more satellites must cooperate to acquire the necessary data. One example is a system for frequent monitoring, whereby a dedicated radar transmitter located in geostationary orbit illuminates the scene and multiple receivers in low Earth orbit collect the scattered energy (Figure 2.88). This distribution of tasks allows the use of small, low-cost microsatellites as receivers, thereby reducing the revisit time without excessive cost.

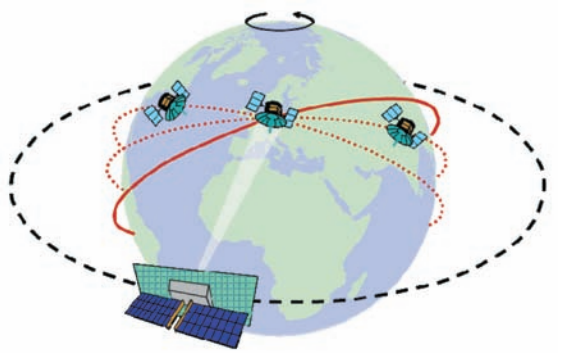

Figure 2.88 Bistatic SAR system consisting of a geostationary illuminator with multiple receivers mounted on small satellites in low Earth orbit.

An alternative concept for frequent monitoring is to deploy satellite constellations in medium Earth orbits, where each satellite accesses a huge area.

Different requirements arise for multistatic SAR interferometry, which calls for close satellite formations. Several concepts suitable for across-track and along-track interferometry have been studied and patented [25] [149]. Some of these formations are described in section 2.1.4.

A major challenge is the avoidance of collision between satellites. This is achieved by using the patented Helix concept [620], which ensures a safe satellite separation for arbitrary along-track displacements and which will be used for TanDEM-X (section 2.1.3).

Performance Estimation

The geometry of a bistatic SAR differs significantly from that of a monostatic SAR. An example is the geostationary illuminator concept of Figure 2.88, where the long transmit path remains almost constant while the relatively short and fast varying receiver path provides the Doppler modulation for high resolution SAR imaging.

Such systems require new algorithms for performance analysis necessitating the development of a bistatic performance estimator (section 2.3.6) [28] [210]. Figure 2.89 shows the predicted sensitivity for the geostationary illuminator system of Figure 2.88 and demonstrates the feasibility of such a system with a moderate transmit power-aperture product of 10^5 W/m^2.

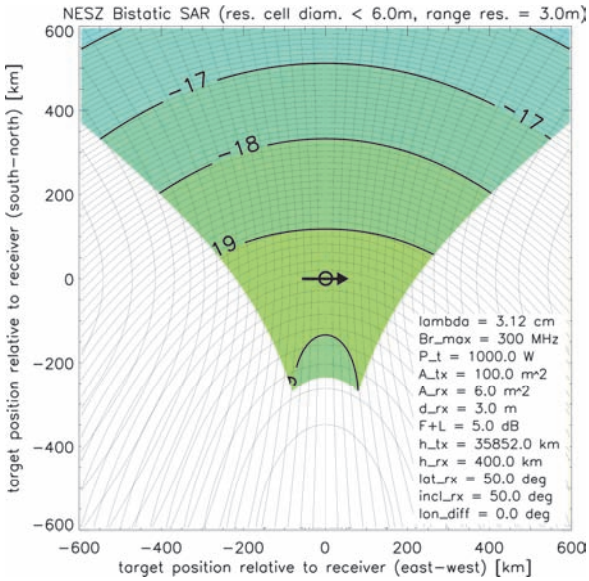

Figure 2.89 Noise equivalent sigma zero (NESZ) in dBm^2/m^2 for a bistatic SAR combining a geostationary illuminator with a LEO receiver. The grey lines show the contours of constant range and Doppler in an Earth tangent plane spanning an area of 1200 km x 1200 km. The receiver motion is indicated by the arrow.

A detailed model was also developed for the analysis of the interferometric performance of multistatic satellite constellations [25]. This model was used, for instance, to predict the height accuracies for the TanDEM-X and Cartwheel concepts (sections 2.1.3 and 2.1.4). For an ESA study on polarimetric and interferometric missions it was used to predict the performance of spaceborne Pol-InSAR systems [29].

Bistatic and Multistatic SAR Processing

The spatial separation of the transmit and receive paths in a bistatic SAR system requires the development of new algorithms for high resolution SAR processing. Bistatic SAR data from stable configurations, where the relative position of the two platforms remains fixed, can often be processed by adapting the monostatic processing algorithms. However, new algorithms are required to focus the bistatic returns from configurations where the transmitter-receiver separation changes during the data take [314].

Multistatic SAR data require different processing approaches. The combination of the signals from multiple receivers can be linear, e.g. linear signal summation, as in the case of digital beamforming (section 2.3.2), or non-linear, as required for the various interferometric modes. By using these techniques in combination, it is possible to significantly improve the performance. An example is the combination of multi-baseline cross-track interferometry with differential ranging [28] [391] (Figure 2.90). This enables the generation of ultra high resolution DEMs with sub-meter height accuracy without the need for phase unwrapping, which can be a challenge for normal interferometry. Large interferometric baselines can be used, the phase ambiguities of individual pixels being resolved by means of differential time delay measurements.

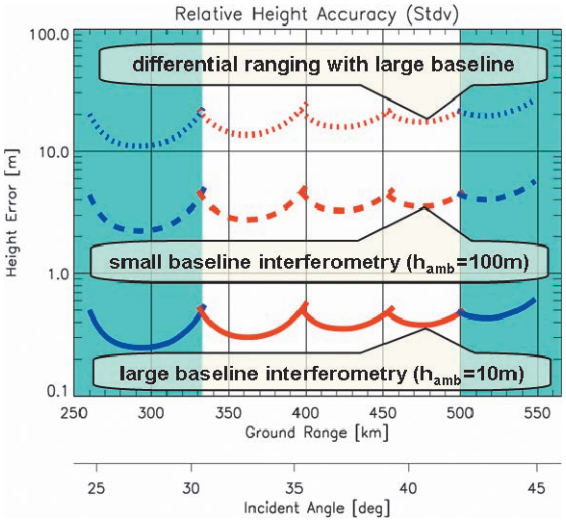

Figure 2.90 Predicted DEM performance for multi-baseline single-pass data acquisition. The interferometric height accuracy is shown for two baselines corresponding to a height of ambiguity of 100 m (dashed) and 10 m (solid). The dotted line is the predicted height accuracy for differential ranging. The height accuracy from differential ranging remains below the height of ambiguity of the small baseline interferometry, thus enabling efficient ambiguity suppression without the need for phase unwrapping.

Further potential arises from multiple aperture sensing for the suppression of range and azimuth ambiguities. For example, a coherent combina-

tion of the signals from multiple receivers separated in an along-track formation, a so-called sparse aperture SAR (Figure 2.91), achieves suppression of azimuth ambiguities by taking advantage of a new multi-aperture signal reconstruction algorithm [27] [155] (section 2.3.2). It is then possible to:

- improve the azimuth resolution
- increase the imaged swath width, and
- reduce the required antenna area.

The sparse aperture configuration is also well suited to GMTI and traffic monitoring applications, since it enables efficient clutter suppression and high accuracy velocity measurements (section 2.3.4).

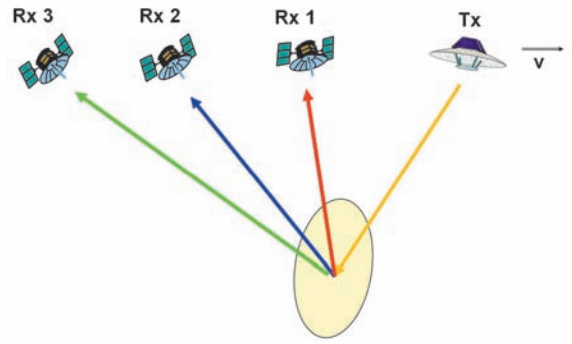

Figure 2.91 Multistatic sparse aperture SAR for high resolution, wide swath imaging with small receiver antennas.

Synchronisation of Bistatic SAR Systems

Further investigations addresses the impact of local oscillator stability during bistatic and multistatic SAR data acquisitions. Oscillator errors deserve special attention in distributed coherent radars, since there is no cancellation of low frequency phase errors as in a monostatic SAR, where the same oscillator signal is used in the transmitter and receiver (Figure 2.92). To investigate the errors, a system model was developed [30] [59], which describes the resulting phase fluctuations. Analytic expressions were then derived for typical errors like the time variant shift, spurious side-lobes, and the broadening of the impulse response, as well as the low frequency phase modulation of the focused SAR signal. To combat the degradation, several synchronisation strategies were developed. Figure 2.93 shows the reduction of the azimuth impulse response deterioration by using a periodic phase referencing concept. This synchronisation technique will be implemented for the TanDEM-X mission
(section 2.1.3), where radar pulses are periodically exchanged between the instruments via dedicated horn antennas.

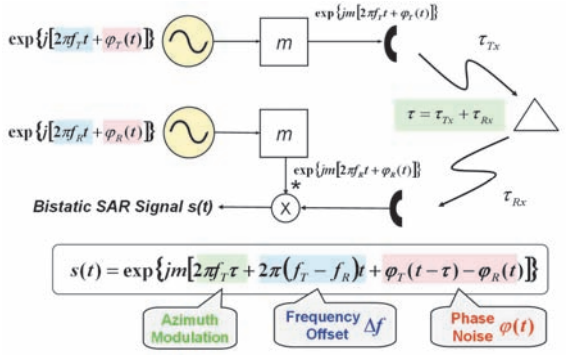

Figure 2.92 Derivation of base-band bistatic phase errors after down conversion. f_T and f_R denote the transmit and receive oscillator frequencies, φ_T and φ_R are the corresponding phase errors, and τ is the travel time of the radar pulse.

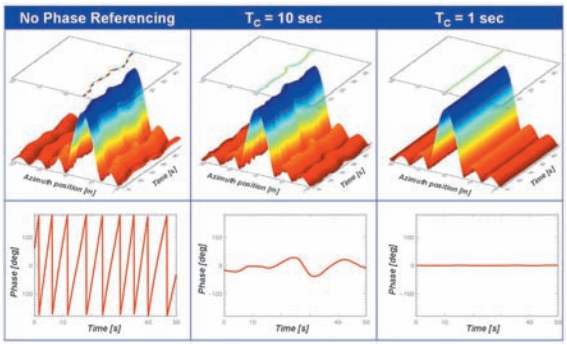

Figure 2.93 Simulated bistatic SAR impulse response in L-band. The upper plots show the simulated profile of the azimuth response without synchronisation (left), phase referencing every ten seconds (middle), and phase referencing every second (right). The lower plots show the corresponding impulse response phase errors in the range from -180° to + 180°.

New Multistatic Imaging Techniques

A wealth of new bistatic and multistatic SAR imaging techniques has been suggested in [28]. Examples are range resolution enhancement beyond the ITU bandwidth limitations, 3-D tomographic mapping, or the measurement of small height changes by double differential SAR interferometry [391]. Further potentials arise from a combination of bistatic radar with digital beamforming on receive (section 2.3.2).

Another opportunity is the parasitic use of communication and navigation satellites, which provide a free illumination source. In order to explore the capabilities and limitations of such parasitic systems, an experimental setup has been built as shown in Figure 2.94. First results are very promising and yield well-focused impulse responses using the television signals from the Astra digital TV satellites for scene illumination. In a future step, the receiving antennas will be moved on tracks to demonstrate synthetic aperture imaging.

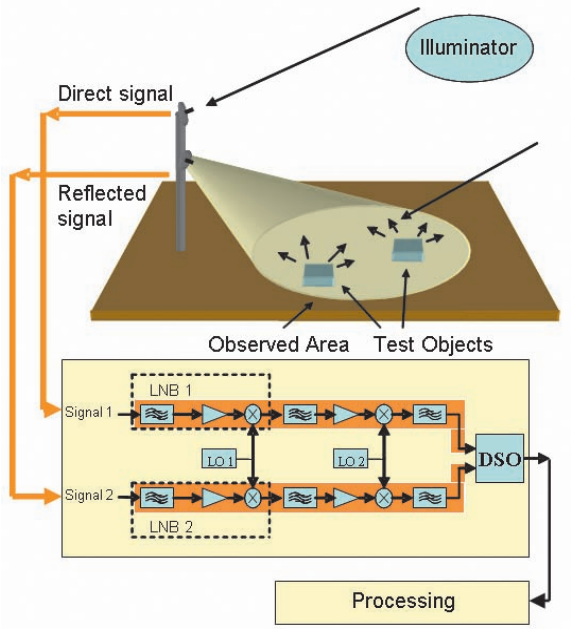

Figure 2.94 Experimental setup for the demonstration of radar imaging based on illumination from a digital TV satellite. One antenna directed at the satellite receives a reference signal while a second antenna directed at the scene receives the reflected signals from the targets. Range focusing is achieved by correlating the two signals.

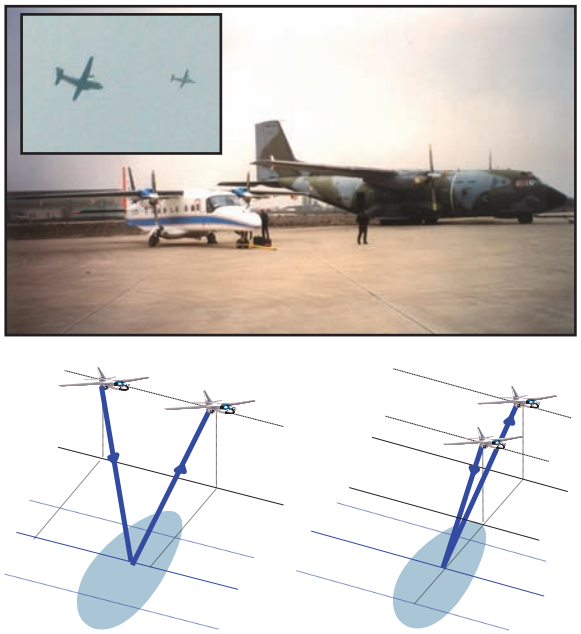

Figure 2.95 Bistatic airborne SAR experiment. Top: the two aircraft on the ground and (inset) in the air; below: the two bistatic configurations, left: quasi monostatic geometry with the aircraft following closely on the same track, right: bistatic geometry.

Bistatic Airborne SAR Experiment

In order to explore the potentials and challenges associated with bistatic radar, DLR and ONERA conducted a joint bistatic airborne SAR experiment with their radar systems E-SAR and RAMSES in February 2003 in southern France (Figure 2.95, top). Two bistatic configurations were flown.

In the first configuration, a quasi monostatic mode, the two planes flew very close to each other to acquire interferometric data in a single-pass across-track configuration with a vertical separation of about 20 m. This successfully demonstrated two-platform bistatic SAR interferometry for the first time [10].

The second geometrical configuration was designed to acquire images with different bistatic angles. An impressive result is shown in Figure 2.96 which is an overlay of three SAR images with different bistatic angles [141]. The strong colour variation between the different areas in the image demonstrates the high information content in multistatic SAR products.

The results from the bistatic airborne SAR experiment clearly demonstrate the technical feasibility of bistatic SAR imaging and the great potential for the extraction of new scene parameters.

Figure 2.96 Colour composite of three SAR images with different bistatic angles, showing the good differentiation of surface features.

Bistatic and multistatic radar is an emerging technique with great potential for a broad range of new remote sensing applications. The combination of practical experience and theoretical expertise makes the Institute a key player in this strategically important field.

In addition to the continuation of theoretical investigations, further bistatic airborne experiments are planned together with ONERA in 2007.

An important outcome of the work has been the successful TanDEM-X mission proposal. A big step forward is expected from the bistatic experiments planned during this mission.

2.3.2 Digital Beamforming

Digital beamforming (DBF) is a technique, whereby the receiving antenna of a radar system is split into multiple sub-apertures. In contrast to analog beamforming, e.g. as employed in TerraSAR-X, the signal from each sub-aperture element is separately amplified, down-converted, and digitised (Figure 2.97). The signals are combined with a digital bus, avoiding the combiners of conventional antennas arrays and, hence, potentially simplifying antenna integration. The coherent combination of the sub-aperture signals allows the formation of multiple beams with arbitrary shapes. The technique does not necessarily require multiple transmit beams, significantly simplifying the antenna design. Hence, digital beamforming on receive is enjoying the greatest interest.

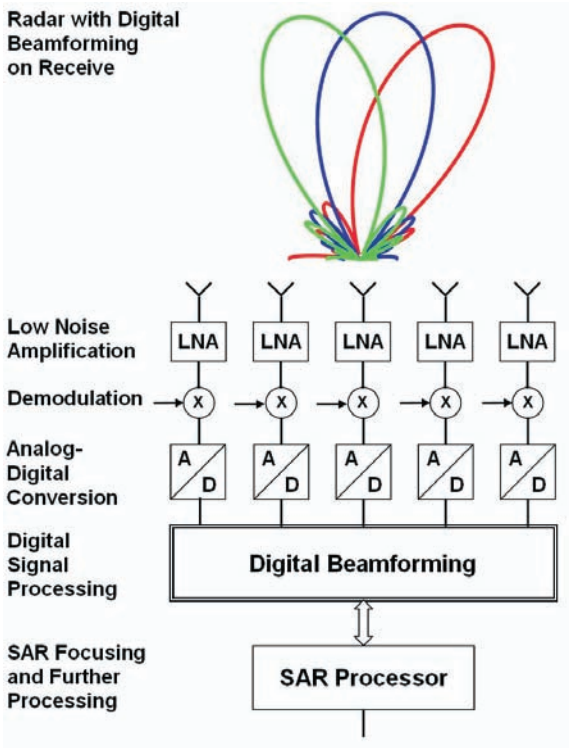

Figure 2.97 Schematic of digital beamforming on receive. The signal from each sub-aperture element is independently amplified, down-converted, and digitised. The digital processing enables flexible and adaptive beamforming after the signal reception.

Digital beamforming is a powerful technique to gather additional information about the direction of scattered radar echoes during the acquisition of SAR images. The flexibility of this a posteriori beamforming process can be used to:

- improve the geometric resolution by combining multiple narrow Doppler spectra to a wide azimuth spectrum,
- improve the radiometric resolution without reducing the imaged area. The receive gain is increased by switching between narrow, high gain beams,
- suppress range and azimuth ambiguities by null-steering,
- suppress interference from specific directions by space time adaptive processing, and
- gain additional information about the dynamic behaviour of the scatterers and their surroundings.

Hence, digital beamforming is regarded as a key technology for the development of powerful, highly flexible SAR systems in the future.

Sector Imaging Radar

A first demonstration of the potentials of digital beamforming on receive was the development of an innovative forward looking imaging radar for enhanced vision. The technique generates high-quality radar images in any desired direction, and is, hence, also suitable for forward looking airborne radars (FLAR).

Figure 2.98 Top: Antenna system attached to the skids of the helicopter. Bottom: SIREV antenna with 56 receiving subarrays.

The system is based on a DLR patent [627] and denoted Sector Imaging Radar for Enhanced Vision, SIREV. In contrast to SAR systems, no relative motion is required between the sensor and the targets. The high frame repetition frequency enables the detection and measurement of very rapid changes in dynamic scenes. Further modes are interferometric mapping, as well as a true 3-D tomographic mapping of semi-transparent scatterers.

To verify and demonstrate SIREV an X-band experimental system was assembled and flown on a helicopter [26]. An antenna was built by IHE, University of Karlsruhe with sequential switching of the receiving antenna elements and was connected to existing radar hardware of the company Aerosensing. The available bandwidth of 100 MHz and the wavelength limited the image resolution, but were sufficient to prove the concept. Figure 2.98 illustrates the antenna system and its attachment to the helicopter. Details of the radar hardware and the antenna system can be found in [67]. The work was funded by Atlas Elektronik GmbH.

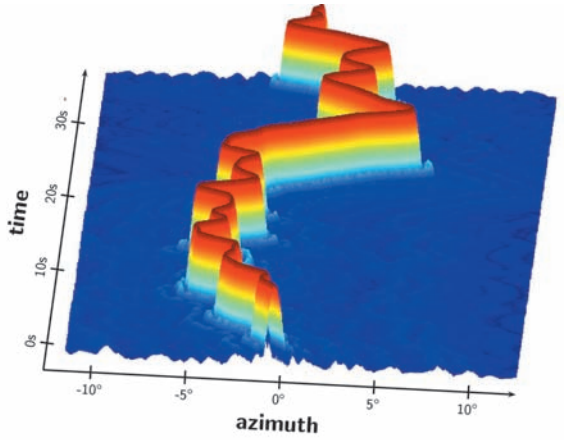

Figure 2.99 Temporal sequence of a corner reflector response obtained as the helicopter moved forward. The result shows good azimuth focusing in spite of the helicopter motion.

A fast processing algorithm was developed for SIREV, which allows accurate, phase preserving image formation. Raw data were obtained from a demonstration flight close to Oberpfaffenhofen. Motion errors of the platform were extracted from an analysis of the recorded data, avoiding the necessity of an inertial navigation system (Figure 2.99).

The results show good agreement with theory. After the image formation, coherent and incoherent averaging were applied to improve the image quality. The required motion compensation for coherent averaging was derived directly from the recorded data by computing the interferometric phase difference between subsequent SIREV images (Figure 2.100, left). The final result was an image sequence composed of several thousand images. An animation of the image sequence is available at:
http://www.dlr.de/hr/sirev/home.html.
The right hand side of Figure 2.100 shows one image of this sequence.

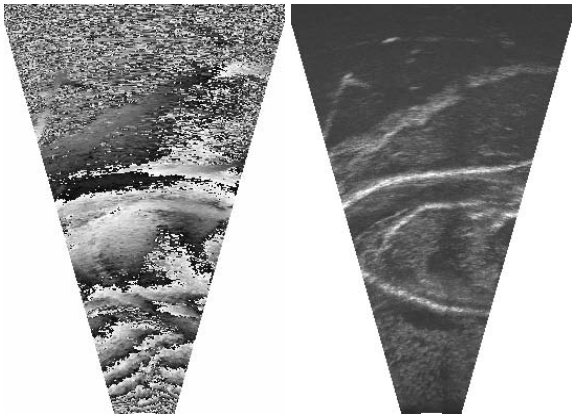

Figure 2.100 Left: interferogram between successive SIREV images. Right: SIREV image of the river Lech.

High Resolution Wide Swath SAR Imaging

The unambiguous swath width and the achievable azimuth resolution pose contradicting requirements on SAR system design. To overcome this inherent limitation of a spaceborne Stripmap SAR, several innovative techniques have been suggested based on splitting the receiving antenna into multiple sub-apertures with individual receiver channels. By combining the digitally recorded sub-aperture signals a posteriori in a linear space-time processor it is possible to form multiple independent beams and to gather additional information about the direction of the scattered radar echoes. This technique is especially promising in combination with small aperture transmitters illuminating a large footprint on the ground.

An example for such a system is the High Resolution Wide Swath (HRWS) SAR which combines the displaced phase center (DPC) technique in azimuth with time variant beam steering in elevation (Figure 2.101). The DPC technique is used to gain additional samples along the synthetic aperture to suppress azimuth ambiguities. The time variant beam steering in elevation is used to improve the SNR without reduction of the swath width. This is achieved by steering the receive beam to follow the radar pulse as it travels over the ground.

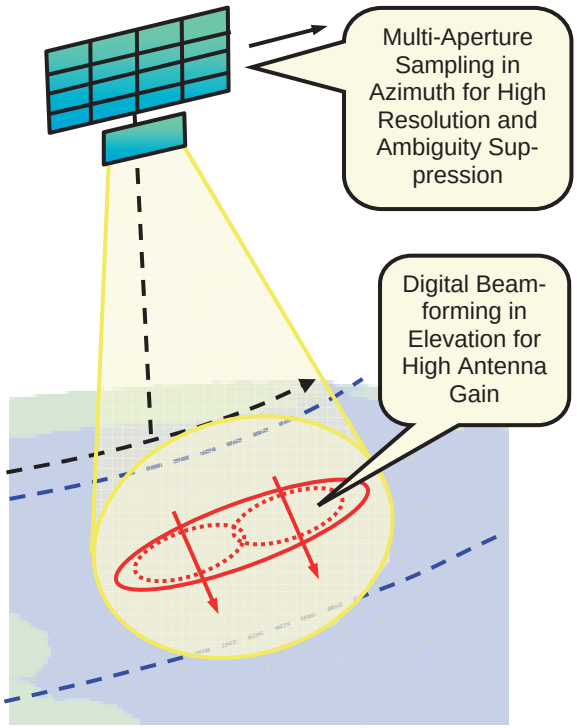

Figure 2.101 High Resolution Wide Swath (HRWS) SAR system. The combination of the displaced phase center technique with time variant beam steering in elevation enables large area imaging with high resolution.

Azimuth Processing Techniques

The application of the classical displaced phase center technique in a HRWS SAR system puts a stringent requirement on the PRF, which has to be chosen such that the SAR platform moves half the antenna length between successive radar pulses. However, such a rigid selection of the PRF in order to obtain a uniformly sampled synthetic aperture may be in conflict with the timing diagram of the SAR for some incidence angles. It also precludes the use of a higher PRF for improved azimuth ambiguity suppression.

To avoid such a restriction, a new reconstruction algorithm was developed, which can recover the unambiguous Doppler spectrum even in the case of a non-uniform DPC sampling [27] [155]. The raw data acquisition in a multiple aperture SAR is described using a linear multi-channel systems model, as shown in Figure 2.102.

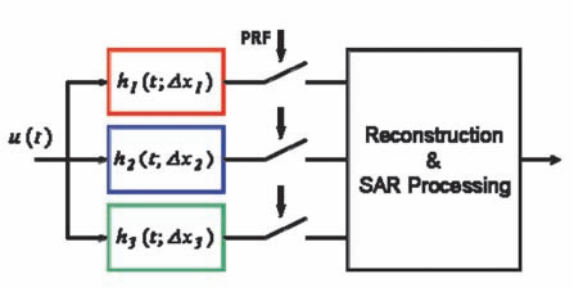

Figure 2.102 Multi-channel linear systems model for multiple aperture SAR. The SAR data acquisition is described by the linear filters on the left. The sampling with a pulse repetition frequency PRF, which is lower than the Nyquist rate, introduces ambiguities for each channel. The unambiguous SAR signal can then be recovered by a joint coherent processing of the recorded signals from all receiver channels.

Each channel on the left-hand side of Figure 2.102 describes the bistatic data acquisition by one sub-aperture element. The signals are sampled with a PRF which is lower than the (Doppler) bandwidth, making the output of each channel highly aliased. The unambiguous SAR signal spectrum is then recovered by coherent multi-channel SAR processing which eliminates the ambiguous parts of the individual Doppler spectra (Figure 2.103). This reconstruction algorithm can also be regarded as a time-variant digital beamforming on receive process, which combines the individual receive signals in a general space-time processing framework.

Use of this algorithm means that the stringent PRF restriction is avoided and it is applicable to systems relying on the DPC technique, like the HRWS SAR or the dual receive antenna concept in TerraSAR-X and Radarsat-2.

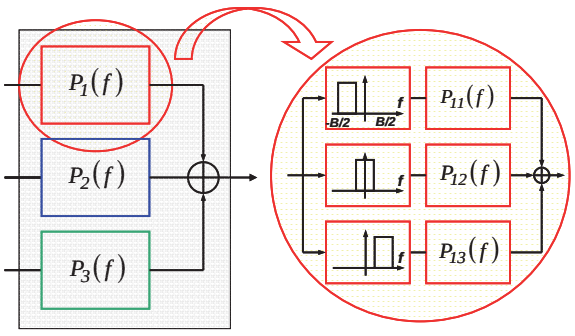

Figure 2.103 Unambiguous signal reconstruction in a multiple aperture SAR with three channels. Each reconstruction filter $P_i(f)$ consists of n=3 band-pass filters $P_{ij}(f)$. The transfer functions $P_{ij}(f)$ are derived from a generalised multiple channel system matrix describing the data acquisition in Figure 2.102.

The validity of the algorithm has been tested by simulation. Figure 2.104 shows the predicted response of the TerraSAR-X dual receive antenna mode to an extended scatterer before (top) and after (bottom) applying the reconstruction algorithm. It is evident that the ambiguous responses are suppressed.

The algorithm has also been applied to real SAR data acquired by the DLR E-SAR system. Figure 2.105 compares the reconstructed image (right) to the ambiguous image for one channel with a highly non-uniform sampling (left).

The azimuth processing for multiple aperture SAR systems is further being investigated in an ongoing contract from EADS Astrium. The goal of this study is the development of a technology demonstrator for a future spaceborne HRWS mission. It has been seen that azimuth processing plays a key role in designing such systems.

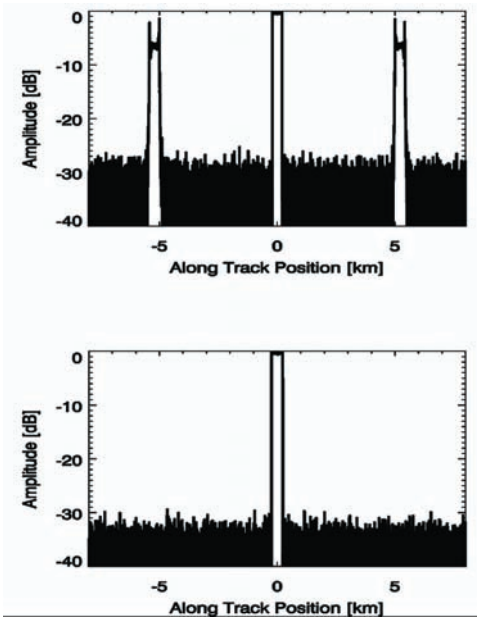

Figure 2.104 Azimuth response for one sub-aperture (top) and after non-uniform DPC antenna reconstruction (bottom) showing the suppression of the ambiguous responses.

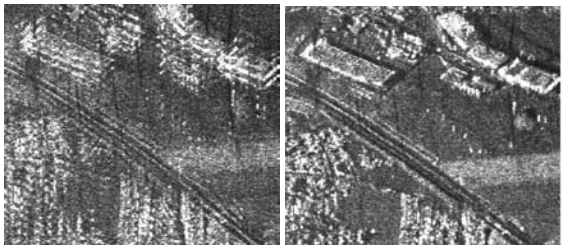

Figure 2.105 Ambiguous image for one channel with non-uniform DPC sampling (left) and after reconstruction with the ambiguities suppressed (right).

Beamforming in Bistatic and Multistatic SAR

Digital beamforming on receive is also of great interest in combination with bistatic SAR systems, such as the example of the geostationary illuminator in combination with passive LEO receivers (section 2.3.1). Such a system has the peculiarity that the length of the transmit path exceeds by far the distance from the target area to the receiver. As a result, the antenna footprint of the geostationary illuminator will be much larger than the footprint of the LEO receiver. Hence, a receiver with a fixed aperture antenna will only see a part of the illuminated footprint. Such a waste of energy can be avoided by splitting the receive antenna into multiple sub-apertures with individual receiver channels (Figure 2.106). Each element then sees a larger area on the ground, and by combining the receiver data it is possible to obtain additional information on the target area. Additional information can be used to:

- increase the azimuth resolution
- reduce range and azimuth ambiguities
- detect moving objects, and
- improve the radiometric resolution.

The concept of digital beamforming on receive can further be extended to multistatic satellite configurations, where each satellite antenna forms one element of a huge, but sparsely populated aperture. The new ambiguity suppression techniques introduced in the previous section can be adjusted to such satellite formations. This enables the use of microsatellites for large satellite clusters with reconfigurable baselines. Flexible baseline selection allows new, powerful imaging modes to be realised. These can be dynamically adapted to changing requirements, thus serving a broad range of remote sensing applications [28] [391].

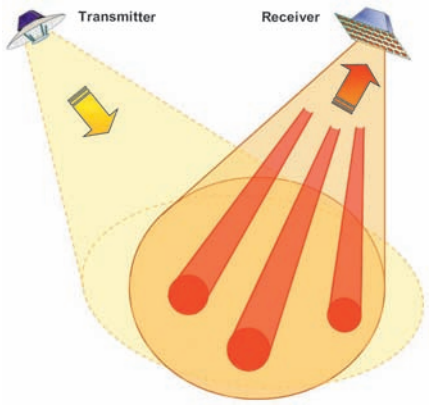

Figure 2.106 Bistatic SAR with digital beamforming on receive. The transmitter illuminates a wide area on the ground. Digital beamforming on receive allows for the formation of multiple narrow beams with high antenna gain. This improves the sensitivity without reduction of the coverage area, as required for high resolution wide swath SAR imaging.

Digital beamforming on receive is a promising technique to overcome fundamental limitations of conventional SAR systems. An important application is high resolution wide swath imaging, as required for many remote sensing applications. This is of special importance for applications dedicated to the observation of dynamic processes like differential and permanent scatterer interferometry which enable the measurement of millimeter displacements from subsidence, landslides, and seismic deformations. Here, a wider image swath allows the use of orbits with shorter revisit times without sacrificing full coverage.

The beamforming techniques developed in the Institute will play a key role in designing future multi-channel radar systems. The technology for such radars is currently being developed in a joint DLR/ESA project.

A first demonstration of high resolution wide swath SAR imaging is planned with the dual receive antenna mode in TerraSAR-X. More advanced demonstrations will become possible with TanDEM-X which provides four independent channels with distributed phase center positions.

Much research is still required to fully exploit the potentials of the DBF technique for spaceborne radar remote sensing. One current example of research at the Institute is the suppression of interference from specific directions. This may gain in importance as the frequency spectrum becomes more and more congested. Another example is the combination of azimuth ambiguity suppression techniques with moving target indication, supporting applications like wide area traffic monitoring (section 2.3.4). Yet another is digital beamforming on transmit with non-separable space-time waveforms. This enables a systematic distribution of the signal energy on the ground together with a significantly improved ambiguity suppression capability. Such systems can be operated in a hybrid mode, devoting more system resources to a limited area of high interest without losing wide coverage.

A potential spin-off could be the use of the DBF techniques to develop a Tsunami Early Warning System (TEWS), which is currently being investigated in a nationally funded study (2.3.11).

Further work is being devoted to the development of efficient data reduction strategies for multiple aperture SAR systems, alternative DBF architectures for improved ambiguity suppression by pre-beam shaping and new and more efficient multi-channel processing algorithms.

2.3.3 Inverse SAR Imaging - ISAR

Reliable global reconnaissance using remote sensing techniques requires a weather and time independent detection, recognition, and identification capability. High resolution spaceborne radar systems, such as planned for reconnaissance (2.1.10) or implemented on TerraSAR-X (2.1.2), are appropriate instruments. When designing such a mission the availability of representative radar data from ground measurements is important, i.e. for the analysis, understanding and simulation of complex target signatures and to provide reference signatures for automatic target recognition (ATR).

Inverse SAR (ISAR) imaging allows the collection of very precise high resolution radar signatures from targets of interest. For a spaceborne radar system, the imaging geometry is similar and differs only by geometrical transformation and rotation as shown in Figure 2.107. With ISAR, a high spatial resolution in the decimeter range is accomplished by rotating an object on a turntable with respect to a spatially fixed broadband radar system, and by recording a sequence of corresponding radar echoes within a specific azimuth angle range.

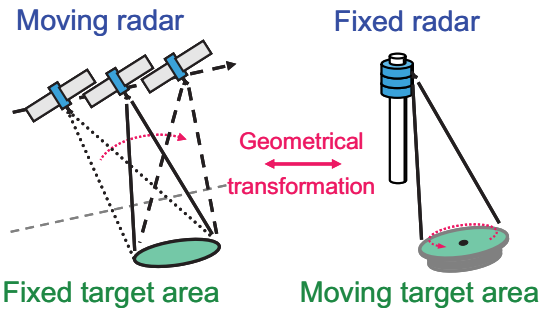

Figure 2.107 Geometry of a Spotlight SAR (left) and tower-turntable ISAR (right). Azimuth resolution is achieved by the relative rotary motion between sensor and target. For far field conditions the measured signatures are identical for both scenarios.

The measurements are performed at a range distance to the turntable of about 60 m. The typical incidence angles are from 24° to 50°, since only this angular range is feasible for a spaceborne radar, due to transmit power limitations.

Figure 2.108 shows the tower and the turntable, which was covered with soil and grass to provide a natural background. Calibration targets (e.g. corner reflectors and top hats) are arranged close to the turntable to allow an off-line data correction. In front of the turntable, a radar fence prevents disturbing reflections caused by the machinery from below the table.

The experimental radar system is based on a pulsed stepped-frequency waveform, offering a high degree of flexibility for the data processing and an inexpensive implementation for the signal generation and data acquisition.

However, corresponding longer measurement duration for a complete signature over an angular range of 360° has to be accepted. A network analyser (NWA) is used to generate the stepped frequency continuous wave signal. A unit containing a transmitter and receiver, including the pulse modulator, was developed. The received and low-noise amplified signal is transferred to the NWA for I/Q detection. An angle encoder delivers the azimuth position of the turntable, and a PC controls the whole measurement system and stores the data [185].

Figure 2.108 Photograph of the tower-turntable arrangement at the Meppen proving ground. Left: The tower with different platforms at heights between 30 m and 50 m. Right: the turntable about 9 m in diameter.

The recorded complex radar backscatter signals are processed coherently off-line to produce an image. The range resolution is determined by the signal bandwidth used, and the cross-range resolution by the extent of the azimuthal angular range, which is analogous to the synthetic aperture of a SAR. A straight forward implementation of a SAR matched filter commonly demands high computational effort. A variety of algorithms reducing the computations exists with various approximations and limitations. As the ISAR data are sampled on a polar grid, a straight-forward application of a two-dimensional (2-D) FFT would result in defocusing errors. For our purposes, the back-projection method, the adapted polar format algorithm and derivatives are convenient.

The back-projection algorithm first calculates the range profile from the spectral samples for each turntable position via a one-dimensional (1-D) FFT. Afterwards the consecutive 1-D interpolated range profiles are back-projected and coherently superimposed in the image plane, according to their specific range direction. This method offers the advantage of an inherent spatial adjustment to the polar grid of the raw radar data. The computational effort of using the back-projection is primarily determined by the image size and can be reduced by selecting only the interesting parts of the image area [186].

The polar format method enables the use of a 2-D FFT by correct localisation of the data samples in the spectral domain. Usually, an interpolation is applied to resample the spectral data on a rectilinear equidistant grid. Due to the limited size of the illuminated scene and available computer performance, a fast and precise method was established by relocating the samples accurately on a finer zero-filled grid. In this way, the data is correctly sampled and the image is formed in one computational step. However, for the imaging of larger scenes, the extended data space can be a drawback. For the near-range geometry and the steep incidence angles used, a rectification method was adapted to correct the image [188].

In order to benefit from both methods, a hybrid of back-projection and a precise linear subaperture version of the polar format was used. The hybrid processing starts with a pixel preselection of a polar format image with a small extension of the data space. It is completed with a back-projection of the highly resolved range profiles onto the selected pixel grid. The subaperture method consecutively transforms rectilinear parts of the fine zero-filled grid in the frequency domain into the image domain. After selection of each focused unambiguous area, the coarsely resolved images are resampled, and then coherently superimposed to form the final image [188] [190].

Figure 2.109 shows some results. The first column represents the coarse target orientation on the turntable, the second column the distribution of the scattering centers and the third the distribution of the persistent scatterers. The signatures were generated using the polar format processing. These images illustrate the different characteristics of radar images compared to optical images even for almost completely metallic objects. This is mainly due to the coherent signal processing, the steep incidence angle, and the monostatic illumination.

For a better visual comparison, an incoherent overlay was generated (Figure 2.110). The shape and the size of the target can be determined very accurately, as well as the turret orientation.

Once the corrected processing of the radar raw data has been performed to obtain radar cross-section (RCS) images of the target, an ATR approach is required to extract a maximum of information from the scene of interest. Because the typical objects of interest very often produce up to 30 characteristic scattering centers, sufficient suppression of noise, artefacts, and sidelobes is mandatory.

Weighting functions in the spatial frequency domain are commonly used to reduce the sidelobes in SAR imagery, usually accompanied by a degradation of spatial resolution. Because maxi-

mum resolution is normally required for target recognition, a method called spatial variant apodisation (SVA) was used to achieve maximum spatial resolution with a simultaneous reduction of side-lobes. This method was successfully adapted to the constraints of our near-range geometry and the steep incidence angles [185].

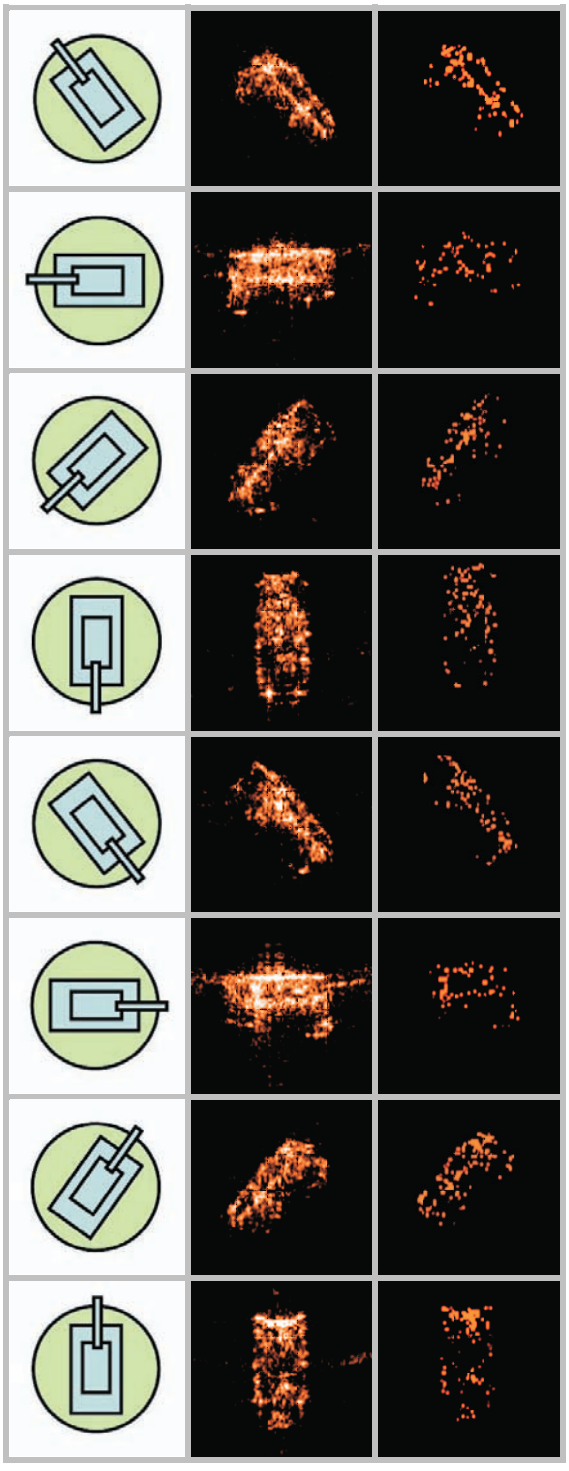

Figure 2.109 Left column: sketch of the target orientation; center column: reconstructed RCS image; right column: image showing the position of persistent scatterers.

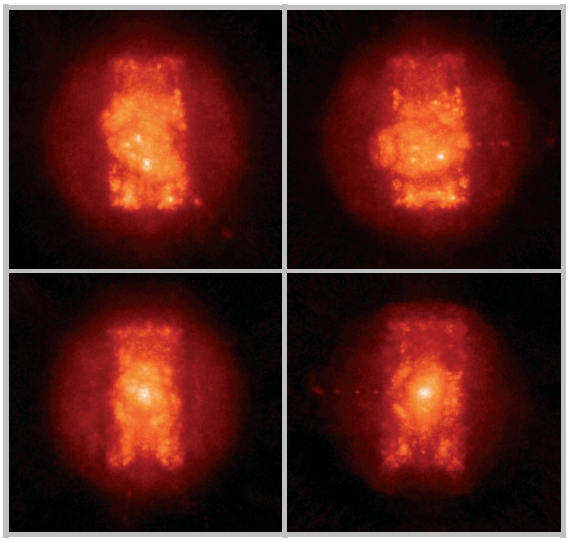

Figure 2.110 Incoherent superposition of single RCS images generated for various azimuthal aspect angles around 360°. The images show two different tanks with a different orientation of the turret.

The turntable measurement system can produce an irregular sampling in azimuth, due to the very low rotational speed and the very high weight of a tank. This can cause speckle noise and ambiguities in the reconstructed RCS images. In order to overcome such problems, a special filtering method was developed using the analysis of the phase to extract the most robust scattering centers of the target. These scattering centers behave like ideal point scatterers over a wide angular range, and typically the trihedral structures act similar to a corner reflector [186].

The right column in Figure 2.109 shows the images of the extracted robust scatterers after applying the phase analysis method. In order to investigate the ATR capabilities and the performance of such 2-D signatures, a template matching method was selected. This recognition and/or identification approach is designed to be tolerant with respect to moderate differences between test and training data. A principal advantage is the robustness against small differences in objects of the same type. For the application of this approach, an experimental database of several thousand images of about two dozen civil and military vehicles was collected.

The investigations also focused on the determination of robustness against variations in the articulation of the test objects, e.g. the different turret orientations in Figure 2.110. Also, the influence of camouflage, deception and multipath effects was explored; for the latter, an example is shown in Figure 2.111.

The results show promising recognition performance; a low false alarm rate, adequate in-class robustness combined with satisfactory inter-class separation was achieved, at least for large armoured vehicles [187] [193] [379] [380].

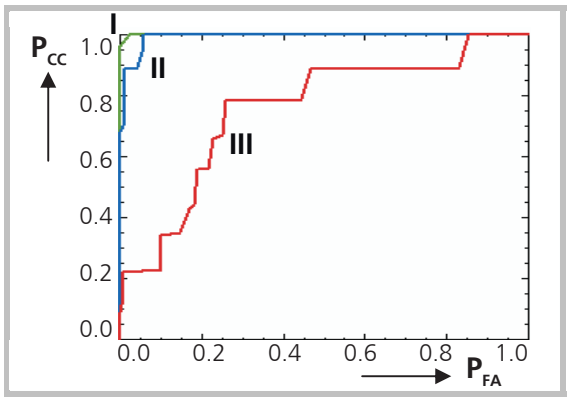

Figure 2.111 Influence of multipath effects on the percentage of correct classification (P_{CC}) as a function of the false alarm rate (P_{FA}), curve I: Test object on rural ground, curve II: Test object orientated in non cardinal directions on metal covered ground, curve III: Test object in cardinal directions on metal covered ground. The curves indicate decreasing recognition performance in urban environments.

Future goals are the identification and analysis of the scattering behaviour of complex targets and to make measurements of more objects to complete the data base.

2.3.4 Traffic Monitoring

The DLR is pursuing three coordinated traffic monitoring projects. One investigates the processing segment for traffic data based on satellite or airborne sensor data and formulates the requirements, also for the other two projects, TerraSAR-X and TRAMRAD (Traffic Monitoring with Radar), in which the Institute is active. As described in 2.1.2, TerraSAR-X will have a mode allowing dual channel operation for moving target detection, and the provision of dedicated traffic monitoring products.

The project TRAMRAD was established to investigate the possibilities of using airborne or spaceborne radar for the monitoring and control of road traffic [457] [102]. The goal is the definition of realizable system concepts for radar systems, which are able to frequently extract wide-area traffic data for traffic monitoring or, in extended time intervals, for traffic planning. Presently, such data are not available for traffic management. Although systems utilizing Floating Car Data (FCD) are candidates for this task, they have severe limitations outside urban conurbations. TRAMRAD is intended to pave the way to a dedicated future traffic monitoring system.

Especially spaceborne missions exhibit a large diversity of orbit and system concepts. Section 2.3.1 describes multistatic concepts, like the geostationary illuminator, which could be exploited for TRAMRAD. Before developing concrete system concepts, MTI (moving target indication) methods have to be studied and evaluated with respect to their suitability.

The first phase of TRAMRAD, which was completed with a review [457], comprised fundamental studies and first simulations of existing MTI methods and techniques [456] [486] [487]. Advantages and limits were studied in order to identify and assess the most promising methods for collecting traffic data in a wide area. Also, extensive simulation results regarding the radar signatures of road vehicles, as well as the surrounding clutter environment have been conducted [479].

An important step forward will be the formulation of consolidated user requirements which are the basis for reliable mission and system requirements. For defining user requirements at first hand, a user workshop was organised at the Institute with attendance from traffic management centers, industry and responsible authorities.

The preliminary conclusions are that there is a short-term need for non-cooperative systems capable of providing wide area traffic data at short time intervals. Hence, airborne platforms also need to be considered. Also, the performance analyses are promising, giving confidence that a suitable system can be found. TRAMRAD continues with a demonstration phase, whereby the F-SAR airborne SAR will be suitably modified and an experimental campaign will be performed. Finally, the overall system has to be defined, so that a dedicated mission can be planned.

SAR/MTI

In general, with standard SAR processing it is not possible to detect and focus moving targets on the ground, because SAR assumes stationary scenes. One major challenge of MTI is the detection of slowly moving targets in the presence of clutter. To perform effective clutter suppression, at least two antennas arranged in the along-track direction are necessary (Figure 2.112). The achievable improvement of clutter suppression was demonstrated by processing dual-channel experimental E-SAR data (Figure 2.113) and by simulation [456].

A further challenge is the correct estimation of target velocities. After processing E-SAR data, it could be shown that the estimation of across-

track velocities and Doppler slopes of moving targets is possible with high accuracy by applying a matched filter bank and fractional Fourier transform in combination with along-track interferometry (ATI) and time-frequency analysis. The correct estimation of along-track velocity without using a priori knowledge, like a digital road map, is still unsolved for dual channel systems, because the effect of along-track velocity and across-track acceleration on moving target's Doppler cannot be separated [456]. Further investigations are necessary to overcome the problem of reliable along-track velocity estimation.

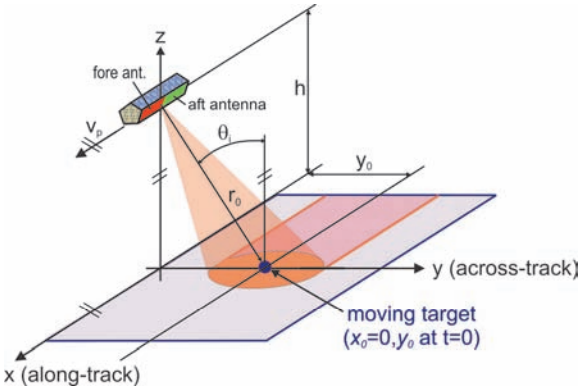

Figure 2.112 Example of two-channel side-looking radar-target geometry used for the SAR/MTI simulations. The antennas (marked in red and green colour) are arranged in along-track direction for clutter suppression and velocity estimation.

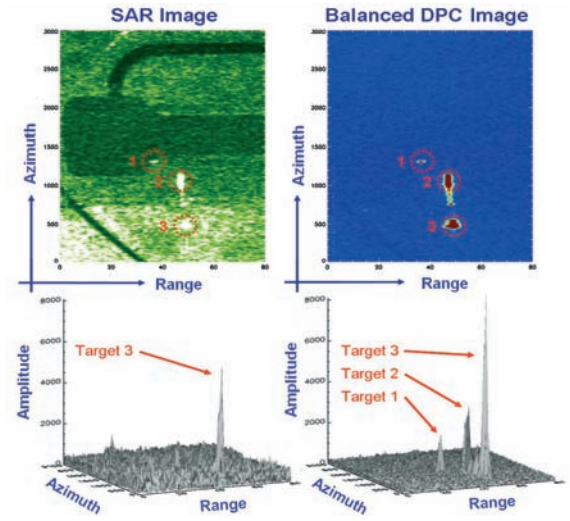

Figure 2.113 Clutter suppression using DPC technique and channel balancing. All moving cars no. 1-3 could be detected from the DPC image on the right. The results were derived from experimental E-SAR data. Left: normal processed SAR image.

Depending on the system and antenna configuration, MTI performance can be further increased with multi-channel systems. A third receiving antenna can improve clutter suppression, eliminate blind velocities and resolve ambiguities in the measurement of across-track velocity [486].

Multiple Channel Systems

Multiple channel techniques combine adaptive array techniques with SAR processing. While classical SAR systems process the received signals either in the time domain or frequency domain, multi-channel systems can spatially separate signals by beamforming on receive (section 2.3.2). This is necessary especially for the detection of slowly moving targets, because the received signals are ambiguous in the frequency domain but resolvable in the spatial domain. Thus, the sensitivity of systems in the angle-Doppler plane was also studied. The sensitivity plane of a non-equidistant four-channel along-track configuration is shown in Figure 2.114. The main diagonal passing through zero Doppler at 90° (broadside direction) exhibits a sharp notch, which suppresses the clutter. Even slow moving targets will be outside this clutter notch and, hence, remain unattenuated. As can also be seen, additional clutter notches result from spatial or temporal subsampling. Their positions are defined by the PRF and the antenna separations [456]. The width of the clutter notch mainly depends on the overall length of the antenna. To obtain suitable multiple channel data for developing the processing algorithms, a first experimental campaign with an airborne four-channel system (section 2.2.6, F-SAR) is planned for the end of 2006.

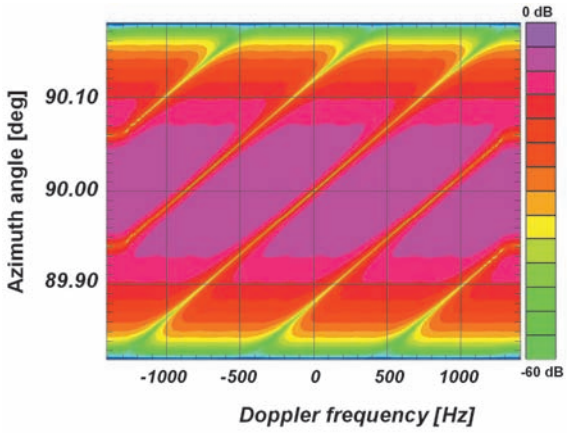

Figure 2.114 Transfer function of a four-channel non-equidistant along-track configuration plotted as a function of azimuth angle and Doppler frequency. Yellow shows the areas where signals are suppressed. Violet is maximum gain.

Furthermore, Space-Time Adaptive Processing (STAP) techniques were studied and the differences between airborne and spaceborne systems investigated [487]. Fundamental differences mainly result from the different height, velocity and stability of the platform. At present, the performance bounds on the detection probability and motion parameter estimation accuracy are being derived for comparison of different system concepts.

Radar Signatures of Road Vehicles

To estimate the requirements for the radar instrument and to assess MTI methods and techniques, representative radar signatures of road vehicles need to be known. The Institute's radar signature modelling tools SIGMA and BISTRO are used (section 2.3.9). With SIGMA, the monostatic radar cross-section (RCS) of electrically large structures such as cars can be computed [479]. The target and the background are modelled by flat panels as shown in Figure 2.115. The top row of images shows the target, a Volkswagen Golf car, whereby the red coloured panels indicate an orientation perpendicular to the path of propagation, representing the specular points, which contribute most to the RCS. The bottom row of images shows the double reflections between the road and the vehicle, and it can be seen that they can significantly raise the total RCS**.** High RCS values for most vehicles occur when they are viewed from the front, back and, especially, from the side.

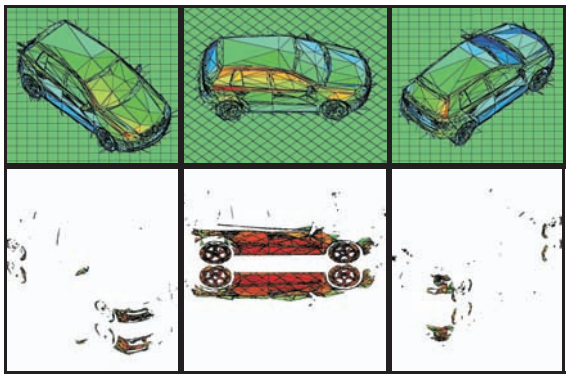

Figure 2.115 Single (direct) reflections (top row) and double reflections (bottom row) of a Golf V car; incidence angle 45°; azimuth angle: 45°, 90°, and 135°. Top: red panels indicate specular reflection; blue: grazing incidence. Bottom: double reflection contributions (vehicle to road and vice versa).

Bistatic radar signatures are also under investigation because bistatic radar offers promising system concepts for TRAMRAD. Since both SIGMA and BISTRO require large computation time, very simple representative geometrical structures are needed as substitutes that allow fast modelling of the scattering and, hence, fast analysis of system parameters. First attempts show that for small ranges of aspect angle a car can be substituted by groups of simple metallic shapes. In Figure 2.116, the monostatic signature of a car is compared with that of a substitute model comprising four metal cylinders. The substitute is a good likeness and can be used for SAR and MTI performance modelling.

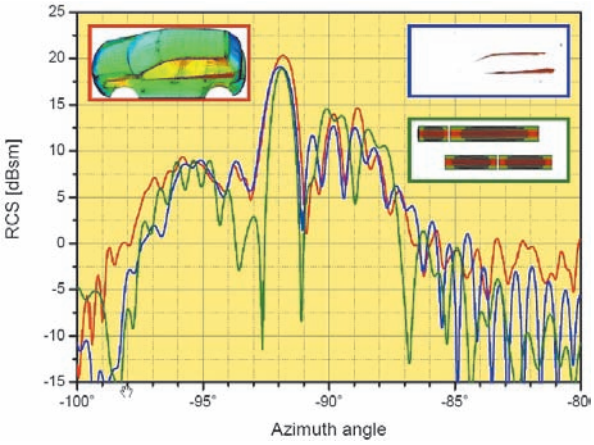

Figure 2.116 Monostatic signature (red curve) of a car (top left inset), signature (blue curve) of the dominant panels (top right inset) and the signature (green curve) of the substitute model consisting of four metallic cylinders (middle right inset). The substitute cylinders exhibit a good RCS likeness.

Encoding Transponders

In spite of the high resolution achieved by SAR instruments, the resolving power is generally insufficient to identify small objects. A transponder technique using encoding has been developed with a view to tagging objects, so that they can be unambiguously identified in a SAR image [17]. The encoding technique requires no modification of the SAR. The SAR data can be processed to image the transponders with the background suppressed.

The encoding transponder has applications in many areas of RFID (radio frequency identification). As the technique augments the capability of a SAR to image the Earth's surface with high resolution, even from space, the encoding transponder has unique powers for wide-area, long range RFID. This could be very useful for monitoring vehicles tagged with encoding transponders.

2.3.5 End-to-End SAR Simulation

The generation of experimental SAR data representative of the new advanced systems is both expensive and time consuming, particularly where parameters and scenarios need to be varied. This is especially true for spaceborne systems. The need for simulation tools for analysis and evaluation is, therefore, essential and led to the development of the **S**AR **E**nd-**T**o-**E**nd **S**imulator SETES [336].

SETES is based on realistic mathematical modeling of an overall SAR system chain and generates information on the quality of the image data and its suitability to interpret target and background signatures. The simulator fulfills several objectives:

- Estimation of SAR system's capabilities and determination of trade-offs during the design phase
- Analysis and demonstration of the system's reaction to changes of operational requirements under space conditions
- Analysis and elimination of system defects and determination of their effects on the image quality
- Support for training SAR operators and image interpreters

The flexible and modular structure of the simulator allows for adjustment and extension to fulfill different tasks. The principal components of SETES are:

- The generation of the scene, including the fully polarimetric scattering behaviour of the 3-D surface and objects, and including typical SAR effects like overlay, speckle noise, shadowing, etc.
- An accurate SAR sensor simulation (antenna, transmit and receive path)
- Generation of the raw data
- Image processing and evaluation

Simulation Preparation

For the preparation of an end-to-end simulation, SETES includes several graphical editors for selecting the simulation parameters, i.e. for the orbit data, the timing parameters, and two editors for the interactive scenario generation.

Background Module

Input data for the background module are a high resolution Digital Elevation Model (DEM), and photos or maps supporting the definition of the electromagnetic properties of the different classes of the background environment. The tasks of the module are the co-registration of the various data sources and the creation of a material map containing the electromagnetic properties of all facets of the DEM. For this purpose user-defined material classes, e.g. asphalt, concrete, grass, soil, can be created. The module allows the assignment of the facets to the material classes in two different ways; these can be used separately or in combination:

- Automatic classification based on image intensities,
- Interactive selection by defining polygon areas.

The material classes contain all information necessary for the subsequent simulation.

Scene Module

The functionality of the scene module includes the visual creation or editing of target scenes with a Graphical User Interface (GUI). Selected targets are positioned (with translation and/or rotation) onto the background scene. The collateral information of the generated scene, e.g. the selected target types and positions, name of the background scene, is saved in a specified file.

Simulation Concept

The principal structure of the simulator is illustrated in Figure 2.117.

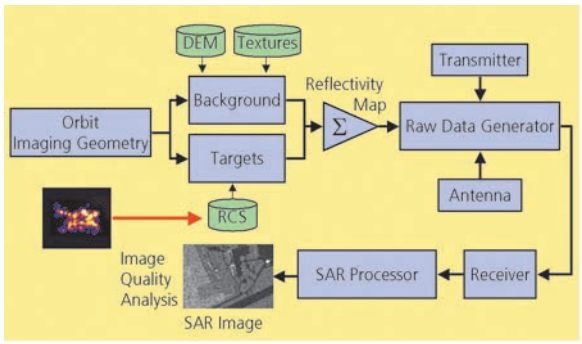

Figure 2.117 Principal structure of SETES with the main modules for orbit and imaging geometry calculations, the generation of the backscattering values, the generation of the raw data, and image processing.

The orbit and imaging geometry module calculates the state vectors of the sensor at all the time steps needed and delivers the coefficients for the coordinate system transformations between the Earth, platform, antenna, and scenario. The next two modules in Figure 2.117 are used for the calculation of radar cross-section values of the background for each facet (resolution cell) depending on geometry, permittivity, speckle, surface roughness and embedded targets. The module reflectivity map includes the projection of the reflectivity data onto the slant range plane of the SAR sensor. The resulting reflectivity map is the input to the raw data generator, which calculates the raw data depending on the desired SAR

mode. The system transfer function of the transmitter and azimuth antenna pattern are taken into account. Non-linear and time variant parts of the sensor are modelled in the receive path module before the image formation by the SAR processor. It is possible to use different types of processor algorithms, like the Chirp Scaling and wavenumber algorithm. Below, the main modules reflecting the basic physical models are described in more detail.

Reflectivity Map

The tasks of this module are to generate the backscattered reflectivity and to superimpose the RCS signatures of targets, and to perform the transformation of the reflectivity data onto the slant range plane of the SAR sensor.

To simulate realistic SAR raw data of extended background scenarios, the use of altitude profiles is necessary, since the influence of the relief plays a great role in the formation of the final image. It is essenetial to make allowance for specific SAR effects like layover, foreshortening and shadowing. Moreover, the change of the backscatter mechanism caused by different incidence angles and polarisations of the waves can be taken into account. The input DEM will be approximated by square plane facets, where each facet is characterised by its coordinates and the electromagnetic properties of the underlying material (defined by the background module). The backscattering coefficient of natural materials like soil or vegetation is the sum of contributions caused by surface and volume scattering. At L-, C- and X-band, volume scattering contributions are expected to be secondary in comparison to surface scattering and are neglected.

A great number of methods for calculation of the backscattering coefficients of rough surfaces have been described in the literature. Two robust and broadly used approximate analytic approaches are the Small Perturbation Model (SPM) and the Kirchhoff Model (KM). Both are implemented in SETES.

The SPM is valid at low frequencies, where the surface variations are much smaller than the incident wavelength and the slopes of the rough surface are relatively small. The KM is applicable at high frequencies for rough surfaces with radii of curvature that are large compared with the wavelength. A drawback of KM is its limitation to relatively small incidence angles. To overcome this, the Integral Equation Method (IEM) was implemented.

In addition to the theoretical models, empirical models for wide ranges of frequency, incidence angles and roughness are implemented. An empirical model using directly measured curves can also be used. Unlike the theoretical models, only the magnitudes of the backscattering coefficients are supplied.

In contrast to natural backgrounds, the surfaces of man-made targets, like vehicles, are smooth compared to the wavelength and have to be handled differently. Presently, the precise simulation of their RCS poses a great challenge, due to the complexity of geometrical models, and the fact that multiple scattering dominates the RCS signature. A possibility to fulfill this gap is the use of measured data. As described in 2.3.3, a database of several thousand high resolution RCS images of about two dozen civil and military vehicles was built up using turntable measurements and appropriate signal processing.

Using the information about position and orientation of the targets provided by the scene description file, the appropriate RCS signatures are selected, resized to the background pixel spacing before being inserted into the background reflectivity map. The resulting reflectivity map of the scenario is finally input to the raw data generation module.

Raw Data Generation

The flow chart of the raw data generation module is illustrated in Figure 2.118. It shows the basic structure of the algorithm for the Stripmap mode.

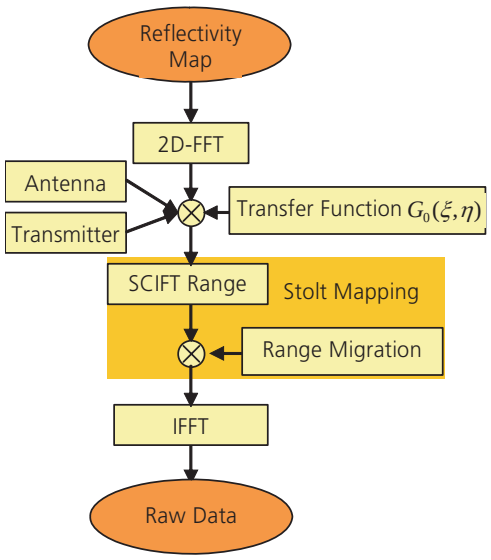

Figure 2.118 Flowchart for the raw data generation of the Stripmap mode with the space-independent part of the system transfer function, and the space-variant part referred to as Stolt mapping.

The raw data collected by a SAR sensor are not separable in azimuth and range directions, because of the range migration and curvature effects. In an analytical expression of the impulse response function, this dependence is given by

coupling terms in the azimuth and range directions. A precisely modelled impulse response function must be considered in two dimensions. In the time domain the range dependence can be taken into account easily, but the computing time is unacceptable for the required scenario sizes. A more efficient solution is obtained by calculating the raw data in the two-dimensional frequency domain. The algorithm used is based on an analytical evaluation of the system transfer function via the stationary phase method. A detailed evaluation of the system transfer function in the Fourier domain shows that it can be formulated as the product of two factors, a space-invariant factor and a space-dependent one. The latter requires non-linear mapping of the range frequencies, usually referred to as Stolt mapping. This algorithm avoids time-consuming interpolations. It uses a Scaled Inverse Fourier Transform (SCIFT), followed by a phase shift in the azimuth-frequency, range domain.

Receive Path Module

Figure 2.119 shows the flowchart of the receive path module. It has five main parts: the ideal modulation segment, carrier frequency segment, intermediate frequency segment, video segment, and digital storage.

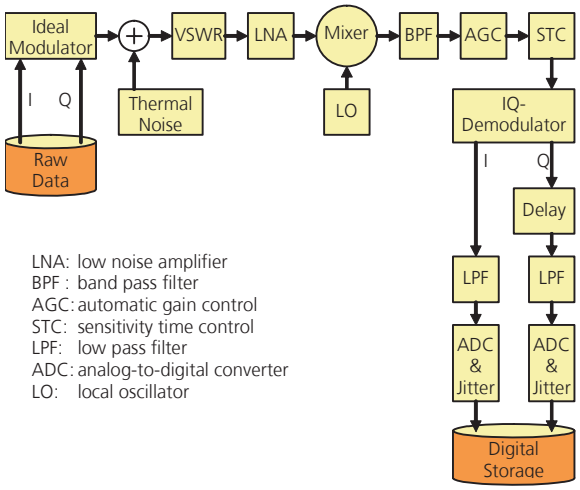

Figure 2.119 Receive path module of SETES with the particular modules for the carrier frequency segment, the intermediate frequency segment, and the video segment.

Only the first part, the ideal modulator, has no physical reference to a system component. The output data of the raw data generator are complex, i.e. I/Q samples. For reasons of compu tational efficiency, for the carrier frequency part, the simulator works in the intermediate frequency band. The modulator takes both I/Q signals and modulates them on the intermediate frequency to obtain a representation of the real signal.

The carrier frequency segment simulates the signal transmission from the antenna to the mixer. Thermal noise is introduced at the beginning of the chain. The other parts are supposed to be noise free. The Voltage Standing Wave Ratio (VSWR) module generates the effect of the mismatches in this receiver chain. The low noise amplifier and the mixer are treated as non-linear devices using polynomial approximations for the gain characteristics.

The intermediate frequency step is simulated as a band-pass filter, adaptive gain control and sensitive time control. The band pass filtering is performed by a Tschebyscheff FIR filter.

The video-segment begins in the I/Q detector module and ends in the ADC. The I/Q detector is simulated as an ideal demodulator with added phase and gain errors. A small time delay between both channels can also be introduced. After low-pass filtering, the analogue/digital conversion of the I and Q signals is simulated. ADC gain and offset errors are superimposed. The jitter effect due to clock errors is simulated by a random shift of the sampling time.

Simulation Examples

In Figure 2.120 the results of a parametric end-to-end simulation are shown. The underlying background scenario is based on the digital elevation model as a part from a real military typical airbase. The DEM has a pixel spacing of 0.5 m. The simulated spatial resolution is 1.5 m in both azimuth and range directions. The resulting SAR images in Figure 2.120 (a) - (d) illustrate the influence of the system noise, measured as the Noise Equivalent Sigma Zero (NESZ).

The distorted SAR image of Figure 2.121 demonstrates the effect of antenna mispointing in the flight direction, leading to Doppler errors. Such an effect can be caused in SAR systems with non-optimal beam steering.

The example shown in Figure 2.122 is a virtual scenario composed of a small residential area on the outskirts of a forest. The profiles of the buildings drawn in blue in the material map and the forest texture were superimposed on the DEM. Two vehicles were placed onto the roads, marked by red arrows. The associated RCS patterns were selected from the database using the appropriate azimuth and elevation angles.

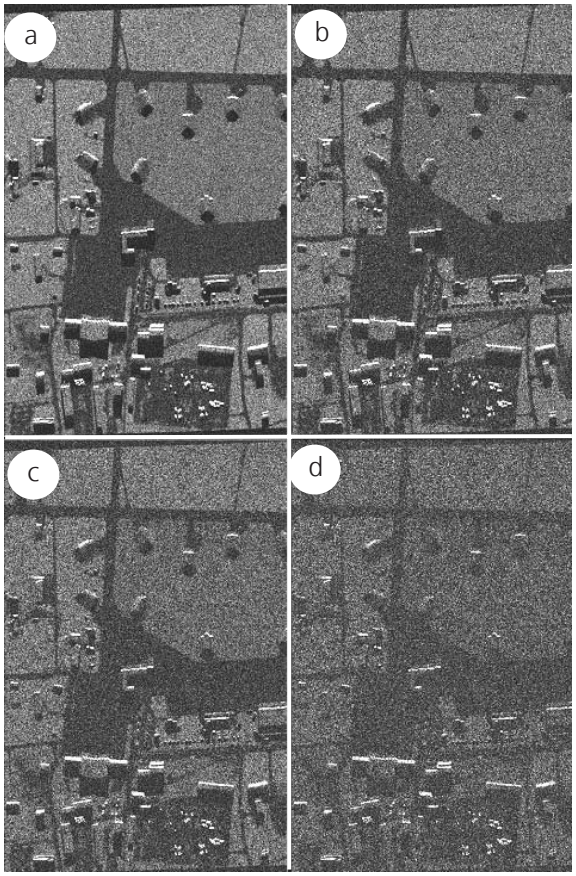

Figure 2.120 End-to-end simulations with variations of NESZ based on a realistic airport scenario: a) NESZ=-26 dB, b) NESZ=-20 dB, c) NESZ=-18 dB, d) NESZ=-13 dB.

The scenario was used for demonstrating the visibility of vehicles in urban areas depending on the orbit and the depression angle of the SAR sensor. In spite of the simple layout of the scene, all typical SAR effects like overlay, foreshortening, and shadowing can be easily recognised.

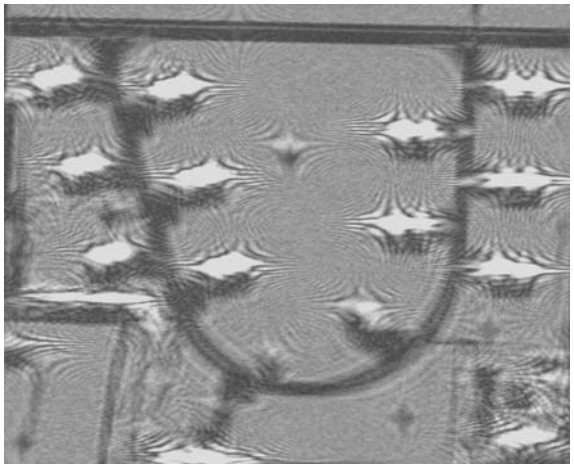

Figure 2.121 Simulation of antenna mispointing in flight direction leading to the wrong Doppler centroid in the processing and resulting in azimuth defocusing.

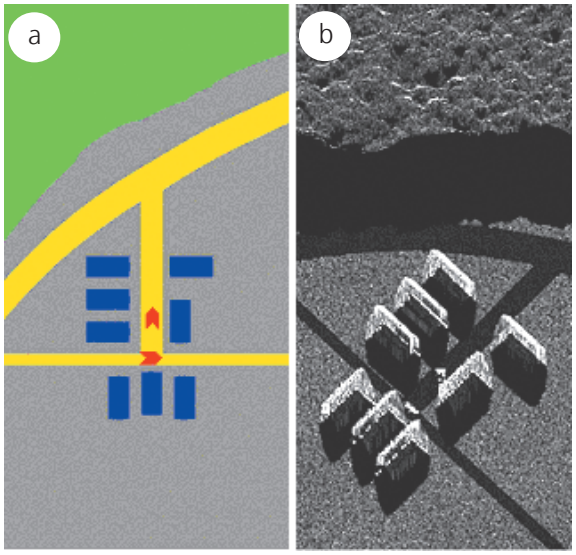

Figure 2.122 Virtual scenario: a) Material map (green: forest, yellow: roads, blue: buildings, red: vehicles). b) Simulated SAR image rotated according to the flight direction. The long shadows are due to the high incidence angles.

The development of SETES will continue by extending the geometrical resolution to meet the needs of upcoming reconnaissance systems. Especially the core modules, i.e. the reflectivity map and raw data generation need to be updated.

Another important future objective is to combine the mission simulator described in 2.1.10 and SETES into one integrated end-to-end simulation environment for analysing reconnaissance systems.

2.3.6 SAR Performance Analysis

Airborne and spaceborne SAR systems are characterised by a huge number of parameters, which are interconnected in a very complex way. The development and optimisation of SAR systems therefore requires efficient software tools. The tools developed by the Institute use a modular approach to allow easy adjustment for different mission requirements or operating modes (Stripmap, ScanSAR, Spotlight, along-track and across-track interferometry) [54].

The general approach for the SAR performance analysis is shown in Figure 2.123. The SAR system parameters are depicted as logical blocks, the most important ones being the antenna parameter computation, the imaging geometry description (including the orbit) and the timing. A key parameter in the design process is the selection of the PRF, which is a highly constrained parameter.

Once these parameters are determined in a first iteration, the quality parameters can be evaluated analytically. Examples of quality parameters in a SAR image are the spatial resolution, radiometric resolution and ambiguity ratios, or, in the case of an interferometric SAR, the estimated height errors of the digital elevation model. By assessment of these quality parameters the SAR system parameters can be optimised.

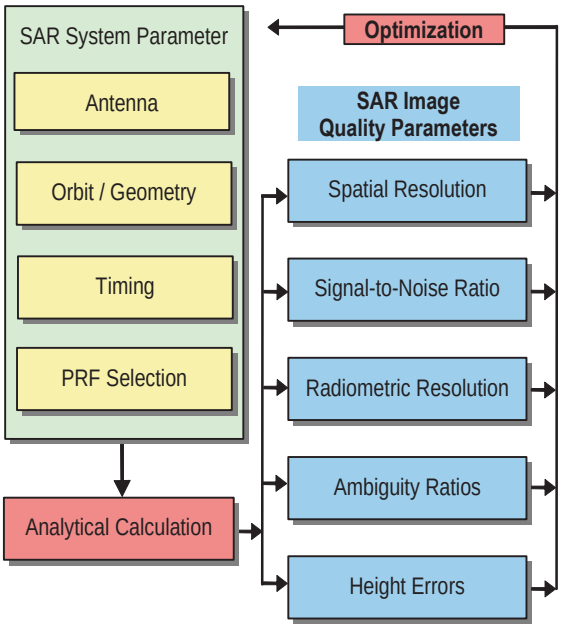

Figure 2.123 General approach for SAR performance analysis with building blocks to describe the system parameters and optimisation loops based on a trade-off with image quality parameters.

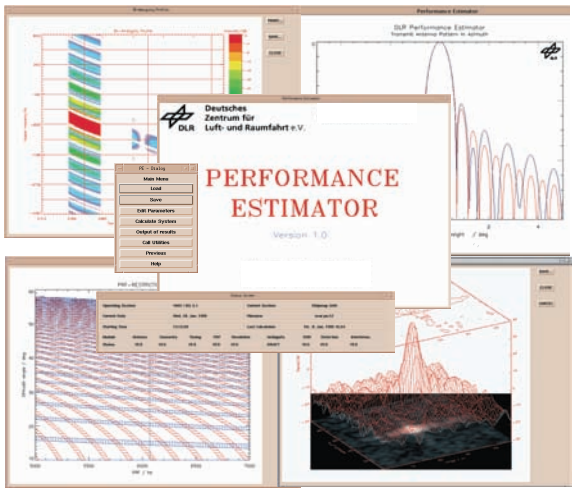

Figure 2.124 Screen shot of the Performance Estimator featuring some of the graphical analysis tools. From top left to bottom right: ambiguous areas, antenna patterns, PRF restrictions and the impulse response.

The software to perform this task is embedded in a graphical user interface and offers a variety of visualisation tools to support the interactive optimisation process (Figure 2.124). For operational purposes the calculation modules can be controlled independently from the graphical user interface to allow performance calculations as a function of arbitrary input parameter variations. With spaceborne SAR systems, for example, this allows the calculation of quality parameters as a function of the orbit position, accounting for the variation in height over ground.

Application Examples

The software modules offer various possibilities to model the system parameters with a high degree of detail. The beam patterns of planar array antennas can be synthesised with the phase and amplitude coefficients of the radiating subelements or with analytical taper functions. Excitation phase coefficients can be calculated from the required steering angles of the antenna. Figure 2.125 shows an example for the synthesis of the X-SAR elevation pattern.

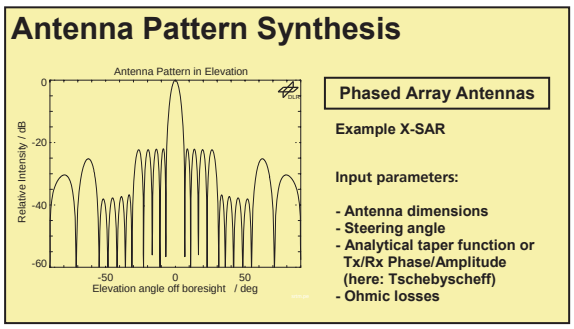

Figure 2.125 Phased array pattern synthesis (example X-SAR elevation pattern with Tschebyscheff tapering).

Parabolic reflector antennas are modelled by a two-parameter analytical model based on the main reflector, and, where applicable, subreflector diameters and on analytical taper functions of the feed. For full flexibility and highest accuracy, the software supports an ASCII-file interface to read in patterns from dedicated antenna calculation programs or from antenna far-field measurements.

The orbit and imaging geometry module supports an elliptical orbit model to determine the platform velocity and position vectors by Kepler's theory in a geodetic coordinate system. For operational purposes (e.g. TerraSAR-X), an ASCII-file interface to dedicated orbit propagators is available to read in the state vector of the platform.

The selection of the PRF is one of the most critical steps in the optimisation process. In SAR systems, the time when echo data can be received

is limited to the time interval between transmit pulses. Also, interference with the strong nadir echo should be avoided. The two interference conditions with transmit pulses and nadir echoes define bands of unacceptable combinations of PRF and off-nadir angle. Figure 2.126 shows these bands and several suitable swath positions for the TerraSAR-X system. To access a wide incidence angle range, several sub-swaths are necessary using different PRFs.

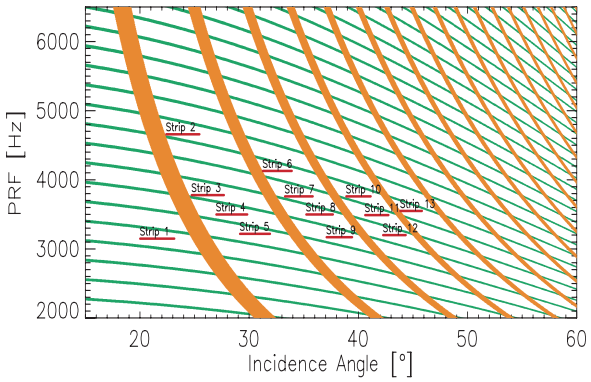

Figure 2.126 PRF restrictions due to transmit pulses (orange) and nadir echoes (green) for TerraSAR-X. The distribution of suitable sub-swaths is indicated in red.

Once the PRF has been selected, the image quality parameters can be derived. Figure 2.127 shows an example of the azimuth impulse response analysis determining the spatial resolution and Peak-to-Side-Lobe Ratio (PSLR). The software tools support the simulation of impulse response distortions in azimuth and range due to systematic and random phase and amplitude errors. For military SAR systems, a new module was developed to process real or simulated orbit data to analyse, for example, the effects of a GPS based motion compensation and to study the possibilities of improve the spatial resolution of future SAR systems.

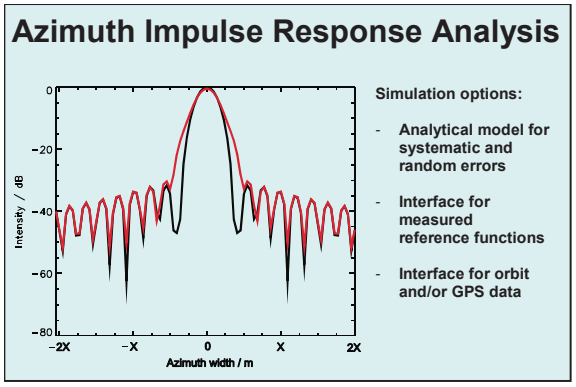

Figure 2.127 Impulse response analysis (black curve: ideal impulse response with Hamming weighting, red curve: distorted impulse response due to GPS position and velocity errors).

Figure 2.128 illustrates an example for a range ambiguity analysis. The ambiguity ratios describe the intensities of all ambiguous areas illuminated by the antenna side-lobes compared to the desired echo signal intensity. The blue areas indicate the ambiguous areas and the red area the desired echo. The range ambiguity profile (intensity) mainly depends on the antenna pattern, the slant range and the radar reflectivity at a certain off-nadir angle. Similar analysis tools are available for azimuth ambiguity analysis, which allows a trade-off between range and azimuth ambiguity suppression.

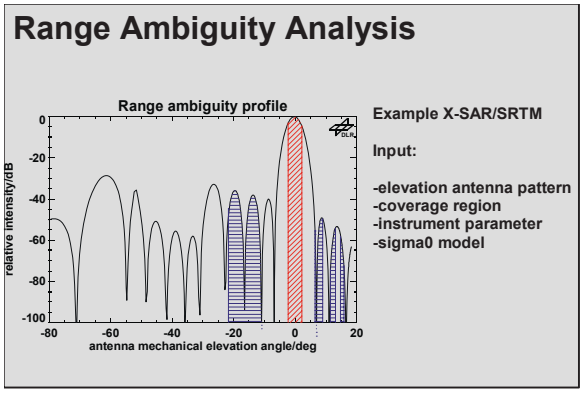

Figure 2.128 Range ambiguity analysis of X-SAR/SRTM (red: desired echo, blue: ambiguous echoes).

Another important quality parameter in the radiometric analysis of a SAR system is the NESZ. This value specifies the radar reflectivity level equivalent to the noise level and is often used to describe the limiting sensitivity of the SAR. The statistics of various scattering classes at different frequencies and polarisations are included in the software tools. Figure 2.129 illustrates a radiometric analysis of the TerraSAR-X system for several sub-swaths.

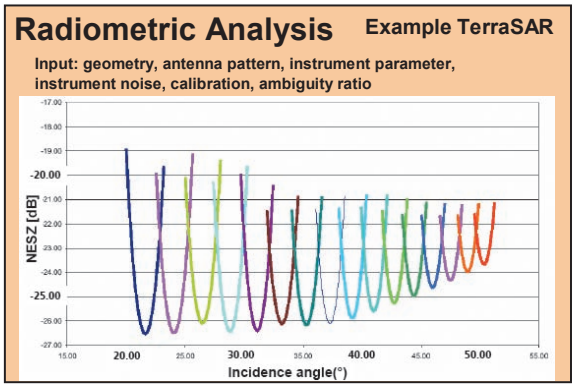

Figure 2.129 Radiometric analysis for TerraSAR-X. The NESZ performance for the sub-swaths is shown in different colours.

The available software tools described here were tested and evaluated with data of existing spaceborne systems like ERS-1/2, SIR-C/X-SAR, SRTM and Radarsat, as well as airborne systems like the Institute's E-SAR. Also verification tools [330] have been developed to comprehensively analyse measured SAR data and to verify the analytically calculated image quality parameters.

Figure 2.130 gives an example of one of the SAR image analysis tools. It supports the analysis of point targets, as well as the analysis of distributed targets to determine the NESZ values or the radiometric resolution. Such software tools also offer a 3-D visualisation of the backscatter characteristic of selected areas.

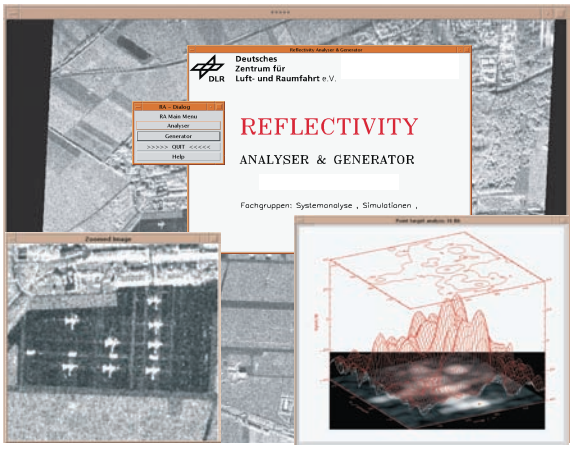

Figure 2.130 Screen shot of the SAR image analysis tool. Background, the complete SAR image; left, close up of an area of interest; right, 3-D visualisation of a target (aircraft).

The software tools for performance estimation and image analysis are being continuously adjusted to the requirements of new and evolving SAR systems. The future trends for spaceborne SAR systems are monostatic and multistatic SAR systems provided by constellations of small satellites with a view to improving the system response time or to realise special modes. The use of airborne SAR systems will be extended to high altitude platforms such as UAVs or air ships.

2.3.7 Radar Calibration

Radar calibration is a traditional R&D field in the Institute with almost 20 years of experience. The primary tasks of SAR calibration are to estimate and correct systematic error contributions throughout the complete SAR system and to convert the image parameters (magnitude and phase) into geophysical units. This could be maps of RCS or backscattering coefficients in the case of standard SAR images, or Digital Elevation Models acquired by interferometric systems like SRTM or TanDEM-X (Figure 2.131).

The quality of this calibration process is dependent on the inherent stability of the radar system and the ability to determine and monitor the radiometric and geometric characteristics [328].

The propagation can have an important influence on imaging performance. Several propagation effects occur inside the atmosphere, which need to be monitored and, where possible, corrected:

- Ohmic losses
- Atmospheric attenuation
- Scintillation
- Dispersion effects
- Tropospheric delay effects
- Polarisation distortion, due to Faraday rotation

These effects have been analysed and are used as a basis for the calibration of SAR satellite products. In addition, the knowledge is used to augment the SAR systems to remotely sense atmospheric parameters.

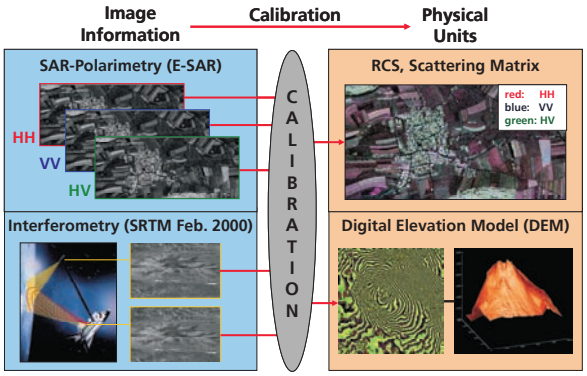

Figure 2.131 The calibration process transforms the image information into geophysical units like RCS maps or digital elevation models.

Interferometric calibration was performed for SRTM, which is described in section 2.1.1. The following sections concentrate on radiometric calibration.

New Calibration Concepts

In recent years, SAR antenna technology has developed from passive slotted waveguide arrays (e.g. ERS-1/2 or X-SAR) to active phased arrays (e.g. ASAR or TerraSAR-X), offering electronic beam steering capabilities required for acquisitions in different swath geometries and for operation in ScanSAR and Spotlight modes. Furthermore, with an increasing number of operational applications and services, the requirements on radiometric and geometric calibration become increasingly demanding.

TerraSAR-X is an ideal example of a multiple mode high resolution SAR and features the following operational modes (Figure 2.132):

- Stripmap Mode at up to 26 different look angles (swath positions)
- ScanSAR Mode in 9 different wide swath configurations each consisting of 4 sub-swaths
- Spotlight Mode at up to 125 different look angles implemented by switching between more than 100 different azimuth beams

On top of the nominal right-looking mode, by performing a roll manoeuvre of the satellite, data can also be acquired in left-looking geometry. Beyond the 3 basic modes, operation in the following experimental modes is planned:

- Wide-band Operation with up to 300 MHz bandwidth
- Dual-Receive-Antenna (DRA) mode achieved by electronically splitting the antenna in flight direction, enabling along-track interferometry and quad-pol operations

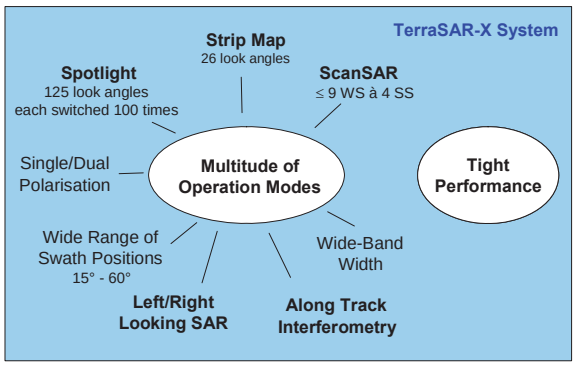

Figure 2.132 Challenges to calibrate a multiple mode high resolution SAR such as TerraSAR-X.

For conventional SAR systems like ERS or X-SAR, calibration involves internal calibration of a single transmit/receive chain (via special calibration loops), the determination of a single antenna beam pattern and the absolute calibration in one or two operational modes. For current multiple beam (~10000 beams in the case of TerraSAR-X), multi-mode systems based on active phased array antennas with hundreds of TRM, this conventional approach is not feasible and new, more efficient, and affordable methods have been developed [416]. The two most important innovations, namely the PN-Gating method and the Antenna Model Concept are presented below.

TRM Characterisation - PN-Gating

Monitoring the gain and phase variations in the transmit and receive paths of each of the 384 TRM in the TerraSAR-X front-end could be performed module by module, the so-called Module Stepping mode on ASAR. Greater accuracy can be achieved using coding techniques, because measurements can be made with the antenna, or parts of the antenna, operating under realistic conditions, e.g. power supply loading.
In this mode, a series of n characterisation pulses are fed through the complete front-end and routed back via a special calibration loop. In each TRM, a unique code sequence of length n is applied. The characteristics of individual TRM can then be extracted by cross-correlating the recorded sum signal with the code sequences. As it was originally planned to use PN codes the method was called PN-Gating and the special module characterisation mode on TerraSAR-X is termed the PN-Gating mode [176] [177]. Unlike the PN codes, the cross-correlation of optimised orthogonal codes whose length is an even number of bits, is zero; consequently the inherent code error disappears. Therefore, the PN-Gating mode was implemented using orthogonal Walsh codes.

In Figure 2.133, results for the TerraSAR-X antenna are plotted for two different types of codes, a PN code and a Walsh code. The estimation error of the amplitude and phase are plotted as a function of SNR, for different phase distributions of the modules and across the antenna array. The results show, that for the TerraSAR-X instrument with 384 modules individual TRM can be characterised with a phase and amplitude accuracy of better than 2° and 0.2 dB, respectively. Hence, PN-gating is a promising method for precisely characterizing individual TRM during the lifetime of an active SAR antenna.

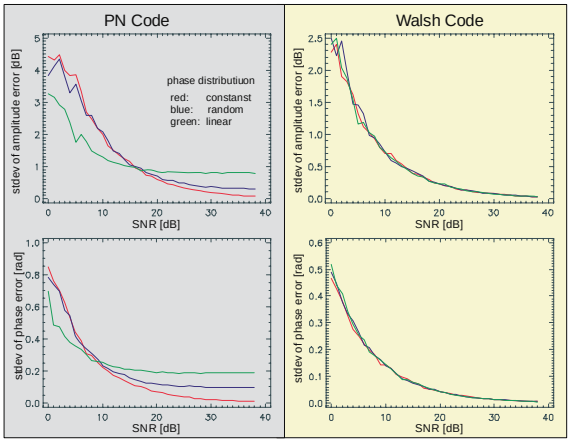

Figure 2.133 Simulated results of the PN-Gating method. Standard deviation of the amplitude and the phase error as a function of SNR for a pseudo noise code and a Walsh code and for different phase distributions across the antenna array: red - constant, blue - random and green - linear phase settings of the TRM.

Antenna Model Approach

Active phased array antennas do not only have the advantage of fast and flexible control of the patterns but also the ability to be mathematically modelled. Such an antenna model provides a software tool to accurately determine the antenna beam patterns based on detailed characterisation of the antenna hardware and knowledge of the antenna control parameters. To achieve the required radiometric quality, this concept requires highly accurate pre-launch characterisation data. After pre-launch validation against near field range pattern measurements and in-flight verification, the antenna model will be used throughout the satellite lifetime to generate the in-orbit calibrated beam patterns, as required for the radiometric corrections in the SAR processing.

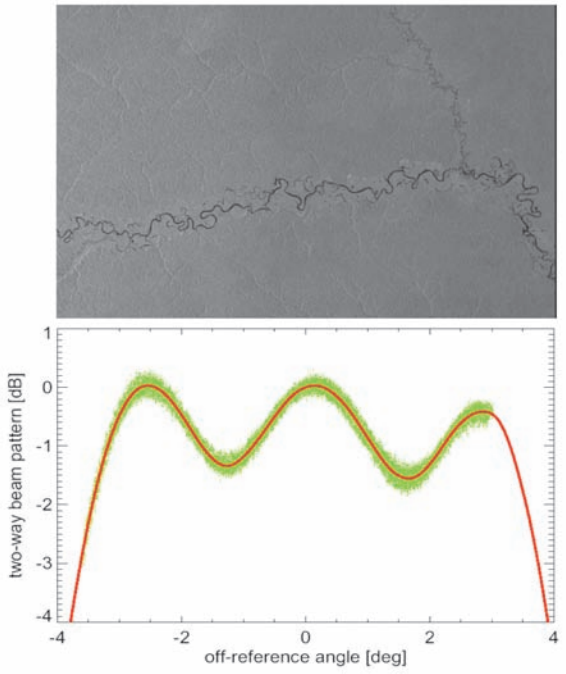

Figure 2.134 ASAR elevation pattern (red line) derived from the range profile (green points) of the above rain forest scene.

The model has to be capable of accurately determining not only the individual beam patterns but also the relative gain variations from beam to beam. Determination of the absolute gain from measurements over external calibration targets can then be reduced to a few beams. As part of the external calibration activities during commissioning, the antenna model has to be verified using rain forest data (Figure 2.134) and azimuth patterns recorded by ground receivers.

A further important task is the determination of beam pointing offsets using monopulse (notch) patterns over both the rain forest and ground receivers. Beam to beam relative calibration can be verified in ScanSAR mode over homogeneous targets.

In the case of TerraSAR-X, the antenna model verification as well as the absolute calibration will be performed for three (low, medium, and high incidence angle) beams. Traditional in-flight calibration would require calibration transponder deployment, maintenance and data collection, and extensive antenna beam characterisation using repetitive passes over the rain forest for at least all the performance controlled beams. With the antenna model approach, the required effort and the duration of the commissioning phase can be significantly reduced, allowing early release of the data products.

This antenna model is the key element of the antenna pattern section (Figure 2.135), which has been implemented into the TerraSAR-X IOCS (section 2.1.2) [568]. In addition to the above capabilities, the antenna pattern module also features a tool for generating optimised beam coefficients under given constraints (e.g. sidelobe suppression, main lobe width and gain, gain ripple). This so-called Antenna Excitation Generator was used to calculate the launch set of TerraSAR-X beam coefficients and will be used for beam optimisation in the event of major degradations of the antenna during the mission (section 2.3.8).

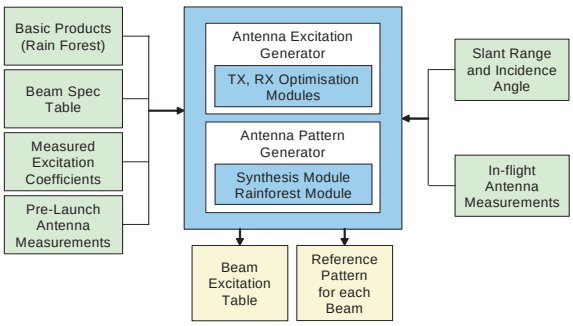

Figure 2.135 Block diagram of the antenna pattern section implemented in the TerraSAR-X IOCS.

Calibration Facility Oberpfaffenhofen CALIF

The Institute is well equipped with calibration targets and operates and maintains a large calibration site in southern Germany. Three different types of calibration targets are used, as shown in Figure 2.136:

- Trihedral and dihedral corner reflectors as passive targets precisely surveyed (with differential GPS) and therefore well suited for geometric calibration
- Transponders with high radar cross-section providing accurately defined point targets within the SAR scene
- Ground receivers measuring the transmit pulses as function of time and consequently the 1-way antenna beam pattern of the SAR antenna during an overflight

Six corner reflectors with a side length of 3 m are permanently installed around Oberpfaffenhofen. They have been regularly utilised for campaigns with different SAR missions (e.g. ERS-1/2, JERS-1, ASAR, ALOS, TerraSAR-X), as well as for the E-SAR calibration.

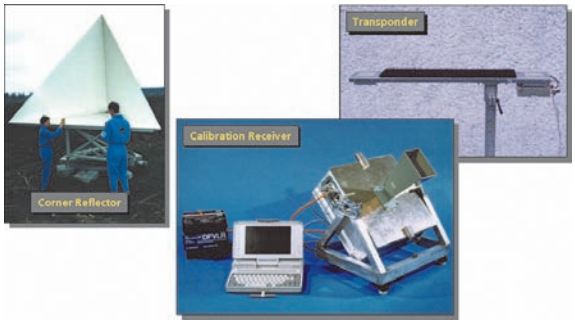

Figure 2.136 Examples of the Institute's calibration ground equipment; left: a corner reflector with 3 m leg length, middle: a ground receiver for measuring transmit pulses, and right: a transponder with adjustable RCS.

The ground receivers and the transponders have laptop interfaces for initialisation, synchronisation, and download of the measurements. All calibration targets can be precisely surveyed using differential GPS receivers.

Algorithms and Tools

The implementation of the above calibration and verification concepts requires algorithms and tools to perform specific measurements and analyses. Early developments date back to the SIR-C/X-SAR missions in 1994 and have been subsequently continuously improved and extended. With growing complexity of the sensors, more sophisticated algorithms, e.g. for PN-Gating, distributed target ambiguity analysis or antenna beam pattern optimisation, have been added.

The core for our calibration and verification algorithms is the CALIX software, which is currently being upgraded for TerraSAR-X and ALOS. A key element of CALIX is the point target analysis tool featuring measurement of impulse response function parameters, integrated point target energy (for determination of absolute calibration factors), target/clutter ratios (to weight calibration factor estimates), geometric analyses (internal delay and datation accuracy for accurately surveyed targets), as well as peak phase estimates in the case of multi-channel (e.g. quad-pol) the data. Figure 2.137 shows a screen-shot of this tool.

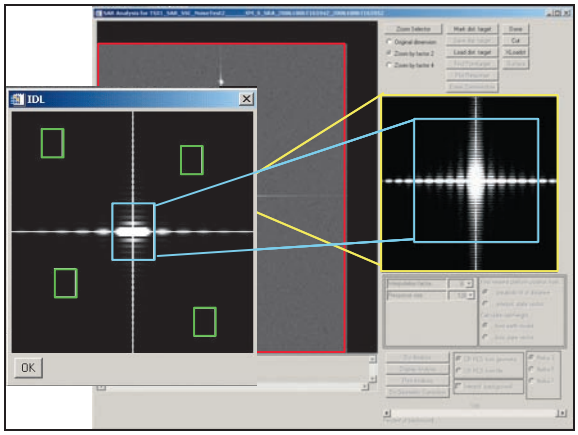

Figure 2.137 Screen-shot of the CALIX point target analysis on simulated TerraSAR-X product.

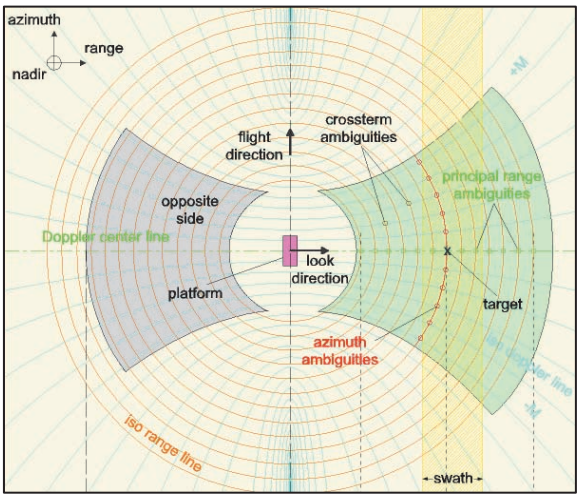

Figure 2.138 Scenario used in the SARCON distributed target ambiguity analysis tool. The position of the ambiguities are shown on plots of the iso-Doppler and iso-range lines.

A contract from ESA/ESRIN was awarded for the development of the SAR product control software (SARCON) for ERS and ASAR products [330]. With BAE Systems Ltd. as software engineering partner, SARCON has been extended and

improved over the last years and is currently the standard software in ESRIN's product control service. The limited ambiguity performance of ASAR in some beams was the driver for the development of a special distributed target ambiguity analysis tool that allows the estimation of ambiguity noise levels for a given scenario (Figure 2.138) [329].

Calibration Campaigns

Implementation of the above concepts requires a calibration facility that is well-equipped with software tools and ground calibration hardware. The third element is the infrastructure for the preparation and execution of calibration campaigns over large test sites. Several campaigns have been performed in the last years.

For the SRTM mission in February 2000 a large test site extending over almost 300 km in southern Germany was set up comprising 26 trihedral corner reflectors of different size and a number of ground receivers. All corner reflectors have been precisely surveyed using differential GPS serving not only as references for absolute radiometric calibration but also as absolute height reference points for DEM generation.

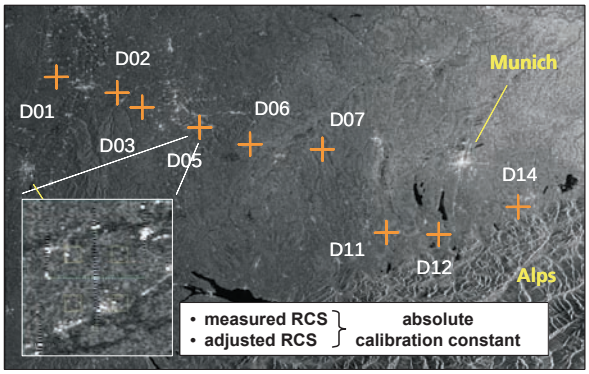

Figure 2.139 SAR image from the ASAR ScanSAR verification campaign in southern Germany showing the calibration sites and (inset) a close-up of a transponder response.

Under contract with ESA/ESTEC and as a contribution to the ASAR commissioning phase a ScanSAR verification campaign was performed in summer 2002. For that purpose, a calibration site extending over the 400 km wide ScanSAR swath was prepared with targets in the center of each of the five sub-swaths and in the overlapping regions between adjacent swaths. Point target analysis on the transponder responses in the ScanSAR image (Figure 2.139) confirmed the beam-to-beam relative calibration as well as the absolute calibration of ASAR Wide-Swath products. Furthermore, using the receiver unit of the transponder, the 1-way azimuth antenna patterns could be measured, as shown in Figure 2.140. The jumps in amplitude indicate the switching from sub-swath to sub-swath in ScanSAR operation.

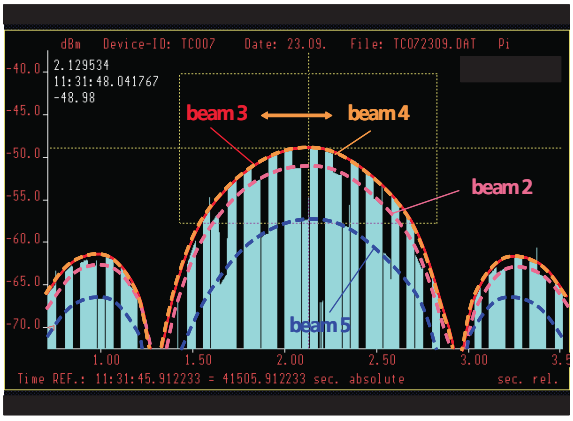

Figure 2.140 Transmit pulses of the ENVISAT/ASAR instrument as function of time recorded by a deployed ground receiver. The reduced amplitudes inidicate the switching of the instrument from beam to beam and the corresponding envelopes represents the one-way (transmit) azimuth antenna patterns of ASAR in ScanSAR operation.

Since 2003, the main efforts have been concentrated on developing the calibration concept for TerraSAR-X. New software tools have been implemented and existing algorithms were updated. CALIX underwent a major upgrade and became part of the IOCS [574] [575]. Further calibration targets are being developed and purchased.

Currently the detailed calibration activities required during the commissioning phase are being planned. Starting from the calibration strategy, different constraints have to be considered here, e.g. the coverage on the Earth's surface, the required number of point target measurements assumed in the radiometric accuracy budget [571].

In order to obtain as many as possible passes over deployed calibration targets, the test sites will be set up in the cross-over points of ascending and descending orbits, as shown in Figure 2.141. Mainly for logistic reasons we aim to select these test sites near Oberpfaffenhofen, as shown in Figure 2.142.

The calibration strategy of TerraSAR-X has been adapted to TerraSAR-L [466] and Sentinel-1 [465] (sections 2.1.5 and 2.1.6).

Worldwide, a number of new SAR missions are being implemented and further innovative concepts are being studied. Current trends point to satellite constellations employing bistatic and multistatic concepts. Innovative calibration approaches are required to keep track with the growing complexity of SAR systems and the de-

mand to cut down the duration of the commissioning phase and to reach operational readiness as early as possible. Furthermore, the effort has to be taken into account and cost efficient methods need to be developed.

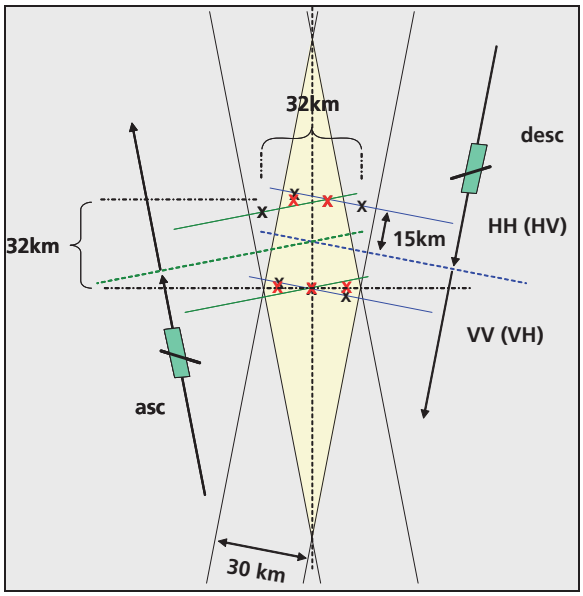

Figure 2.141 Test site configuration for TerraSAR-X Stripmap calibration with 7 target positions (black and red crosses). The yellow region on the Earth surface is the crossing area covered by an ascending and a descending pass, whereby the red crosses are covered by both passes.

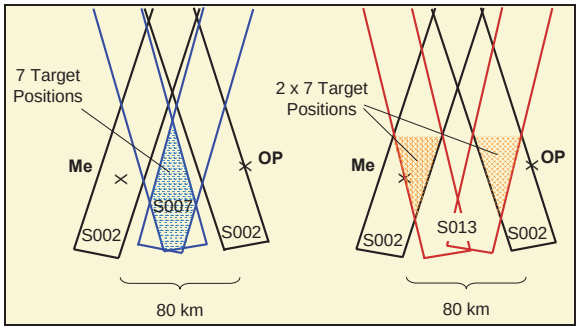

Figure 2.142 Three test sites near Oberpfaffenhofen (OP) for TerraSAR-X Stripmap calibration: blue for beams S007 and orange for beam S002 and S013 (Me: Memmingen).

Given the challenging but also very promising situation, it is suggested to introduce more standardisation into SAR calibration. In this context we intend to certify our calibration facility and to offer our services to SAR mission operators globally. In the long-term the Institute aims to become an accreditation body certifying other calibration centers.

2.3.8 Antenna Technology

Technology is developed in the Institute, where suitable products are not available on the market and where the development requires close interaction with the rest of the system. The SAR antennas are an example of particular importance for the many SAR activities in the Institute. The main challenges to achieve are:

- Receive and transmit (high power) operation
- Coverage of the radar wavelengths
- Operation in various polarisations
- High gain
- Uniform illumination of the imaged swath (for high relative radiometric accuracy)
- High side-lobe suppression (for low range and azimuth ambiguities)
- Thermal stability
- Beam steering and shaping (for advanced SAR modes)

For spaceborne SAR systems, work in the Institute is concentrated on antenna optimisation and characterisation, as required for system verification and calibration (section 2.3.7). For the airborne systems E-SAR and F-SAR the mounting, operating and licensing the SAR antennas and their mounts are additional tasks.

Spaceborne Satellite Antennas

Although the Institute does not construct satellite antennas, an important field is the specification, prediction and optimisation of antenna performance, particularly for active arrays as used for SAR instruments. Pattern prediction is based on the excitation coefficient settings for the array's sub-elements, on the electrical characteristics of the TRM and on the sub-element radiation patterns.

In satellite SAR missions it is of great importance to achieve high sensitivity over a large angular range (TerraSAR-X: 20° to 45° look angle), as well as good suppression of ambiguities. Hence, there is need for a software tool that optimises the antenna patterns of the satellite's electronically steered array antenna. The shaping of the pattern is obtained by varying the excitation coefficients and setting up each TRM with these coefficients. In operation, the setting is performed by up-linking appropriate commands to the SAR.

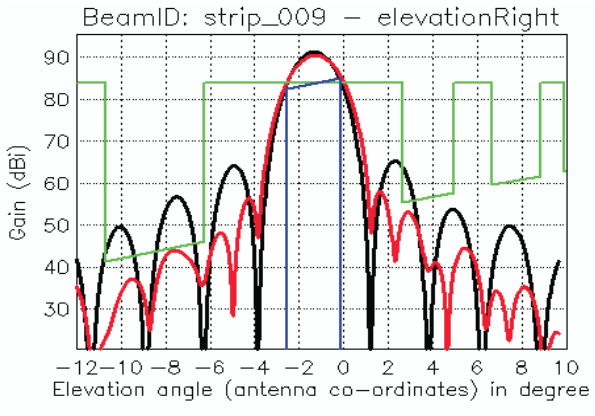

Figure 2.143 Antenna pattern of Stripmap beam S009 for TerraSAR-X. Red curve: Optimised pattern, black curve: unoptimised pattern, green curve: Mask to be fulfilled, blue ramp: coverage region.

Figure 2.143 shows the mask, the blue line being the minimum gain mask in the coverage region and the green line, the maximum gain mask in the ambiguity regions. The black curve is the pattern without optimisation and violates the mask. The red curve is the optimised pattern which doesn't violate the ambiguity mask, while the achieved gain in the coverage region reaches the minimum required.

The Antenna Pattern Optimisation Software was first developed for the ASAR front-end under ESA/ESTEC contract [93] [94]. The ASAR antenna consists of 320 sub-arrays and transmit/receive modules, respectively. For TerraSAR-X, two optimisation approaches were realised and compared, an analytical method and a randomising method. The first approach uses a genetic algorithm on top of a deterministic inversion. The solution is achieved by calculating several "generations" with certain "individuals" of patterns and recombining the associated excitation coefficients through mutation. The second method calculates thousands of different pattern realisations by randomly varying the excitation coefficients to find the optimum solution (500 realisations per second on a Pentium IV, 3.4 GHz). In case of TerraSAR-X, the second method showed better performance and results.

Antennas for Airborne Radar Systems

The airborne SAR activities cover microwave frequencies ranging from 300 MHz to 10 GHz and require various antenna technologies, i.e. microstrip array, slotted waveguide or horn antennas.The prototype antenna development for airborne SAR has to meet airworthiness requirements, as well as the requirements given by the application.

Figure 2.144 P-band antenna with the wind deflector mounted under the fuselage of DLR's Dornier Do 228.

The Institute has established a complete design and development chain for the production of prototype airborne antennas. Airworthiness certification and payload approval are carried out in cooperation with other DLR institutions. This has proven to be very successful as the example of the P-band antenna for the DLR airborne SAR shows (Figure 2.144) [221].

The antenna is designed for wide-band operation in P-band, i.e. in the 300 to 400 MHz frequency range. At the 80 cm wavelength the antenna has small physical dimensions of only 1.4 m by 1.4 m constrained by the width of the aircraft's fuselage. The use of materials with a high dielectric constant was required. To achieve the bandwidth of 28%, an aperture coupled, triple stacked patch element was developed (Figure 2.145) [225]. Sixteen elements form the electrically steered array. Thus, the configuration of 4 rows was chosen with 125° phase shift per row to obtain a main beam pointing 42° off nadir, necessary for the side-looking SAR imaging geometry.

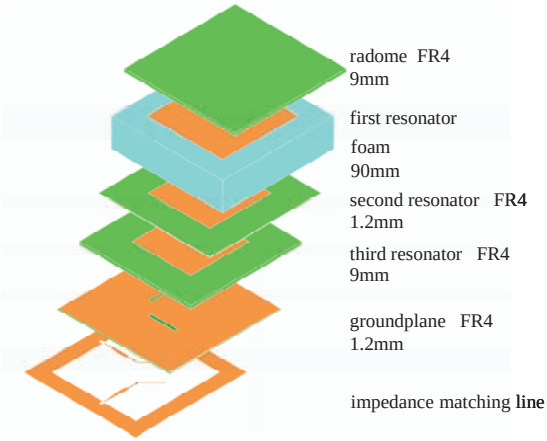

Figure 2.145 Structure of the different layers of one radiating P-band element. Three resonating patches contribute to the radiated field.

The P-band antenna is dual polarised and has a high cross-polarisation suppression of 25 dB over the useful bandwidth of 100 MHz. The design meets the specification for beam width in elevation and azimuth for both polarisation directions. In close collaboration with the Department for Flight Operations, a wind deflector was designed, built and certified together with the antenna (Figure 2.144). The whole equipment comprising antenna, power dividing network, mounting frames and deflector is 3.4 m in length and has a weight of 130 kg. Figure 2.146 shows the antenna and the results of the antenna pattern measurements.

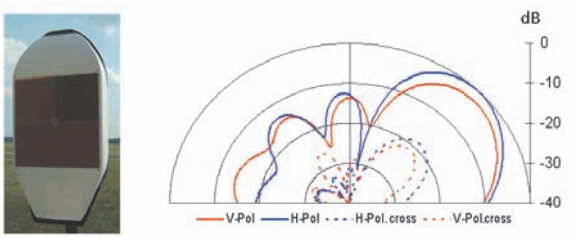

Figure 2.146 Left: Photograph of the P-band antenna mounted on the far-field measurement facility. Right: Antenna diagrams (solid blue: HH, solid red: VV, dashed: cross-pol).

A new L-band antenna to be used for the F-SAR system (section 2.2.6) is an example of a phased array using patches. The antenna has a beam steering capability as well as wideband operation, high pulse power ability and low cross-polarisation level (Figure 2.147).

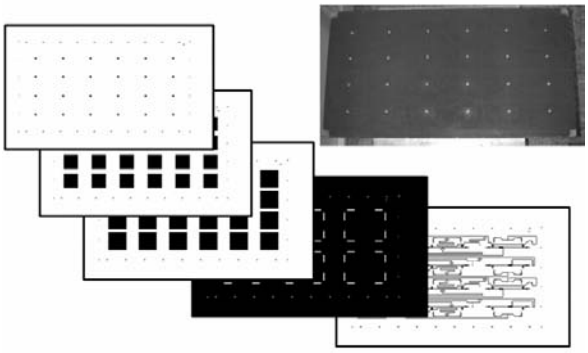

Figure 2.147 Top right: photograph of the L-band antenna for the new airborne SAR, F-SAR, together with the masks for etching the various layers.

For specific applications requiring quick solutions, slotted waveguide antennas are convenient. Figure 2.148 shows an X-band slotted waveguide antenna for SAR interferometry application. Three of these antennas are mounted on the side of the aircraft's fuselage to form an interferometer with both along-track and cross-track baselines.

Antenna Design and Development Infrastructure

The Institute maintains a number of antenna software design tools running on a high-performance PC. Agilent's Advanced Design System (ADS) is used for the development of planar radiating elements. The software supports the design of planar structures using a 2.5-dimensional simulator. The simulation of small groups of elements is possible, as well as the associated feed network.

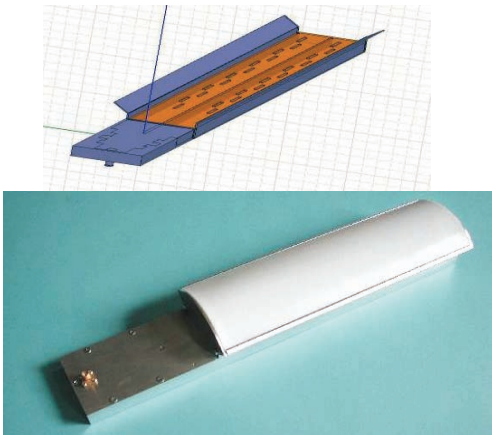

Figure 2.148 Top: Design of the X-band slotted waveguide antenna. Bottom: the prototype antenna with a Teflon radome. The box with the connector contains the power divider.

For designing real 3-D structures, Ansoft's High Frequency Structure Simulator (HFSS) is better suited. Complex topologies are possible limited only by the available computing power. Feko, a third software tool, produced by EM Software&Systems, is available for analysing the placement of antennas on structures.

Figure 2.149 Examples of horn antennas for millimeter wavebands. Because the machining of the inaccessible internal surfaces is impossible with conventional machines, galvanoplastic techniques have to be used.

The Institute's precision mechanics workshop handles most aspects of antenna manufacturing. The workshop is specialised in small structures and high quality products. Antennas and other microwave components are manufactured up to W-band using manual and numerically controlled machines, as well as galvanic techniques (Figure 2.149).

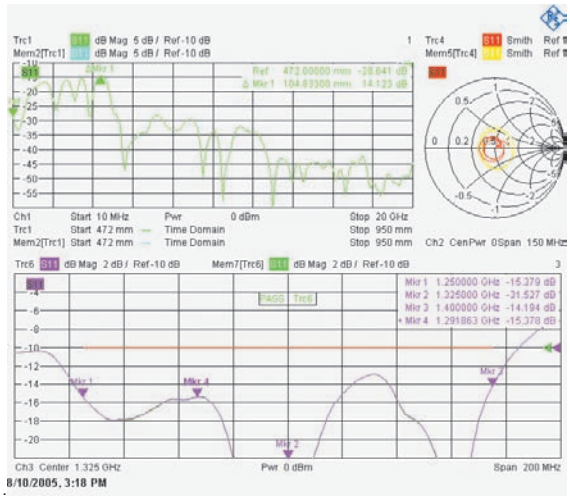

Figure 2.150 Screen-shot of the network analyser with the input impedance measurement of the L-band antenna described above. Top left: reflected power in the time domain. Top right: Smith chart of the normalised input impedance. Bottom: magnitude of the reflected power in the frequency domain.

Figure 2.151 DLR's airborne P-band SAR antenna mounted with its wind deflector on the antenna measurement facility AMA.

The Institute maintains a laboratory equipped with latest instrumentation for antenna development. Several high-performance network analyser is used to characterise the properties of the microwave components. The new F-SAR L-band antenna is given as an example (Figure 2.150).

For antenna measurements, the far-field antenna measurement range (AMA) operated by the Institute of Communication and Navigation, is used (Figure 2.151). The major advantage is the possibility to operate the facility at very low frequencies, practically down to a few MHz, not possible in a closed chamber. However, because of the open arrangement the measurements are weather dependent and radio frequency interference with other services cannot be excluded. Thus, the far-field antenna measurement range is unsuitable for sensitive antennas. It is limited with respect to the accuracy and not all kind of measurements can be performed. For this reason, a new microwave laboratory complex containing a compensated compact range is in planning. The compact range will add new antenna measurement facilities and a big improvement in accuracy.

2.3.9 Radar Signatures

The knowledge of the radar signature of a target and the scattering from the surroundings is essential for estimating the performance of radar systems used in both military and civil scenarios. The complexity and variability of these quantities mean that accurate models have to be relied upon.

Simulation of Target Scattering

As the experimental determination of radar cross-section (RCS) distributions of real targets is very laborious and expensive, the development and maintenance of numerical simulation programs is of great importance. Several software tools using different methods for mono- and bistatic calculations are under development.

The monostatic RCS model SIGMA is based on the method of Physical Optics (PO). A module is included, which calculates edge correction contributions. Simulation in two dimensions is possible [479]. SIGMA is able to simulate the radar signatures of complex metallic objects, also coated with dielectric materials. The dielectric coating can be defined either by the dielectric constants or the Fresnel reflection coefficients as a function of the incidence angle.

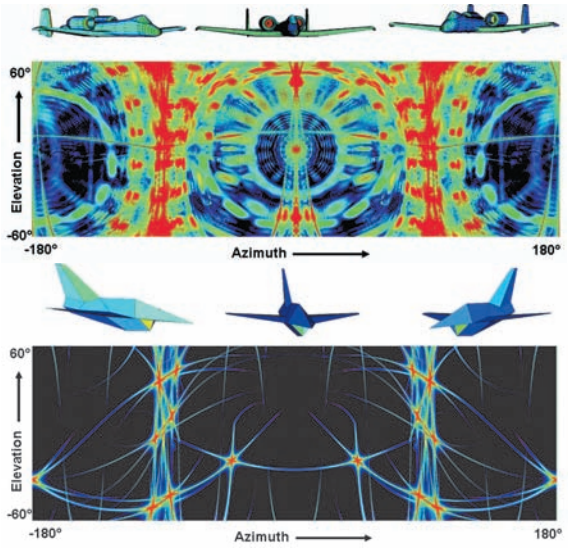

Figure 2.152 2-D signature of a Fairchild A-10 Thunderbolt (top) and the DLR stealth concept aircraft F7 (bottom); horizontal axis: azimuth angle, vertical axis: elevation angle. From the front (center), the Thunderbolt has high reflectivity and would be easily detected by a radar, whereas the F7 is practically invisible.

In Figure 2.152 the 2-D RCS distributions of two aircraft are shown. In the front view region (center of the images) the stealth behaviour of the F7, which has been optimised to minimise detection on approach, is obvious, whereas the Thunderbolt has high reflections.

SIGMA is able to simulate RCS distributions for several stepped frequencies at once. With this facility, a range profile can be processed by applying an inverse Fourier transform. Figure 2.153 shows the fully polarimetric range profiles of an armoured vehicle. It shows that a range profile can be sufficient to characterise a vehicle, which is very useful if only a polarimetric ranging radar is available. The result shows good discrimination of target features, i.e. good classification possibilities.

Because of the increasing importance of bistatic radar systems, a bistatic RCS simulation code BISTRO has been developed. The program is aimed at the simulation of the bistatic high-frequency electromagnetic scattering from man-made targets. Figure 2.154 shows a computed scattering diagram of a 10λ perfectly conducting sphere for a fixed direction of illumination and varying observation aspects. This illustrates typical features of bistatic scattering, namely the dominance of forward scattering compared to back-scattering and the complex structure of the scattering diagram, due to the presence of multiple sidelobes.

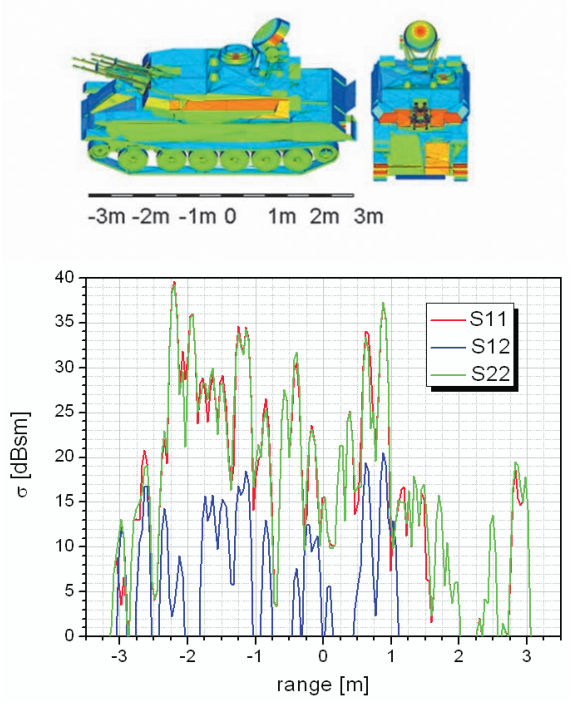

Figure 2.153 Bottom: Polarimetric signature of the armoured vehicle shown at the top (frequency = 32 GHz, incidence angle θ = 60°). Red and green are the co-polar components and blue the cross-polar.

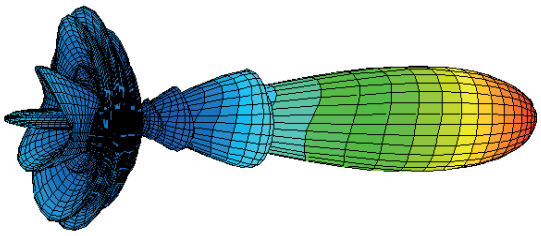

Figure 2.154 3-D bistatic RCS of a sphere; on the left, back scattering: on the right, forward scattering: It can be seen that forward scattering dominates.

The developed modules of the program have been successfully applied to various types of canonical scatterers (spheres, plates, cylinders, etc.) and complex targets (cars, aircraft). Additional modules for hidden surface detection, edge corrections and dielectric coatings are under development, further improving the simulation accuracy. Modelling the edge corrections for edges in non-metallic surfaces requires more research [40], [41], [398], [399], [400].

In order to simulate high-order (>2) reflection contributions for mono- and bistatic scattering problems, the software tool SIGRAY applying the Shooting and Bouncing Rays Method has been developed. In comparison to PO, this method is time-consuming but very well suited to calculate

the RCS contributions of high order reflections. For reflections of the order n, the geometrical optics method is applied n – 1 times. Finally, only one application of PO is used.

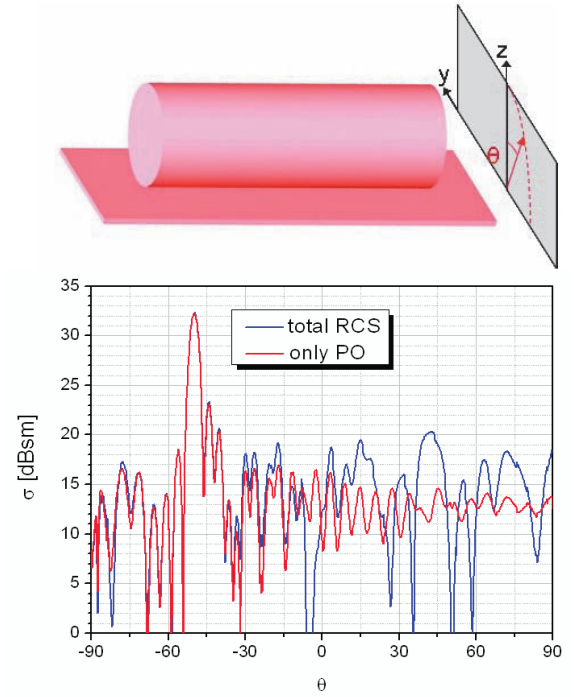

Figure 2.155 Bistatic signature of a cylinder close to a flat panel; Transmitter: θ = +50°; Red: only PO (Physical Optics) contributions; Blue: PO plus multiple reflection contributions. At θ = +50° (monostatic scattering) the RCS is low, whereas at θ = -50° (specular reflection) it is very high.

Figure 2.155 shows the simulation results from SIGRAY for the interaction between a cylinder and a flat panel [158]. The discrepancy between the curves shows that multiple reflections have a major influence and need to be taken into account.

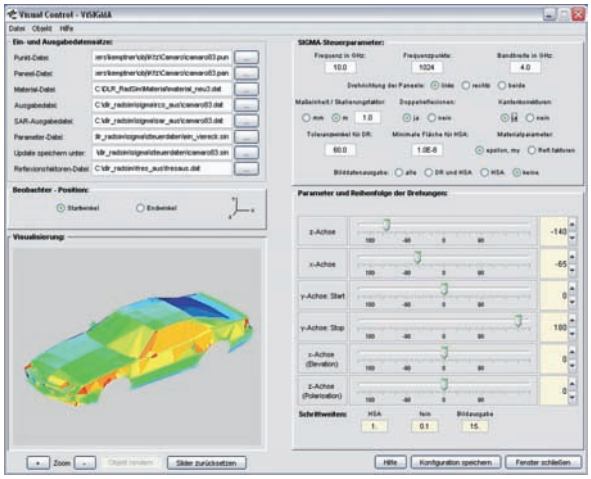

Figure 2.156 Screen-shot of the configuration tool for a SIGMA simulation showing the file and parameter selection, and the viewer with the simulated object coloured according to the normal vector.

For preparing numerical simulations, important tasks are the importing of 3-D geometry datasets of anthropogenic targets from popular CAD formats, their modification and repair and the export in the data format used by SIGMA, BISTRO and SIGRAY.

In order to ensure easy and reliable configuration of the simulations, a common graphical user interfaces for SIGMA and SIGRAY has been developed (Figure 2.156). The object to be simulated is visualised in the required orientation. It is coloured according to the normal vector, which corresponds to the areas of highest reflectivity. After starting the simulation the RCS data are shown on a graph synchronised with the position of the target [599].

To validate the simulation tools, the Institute maintains a monostatic and bistatic RCS measurement facility (Figure 2.157). It is set up in an 10 x 5 x 5 m^3 anechoic chamber and consists of a W-band (92 GHz) reflection measurement system based on a NWA. The test object is mounted on a rotator, which is concentric with an arm carrying the receive antenna. Using the time domain option of the NWA a range gate is applied for suppressing disturbing signals. Measurements are performed on scaled models of reference objects to compare the simulated results with real ones. More results on RCS simulation of vehicles are presented in 2.3.4 “Traffic Monitoring”.

Figure 2.157 Monostatic and bistatic RCS measurement facility with the reflection measurement system on the right. The test object is located on the rotator in the center, and the transmitter antenna is mounted on the arm.

Radar Range Model

In order to determine the detectability of artificial objects embedded in a natural environment it is essential to assess the clutter contribution of the surrounding area. Thus, the software tool DORTE (Detection of Objects in Realistic Terrain) was developed [312]. DEMs are used to describe the topography and determine shadowed areas and local incidence angles. The specific radar backscattering coefficient of each terrain cell is calculated using semi-empirical and statistical clutter models. The land use database CORINE of the EEA (European Environment Agency) is currently employed to assign clutter models to different areas within a DEM.

CORINE data are available for almost every European country. Figure 2.158 shows an example of a simulated clutter map for the northern end of the lake Ammersee close to Oberpfaffenhofen. The radar is located in the lower left corner [479].

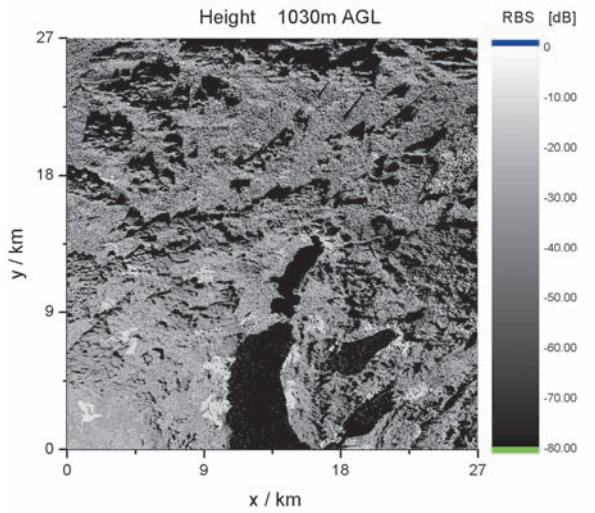

Figure 2.158 Simulated radar clutter map of the northern Ammersee region. The radar is located at the bottom left corner (0, 0) at a height of 1030 m. The shadowing due the topography can be seen clearly.

DORTE can be used for a quick and inexpensive estimation of the expected clutter level for virtually every place on the Earth, as long as a DEM and land cover information is available. For the future it is planned to extend the code capabilities to allow for multistatic configurations and to take different radar hardware characteristics into account.

Electromagnetic Properties of Materials

For the simulations, the influence of dielectric coatings of metallic targets is of great importance. In order to determine the properties of different types of material samples in the microwave range, three different measurement facilities are operated.

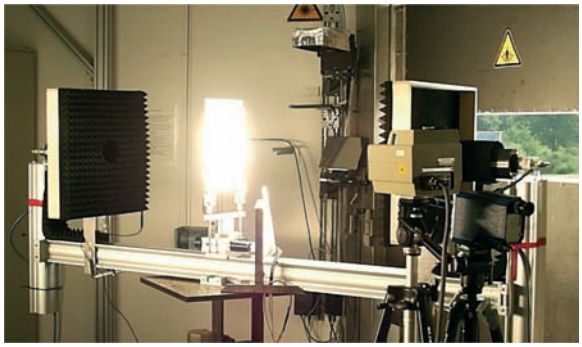

Figure 2.159 Ka-band transmission measurement setup in the DLR solar furnace. The material sample in the center is illuminated by focused sun light and heated to a temperature of 1000 °C.

A Ka-band (35 GHz) transmission measurement setup can be used for measuring the dielectric constants of material samples in the form of sheets or plates. The measurements are automated and real-time data acquisition is realised. One example of the use of the setup was for high temperature measurements on materials for a nose cone, making use of the DLR solar furnace in Cologne (Figure 2.159). These measurements [4][145] [156] were part of a DLR project Hochagile Flugkörper (HaFK) to develop technologies for missiles.

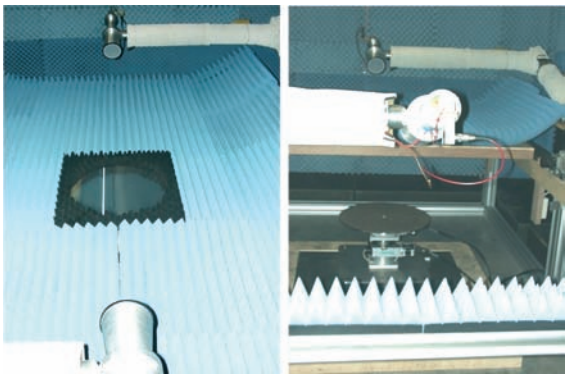

Figure 2.160 Free space reflection measurement facility. Left: a measurement in progress with the sample in the center and the two arms carrying the receive and transmit antennas. Right: the precision turntable for the sample.

An X-band reflection measurement setup (Figure 2.160) is used for measuring materials in the form of plates. The sample can be rotated and shifted by remote control. It is possible to measure fully polarimetric data at a large range of bistatic angles by rotating the antenna arms. A number of different flat and rough metallic or dielectric surfaces have been measured and analysed with the aim of finding methods to isolate the measurement of surface roughness and of the dielectric properties. It has recently been shown that the bistatic phase is strongly related to the dielectric properties of the surface [435]. This indicates that a bistatic radar system could be a useful tool for measuring soil moisture, etc.

A waveguide measurement setup for transmission and reflection measurements is used for material samples in the form of blocks, which can be shaped to fit into a waveguide. It operates in and L-, X-, Ku-, K-, Ka-, V- and W-band. Automatic procedures are implemented for the calibration and measurement procedures. ε and μ (permittivity and permeability) are derived using a Newton-Raphson algorithm. Some of the experiments have been performed for the DLR projects HaFK and UCAV structures.

2.3.10 Microwave Radiometry

Microwave radiometry has a long tradition in the Institute going back more than thirty years [304]. The research on passive measurement and imaging technologies is a main working area within the radiometric activities. New requirements in spatial resolution, sensitivity, spectral diversity, penetration depth, environmental conditions, and real-time capabilities, and also new applications demand the investigation and introduction of new principles, and the refinement of existing techniques.

Since the sky temperature varies strongly with frequency due to atmospheric attenuation as shown in Figure 2.161, Earth observation is mostly performed in the atmospheric windows around 35, 94, 140 and 220 GHz or at lower microwaves below 20 GHz. Atmospheric research is carried out close to the absorption lines. In general, the benefits of passive microwave techniques are a) almost independence of poor weather and daytime, b) covert operation and, hence, hard to be detected, c) no exposure of observed objects (e.g. persons), and d) the capability of nadir imaging in highly mountainous or urban areas.

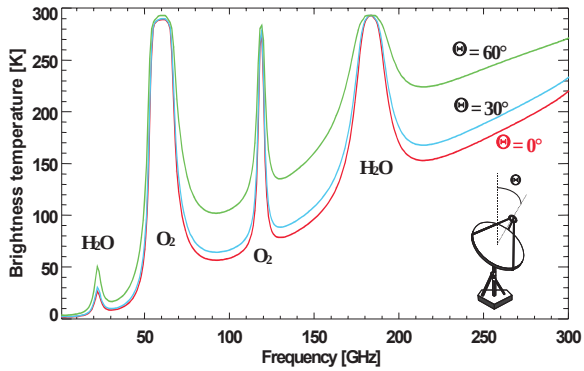

Figure 2.161 Computed brightness temperature of the sky for various observation angles as a function of frequency.

The research on imaging technologies is presently focused on three main areas:

- Line-scanner systems, which follow a more classical approach with the benefits of rather simple hardware and low cost, but with the drawbacks of limited resolution and real-time capabilities
- Aperture synthesis systems, which are a new approach for passive Earth observation and terrestrial imaging with the benefits of high spatial resolution and real-time capabilities, but with the drawbacks of higher cost and more complicated development and operation
- Hybrids of both in order to combine benefits and reduce the drawbacks, costs, and expense

Line-scanner Radiometers

Various line-scanner systems for airborne applications have been developed in the Institute during the last thirty years. The line-scanner principle is illustrated in Figure 2.162. The spatial resolution is determined and limited by the moving antenna and was in the order of 1° at 90 GHz. A sensitivity of about 1.5 K was achieved. The system was also operated at 37 GHz.

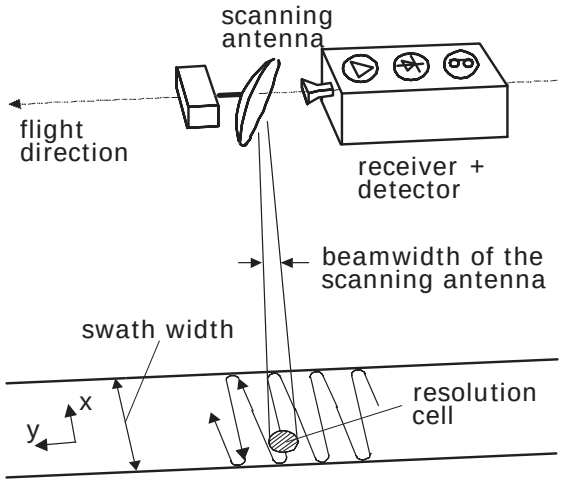

Figure 2.162 Imaging principle of an airborne linescanner system. An oscillating parabolic mirror causes an across-track scan of the antenna beam on the ground.

In order to support the development of new imaging method, and in order to be able to also acquire radiometric signatures on the ground, a ground-based imager was developed. The imaging principle of this system is shown in Figure 2.163, whereby the main goal was the capability to image a full hemisphere and have high flexibility to make modifications.

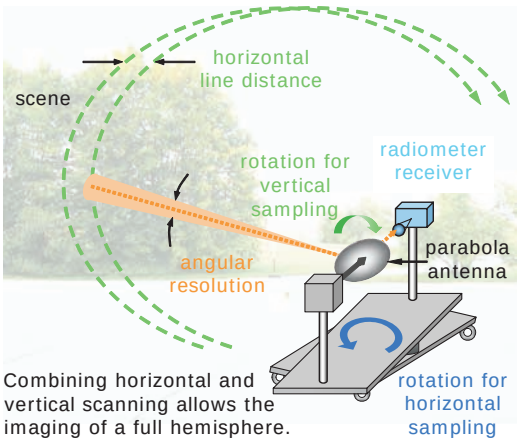

Figure 2.163 Imaging principle of the ground-based linescanner system. A rotating parabolic mirror provides an image row, and the azimuth movement of the whole unit delivers the second image dimension.

The system operates at 90 GHz, 37 GHz and 9.6 GHz with about 0.6°, 1.5°, and 5.8° of angular far-field resolution, but it can be extended to any frequency band where a receiver is available and the spatial resolution is still sufficient. The measurement duration for the complete hemisphere is less than 5 minutes and the sensitivity is in the order of 0.1 K. An image taken from the roof of the Institute building is shown in Figure 2.164.

The scene contains various metallic objects like containers and metal plates, a small water-filled pool, buildings with the sun blinds partly lowered, a concrete yard, grassy areas partly covered by groups of bushes, and clouds in the sky. It is remarkable, that the radiometric image has a strong optical appearance, greatly simplifying image interpretation. Due to the imaging geometries the photograph and the radiometer image are differently warped. Note that the radiometric image shows no shadows, since the whole sky acts as an illumination source.

Figure 2.164 Top: line-scanner image of a complex scene at 90 GHz taken from the roof of the Institute; bottom: a corresponding panoramic photograph.

Aperture Synthesis Radiometer

Since the nineties the work has focused on aperture synthesis techniques, a method capable of achieving considerably higher spatial resolution and coming from radio astronomy. Aperture synthesis uses a highly thinned aperture as shown in Figure 2.165 to perform low-redundancy imaging in the spatial frequency domain. Antennas are only mounted along the arms of the T-array to simulate the corresponding two-dimensional aperture. There is no mechanical movement. The image in the spatial domain has to be reconstructed via a dedicated algorithm, in the theoretically ideal case, an inverse Fourier transform. Since all receiver signals are simultaneously correlated in pairs, a real-time image of the scene defined by the single-element antenna pattern can be obtained. The applicability of this imaging principle was demonstrated using a two-element interferometer at 37 GHz with variable baselines synthesizing a 0.6° antenna beam. It was shown that high resolution imaging of complex terrestrial scenes is possible, and that the focusing from far field to the extreme near field can be adjusted purely by mathematical means.

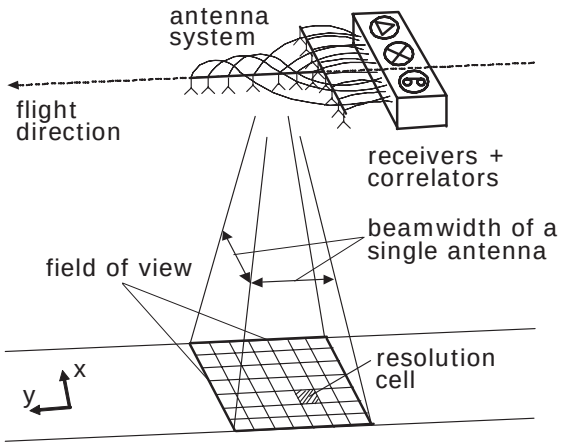

Figure 2.165 Imaging principle of an airborne aperture synthesis imaging radiometer with a T-shaped arrangement of the receivers.

In order to save costs, hybrids of scanner and aperture synthesis systems are very attractive. Such a system is presently under development (Figure 2.166).

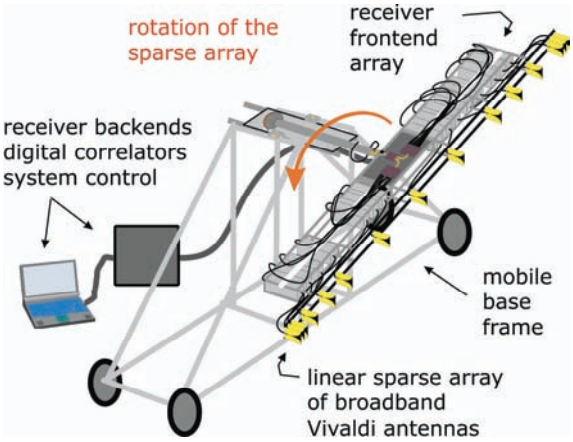

Figure 2.166 Sketch of a hybrid radiometer system combining aperture synthesis and scanning for two-dimensional imaging. Antennas are arranged at defined positions along the linear axis for the aperture synthesis. Scanning in the other plane is achieved by rotating the linear axis.

The antennas along the linear axis are arranged in a thinned, well-defined pattern for aperture synthesis on the linear axis. By rotating the linear axis in well-defined steps around its center over 180° and performing the measurement for each step, a final brightness temperature image can be constructed in the spatial domain. The hybrid system requires 15 receivers and 105 correlators. An image is expected to be formed within a few minutes in a multi-spectral imaging mode [182].

While a simple, two-element system would require several hours to produce one image, a full two-dimensional synthesis would need scores of elements and even more correlators, although the imaging could be performed in real-time. Hence, the hybrid radiometer represents a useful compromise.

SMOS (Soil Moisture and Ocean Salinity) Mission

Radiometric spaceborne instruments have long been contributing to Earth observation, both for scientific research and operational services, e.g. weather prediction and climate research. Since these applications demand an increase in reliability and precision, requiring higher spatial resolution of the radiometer, also at lower frequencies, aperture synthesis techniques have become attractive candidates for new and innovative spaceborne systems. Such an approach is currently being implemented for the ESA's Earth Explorer Mission SMOS, planned for launch in autumn 2007. The goal of SMOS is to globally map soil moisture and ocean salinity using an L-band aperture synthesis radiometer in a Y-configuration.

The Institute supports the mission by participation in the SMOS Science Advisory Group and various ESA contracts to develop image reconstruction techniques, which are mandatory for such a complex instrument. Figure 2.167 shows an artist view of the SMOS aperture synthesis radiometer. Since the array has a Y-shape, the corresponding sampling grid in the spatial frequency domain is hexagonal. Hence, the alias-free field of view in the spatial domain is also hexagonal. Image reconstruction has to account of all the errors introduced by mismatches and imperfections in the antenna patterns, the receiver transfer functions and the correlators, these being the ones with the largest impacts. Finally, a suitable calibration is mandatory.

An alternative image reconstruction method, a so-called G matrix approach was proposed, which allows full characterisation and calibration of the sensor from a pre-launch measurement of the transfer functions and an in-orbit determination of the G matrix by measurements of a comprehensive set of known brightness temperature scenes in space [555]. These scenes were chosen to contain the moon as a point source. Extensive simulations were performed to assess the performance of the developed approach. According to the G matrix approach, the complex integral equation describing the measured values of the aperture synthesis system can be described by discrete samples. Then the discrete representation can be converted to a matrix equation summarizing the imaging process for a certain number of different calibration scenes. Finally the matrix equation is solved to determine the G matrix, describing the system transfer function. This matrix is used for correcting and calibrating the radiometric measurements.

Figure 2.167 Artist view of the SMOS aperture synthesis radiometer satellite in space (© ESA).

Figure 2.168 shows a simulated result for a highly imperfect system including the unavoidable system noise. The system was assumed to have very different antenna patterns and receiver frequency responses. The non-ideal system was modeled and the corresponding correlation outputs for each baseline have been computed for each single point source scene of a whole calibration process. The resulting G matrix was then applied to simulated measurements of a typical scene including system noise. In the calibration mode in space, a set of independent calibration scenes can be produced by tilting the satellite so that the moon moves within the sensor's field of view and for each resolution cell. It was shown that by a suitable selection of calibration scenes and with sufficient calibration time (a few days) the post-launch G matrix approach can produce satisfying image reconstruction results. Note that only the post-launch approach can recover uncontrolled changes in the system response, e.g. due to aging or the exposure of the hardware to the space environment.

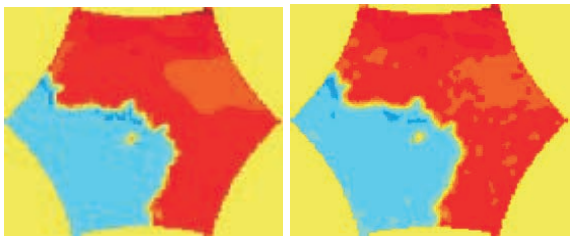

Figure 2.168 Original (left) and reconstructed brightness temperature image (right) of a scene of the Gulf of Guinea using the pre-launch generated G matrix.

Security Applications

Contamination by landmines is increasingly recognised as an inhumane burden on countries ravaged by war, many of these poor. Conventional techniques, like metal detectors or trained dogs are too inefficient to solve this problem. Also, plastic materials are increasingly being used to avoid detection. International terrorism has reached a level where adequate countermeasures to protect the population have to be provided by the authorities. A passive microwave sensor is a potential candidate to construct detectors, which are both reliable and convenient to use.

Within the scope of an EC project HOPE (Handheld OPerational dEmining system), a special radiometer for buried landmine detection was developed [544]. The HOPE multi-sensor system consisted of a metal detector, a ground penetrating radar, and a microwave radiometer, all integrated in one system intended for handheld operation. The radiometer was designed to perform imaging for detection in the extreme near field of the antenna close to the ground. Also, a multi-frequency mode covering about 1.5-7 GHz was developed in order to allow the discrimination of mines from false targets. Figure 2.169 shows laboratory measurements of buried objects like dummy mines and false targets, together with a photograph of the scene with the objects placed on the surface. A high detection rate can be achieved by using multiple frequency bands, but discrimination of the object type is still a challenge.

For a proper discrimination from false targets, more detailed frequency profiles were investigated in a separate study (Figure 2.170) [297]. Here, the sensor is kept at a single position above the suspected area and the radiometer's broad frequency range is swept in sufficiently small steps. The results indicated that an improved detection and the possibility of discrimination is feasible using this multi-spectral approach.

Based on the mine detection results, the method was extended to the more general detection of hidden objects using a multi-spectral system with higher spatial resolution and capable of near real-time processing. The hybrid radiometer system of Figure 2.166 is currently under construction. Using a 3 m aperture and a range of center frequencies from 1.4-7 GHz, a multitude of spectral images with a bandwidth of 20 MHz will be recorded within a few minutes. The array design was optimised in order to get mostly alias-free imaging with the lowest number of single elements, i.e. 15. The angular resolution is expected to be between 5.2° and 0.75° depending on the center frequency.

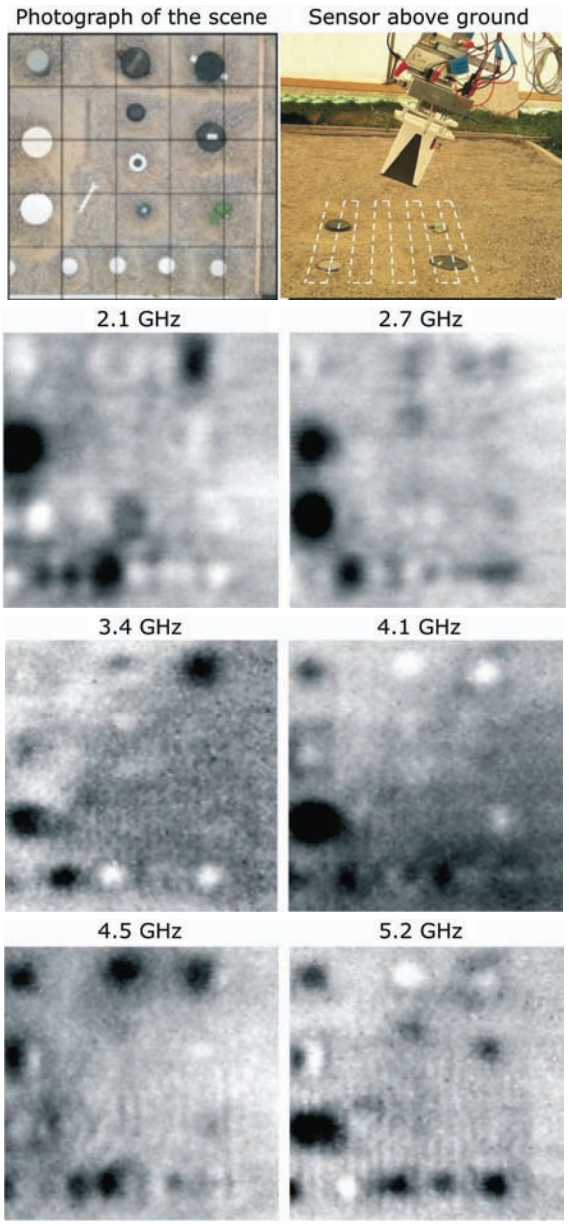

Figure 2.169 Top left: photograph of the objects before being buried. Top right: view of the scanner. Beneath: measured images for various frequencies of the scenario.

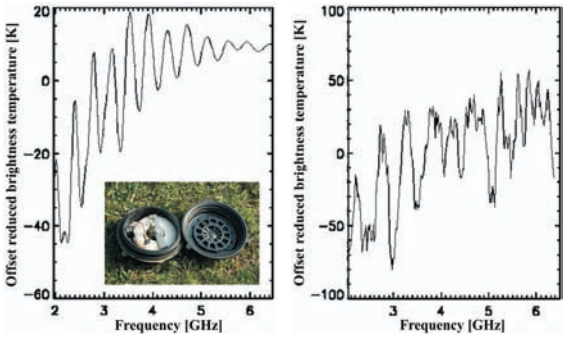

Figure 2.170 Simulated (left) and measured (right) frequency profiles of a so-called PPM-2 mine, largely made of plastic. For clarity, the average brightness temperature level has been subtracted in each case. The interference behaviour due to the layered structure is comparable for the simulation and the measurement.

The use of millimeter-wave radiometry for the purpose of change detection behind optically opaque dielectric walls was also investigated. The experimental line-scanner shown in Figure 2.163 was used.

Figure 2.171 shows the result at a distance of 6 m for a person with upraised arms behind a fibre-glass radome. Although the radome was not optimised for microwave penetration, the person can be clearly detected.

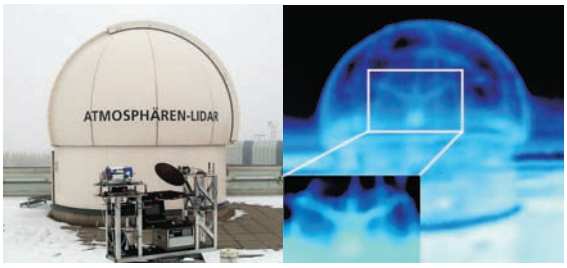

Figure 2.171 Right 37 GHz radiometer image with a person clearly detected inside the optically opaque radome photographed on the left.

Figure 2.172 illustrates the detection capability with the same system inside another radome from a distance of about 45 m [551]. In addition to terrestrial applications, spaceborne radiometers were investigated with respect to the capability of ship detection for the EU EUCLID programme. The study focused on classical imaging approaches using a conical scanner and showed satisfying detection results for large ships.

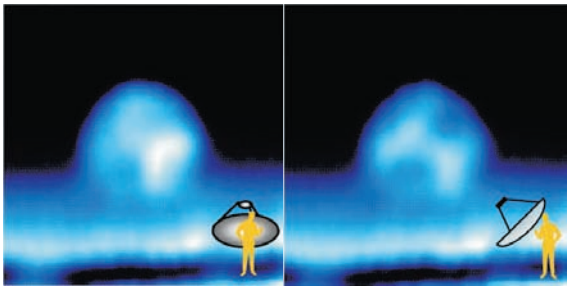

Figure 2.172 37 GHz radiometer images of an optically opaque radome containing a person and a parabolic antenna inside in different positions (see drawings).

Airborne Radiometers

The research into airborne sensors concentrates on the development of very high-resolution passive imaging sensors for UAV (Unmanned Aerial Vehicle) platforms intended for reconnaissance. For a UAV altitude of about 5 km and a required ground resolution in the meter range, an aperture synthesis radiometer in W-band was considered optimal. With a view to reducing cost, the minimum number of receivers and correlators was found by analysing different array geometries and image reconstruction methods. Ground based measurements were used to investigate the techniques. Figure 2.173 shows various array designs and the corresponding reconstruction results using an advanced CLEAN algorithm [285]. The scene was measured at 37 GHz and resampled and thinned out to the required array grid. Only the full U array fulfills the Nyquist sampling criterion on a rectangular grid.

It can be seeathr Radarn that a simple inverse Fourier transform is not a suitable reconstruction method. However, a highly thinned array of a suitable shape in conjunction with an adequate image reconstruction approach can deliver acceptable results compared to the Nyquist array, at least for target detection.

Within a NATO Research and Technology Organisation (RTO) research group this approach was applied to a strawman design of an aperture synthesis radiometer fitted to a typical UAV platform [300] [306]. A Y-array was found to be most useful, as it most easily fits to an aircraft structure while yielding adequate results. Various degrees of thinning error sources such as wing movement were analysed with respect to the reconstructed image quality.

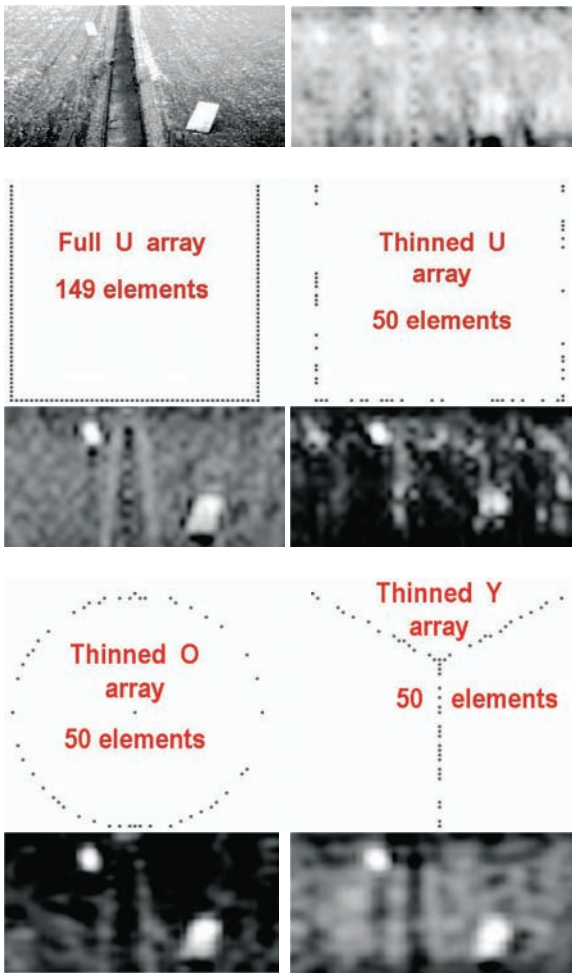

Figure 2.173 Top left: photograph of the scene imaged with a 37 GHz aperture synthesis radiometer. Top right: reconstructed image for the thinned U array using a simple inverse Fourier transform. The other images show the results using the advanced CLEAN algorithm for the various array geometries above [285].

The use of airborne radiometric sensors for the purpose of disaster monitoring and prevention is also of major interest. In this context, the application of radiometric imaging for the monitoring of the seepage condition of dikes was investigated in a project funded by the German Federal Ministry of Education and Research (BMBF) and in cooperation with the Franzius Institute for Hydraulic, Waterways and Coastal Engineering of the University of Hanover. The goal was to develop an efficient sensor for the timely detection of areas susceptible to breaching. Ground based measurements were performed with the line-scanner shown in Figure 2.163 on an artificial but representative dike under controlled conditions. Figure 2.174 shows the results in a time sequence for different frequencies [554].

The basin on the right was filled with water to simulate flooding. Then small artificial channels on the water side were opened in a controlled manner to simulate damage to the dike. After about 36 hours the water starts to leak to the left-hand, dry side of the dike. If this event can be detected in time by a suitable sensor, countermeasures can be taken to prevent a burst. It was demonstrated that an imaging radiometer is able to detect the leakage early for all the frequencies used, in spite of the different spatial resolutions. Hence, an airborne imaging radiometer can also be used for the prevention of potential dike bursts.

The increasingly demanding requirements for very high resolution and near real-time imaging capabilities mean that the principles and technology of aperture synthesis radiometers need further research. Depending on the requirements, the operating conditions and the funds available, real-aperture radiometers, aperture synthesis radiometers and hybrids all have their place. In addition to ground-based systems, the development of a new airborne system is planned.

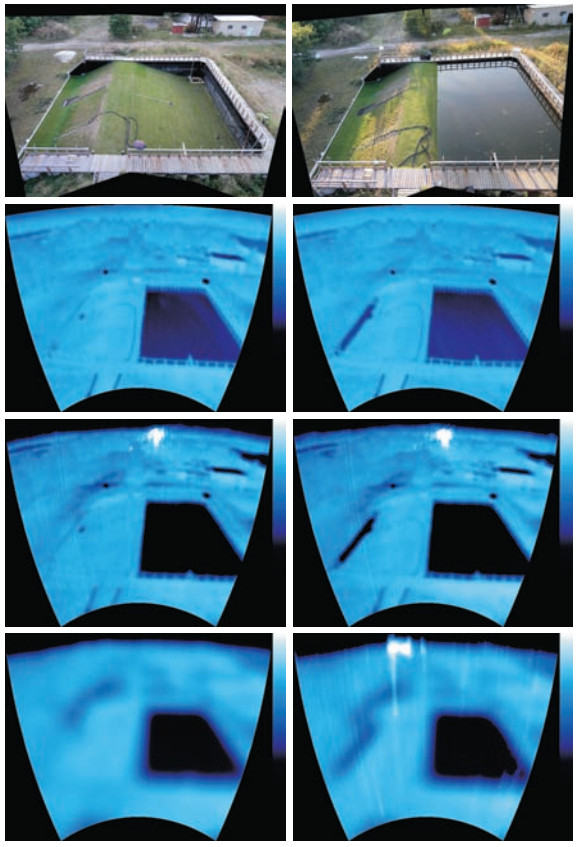

Figure 2.174 Top row: photograph of the artificial dike facilities with the dry (left) and filled (right) water basin. The images below correspond to measurements at three frequencies, 90 GHz, 37 GHz, and 9.6 GHz. The left-hand images show the results before seepage and the right-hand images with seepage (dark blue strips).

The potential for the use of microwave radiometry is clearly evident in the security domain, namely screeners for hidden object detection on persons, through-the-wall imaging and the surveillance of sensitive areas, like nuclear power plants or border areas.

The application of passive microwave systems for disaster monitoring is becoming increasingly important as the likelihood of such events rises. The monitoring of surveillance of dikes and other stretches of water with respect to oil pollution is only one example.

A third important application of passive systems is expected in the radio interference detection and localisation, particularly as the frequency spectrum becomes more and more congested.

2.3.11 Weather Radar

The Institute is inevitably confronted by the influence of the propagation path on the imaging sensors, it being an important element in the performance computation and the system calibration (sections 2.3.7 and 2.3.10). In addition, the Institute participates in European projects in the field of weather radar collaborating with other DLR institutes. Of particular importance is the Institute of Atmospheric Physics with which the Institute shares a fully polarimetric weather radar facility (POLDIRAD). This radar is able to provide unique data for the development and verification of algorithms.

EU AMPER Project

The AMPER project (**A**pplication of **M**ulti-parameter **P**olarimetry in **E**nvironmental **R**emote Sensing) was funded by the European Commission over the period from January 2003 until December 2005. The Institute was responsible for the overall coordination of the project and research contributions in the field of modelling and understanding atmospheric effects and distortions on coherent polarimetric radar data, as well as in the field of polarimetric target decomposition theory.

The main aim of the project was the training and research of young scientists in the area of multi-parameter polarimetry at partner organisations spread all over Europe (i.e. DLR, TU Chemnitz and Definiens Imaging GmbH, Germany; University of Essex, UK; DDRE, Denmark; UPC, Spain; MOTHESIM and University of Rennes, France; JRC, Italy). The scientific activities of the network fall into three main areas dealing with sensor systems and measured data, the underlying physics and scattering models, parameter retrieval and product generation.

The focus of modelling atmospheric effects was on the scattering of hydrometeors, particularly rain drops. The main purpose is not only to have a coherent model for simulating weather radar data, but also to create a link between observations by weather radar systems and SAR systems. Polarimetric propagation effects play an important role for both systems, and, hence, the model can be used to predict or describe the influence of propagation through a medium containing rain drops for polarimetric radars, regardless of whether they are ground-based or airborne/spaceborne. Raindrops are oblate scatterers, where the oblateness increases with the size of the rain drop, and thus rainfall produces anisotropic scattering, which can be measured with polarimetric radars. One particular problem occurs, because the four elements of the scattering matrix are not all measured at the same time but with a certain time delay, which is usually around 1 ms. During this time, the observed scattering volume (containing falling rain drops) changes and, thus, decorrelation will be seen (Figure 2.175) [113][115].

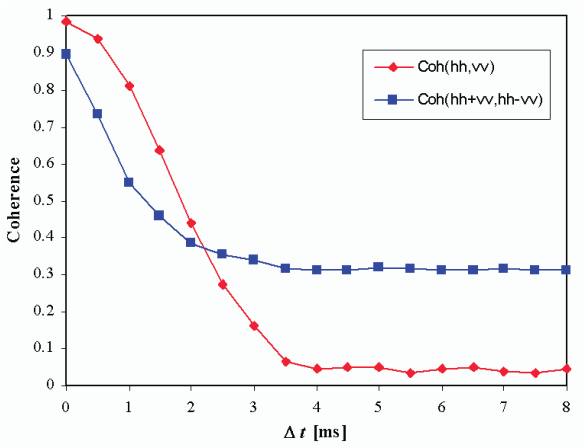

Figure 2.175 Dependence on the measurement interval Δt of the coherence for HH and VV polarisations (red) and the Pauli base. It shows that the decorrelation is strongly dependent on the initial polarisation base, and that this is important for the correct extraction of information.

Using model results and experience drawn from the literature, phase delays and amplitude effects on radar data can be predicted. Special attention has been given to the impact of such effects on the processing of SAR images. Phase changes due to atmospheric distortions have a similar behaviour to motion errors of the sensor platform and thus might not be separated from such additional error sources [134][136].

With regard to polarimetric decomposition theorems, two signal processing approaches have been applied for the first time to fully polarimetric SAR and weather radar signatures. Considerable attention is paid to the eigenvectors of the covariance matrix [9].

EU CARPE DIEM Project

In the framework of the European project CARPE DIEM (**C**ritical **A**ssessment of available **R**adar **P**recipitation **E**stimation techniques and **D**evelopment of **I**nnovative approaches for **E**nvironmental **M**anagement) several work packages with regard to polarimetric techniques have been investigated. The project contributed to the Energy, Environment and Sustainable Development Programme for Research, Technology Development and Demonstration under the fifth Framework Programme with the goal of improving flood forecasting capabilities. The Institute's tasks comprised the exploitation of advanced radar capabilities to allow the enhanced assimilation of weather radar data from operational networks in hydrological and numerical weather prediction models. As the data source, the coherent and fully polarimetric C-band weather radar POLDIRAD was used.

The first task dealt with the use of polarimetric measurements to estimate effects of variation in drop-size distributions on the uncertainty inherent in rainfall estimates collected at different spatial and temporal scales. The parameters particularly taken into account are the differential reflectivity and phase, which occur due to the oblate nature of rain drops. The outcome was that the differential phase could potentially still provide a more accurate estimate of the average rainfall across an area (or equivalently from a series of rapid scans averaged over a period of time).

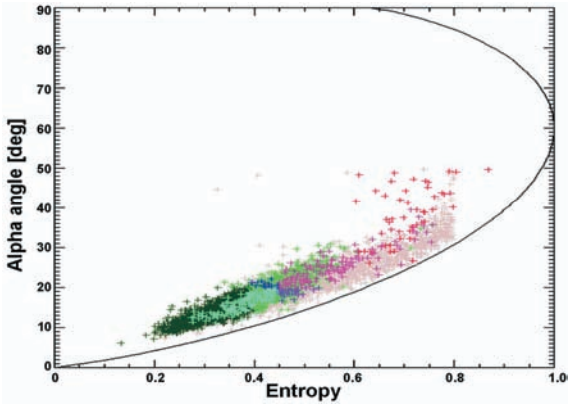

Figure 2.176 Distribution of data points of a thunderstorm in the Entropy-Alpha plane derived from a time series measured with POLDIRAD on 2nd November 2005 [66].

The second task was dedicated to the problem that there is a significant lack of "ground truth" for weather radar observations, i.e. the scattering particles are usually pretty much unknown or have to be guessed by using empirical methods (mostly based on fuzzy logic classification). Polarimetry has the great advantage that the scattering can be related to the physics without a priori or empirical knowledge. Hence, Entropy-Alpha decomposition and classification (originally used for land classification in SAR imaging) has been used in order to identify different types of hydrometeors. The most important premise for a precise decomposition is the correction of differential propagation errors, which can only be performed on time series (raw) data. This type of data is usually not available, but POLDIRAD is now able to deliver also the required time series. Figure 2.176 shows a typical distribution of Entropy-Alpha values in the case of a thunderstorm, which provides a broad variation of scatterers (light rain, heavy rain, hail, sleet, snow) [66]. Using this distribution and an additional weighting with reflectivity values, a classification scheme could be compiled.

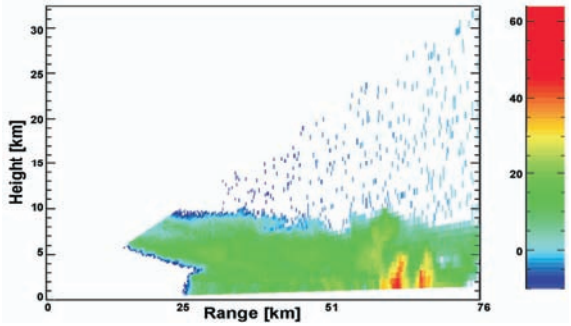

Figure 2.177 Range-height plot of the thunderstorm in the previous image with high reflectivity values. The colours represent volume scattering in dBZ as shown in the colour scale.

In Figure 2.177 and Figure 2.178, the reflectivity can be compared with the classification result. The first impression is that this purely physically derived result is very promising, although a comparison with common techniques has still to be performed and will be part of future activities [116]. The method could not only improve the ability to extract weather information from terrestrial radars, but also from radars on airborne and spaceborne platforms

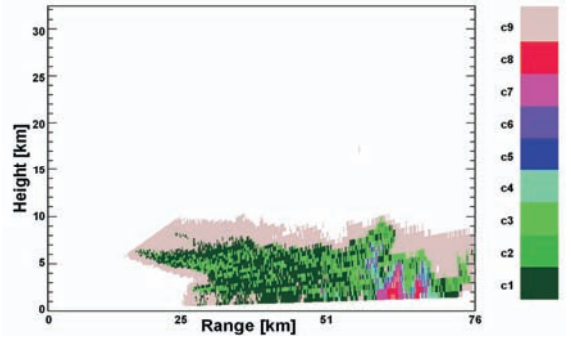

Figure 2.178 Classification of hydrometeors for the thunderstorm shown in the previous figures. Dark green denotes light rain, lighter greens transition to heavy rain, cyan and blue is assumed to be very heavy rain, whereas purple, pink and red denote highly anisotropic scattering from very heavy rain mixed with sleet and/or hail.

3 Documentation

3.1 Academic Degrees

3.1.1 Diploma Theses

Name	Subject	University	Year
1. Bär, Matthias	Klassifizierung polarimetrischer SAR-Daten	Universität der Bundeswehr, Neubiberg	2000
2. Domke, Peter	Entwicklung einer Mikrocontroller-Echtzeiterweiterung für die denzentrale Steuerung des flugzeuggetragenen Radar-systems F-SAR 2000 über CAN-Bus	Technische Universität, Leipzig	2000
3. Guillaso, Stephae	Range Resolution Improvement of Full-Polarimetry Airborne SAR Images using Multiple Parallel Tracks	University of Rennes 1, France	2000
4. Stelzl, Stefan	Validierung eines digitalen Geländemodells aus SAR-Daten	Universität der Bundeswehr, Neubiberg	2000
5. Zeiler, Markus	Nutzung der thermischen Mikrowellen-strahlung zur Detektion von vergrabenen Anti-Personen-Minen	Universität Regensburg	2000
6. Bach, Robert	Aufbau eines digitalen Korrelators für ein Apertur-Synthese-Radiometer	Universität der Bundeswehr, Neubiberg	2001
7. Engwall, Maria	Evaluation of the Monostatic Radar Signal in the Case of Tripple Reflections at Flat Panels	University of Chalmers, Sweden	2001
8. Liebert, Thomas	Aufbau eines experimentellen ISAR-Messsystems im S- und X-Band für hoch-auflösende Radarabbildungen	Universität der Bundeswehr, Neubiberg	2001
9. Pipia, Luca	Anwendung der kohärenten Huynen-Zerlegung zur Gewinnung von optimierten Amplituden-Verhältnissen und relativen Phasen, um effizientere Klassifikations-Observablen zu erhalten	University Cagliari, Italy	2001
10.Weller, Martin	Untersuchung eines adaptiven Filters zur Unterdrückung von Nebenkeulen in hoch-aufgelösten Radarbildern	Universität der Bundeswehr, Neubiberg	2001
11.Fischer, Christian	Studie zur Trennung von Volumen und Oberflächenstreuung mit interfero-metrischen Multi-Baseline SAR-Daten	Technische Univer-sität, München	2002

12.Jirousek, Matthias	Weiterentwicklung eines experimentellen Apertur-Synthese-Radiometers für hochaufgelöste passive Abbildungen im Millimeterwellen-Mikrowellen-Bereich	Universität Karlsruhe	2002
13.Párraga Niebla, Cristina	Block Adaptive Quantization for Interferometric SAR	Univers. Politècnica de Catalunya, Barcelona, Spain	2002
14.Shishkova, Olga	Bestimmung von Oberflächenparametern unter Verwendung von polarimetrischen SAR-Daten	Russian Academy of Sciences – Inst.of Radio Engineering and Electronics	2002
15.Schulteis, Stephan	Entwicklung von Mehrschichtmodellen zur Verbesserung der Detektionswahrscheinlichkeit von Antipersonen-Minen mit Hilfe von Mikrowellenradiometern	Universität Karlsruhe	2002
16.Werl, Guido	Einfluss der Vegetation auf die quantitative Bestimmung von Bodenfeuchte am Beispiel des Ampermooses unter Verwendung von polarimetrischen SAR- und Hyperspektralen Daten	Universität Würzburg	2002
17.Nannini, Matteo	Development and Implementation of Software Moduls for Simulation of Receive Paths of Spaceborn SAR Systems	Universita degli Studi di Firence	2003
18.Hentschel, Mirko	Analysen zur Ein- und Zweipassinterferometrie	Universität der Bundeswehr, Neubiberg	2003
19.Rauh, Christian	Entwicklung und Implementierung eines Prozessors zur Fokussierung bistatischer SAR-Impulsantworten	Technische Universität, Dresden	2003
20.Castell Calderon, Marc	Antenna Pattern Specifications and Optimization for TerraSAR-X	Univers. Politècnica de Catalunya, Barcelona, Spain	2004
21.Chiari, Martin v.	Untersuchung spektraler radiometrischer Mikrowellensignaturen zur Detektion verborgener Objekte in geschichteten Medien	Technische Universität, Chemnitz	2004
22.Gabele, Martina	SAR-Mehrkanalverfahren zur Detektion bewegter Objekte	Universität Karlsruhe	2004
23.Kugler, Florian	Studie der zeitlichen Kohärenzanalyse am Beispiel eines temperaten Mischwaldes	Technische Universität, München	2004
24.Márquez-Martinez, José	Development of a Range Ambiguity Simulator and Investigation of Methods for Range Ambiguity Suppression in SAR	Univers. Politècnica de Catalunya, Barcelona, Spain	2004

25.Meier, Frank	Automatische Bestimmung von ARC/STC-Stellgrößen für ein flugzeuggetragenes Radar mit synthetischer Apertur (SAR)	Fachhochschule Schweinfurt	2004
26.Müller Sánchez, Francisco	Velocity Estimation of Moving Targets using Along-track SAR Interferometry	Universität Karlsruhe	2004
27.Pouria, Sanae	Real Time Pulse Compressor based on 1-bit Quantisation	University Lulea, Schweden	2004
28.Ruiz, Guillermo	Entwicklung und Untersuchung eines schnellen Algorithmus zur Prozessierung hochaufgelöster Drehstand-ISAR-Bilder	Technische Universität, Darmstadt	2004
29.Roca-Cusachs Maennicke, Oliver	Performance Analyses of Hardware Optimized Block Adaptive Quantizer Algorithm for TerraSAR-X Parameter	Univers. Politècnica de Catalunya, Barcelona, Spain	2004
30.Vögele, Andreas	Weiterentwicklung eines digitalen Korrelators für ein Apertur-Synthese-Radiometer	Universität Karlsruhe	2004
31.Aulinger, Thomas	Vergleich von Höhenmodellen aus InSAR- und Lidar-Daten über einem Naturwald im Nationalpark Bayerischer Wald	Fachhochschule München	2005
32.Alban, Francois	L'amèlioration des performances en résolution spectrale d'un radiomètre à large bande et en champ proche, destiné à la détection d'objects enfouis	Royal Military Academy, Belgium	2005
33.Andres, Christian	Topographieabhängige spektrale Filterung für flugzeuggestützte Mehrpass-SAR-Interferometrie	Fachhochschule Wien	2005
34.Daniel, Sandrine	Quantitative Bodenparameterbestimmung unter Verwendung von polaimetrischen und interferometrischen SAR	University of Rennes 1, France	2005
35.Emaer, Jerome	Détermination de l'humidité du sol à partir de mesures radiométriques en bande L	Royal Military Academy, Belgium	2005
36.Hübner, Anna	Entwicklung einer kompakten Antenne für einen Radartransponder	Technische Universität, München	2005
37.Norrman, Helen	Entwicklung einer kompakten Antenne für einen Radartransponder	University Lulea, Schweden	2005
38.Streicher, Veit	Genauigkeitsuntersuchungen von Höhenmodellen, erzeugt mit der SAR-Interferometrie	Universität der Bundeswehr, Neubiberg	2005
39.Wachtl, Stefan	Untersuchung von digitalen Empfängerkonzepten für die Anwendung bei Mikrowellenradiometern	Fachhochschule Würzburg	2005

3.1.2 Doctoral Theses

Name	Subject	University	Year
1. Börner, Thomas	Kohärente Modellierung von Radarrückstreuung für die Anwendung in Polarimetrischer SAR Interferometrie	Ludwig-Maximilians-Universität, München	2000
2. Hellmann, Martin	Classification of Fully Polarimetric SAR-Data for Cartographic Applications	Technische Universität Dresden	2000
3. Mittermayer, Josef	Hochauflösende Verarbeitung von Radardaten mit synthetischer Apertur	Universität Siegen	2000
4. Lamprecht, Katja	Polarimetrische Methoden der Fernerkundung der Atmosphäre: Bestimmung der Tropfengrößendichteverteilung von Niederschlag und Bestimmung der Regenrate bei der Wahl unterschiedlicher Polarisationsbasen	Technische Universität Graz	2000
5. Ulbricht, Andreas	Flugzeuggetragene Repeat-Pass-Interferometrie mit dem E-SAR	Ludwig-Maximilians-Universität, München	2000
6. Fuchs, Frank	Entwicklung und Verifikation eines RCS-Rechenmodells basierend auf den finiten Differenzen im Zeitbereich (FDTD) mit dem Ziel der Hybridisierung mit der Physikalischen Optik (PO)	Universität Saarland	2001
7. Hajnsek, Irena	Inversion of Surface Parameters Using Polarimetric SAR	Universität Jena	2001
8. Potsis, Athanasios	Radio Frequency Interference Suppression for Synthetic Aperture Radar	National Technical University, Athens	2001
9. Dietrich, Björn	Fähigkeiten eines Metalldetektors zur Parameterbestimmung und Objektdiskriminierung	Universität Karlsruhe	2002
10. Greiner, Matthias	Entwicklung neuartiger Bildrekonstruktionsverfahren für das Apertur-Synthese-Radiometer	Universität Karlsruhe	2002
11. Reigber, Andreas	Airborne Polarimetric SAR Tomography	Universität Stuttgart	2002
12. Àlvarez Pérez, José Luis	Two Novel Studies of Electromagnetic Scattering in Random Media in the Context of Radar Remote Sensing	University of Nottingham, UK	2003
13. Alberga, Vito	Comparison of polarimetric methods in image classification and SAR interferometry applications	Technische Universität Dresden	2004
14. Scheiber, Rolf	Hochauflösende Interferometrie für Radar mit Synthetischer Apertur	Universität Karlsruhe	2004
15. Rathgeber, Wolfgang	Superresolution durch den Einsatz spektraler Schätzverfahren in der SAR-Prozessierung	Universität Karlsruhe	2005

3.2 Guest Scientists

Name	Home Institution	Period
1. Dimou, Alexandros	National Technical University, Athens, Greece	Oct. 1998 – Oct. 2000
2. Potsis, Athanasios	National Technical University, Athens, Greece	Oct. 1998 – Oct. 2000
3. Alberga, Vito	EU Research Assistant	Feb. 1999 – Mar. 2002
4. Sood, Khagindra Kumar	Indian Space Research Organization, India	Aug. 1999 – Apr. 2000
5. Bara, Marc	Universitat Politècnica de Catalunya, Barcelona, Spain	Feb. 2000 – Apr. 2000
6. Àlvarez Pérez, José Luis	EU Research Assistant	Mar. 2000 – Feb. 2001
7. Breuer, Axel	University of Rennes 1, France	Jul. 2000 – Jan. 2003
8. Robert, Paulraj	Indian Space Research Organization, India	Sep. 2000 – Jun. 2001
9. Papathanassiou, Konstantinos	EU Research Assistant	Oct. 2000 – Jun. 2001
10.Lopez Martinez, Carlos	EU Research Assistant	Oct. 2000 – Mar. 2002
11.Ewan, Archibald	EU Research Assistant	Jan. 2001 – Mar. 2002
12.Bothale, Vinod M.	Indian Space Research Organization, India	Apr. 2001 – Dec. 2001
13.Olmedo, Rafael	Instituto Nacional de Tecnica Aerospacial, Madrid, Spain	May 2001 – Aug. 2001
14.Fabregas, Xavier	Universitat Politècnica de Catalunya, Barcelona, Spain	May 2001 – Aug. 2001
15.Chokkanathapuram, Rajaraman	Indian Space Research Organization, India	Jun. 2001 – Sep. 2001
16.Ben Khadhra, Kais	Télécom Paris École Nationale Supérieure des Télécommunications, Paris, France (DAAD scholarship)	Oct. 2001 – Sep. 2005
17.Singh, Dahrmendra	University Delhi, India	Jun. 2002 – Feb. 2003

Name	Home Institution	Period
18.Huether, Brian	National Air Intelligence Center, USA	Sep. 2002 – Aug. 2004
19.Kohlhase, Andreas	Deutsche Forschungsgemeinschaft	Sep. 2002 – Sep. 2004
20.Vandewal, Marijke	Royal Military Academy, Belgien	Oct. 2002 – Nov. 2005
21.Misra, Arundhati	Indian Space Research Organization, India	Nov. 2002 – Jul. 2003
22.Ilundain Gorriti, Gorka	Instituto Nacional de Tecnica Aerospacia, Madrid, Spanien	Feb. 2003 – May 2003
23.Liseno, Angelo	EU Research Assistant	Feb. 2003 – Sep. 2003
24.Danklmayer, Andreas	EU Research Assistant	Mar. 2003 – Dec. 2005
25.Zandona Schneider, Rafael	Instituto Tecnológico de Aeronáutica, Brazil (DAAD scholarship)	Mar. 2003 – Sep. 2006
26.Camera de Macedo, Karlus Alexander	Instituto Tecnológico de Aeronáutica, Brazil	Apr. 2003 – Mar. 2007
27.Hiroshi, Kumura	Gifu University, Japan	Sep. 2003 – Nov. 2003
28.Sanz Marcos, Jesus Manuel	Universitat Politècnica de Catalunya, Barcelona, Spain	Jan. 2004 – Apr. 2004
29.Garrestier, Franck	ONERA, France	Jun. 2004 – Aug. 2004
30.Stryker, Amy	National Air Intelligence Center, USA	Sep. 2004 – Aug. 2006
31.Erten, Esra	Technische Universität Berlin (DAAD scholarship)	Sep. 2005 – Nov. 2005
32.Sharma, Jayanti	Universität Karlsruhe (DAAD scholarship)	Oct. 2005 – Jul. 2006

3.3 Scientific Awards

2000

Reigber, Andreas, Best Student Paper Award: "*SAR Tomography and Interferometry for the Remote Sensing of Forested Terrain*", VDE-Verlag, Berlin-Offenbach, European Conference on Synthetic Aperture Radar (EUSAR), ISBN 3-8807-2544-4, München, 23-25 May 2000.

2001

Keydel, Wolfgang, IEEE GRSS Dinstinguished Achievement Award, Geoscience and Remote Sensing Society, 2001.

Mittermayer, Josef, DLR-Wissenschaftspreis 2001: "*Spotlight SAR data processing using the frequency scaling algorithm*", IEEE Geoscience and Remote Sensing Society (IGARSS), vol. 37, No. 5, Sep. 1999, pp. 2198-2114, 2001.

Reigber, Andreas und Moreira, Alberto, IEEE-GRSS Prize Award 2001: "*First Demonstration of Airborne SAR Tomography Using Multibaseline L-Band Data"*, IEEE Transactions on Geoscience and Remote Sensing Society, vol. 38, No. 5, pp. 2142-2152, 2000.

2002

Hajnsek, Irena, Promotionspreis der Friedrich-Schiller-Univerität Jena, *„Inversion of Surface Parameters Using Polarimetric SAR",* DLR-FB-2001-30, pp. 224.

Papathannassiou, Konstantinos, IEEE Senior Member, 2002.

Papathannassiou, Konstantinos, DLR-Wissenschaftspreis 2002: *„Beiträge in der Entwicklung von Polarimetric SAR Interferometry",* IEEE Geoscience and Remote Sensing Society (IGARSS), pp. 2352-2363, 2001.

Papathannassiou, Konstantinos, Best Paper Award 2002, "*A Three Stage Inversion Process for Polarimetric SAR Interferometry*", European Conference on Synthetic Aperture Radar (EUSAR), VDE-Verlag, ISBN 3-8007-2697-1, Cologne, pp. 279-282., 02-04 Jun. 2002.

Werner, Marian, Wernher-von-Braun-Ehrung der Deutschen Gesellschaft für Luft- und Raumfahrt - Lilienthal-Oberth e.V. in Anerkennung der besonderen Leistung als Mitglied des Teams für die erfolgreiche Entwicklung, Vorbereitung und Durchführung der Shuttle Radar Topography Mission (SRTM).

2003

Hajnsek, Irena, DLR-Wissenschaftspreis 2003: *„Inversion of surface parameters from polarimetric SAR*", IEEE Transactions and Geoscience Remote Sensing Society, pp. 727-745, 2003.

Keydel, Wolfgang, Verleihung des akademischen Grades und der Würde eines Doktors der Ingenieurwissenschaften ehrenhalber durch die Technische Fakultät Erlangen-Nürnberg.

2004

Mette, Tobias, Student Paper Prize 2004, "*Applying a Common Allometric Equation to Convert Forest Height from PolInSAR Data to Forest Biomass",* IEEE Geoscience and Remote Sensing Society (IGARSS), Anchorage, Alaska, Sep. 2004.

Moreira, Alberto, IEEE Fellow, citation: "*For Contributions to Synthetic Aperture Radar Systems, High Resolution Signal Processing and Image Formation Algorithms",* 2004.

2005

Gabele, Martina, EADS Argus Award 2005, „SAR-Mehrkanalverfahren 2. Detektion bewegter Objekte", Diploma Thesis, DLR-IB-551-6/2004.

Keydel, Wolfgang, DGON-Ehrenpreis für die Verdienste um die Förderung der Wissenschaft und Forschung auf dem Gebiet der Radartechnik, International Radar Conference (IRS), Berlin, 2005.

3.4 Participation in External Professional Committees

- Chairman of NATO SET-045 (TG26) "Civil Spacebased Radar Technology for Military Applications"
- Chairman of NATO SET-102 "High resolution spaceborne SAR-systems for geospatial intelligence "
- Permanent Guest at NATO RTO Space Science and Technology Advisory Group (SSTAG)
- Permanent Guest of the EUCLID CEPA 9 Steering Committee: Satellite Surveillance and Military Space Technology
- Member of the CEOS SAR Calibration Working Group
- Member of the Board of Directors of the ITG/VDE Society 2003-2005, 2006-2008
- Member of Techn. Committee 7.4 on Microwave Techniques of ITG/VDE (Information Technology Society of German Association for Electrical, Electronic & Information Technologies)
- Member of the ESA SAR Science Advisory Group since 2003
- Member of the Technical/Scientific Council (WTR) of DLR 2005-2006
- Member of Institute of Electrical and Electronics Engineers (IEEE)
- Member of "The Electromagnetics Academy", Massachusetts, Cambridge, USA
- Member of VDE/ITG, German Association of Engineers
- Member of the Administrative Committee (AdCom) of the IEEE Geoscience and Remote Sensing Society, 1999-2001, 2004-2006
- Guest Editor of the Special Issue of the Journal of Telecommunications (Frequenz), Special Issue of the 3rd EUSAR conference, Mar. 2001.
- Associate Editor for IEEE Geoscience and Remote Sensing Letters (GRSL)
- Guest Co-Editor for the IEEE Transactions on Geosc. and Remote Sensing (TGARS) for the Special Issue on Retrieval of Geo/Bio Parameters over Land Surfaces
- Chair (and founder) of the IEEE GRSS German Chapter
- Member of Fellow Evaluation Committee for IEEE OES 2004-2005
- Member of the IEEE AdHoc Committee on Earth Observation for GEOSS recommendation
- Guest Editor of Special Issue of Journal of Telecommunications, Special Issue of the 3rd EUSAR Conference, 2001
- Member of ESA SMOS Science Advisory Group (Soil Moisture and Ocean Salinity)

3.5 Paper Reviews

- Aerospace Science and Technology
- AEÜ - International Journal of Electronics and Communication
- Computers & Geosciences
- EURASIP Journal on Applied Signal Processing
- Fluctuation and Noise Letters
- IEE Proceedings on Radar, Sonar and Navigation
- IEEE Geoscience and Remote Sensing Letters
- IEEE Transactions on Aerospace and Electronic Systems
- IEEE Transactions on Antennas and Propagation
- IEEE Transactions on Geoscience and Remote Sensing
- IEEE Transactions on Image Processing
- IMA - Journal of Applied Mathematics
- Indian Journal of Radio & Space Physics
- International Journal of Numerical Modeling: Electronic Networks, Devices and Fields
- International Journal of Radio and Space Physics
- International Journal of Remote Sensing
- Journal of Applied Physics
- Korean Journal of Remote Sensing
- Meteorologische Zeitschrift
- Photogrammetric Engineering and Remote Sensing
- Proceedings of the Royal Society of London
- Quarterly Journal of Mechanics and Applied Mathematics

- Radio Science
- Remote Sensing of Enviroment
- Reports on Mathematical Physics
- Spatial Vision - International Journal of Computation, Perception, Attention, and Action

3.6 Conferences

IEEE Geoscience and Remote Sensing Symposium (IGARSS), **Member of Technical Program Committee, Sessions Organiser, Invited Papers,** 1999-2006.

European Conference on Synthetic Aperture Radar (EUSAR), **Technical Chairman, Awards Chairman**, Munich, Germany, May 2000.

European Conference on Synthetic Aperture Radar (EUSAR), **Awards Chairman, Member of the Program Board**, Cologne, Germany, Jun. 2002.

European Conference on Synthetic Aperture Radar (EUSAR), **Awards Chairman, Member of the Program Board**, Ulm, Germany, May 2004.

European Conference on Synthetic Aperture Radar (EUSAR), **Conference Chair, Main Organiser; complete paper review process; Member of Program Board**, Dresden, Germany, May 2006.

Committee on Earth Observation Satellites (CEOS), **Member of the Technical Program Committee,** 1999, 2001-2005.

Advanced SAR Workshop (ASAR), **Member of the Technical Program Committee**, 2001-2005.

International Radar Symposium (IRS), **Member of the Technical Program Committee,** 2003, 2005.

ESA Fringe Workshop, **Member of the Technical Program Committee,** 2003, 2005.

International Workshop on Applications of Polarimetry and Polarimetric Interferometry (PolInSAR), **Member of the Technical Program Committee**, 2003, 2005.

Progress in Electromagnetics Research Symposium (PIERS), **Member of the Technical Program Committee**, 2006.

ESA/ENVISAT Workshop, **Member of the Technical Program Committee**, 2004.

European Microwave Conference (EuMC), **Member of the Technical Program Committee,** 2003-2006.

4th International Symposium on Retrieval of Bio- and Geophysical Parameters from SAR Data for Land Applications, ESA, **Member of the Technical Program Committee**, 2004.

German Microwave Conference (GeMiC), **Member of the Technical Program Committee,** 2005-2006.

International Radar Conference (IRC), **Member of the Awards Committee**, Toulouse, France, 2004.

Union Radio-Scientifique Internationale (URSI) XXVIII General Assembly, **Member of Technical Committee,** New Delhi, India, Oct. 2005.

Union Radio-Scientifique Internationale (URSI) XXVIII General Assembly, **Member of Technical Committee,** Maastricht, The Netherlands, Aug. 2002.

Union Radio-Scientifique Internationale (URSI) Commision F Symposium on Propagation and Remote Sensing, **Conference Chair, Main Organiser; complete paper review process; Member of Program Board,** Garmisch-Partenkirchen, 12-15 Feb. 2002.

Soil Moisture and Ocean Salinity (SMOS) Workshop, **Main Organiser,** Oberpfaffenhofen, Germany, 10-12 Dec. 2001.

2. Luftbildsymposium der Bundeswehr, **Main Organiser,** 27-29 Jan. 2004.

2nd X-SAR/SRTM PI Workshop, **Main Organiser,** Oberpfaffenhofen, Germany, 17-18 Oct. 2002.

NATO, **Research and Technology Board and Associated Meeting**, Lisbon, 17 Sep. 2005.

3.7 Lectures at Universities

Lecturer	University	Subject	2000	2001	2002	2003	2004	2005
Chandra, Madhu	Universität Chemnitz	Elektrotechnik	**X**	**X**				
Chandra, Madhu	Universität Chemnitz	HF-Technik			**X**			
Danklmayer, Andreas	Technische Universität Chemnitz	Mikrowellentechnik						**X**
Hajnsek, Irena	Universität Jena	Angewandte Radar-fernerkundung am Beispiel von Landnutzungscharakterisierung		**X**	**X**	**X**		
Younis, Marwan	Universität Karlsruhe	Advanced Radio Communications I						**X**
Moreira, Alberto	Universität Karlsruhe	Spaceborne SAR Remote Sensing				**X**	**X**	**X**
Süß, Helmut	Universität Karlsruhe	Mikrowellenradiometrie – neue Verfahren und Anwendungen	**X**	**X**	**X**	**X**	**X**	**X**
Süß, Helmut	Universität der Bundeswehr, Neubiberg	Radar- und Lasermethoden	**X**	**X**	**X**	**X**	**X**	**X**

3.8 Publications

3.8.1 Articles in Refereed Journals

[1] **Alberga**, **V**., **Chandra**, **M**., *Volume decorrelation resolution in polarimetric SAR interferometry*, IEE Electronics Letters, vol. 39, pp. 314 - 315, 2003.

[2] **Alberga**, **V**., *Volume decorrelation effects in polarimetric SAR interferometry*, IEEE Transactions on Geoscience and Remote Sensing, vol. 42, pp. 2467 - 2478, 2004.

[3] Bara, M., **Scheiber**, **R**., Broquetas, A., **Moreira**, **A**., *Interferometric SAR Signal Analysis in the Presence of Squint*, IEEE Transactions on Geoscience and Remote Sensing, Vol. 38, pp. 2164 - 2178, 2000.

[4] **Börner**, **T**., **Thurner, S.**, **Kemptner**, **E**., *Ka-Band Transmission Measurements of Dielectric Coplanar Plates at High Temperatures Using Solar Energy*, Frequenz - Journal of Telecommunications, vol. 11/12, pp. 242 - 245, 2005.

[5] Böttger, U., Beier, K., Biering, B., Müller, C., **Peichl**, **M**., Spyra, W., "*easyMine*" *Realistic and systematic Mine Detection Simulation Tool*, Advances in Radio Science (ARS), vol. 2, pp. 237 - 239, 2004.

[6] **Alvarez-Perez, J.L.**, *An extension of the IEM/IEMM suface scattering model*, Waves in Random Media, vol. 11, pp. 307 - 329, 2001.

[7] Cloude, S.R., **Papathanassiou**, **K**., Pottier, E., *Radar Polarimetry and Polarimetric Interferometry*, IEICE Transactions on Electronics, vol. E84-C, pp. 1814 - 1822, 2001.

[8] Cloude, S.R., **Papathanassiou**, **K**., *Three-stage inversion process for polarimetric SAR interferometry*, IEE Proceedings - Radar Sonar and Navigation, vol. 150, pp. 125 - 134, 2003.

[9] **Danklmayer**, **A.**, **Lüneburg, E.**, Boerner, W.-M., *Principal Component Analysis in Radar Polarimetry*, Frequenz - Journal of Telecommunications, vol. 5-6/2005, pp. 158 - 163, 2005.

[10] Dubois-Fernandez, P., Cantalloube, H., Vaizan, B., **Krieger**, **G**., **Horn**, **R**., **Wendler**, **M**., Giroux, V., *ONERA-DLR bistatic SAR campaign:Planning, data acquisition, and first analysis of bistatic scattering behavior of natural and urban targets*, IEE Proceedings - Radar Sonar and Navigation, 2004.

[11] **Fiedler**, **H**., Börner, E., **Mittermayer**, **J.**, **Krieger**, **G.**, *Total Zero Doppler Steering - A New Method for Minimizing the Doppler Centroid*, IEEE - Geoscience and Remote Sensing Letters, vol. 2, pp. 141 - 145, 2005.

[12] **Fuchs, F., Kemptner**, **E.**, **Klement**, **D.**, Planta, K., *Bistatic RCS Computations by FDTD and Comparison with other Rigorous Methods and Experiments*, Frequenz - Journal of Telecommunications, vol. 54, pp. 141 - 144, 2000.

[13] **Geudtner**, **D**., Vachon, P., Mattar, K., Schättler, B., Gray, A.L., *Interferometric Analysis of RADARSAT Strip-Map Mode Data*, Canadian Journal of Remote Sensing, vol. 27, pp. 96 - 108, 2001.

[14] **Geudtner, D., Zink, M.,** Gierull, Ch., Shaffer, S., *Interferometric Alignment of the X-SAR Antenna System on the Space Shuttle Radar Topography Mission*, IEEE Transactions on Geoscience and Remote Sensing, vol. 40, No. 5, pp. 995 - 1006, 2002.

[15] **Hajnsek**, **I.**, Pottier, E., Cloude, S.R., *Inversion of surface parameters from polarimetric SAR*, IEEE Transactions on Geoscience and Remote Sensing, vol. 41, pp. 727 - 745, 2003.

[16] **Hajnsek**, **I.**, Cloude, S., *The Potential of InSAR for Quantitative Surface Parameter Estimation*, Can. J. Remote Sensing, vol. 31, pp. 85 - 102, 2005.

[17] **Hounam**, **D., Wägel, K**., *A Technique for the Identification and Localization of SAR Targets using Encoding Transponders*, IEEE Transactions on Geoscience and Remote Sensing, vol. 39, pp. 3 - 7, 2001.

[18] **Jäger, G**., **Benz, U**., *Measures of classification accuracy based on fuzzy similarity*, IEEE - Transactions on Geoscience and Remote Sensing, vol. 38, pp.1462 - 1467, 2000.

[19] **Jäger, G.**, *Even continuity and equicontinuity in fuzzy topology*, Fuzzy Sets and Systems, vol. 123, pp. 159 - 167, 2001.

[20] **Jäger**, **G.**, *Degrees of Compactness in Fuzzy Convergence Spaces*, Fuzzy Sets and Systems, vol. 125, pp. 167 - 175, 2002.

[21] **Keydel**, **W**., *Perspectives and Vision for future SAR Systems*, IEE Proceedings - Radar Sonar and Navigation, vol. 150, pp. 97 - 103, 2003.

[22] Kimura, H., Nakamura, T., **Papathanassiou**, **K**., *Suppression of Ground Radar Interferences in JERS-1 SAR Data*, IEICE Transactions on Communications, vol. 87, pp.3759-3765, 2004.

[23] **Kohlhase, A.O.**, Feigl, K.L., Massonnet, D., *Applying differential InSAR to orbital dynamics: a new approach for estimating ERS trajectories*, Journal of Geodesy, vol. 77, pp. 493 - 502, 2003.

[24] **Krieger, G**., Rentschler, I., Hauske, G., Schill, K., Zetzsche, C., *Object and scene analysis by saccadic eye-movements: an investigation with higher-order statistics*, Spatial Vision, vol. 13, pp. 201 - 214, 2000.

[25] **Krieger**, **G., Fiedler, H., Mittermayer, J., Papathanassiou**, **K., Moreira, A.**, *Analysis of multistatic configurations for spaceborne SAR interferometry*, IEE Proceedings - Radar Sonar and Navigation, vol. 150, pp. 87 - 96, 2003.

[26] **Krieger**, **G., Mittermayer, J., Buckreuss**, **S., Wendler**, **M**., **Sutor, T.**, **Witte**, **F.**, **Moreira**, **A.,** *Sector Imaging Radar for Enhanced Vision*, Aerospace Science and Technology, vol. 7, pp. 147 - 158, 2003.

[27] **Krieger**, **G**., **Gebert, N., Moreira, A.**, *Unambiguous SAR Signal Reconstruction from Nonuniform Displaced Phase Center Sampling*, IEEE Geoscience and Remote Sensing Letters, vol. 1, pp. 260 - 264, 2004.

[28] **Krieger, G., Moreira, A.,** *Spaceborne Bi- and Multistatic SAR: Potentials and Challenges*, IEE Proceedings - Radar Sonar and Navigation, in press, 2005.

[29] **Krieger, G., Papathanassiou, K.**, Cloude, S., *Spaceborne Polarimetric SAR Interferometry: Performance Analysis and Mission Concepts*, EURASIP Journal of Applied Signal Processing, pp. 3272 - 3292, 2005.

[30] **Krieger, G., Younis, M**., *Impact of Oscillator Noise in Bistatic and Multistatic SAR*, IEEE Geoscience and Remote Sensing Letters, in press, 2005.

[31] Lee, J.S., Cloude, S.R., **Papathanassiou**, **K.**, Grunes, M.R., Woodhouse, I.H., *Speckle filtering and coherence estimation of polarimetric SAR interferometry data for forest applications*, IEEE Transactions on Geoscience and Remote Sensing, vol. 41, pp. 2254 - 2263, 2003.

[32] Lee, J.S., Boerner, W.M., Schuler, D.L., Ainsworth, T.L., **Hajnsek**, **I**., **Papathanassiou**, **K**., Lüneburg, E., *A Review of Polarimetric SAR Algorithms and their Applications*, Journal of Photogrammetry and Remote Sensing, China, vol. 9, pp. 31 - 80, 2004.

[33] **Liseno**, **A**., Pierri, R., *Imaging of voids by means of a physical-optics-based shape-reconstruction algorithm*, J. Opt. Soc. Am. A, vol. 21, pp. 968 - 974, 2004.

[34] **Liseno, A**., Pierri, R., *Shape Reconstruction by the Spectral Data of the far-field Operator: Analysis and Performances*, IEEE Trans. Antennas and Propagation, vol. 52, pp. 899 - 903, 2004.

[35] **Liseno, A**., Tartaglione, F., Soldovieri, F., *Shape reconstruction of 2d buried objects under a Kirchhoff approximation*, IEEE Geoscience and Remote Sensing Letters, vol. 1, pp. 118 - 121, 2004.

[36] **Macedo**, **K.A.C**., **Scheiber, R**., *Precise Topography- and Aperture-Dependent Motion Compensation for Airborne SAR*, IEEE Geoscience and Remote Sensing Letters, vol. 2, pp. 172 - 176, 2005.

[37] Martinez, C.L., Canovas, X.F., **Chandra**, **M**., *SAR Interferometric Phase Noise Reduction using wavelet transform*, IEE Electronics Letters, vol. 37, pp. 649 - 651, 2001.

[38] **Mittermayer, J**., *The Frequency Scaling Algorithm and interferometric Spotlight SAR pro-cessing*, Aerospace Science and Technology, vol. 6, pp. 147 - 158, 2002.

[39] **Osipov**, **A.**, *Zeros of the Bessel function and the role of continuous spectrum in the problem of electromagnetic diffraction by a finitely conducting sphere*, Vestnik St. Petersburg University, Physics and Chemistry, pp. 29 - 38, 2000.

[40] **Osipov, A**., Hongo, K., Kobayashi, H., *High-frequency approximations for electromagnetic field near a face of an impedance wedge*, IEEE Transactions on Antennas and Propagation, vol. 50, pp. 930 - 940, 2002.

[41] **Osipov**, **A.**, *A Simple Approximation of the Maliuzhinets Function for Describing Wedge Diffraction*, IEEE Transactions on Antennas and Propagation, vol. 53, pp. 2773 - 2776, 2005.

[42] **Öttl**, **H.**, **Moreira**, **A.**, **Süss**, **H.**, *Some Results of New Microwave Remote Sensing Experiments*, Acta Astronautica, vol. 47, pp. 355 - 363, 2000.

[43] **Öttl**, **H.**, Briess, K., Lorenz, E., Oertel, D., Skrbek, W., Walter, I., Zhukov, B., *The Disaster "Fires", its Detection and Means to Improve Information*, Space Technology, vol. 23, pp. 249 - 256, 2003.

[44] **Papathanassiou**, **K.**, Cloude, S.R., *Single Baseline Polarimetric SAR Interferometry*, IEEE Transactions on Geoscience and Remote Sensing, vol. 39, pp. 2352 - 2363, 2001.

[45] **Parraga Niebla, C., Krieger, G.**, *Optimization of Block-Adaptive Quantization for SAR Raw Data*, Space Technology, vol. 23, pp. 131 - 141, 2003.

[46] Potsis, A., **Reigber, A., Mittermayer, J**., **Moreira, A.**, Uzunoglou, N., *Sub-aperture algorithm for motion compensation improvement in wide-beam SAR data processing*, IEE Electronics Letters, vol. 37, pp. 1405 - 1407, 2001.

[47] **Reigber, A., Moreira, A.**, *First Demonstration of Airborne SAR Tomography Using Multibaseline L-Band Data*, IEEE Transactions on Geoscience and Remote Sensing, vol. 38, pp. 2142 - 2152, 2000.

[48] **Reigber, A**., *Correction of Residual Motion Errors in Airborne SAR Interferometry*, IEE Electronics Letters, vol. 37, pp. 1083 - 1084, 2001.

[49] **Reigber**, **A**., **Papathanassiou**, **K**., Cloude, S., **Moreira**, **A.**, *Tomography and Interferometry for Remote Sensing of Forested Terrain*, Frequenz - Journal of Telecommunications, vol. 55, pp. 119 - 122, 2001.

[50] **Reigber**, **A., Scheiber, R**., *Airborne Differential SAR Interferometry: First Results at L-band*, IEEE Transactions on Geoscience and Remote Sensing, vol. 41, pp. 1516 - 1520, 2003.

[51] **Scheiber, R., Moreira, A.**, *Coregistration of Interferometric SAR Images Using Spectral Diversity*, IEEE Transactions on Geoscience and Remote Sensing, vol. 38, pp. 2179 - 2191, 2000.

[52] Scheuchl, B., Cumming, I., **Hajnsek, I.**, *Classification of fully polarimetric single and dual frequency SAR data of Sea Ice using the Wishart Classifier*, Canadian Journal of Remote Sensing, vol. 31, pp. 61-72, 2005.

[53] Schill, K., Umkehrer, E., Beinlich, S., **Krieger**, **G**., Zetzsche, C., *Knowledge-based scene analysis with saccadic eye-movements*, Journal of Electronic Imaging, vol. 10, pp. 152 - 160, 2001.

[54] **Schröder, R.**, **Süß, H**., **Zeller, K.H**., *Performance analysis of spaceborne SAR systems*, Aerospace Science and Technology, vol. 6, pp. 451 - 457, 2002.

[55] **Schröder, R.**, Puls, J., **Hajnsek, I., Jochim, F., Neff, T**., Kono, J., Paradella, W., Quintino, M., Valeriano, D., Costa, M., *MAPSAR: A small L-band SAR mission for land observation*, Acta Astronautica, vol. 56, pp. 35 - 43, 2005.

[56] **Schwerdt, M**., **Hounam, D., Alvarez-Peres, J.L., Molkenthin, T**., *The Calibration Concept of TerraSAR-X: A Multiple Mode, High Resolution SAR*, Canadian Journal of Remote Sensing, vol. 31, pp. 30 - 36, 2005.

[57] **Süß, H., Söllner, M.**, *Fully Polarimetric Measurements of Brightness Temperature Distributions With a Quasi-Optical Radiometer System at 90 GHz*, IEEE Transactions on Geoscience and Remote Sensing, vol. 43, pp. 1170 - 1179, 2005.

[58] **Werner, M.**, *Shuttle Radar Topography Mission (SRTM) Mission Overview*, Frequenz - Journal of Telecommunications, vol. 55, pp. 75 - 79, 2001.

[59] **Younis, M., Metzig, R., Krieger, G.**, *Performance Prediction of a Phase Synchronization Link for Bistatic SAR*, IEEE Geoscience and Remote Sensing Letters, in press, 2005.

[60] Zetzsche, C., **Krieger, G.**, *Intrinsic Dimensionality: Nonlinear Image Operators and Higher-Order Statistics,* in *Nonlinear Image Processing*, vol. Nonlinear Image Processing, Mitra, S.K. and Sicuranza, G.L., Eds.: Academic Press, 2000, pp. 403 - 448.

[61] Zetzsche, C., **Krieger, G.**, *Nonlinear mechanisms and higher-order statistics in biological vision and electronic image processing: review and perspectives*, Journal of Electronic Imaging, vol. 10, pp. 56 - 99, 2001.

3.8.2 Research Reports and Periodicals

[62] **Alberga, V.,** *Comparison of polarimetric methods in image classification and SAR interferometry applications*, DLR-FB-2004-05, pp. 171, 2004.

[63] **Alvarez-Perez, J.L.,** *Two Novel Studies of Electromagnetic Scattering in Random Media in The Context of Radar Remote Sensing,* DLR-FB-2003-11, pp. 166, 2003.

[64] Bachem, A., Beneke, K., **Süß, H**., Dittler, T., Hayn, D., Klein, J., *Bedarf und Perspektiven für die Beschaffung raumgestützter SAR-Sensoren zur vernetzten Operartionsführung*, in Europas Zukunft zwischen Himmel und Erde, Nomos Verlag, ISBN 3-8329-1410-2, pp. 148 – 166, 2005.

[65] Bamler, R., Dech, S., Meisner, R., Runge, H., **Werner, M.**, *SRTM - Ausschnitte aus der Weltkarte des 21. Jahrhunderts*, DLR Nachrichten, pp. 2-21, 2003.

[66] **Börner, T.**, *Kohärente Modellierung von Radarrückstreuung für die Anwendung in Polarimetrischer SAR Interferometrie*, DLR-FB-2000-11, pp. 123, 2000.

[67] **Buckreuss, S., Krieger, G., Mittermayer, J., Moreira, A., Sutor, T**., **Wendler, M., Witte, F**., Venot, Y., Wiesbeck, W., **Younis, M.**, *Final Report: SIREV - Development of a Functional Model*, DLR-FB-2000-44, pp. 154, 2000.

[68] **Fuchs, F.**, *Entwicklung und Verifikation eines RCS-Rechenmodells basierend auf den finiten Differenzen im Zeitbereich (FDTD) mit dem Ziel der Hybridisierung mit der Physikalischen Optik (PO),* DLR-FB-2001-31, pp.146, 2001.

[69] **Hajnsek, I.**, *Inversion of Surface Parameters Using Polarimetric SAR*, DLR-FB-2001-30, pp. 224, 2001.

[70] **Hellmann, M**., *Classification of Fully Polarimetric SAR-Data for Cartographic Applications*, DLR-FB-2000-19, pp. 170, 2000.

[71] **Keydel, W.**, *Perspectives for the Future of Space Borne Synthetic Aperture Radar for Earth Observation*, Journal Elektrotechnik & Informationstechnik, Springer Verlag, 2003.

[72] **Keydel, W.,** Röde, B., *Radar Research and Development in Oberpfaffenhofen during the 20th Century and beyond,* DGON Report "100 Years of RADAR - Special Issue", May 2005, Bonn, Germany, 2005.

[73] **Lamprecht, K.**, *Polarimetrische Methoden der Fernerkundung der Atmosphäre: Bestimmung der Tropfengrößedichteverteilung von Niederschlag und Bestimmung der Regenrate bei der Wahl unterschiedlicher Polarisationsbasen*, DLR-FB-2000-36, pp. 178, 2000.

[74] **Lopez Martinez, C.**, *Multidimensional Speckle Noise, Modelling and Filtering Related to SAR Data,* DLR-FB-2004-35, pp. 254, 2004.

[75] **Mittermayer, J.,** *Hochauflösende Verarbeitung von Radardaten mit synthetischer Apertur*, DLR-FB-2000-29, pp. 216, 2000.

[76] **Moreira**, **A.**, *IEEE German Section - Geoscience and Remote Sensing Society Chapter*, IEEE Geoscience and Remote Sensing Society Newsletter, pp. 8 - 11, 2003.

[77] **Rathgeber, W.,** *Superresolution durch den Einsatz spektraler Schätzverfahren in der SAR-Prozessierung,* DLR-FB-2005-15, pp. 148, 2005.

[78] **Reigber, A.,** *Airborne Polarimetric SAR Tomography*, DLR-FB-2002-02, pp.132, 2002.

[79] **Scheiber, R.,** *Hochauflösende Interferometrie für Radar mit Synthetischer Apertur*, DLR-FB-2004-12, pp. 153, 2004.

[80] **Ulbricht, A.,** *Flugzeuggetragene Repeat-Pass-Interferometrie mit dem E-SAR*, DLR-FB-2000-12, pp. 157, 2000.

[81] **Wendler, M., Krieger, G.,** Dubois-Fernandez, P., *Bistatic Synthetic Aperture Radar,* Paris Air Show 2003, LeBourget, 15-22 Jun. 2003.

[82] **Werner, M.,** *Status of the SRTM data processing: when will the world-wide 30m DTM data be available?* GIS Fachzeitschrift für Geo Informations Systeme, vol. 6, pp. 6 - 10, 2001.

3.8.3 Conference Proceedings - Published

[83] **Alberga**, **V., Chandra, M.,** *Analysis of amplitude ratios in SAR-polarimetry*, Kleinheubacher Tagung 2000; Kleinheubach, Germany, 25-29 Sep. 2000, pp. 527 - 534, 2000.

[84] **Alberga**, **V., Chandra, M.,** Krogager, E., *A comparison of target decomposition theorems in SAR interferometry applications*, Union Radio-Scientifique Internationale (URSI) Commission F Open Symposium on Propagation and Remote Sensing, Garmisch-Partenkirchen, Germany, 12-15 Feb. 2002.

[85] **Alberga, V., Chandra, M.,** *Combined application of target decomposition methods and polarimetric SAR interferometry: some preliminary results*, International Society for Optical Engineering (SPIE),Toulouse, France, 17-21 Sep. 2001, pp. 140 - 150, 2002.

[86] **Alberga**, **V., Chandra, M., Papathanassiou, K.,** *An Analysis of Volume Decorrelation in Polarimetric SAR Interferometry*, European Conference on Synthetic Aperture Radar (EUSAR), Cologne, Germany, 4-6 Jun. 2002, pp. 613 - 616, 2002.

[87] **Alberga, V., Chandra, M., Papathanassiou, K.,** *An analysis of volume decorrelation in polarimetric SAR interferometry*, European Conference on Synthetic Aperture Radar (EUSAR), pp. 613 - 616, Cologne, Germany, 2002.

[88] **Alberga, V., Chandra, M.**, Pipia, L., *Supervised classification of coherent and incoherent polarimetric SAR observables: comparison and accuracy assessments*, International Society for Optical Engineering (SPIE), Agia Pelagia, Crete, Greece, 22-27 Sep. 2002, pp. 181 - 191, 2003.

[89] Alivizatos, E., **Reigber, A., Moreira, A.,** Uzunoglu, N., *SAR Processing with Motion Compensation using the Extended Wavenumber Algorithm*, European Conference on Synthetic Aperture Radar (EUSAR), Ulm, 25 -27 May 2004.

[90] Allain, S., Ferro-Famil, L., **Hajnsek, I.,** Pottier, E., *Extraction of Surface Parameters from Multi-Frequency and Polarimetric SAR Data*, European Conference on Synthetic Aperture Radar (EUSAR), Cologne Germany, 4-6 Jun. 2002, pp. 295 - 298, 2002.

[91] Allain, S., Ferro-Famil, L., Pottier, E., **Hajnsek, I.**, *Extraction of Surface Parameters from Multi-frequency and Polarimetric SAR Data*, IEEE Geoscience and Remote Sensing Symposium (IGARSS), Toronto Canada, 24-28 Jun.2002, pp.426-428, 2002.

[92] **Alvarez-Perez, J., Hajnsek, I., Papathanassiou, K.,** *Modelling ot the Mueller Matrix for Rough Surface Scattering*, Progress in Electromagnetics Research Symposium (PIERS), Cambridge Massachusetts USA, 1- 5 Jul. 2002.

[93] **Alvarez-Pérez, J.L., Schwerdt, M., Hounam, D.,** Torres, R., Buck, C., **Zink, M.**, *Antenna Pattern Optimization for the ENVISAT ASAR Antenna with Failed Elements*, 25th ESA Antenna Workshop on Satellite Antenna Technology, Noordwijk 2002.

[94] **Alvarez-Pérez, J.L., Schwerdt, M., Hounam, D.,** Torres, R., Buck, C., **Zink, M.,** *Antenna Pattern Synthesis with Optimized Excitation Laws in Use of a Genetic Algorithm for ENVISAT/ASAR*, European Conference on Synthetic Aperture Radar (EUSAR), Cologne 2002.

[95] Amiot, T., **Krieger, G.**, Douchin, F., **Werner, M.**, Fjortoft, R., *TerraSAR-L Interferometric Cartwheel: DEM Performance Estimation*, Radar Conference, pp. 1-6, Toulouse, France, 2004.

[96] Bara, M., Andreu, J., **Scheiber, R., Moreira, A**., Broquetas, A., *Interferometric Phase Corrections during Squinted-data Geocoding*, European Conference on Synthetic Aperture Radar (EUSAR), Munich, 23-25 May, 2000, pp. 193 - 196, 2000.

[97] Bara, M., Andreu, J., **Scheiber, R., Horn, R.**, Broquetas, A., *A Mosaic Technique for the Generation of Wide-Area DEMs with Interferometric SAR Data*, IEEE Geoscience and Remote Sensing Symposium (IGARSS), Sydney, 9-13 Jul. 2001.

[98] **Ben Khadhra, K.**, Singh, D., **Börner, T., Hounam, D.,** Wiesbeck, W., *Analysis of Multi-Frequency Polarimetric Data for Assessment of Bare Soil Roughness*, IEEE Geoscience and Remote Sensing Symposium (IGARSS), Toulouse, France, 2003.

[99] **Benz, U., Fischer, J., Jäger, G.,** *Image Content Dependent Compression of Polarimetric SAR Data*, IEEE Geoscience and Remote Sensing Symposium (IGARSS), Hawaii, 24-28 Jul. 2000.

[100] **Benz, U., Fischer, J., Jäger, G.**, *Image Content Dependent Compression of SAR Data*, Space-Based Observation Technology (SBOT), Samos/Greece, 16-18 Oct., 2000.

[101] **Benz, U., Fischer, J.,** *Adaptive SAR Image Compression in Wavelet Domain*, European Conference on Synthetic Aperture Radar (EUSAR), Munich, 23-25 May, 2000, pp. 297 - 300, 2000.

[102] **Bethke, K.-H., Baumgartner, S., Gabele, M., Hounam, D., Kemptner, E., Klement, D., Krieger, G., Rode, G.**, *TRAMRAD, Traffic Monitoring with Space-Based Radar*, Advanced SAR Workshop, CSA Saint-Hubert, QC, Canada, 2005.

[103] **Börner, T., Chandra, M., Geudtner, D., Hounam, D.,** Schaettler, B., **Schwerdt, M.**, **Zink, M.**, Rye, A.J., Meadows, P.J., Cordey, R.A., Mancini, P., Rosich Tell, B., Esteban, D., *SAR Product Control Software (SARCON)*, European Conference on Synthetic Aperture Radar (EUSAR), pp. 675 - 678, 2000.

[104] Boerner, W.-M., Morisaki, J., **Danklmayer, A., Chandra, M.,** *On the Statistical Aspects of Radar Polarimetry*, IEEE Geoscience and Remote Sensing Symposium (IGARSS), Seoul (ROK), 2005.

[105] Boerner, W.M., Cloude, S.R., Lee, J.S., **Papathanassiou, K.,** Lukowski, T.I., *Advances in Extra Wide-Band Multi-modal Air/Space-borne Radar Polarimetry,POL-IN-SAR Imaging and its Applications*, IEEE Geoscience and Remote Sensing Symposium (IGARSS), Toronto, Canada, 24-28 Jun. 2002, pp. 408 - 410, 2002.

[106] Börner, E., Lord, R., **Mittermayer, J.,** Bamler, R., *Evaluation of TerraSAR-X Spotlight Processing Accuracy based on a new Spotlight Raw Data Simulator*, IEEE Geoscience and Remote Sensing Symposium (IGARSS), Toulouse, France, Jun. 2003.

[107] Börner, E., **Mittermayer, J.**, Lord, R., *Development and Test of the Spotlight SAR Processing for TerraSAR-X using a new Raw Data Simulator*, Advanced SAR Workshop, Montreal Kanada, 25-27 Jun. 2003.

[108] Börner, E., **Fiedler, H., Krieger, G., Mittermayer, J.,** *A New Method for Total Zero Doppler Steering*, IEEE Geoscience and Remote Sensing Symposium (IGARSS), Anchorage Alaska, 20-24 Sep. 2004, pp. 1526 - 1529, 2004.

[109] Börner, E., **Mittermayer, J.,** *TerraSAR-X Sliding Spotlight Realization by Stripmap Sections and Impact on SAR Processing*, IEEE Geoscience and Remote Sensing Symposium (IGARSS), Anchorage Alaska, 20-24 Sep. 2004.

[110] **Börner, T., Chandra, M., Geudtner, D., Hounam, D.**, Schättler, B., **Schwerdt, M., Zink, M.,** Rye, A.J., Meadows, P.J., Cordey, R.A., Mancini, P., Rosich-Tell, B., Esteban, D., *SAR Product CONtrol Software (SARCON)*, European Conference on Synthetic Aperture Radar (EUSAR), Munich, 23-25 May 2000, pp. 675 - 678, 2000.

[111] **Börner, T., Chandra, M., Geudtner, D., Hounam, D.,** Schättler, B., **Schwerdt, M., Zink, M.**, Rye, A.J., Meadows, P.J., Cordey, R.A., Mancini, P., Rosich-Tell, B., Esteban, D., *SAR Product CONtrol Software (SARCON)*, ERS-ENVISAT Symposium, Göteborg, 16-20 Oct. 2000.

[112] **Börner, T.**, *Polarimetric Bistatic X-Band Measurement Facility and its Applications*, Kleinheubacher Tagung, Miltenberg, 2002.

[113] **Börner, T.**, Bebbington, D.H.O., **Chandra, M.**, *Coherent Modelling of Backscatter and Propagation of Precipitation*, Open Symposium on Propagation and Remote Sensing, Garmisch-Partenkirchen, 12-15 Feb. 2002.

[114] **Börner, T.**, *Ermittlung von Materialeigenschaften im Mikrowellenbereich (Ka-Band) mittels Transmissionsmessungen bei hohen Temperaturen*, Wehrtechnisches Symposium „Tarnen und Täuschen", Mannheim, 20-22 Oct. 2003.

[115] **Börner, T.**, Bebbington, D., *Modelling Coherent Scattering of Raindrops in X- and Ka-Band and the Impact of Precipitation on Radar/SAR Data and Applications*, European Conference on Synthetic Aperture Radar (EUSAR), pp. 149 - 152, Ulm, 2004.

[116] **Börner**, **T.,** Hagen, M., Bebbington, D., *A first approach to unsupervised Entropy-Alpha-classification of full-polarimetric weather-radar data*, 32nd Conference Radar Meteorology, Albuquerque, NM (USA), 2005.

[117] Böttger, U., Beier, K., Biering, B., **Peichl, M.**, Spyra, W., *"easyMine" - realistic and systematic mine detection simulation tool*, Kleinheubacher Tagung, Miltenberg, 27 Sep. -1 Oct. 2003.

[118] Breit, H., Börner, E., **Mittermayer, J.**, Holzner, J., Eineder, M., *The TerraSAR-X Multi-Mode SAR Processor - Algorithms and Design*, European Conference on Synthetic Aperture Radar (EUSAR), Ulm, May 2004, pp. 501 - 503, 2004.

[119] Breuer, A., **Hajnsek, I.**, *Analytical solution for a surface scattering model*, International Workshop on Applications of Polarimetry and Polarimetric Interferometry (PolInSAR), Frascatti, Jan. 2003.

[120] Breuer, A., **Hajnsek, I.**, Ferro-Famil, L., Pottier, E., *Full polarimetry versus partial polarimetry for quantitative surface parameter estimation*, IEEE Geoscience and Remote Sensing Symposium (IGARSS), 21-25 Jul. 2003, Toulouse, France, pp. 437 - 439, 2003.

[121] **Buckreuss, S., Scheiber, R., Basler, C**., *The X-SAR/SRTM Radar Data Analyzer*, European Conference on Synthetic Aperture Radar (EUSAR), Munich, 23-25 May 2000, pp. 219 - 222, Munich, Germany, 2000.

[122] **Buckreuss, S.**, Balzer, W., Mühlbauer, P., Werninghaus, R., Pitz, W., *TerraSAR-X, a German Radar Satellite*, International Radar Symposium (IRS), Dresden, 30 Sep. -02 Oct. 2003.

[123] **Buckreuss, S.**, Balzer, W., Mühlbauer, P., Werninghaus, R., Pitz, W., *The German SAR-Satellite TerraSAR-X*, ONERA-DLR Aerospace Symposium (ODAS), Toulouse, 04-06 Jun. 2003, pp. S4-S5, 2003.

[124] **Buckreuss, S.**, Balzer, W., Mühlbauer, P., Werninghaus, R., Pitz, W., *The TerraSAR-X Satellite Project*, IEEE Geoscience and Remote Sensing Symposium (IGARSS) 2003, Toulouse, 21-25 Jul. 2003.

[125] Cantalloube, H., **Wendler, M.**, Giroux, V., Dubois-Fernandez, P., *A first bistatic airborne SAR interferometry experiment - preliminary results*, SAM2004 Third IEEE Sensor Array and Multichannel Signal Processing Workshop, Barcelona, 18-21 Jul. 2004.

[126] Cantalloube, H., **Wendler, M.**, Giroux, V., Dubois-Fernandez, P., **Krieger, G**., *Challenges in SAR processing for airborne bistatic acquisitions*, European Conference on Synthetic Aperture Radar (EUSAR), Ulm, 25-27 May 2004, pp. 577 - 580, Ulm, Germany, 2004.

[127] **Chandra, M., Hounam, D.**, *Tropospheric Propagation Effects in SAR Measurements*, European Conference on Synthetic Aperture Radar (EUSAR), Munich, 23-25 May 2000, pp. 465 - 465, 2000.

[128] **Chandra, M., Danklmayer, A.**, **Lüneburg, E.**, *On the statistical properties of polarimetric weather radar signature*, Kleinheubacher Tagung, Miltenberg (Germany) 29 Sep.-02 Oct. 2003, Miltenberg, Germany, 2004.

[129] Christophe, F., Borderies, P., Millot, P., **Peichl, M., Süß, H.**, **Zeiler, M**., **Dill, S.**, **Reinwaldt, F.**, *Electromagnetic technologies for improved detection of antipersonnel land mines*, ONERA-DLR Aerospace Symposium (ODAS), Berlin, Germany, 15-16 Jun. 2000.

[130] Cloude, S., **Papathanassiou, K.,** *A 3-Stage Inversion Process for Polarimetric SAR Interferometry*, European Conference on Synthetic Aperture Radar (EUSAR), pp. 279 - 282, Cologne, Germany, 2002.

[131] Cloude, S.R., **Moreira, A., Papathanassiou, K**., Pottier, E., **Reigber, A.**, *A Comparison of Algorithms for Vegetation Structure Extraction using Radar Polarimetry and Interferometry*, IEEE Geoscience and Remote Sensing Symposium (IGARSS), Honolulu/Hawaii/USA, 24-28 Jul. 2000.

[132] D'Amico, M., Fulgoni, A., Alberoni, P.P., **Chandra, M.,** *Polarimetric Modelling of Flare Echoes, and Comparisons with Observations at C Band*, 30th International Conference on Radar Meteorology, Munich, 19-24 Jul. 2001.

[133] D'Amico, S., Montenbruck, O., Arbinger, C., **Fiedler, H.**, *Formation Flying Concept for Close Remote Sensing Satellites*, 15th AAS/AIAA Space Flight Mechanics Conference, 2005, pp. 831 - 848, Copper Mountain, Colorado (USA), 2005.

[134] **Danklmayer, A., Archibald, E., Boerner, T., Hounam, D., Chandra, M.,** *"Atmospheric effects and product quality in the application of SAR interferometry"*, European Conference on Synthetic Aperture Radar (EUSAR), Ulm, Germany, 25-27 May 2004.

[135] **Danklmayer, A., Chandra, M.**, **Lüneburg, E.**, *Principal Component Analysis in Radar Polarimetry*, Kleinheubacher Tagung 2004, Miltenberg, Germany 2005.

[136] **Danklmayer, A., Macedo, K., Scheiber, R., Börner, T., Chandra, M**., *Analysis Methods of errors (Motion and Atmospheric) in Synthetic aperture radar (SAR) Images*, Kleinheubacher Tagung, Miltenberg (Germany), 27. Sep. - 01 Oct. 2004, Miltenberg, Germany, 2005.

[137] **Dill, S., Peichl, M., Zeiler, M.**, **Süß, H.**, *Detection of anti-personnel mines using micorwave radiometers*, 1st ONERA-DLR-Workshop, Bonascre, 23-26 Jan. 2001.

[138] **Dill, S., Peichl, M**., **Schulteis, S**., **Süß, H.,** *Microwave radiometry techniques for buried landmine detection*, Progress in Electromagnetics Research Symposium (PIERS), Cambridge, 1-5 Jul. 2002, pp. 432 - 432, 2002.

[139] Dimou, A., **Jäger, G., Benz, U.,** Makios, V., *A Fuzzy Edge Detector for SAR Images*, European Conference on Synthetic Aperture Radar (EUSAR), Munich, 23-25 May 2000, pp. 669 - 702, 2000.

[140] Dimou, A., Uzunoglou, N., Frangos, P., **Jäger, G., Benz, U.**, *Linear features' detection in SAR images using Fuzzy Edge Detector*, Space-Based Observation Technology (SBOT), Samos, Greece, 16-18 Oct. 2000.

[141] Dubois-Fernandez, P., Cantalloube, H., Ruault du Plessis, O., **Wendler, M.**, Vaizan, B., Coulombeix, C., Heuze, D., **Krieger, G.**, *Analysis of bistatic scattering behavior of natural surfaces*, European Conference on Synthetic Aperture Radar (EUSAR), pp. 573 - 576, Ulm, Germany, 2004.

[142] Dubois-Fernandez, P., Cantalloube, H., Ruault du Plessis, O., **Wendler, M., Horn, R.**, Vaizan, B., Coulombeix, C., Heuze, D., **Krieger, G.**, *Analysis of Bistatic Scattering Behavior of Natural Surfaces*, Radar Conference, pp. 1 - 4 (4 Seiten auf CD), Toulouse, France, 2004.

[143] Ebner, H., Riegger, S., **Hajnsek, I., Hounam, D., Krieger, G., Moreira, A., Werner, M.,** *Single-Pass SAR Interferometry with a Tandem TerraSAR-X Configuration*, European Conference on Synthetic Aperture Radar (EUSAR) 2004, Ulm, Germany, 25-27 May 2004, pp. 53 -, 2004.

[144] Eineder, M., **Krieger, G.,** *Interferometric Digital Elevation Model Reconstruction - Experiences from SRTM and Multi Channel Approaches for Future Missions*, IEEE International Geoscience and Remote Sensing Symposium (IGARSS), pp. 2664 - 2667, Seoul, Korea, 2005.

[145] Emunds, H., **Frieß, M**., Göring, J., **Kemptner, E.**, Otto, H., Dankert, C., *Untersuchungen an den vom DLR neu entwickelten Materialien für Suchkopfabdeckungen*, Wirkung und Schutz, Explosivstoffe, Mannheim, 8-10 Nov. 2004.

[146] **Fiedler, H., Krieger, G., Jochim, F.,** Kirschner, M., **Moreira, A**., *Analysis Of Satellite Configurations For Spaceborne SAR Interferometry*, Formation Flying Conference, Toulouse, France, 29-31 Oct. 2002, Toulouse, France, 2002.

[147] **Fiedler, H., Krieger, G., Jochim, F.**, Kirschner, M., **Moreira, A.,** *Analysis Of Bistatic Configurations For Spaceborne SAR Interferometry*, European Conference on Synthetic Aperture Radar (EUSAR), Cologne, 4-6 Jun. 2002, pp. 29 - 32, Cologne, 2002.

[148] **Fiedler, H., Krieger, G.**, *Close Formation Flight of Passive Receiving Micro-Satellites*, 18th International Symposium on Space Flight Dynamics, Munich, 11-15 Oct., pp. 1 - 6 (6 Seiten auf CD), Munich, 2004.

[149] **Fiedler, H., Krieger, G.**, *Close Formation of Micro-Satellites for SAR Interferometry*, 2nd International Symposium on Formation Flying, Washington, 14-16 Sep. 2004, pp. 1 - 8 (8 Seiten auf CD), Washington, DC, USA, 2004.

[150] **Fiedler, H.,** Börner, E., **Mittermayer, J., Krieger, G.**, *Total Zero Doppler Steering*, European Conference on Synthetic Aperture Radar (EUSAR), Ulm Germany, 24-28 May 2004, pp. 481 - 484, 2004.

[151] **Fiedler, H., Krieger, G., Werner, M., Hajnsek, I., Moreira, A.,** *TanDEM-X: Mission Concept and Performance Analysis*, Committee on Earth Observation Satellites (CEOS) SAR Calibration/Validation Workshop, Adelaide, Australien, 2005.

[152] **Fischer, C., Hajnsek, I., Papathanassiou, K., Moreira, A.,** *Separation of Volume and Ground Scattering Using Interferometric and Polarimetric Techniques*, European Conference on Synthetic Aperture Radar (EUSAR), Cologne, Germany, 4-6 Jun. 2002, pp. 609 - 612, 2002.

[153] **Gebert, N., Krieger, G., Moreira, A.**, *Digital Beamforming for High Resolution Wide Swath SAR Imaging*, German Microwave Conference (GeMiC), Ulm, 05-07 Apr. 2005, Ulm, Germany, 2005.

[154] **Gebert, N., Krieger, G., Moreira, A.**, *High Resolution Wide Swath SAR Imaging - System Performance and Influence of Perturbations*, International Radar Symposium (IRS) pp. 49 - 54, Berlin, Germany, 2005.

[155] **Gebert, N., Krieger, G., Moreira, A.**, *SAR Signal Reconstruction from Non-Uniform Displaced Phase Centre Sampling in the Presence of Perturbations*, International Geoscience and Remote Sensing Symposium (IGARSS), Seoul, Korea, 2005.

[156] Göring, J., **Kemptner, E.**, Emunds, H., Frieß, M., *Oxidkeramische Verbundwerkstoffe für Suchkopfabdeckungen hochagiler Flugkörper*, 3. DLR - Flugkörper-Workshop, Cologne, Germany, 6 Nov. 2003.

[157] **Greiner, M., Peichl, M., Süß, H.**, *Advanced image reconstruction and array geometries in aperture synthesis radiometry*, IEEE International Geoscience and Remote Sensing Symposium (IGARSS), Toulouse, France, 21-25 Jul. 2003.

[158] **Hager, M., Anglberger, H., Kemptner, E**., *Results to test case 4 (PLACYL)*, Workshop Journées Internationales de Nice sur les Antennes (EM JINA) – Intern. Symposium on Antennas, Nizza, France, Nov. 2004.

[159] **Hajnsek, I., Papathanassiou, K.**, Cloude, S.R., *Additive Noise Filtering for Polarimetric Eigenvalue Processing*, IEEE Geoscience and Remote Sensing Symposium (IGARSS), Sydney, Jun. 2001.

[160] **Hajnsek, I., Papathanassiou, K.**, Cloude, S.R., *L- and P-band for Surface Parameter Estimation*, IEEE Geoscience and Remote Sensing Symposium (IGARSS), Sydney, Jun. 2001.

[161] **Hajnsek, I., Papathanassiou, K.**, Cloude, S.R., Lee, J.S., *The Effect of Additive Noise on Surface Roughness Estimation from P-band Polarimetric SAR Data*, Progress in Electromagnetics Research Symposium (PIERS), Osaka, Japan, 2001.

[162] **Hajnsek, I., Papathanassiou, K., Horn, R., Scheiber, R.,** Cloude, S.R., *New Techniques for Polarimetric SAR Imaging*, Onera-DLR Aerospace Symposium (ODAS), Paris, France, Jun. 2001.

[163] **Hajnsek, I., Papathanassiou, K., Horn, R., Scheiber, R., Moreira, A.,** *Neue Methoden zur Bestimmung von Bodenoberflächen-Vegetationsparametern entwickelt aus polarimetrischen und interferometrischen E-SAR Daten*, DFD Nutzerseminar, Konstanz, Germany, Sep. 2001.

[164] **Hajnsek, I.**, Pottier, E., Cloude, S.R., *Estimation of Surface Parameters Using Polarimetric Radar Data*, European Geophysical Society (EGS) Symposium, Nice, Mar. 2001.

[165] **Hajnsek, I.,** Scheuchl, B., Caves, R., Cumming, I., *Surface Parameter Inversion from Sea Ice Using Spaceborne Polarimetric SAR Data*, Advanced SAR Workshop, Montreal, Canada, Oct. 2001.

[166] **Hajnsek, I., Papathanassiou, K.**, *Parameter Inversion for Polarimetric SAR*, Union Radio-Scientifique Internationale (URSI) Commission F Open Symposium on Propagation and Remote Sensing, Garmisch-Partenkirchen, Germany, 12-15 Feb. 2002.

[167] **Hajnsek, I., Papathanassiou, K.**, Cloude, S.R., **Moreira, A.**, *Surface Parameters Estimation Using Passive Polarimetric Microsatellite Concept*, European Conference on Synthetic Aperture Radar (EUSAR), Cologne, Germany, 4-6 Jun.2002,pp.275-278, 2002.

[168] **Hajnsek, I., Papathanassiou, K., Moreira, A.**, Cloude, S.R., *Surface Parameter Estimation Using Polarimetric and Interferometric SAR*, IEEE Geoscience and Remote Sensing Symposium (IGARSS), Toronto, Canada, 24-28 Jun. 2002, pp. 420 - 422, 2002.

[169] **Hajnsek, I., Alvarez-Perez, J.L., Papathanassiou, K., Moreira, A.**, Cloude, S.R., *Surface Parameter Estimation Using Interferometric Coherences at Different Polarisations*, International Workshop on Applications of Polarimetry and Polarimetric Interferometry (PolInSAR), ESA/ESRIN, Frascatti, Jan. 2003.

[170] **Hajnsek, I., Papathanassiou, K.**, Cloude, S.R., *A hybrid scattering model for surface parameter estimation using polarimetric SAR interferometry*, IEEE Geoscience and Remote Sensing Symposium (IGARSS), 21-25 Jul. Toulouse, France, pp. 693 - 695, 2003.

[171] **Hajnsek, I., Papathanassiou, K., Moreira, A.**, *Pol-InSAR scenarios for surface parameter estimation*, Advanced SAR Workshop, Montreal, Canada, Jun. 2003.

[172] **Hajnsek, I., Papathanassiou, K., Moreira, A., Krieger, G.,** *Polarimetric SAR Interferometry with a Multistatic SAR Satellite*, International Astronautical Congress, Bremen, Germany, Oct. 2003.

[173] **Hajnsek, I.**, Cloude, S.R., *Pol-InSAR for Agricultural Vegetation*, IEEE Geoscience and Remote Sensing Symposium (IGARSS), Anchorage, Alaska, Sep. 2004, pp. 1224 - 1227, 2004.

[174] Hong, W., **Mittermayer, J., Moreira, A.**, *High Squint Angle Processing of E-SAR Stripmap Data*, European Conference on Synthetic Aperture Radar (EUSAR), Munich, Germany, 23-25 May 2000.

[175] **Horn, R., Moreira, A., Buckreuss, S., Scheiber, R**., *Recent Developments of the Airborne SAR System E-SAR of DLR*, European Conference on Synthetic Aperture Radar (EUSAR), Munich/Germany, 23-25 May 2000.

[176] **Hounam, D., Schwerdt, M., Zink, M.,** *Active Antenna Module Characterisation by Pseudo-Noise Gating*, ESA Antenna Workshop on Satellite Antenna Technology, Noordwijk 2002.

[177] **Hounam, D., Wägel, K., Bauer, R., Schwerdt, M**., *Encoded Reference Target for InSAR Measurements*, European Conference on Synthetic Aperture Radar (EUSAR), Cologne, Germany 2002.

[178] **Hounam, D., Mittermayer, J.**, *Techniques for Reducing SAR Antenna Size*, IEEE Geoscience and Remote Sensing Symposium (IGARSS), Toulouse/France, 21-25 Jul. 2003.

[179] **Hounam, D., Moreira, A., Mittermayer, J., Krieger, G**., *A Small Low-Cost SAR Satellite for InSAR Measurements of Permanent Scatterers*, European Conference on Synthetic Aperture Radar (EUSAR), pp. 49 - 52, Ulm, Germany, 2004.

[180] **Hounam, D., Baumgartner, S., Bethke, K.H., Gabele, M., Kemptner, E., Klement, D., Krieger, G., Waegel, K.,** *An autonomous, non-cooperative, wide-area Traffic Monitoring System using space-based Radar (TRAMRAD)*, International Geoscience and Remote Sensing Symposium (IGARSS), Seoul, 25-29 Jul. 2005.

[181] **Jäger, G., Benz, U., Scheiber, R.,** *Knowledge-based quality assessment and improvement of digital elevation models from interferometric SAR data*, European Conference on Synthetic Aperture Radar (EUSAR), Munich, Germany 23-25 May 2000, pp. 335 - 338, 2000.

[182] **Jirousek, M., Peichl, M., Süß, H.**, *A multi-frequency microwave aperture synthesis radiometer for high-resolution imaging*, International Geoscience and Remote Sensing Symposium (IGARSS), Anchorage, Alaska, USA, 20-24 Sep. 2004.

[183] **Jochim, F.**, Quintino da Silva, M.M., **Schröder, R., Hajnsek, I.,** Puls, J., *Orbit Analysis for Brazilian-German Space Project MapSAR Based on User Requirement*, International Symposium on Small Satellites for Earth Observation, pp. 275 - 283, Berlin, Germany, 2005.

[184] **Keller, M**., Milisavljevic, N., **Süß, H.,** Acheroy, M., *Reduction of Mine Suspected Areas by Multisensor Airborne Measurements - First Results*, International Society for Optical Engineering (SPIE) AeroSense 2002, pp. 857 - 871, Orlando (USA), 2002.

[185] **Kempf, T., Peichl, M., Dill, S., Süß, H.,** *Application of complex dual apodization on high resolution low incidence angle ISAR images*, German Radar Symposium (GRS), Berlin, 11-12 Oct. 2000.

[186] **Kempf, T., Peichl, M., Dill, S., Süß, H**., *An approach for the suppression of ambiguities in ISAR images caused by irregular sampling*, German Radar Symposium (GRS), Bonn, 3-5 Sep. 2002, pp. 159 - 165, 2002.

[187] **Kempf, T., Peichl, M., Süß, H.**, *A Method for Advanced Automatic Recognition of Relocatable Targets*, NATO/RTO-SET Symposium on Complementarity of Ladar and Radar, Prag, 22-23 Apr. 2002.

[188] **Kempf, T., Peichl, M., Dill, S., Süß, H.,** *Advanced tomographic processing for high resolution ISAR imaging*, International Radar Symposium (IRS), Dresden, Germany, 30 Sep. - 02 Oct. 2003.

[189] **Kempf, T., Peichl, M., Dill, S., Süß, H.**, *ATR Perfomance at Extended Operating Conditions for highly resolved ISAR-images of relocatable targets*, Proc. of Radar 2004, Toulouse, France, 18-22 Oct. 2004.

[190] **Kempf, T., Peichl, M., Dill, S., Süß, H**., *Performance of algorithms for high-resolution turntable ISAR imaging*, European Conference on Synthetic Aperture Radar (EUSAR), Neu-Ulm, Germany, 25-27 May 2004.

[191] **Kempf, T.**, *Automatic target recognition of relocatables in X-band ISAR data*, 5th DLR-CNES Workshop 'Information Extraction and Scene Understanding for Meter Resolution Images', Oberpfaffenhofen, 29 Nov. - 1. Dec. 2004.

[192] **Kempf, T**., *Untersuchungen zur automatischen Erkennung militärischer Fahrzeuge*, Workshop ATR-Verfahren für die luft- und raumgestützte Aufklärung, Wachtberg-Werthoven, 06 May 2004.

[193] **Kempf, T., Peichl, M., Dill, S., Süß, H.**, *ATR Performance within an extended X-band Tower-Turntable Database of highly resolved relocatable targets*, NATO SET-080 Symposium on Target Identification and Recognition Using RF Systems, Oslo, 11-13 Oct. 2004.

[194] **Kemptner, E**., *Simulation von Radarsignaturen und deren experimentelle Validation*, „Tarnen und Täuschen", Mannheim, 20-22 Oct. 2003.

[195] **Keydel, W., Hounam, D, Werner, M.**, *X-SAR/SRTM, Part of a Global Earth Mapping Mission*, Symposium on Space-Based Observation Technology (SBOT), Samos, Greece, 16-18 Oct. 2000.

[196] **Keydel, W.**, *Military Remote Sensing Applications with SAR*, Research & Technology Organisation (RTO) Symposium, Prague, Czech Republic, 22-23 Apr. 2002.

[197] **Keydel, W.**, *Visions and Perspectives for Future SAR Systems,* European Conference on Synthetic Aperture Radar (EUSAR), Cologne, Germany, 04-06 Jun. 2002.

[198] **Keydel, W.**, *From Radar Antenna to Antenna Radar Perspectives for Future Antenna Development for Airborne and Space Borne SAR,* Research & Technology Organisation (RTO) Symposium Smart Antennas, Chester, Great Britain, 07-09 Apr. 2003.

[199] Kimura, H., Mizuno, T., **Papathanassiou, K., Hajnsek, I.,** *Improvement of Polarimetric SAR Calibration based*, IEEE Geoscience and Remote Sensing Symposium (IGARSS), Sep. 2004, pp. 184 - 187, Anchorage, Alaska, 2004.

[200] **Kohlhase, A.O.**, Feigl, K.L., Ferretti, A., Massonnet, D., *Estimating Crustal Deformation Fields from Interferometric SAR, Permanent Scatterers, and GPS Measurements*, Fringe Workshop, Frascati, 01- 05 Dec. 2003.

[201] **Kohlhase, A.O**., Feigl, K.L., Massonnet, D., Ferretti, A., *Estimating orbital trajectories from fringe gradients in SAR interferograms for measuring crustal strain*, IEEE Geoscience and Remote Sensing Symposium (IGARSS), Toulouse, France, 21 – 25 Jul. 2003.

[202] Kono, J., Paradella, W.R., Quintino da Silva, M.M., De Morisson Valeriano, D., Farias Costa, M.P., **Schroeder, R.,** Puls, J., **Hajnsek, I., Jochim, F., Neff, T**., *MAPSAR: A new L-band spaceborne SAR mission for assessment and monitoring of terrestrial natural resources*, Simposio Brasileiro de Sensoriamento Remoto (SBSR), Belo Horizonte, Brasil, 5-10 Apr. 2003.

[203] **Krieger, G., Mittermayer, J., Wendler, M., Witte, F., Moreira, A.,** *SIREV - Sector Imaging Radar for Enhanced Vision*, International Symposium on Image and Signal Processing and Analysis, pp. 377 - 382, Pula, Croatia, 2001.

[204] **Krieger, G., Wendler, M., Mittermayer, J., Moreira, A., Papathanassiou, K.**, *Performance Estimation for the Interferometric Cartwheel in Combination with a Transmitting SAR Satellite*, Advanced SAR Workshop, Saint-Hubert, Quebec, Canada, 1-3 Oct. 2001.

[205] **Krieger, G., Fiedler, H., Wendler, M., Mittermayer, J., Moreira, A.,** *Spaceborne Single-Pass Interferometry with Multi-Static SAR*, German Radar Symposium (GRS), pp. 65-69, Bonn, Germany, 2002.

[206] **Krieger, G., Wendler, M., Fiedler, H., Mittermayer, J., Moreira, A**., *Comparison Of The Interferometric Performance For Spaceborne Parasitic SAR Configurations*, European Conference on Synthetic Aperture Radar (EUSAR), pp. 467 - 470, Cologne, Germany, 2002.

[207] **Krieger, G., Wendler, M., Fiedler, H., Mittermayer, J., Moreira, A.**, *Performance Analysis for Bistatic Interferometric SAR Configurations*, IEEE Geoscience and Remote Sensing Symposium (IGARSS), pp. 650 - 652, Toronto, Canada, 2002.

[208] **Krieger, G., Wendler, M., Mittermayer, J., Buckreuss, S., Witte, F.**, *Sector Imaging Radar for Enhanced Vision*, German Radar Symposium (GRS), pp. 219 - 224, Bonn, Germany, 2002.

[209] **Krieger, G., Fiedler, H., Moreira, A.**, *Bi- and Multi-Static SAR Missions: Potentials and Challenges*, Advanced SAR Workshop, Saint-Hubert, Quebec, Canada, 2003.

[210] **Krieger, G., Fiedler, H., Rodriguez Cassola, M., Hounam, D., Moreira, A.**, *System Concepts for Bi- and Multi-Static SAR Missions*, International Radar Symposium (IRS) pp. 331 - 339, Dresden, Germany, 2003.

[211] **Krieger, G., Gebert, N., Moreira, A.**, *Digital Beamforming and Non-Uniform Displaced Phase Centre Sampling in Bi- and Multistatic SAR*, European Conference on Synthetic Aperture Radar (EUSAR), pp. 563 - 566, Ulm, Germany, 2004.

[212] **Krieger, G., Gebert, N., Moreira, A.,** *SAR Signal Reconstruction from Non-Uniform Displaced Phase Centre Sampling*, IEEE Geoscience and Remote Sensing Symposium (IGARSS), pp. 1763 - 1766, Anchorage, USA, 2004.

[213] **Krieger, G., Moreira, A., Hounam, D., Werner, M.**, Riegger, S., Settelmeyer, E., *A Tandem TerraSAR-X Configuration for Single-Pass SAR Interferometry*, Radar Conference, pp. 1–6, Toulouse, France, 2004.

[214] **Krieger, G., Moreira, A., Fiedler, H., Hajnsek, I.,** Eineder, M., **Zink, M**., Werner, M., *TanDEM-X: A Satellite Formation for High Resolution SAR Interferometry*, ESA Fringe Workshop, Frascati, Italy, 2005.

[215] **Krieger, G., Rodriguez Cassola, M., Younis, M., Metzig, R.**, *Impact of Oscillator Noise in Bistatic and Multistatic SAR*, IEEE Geoscience and Remote Sensing Symposium (IGARSS), pp. 1043 - 1046, Seoul, Korea, 2005.

[216] **Krieger, G., Moreira, A., Hajnsek, I., Werner, M., Fiedler, H.,** Settelmeyer, E., *The TanDEM-X Mission Proposal*, International Society for Photogrammetry and Remote Sensing (ISPRS) Workshop: High-Resolution Earth Imaging for Geospatial Information, Hannover, Germany, 2005.

[217] **Krieger, G., Moreira, A., Fiedler, H., Hajnsek, I.**, Eineder, M., **Zink, M., Werner, M.,** *TanDEM-X: A Satellite Formation for High Resolution SAR Interferometry*, Advanced SAR Workshop, Saint-Hubert (Longueuil), Quebec, Canada, 2005.

[218] **Krieger, G., Papathanassiou, K.,** Cloude, S., **Moreira, A., Fiedler, H.**, Völker, M., *Spaceborne Polarimetric SAR Interferometry: Performance Analysis and Mission Concepts*, International Workshop on Applications of Polarimetry and Polarimetric Interferometry (PolInSAR), Frascati, Italy, 2005.

[219] Kutuza, B., Kalinkevich, A., **Shishkova, O.**, **Hajnsek, I.**, *Quantitative Estimation of Subsurface Parameters*, European Conference on Synthetic Aperture Radar (EUSAR), Ulm, Germany, May 2004, pp. 653 - 656, 2004.

[220] Lee, J.S., Cloude, S.R., **Papathanassiou, K.,** Grunes, M.R., Ainsworth, T.L., Schuler, D.L., *Speckle Filtering of Polarimetric SAR Interferometry Data*, IEEE Geoscience and Remote Sensing Symposium (IGARSS), Toronto Canada, 24-28 Jun. 2002, pp. 832 - 834, 2002.

[221] **Limbach, M**., *Design of an Airborne Dual-Polarized Triple Stacked Patch Antenna for Broadband SAR Applications in P-Band*, 25th ESA Antenna Wokshop on Satellite Antenna Technology, pp. 513 - 518, Noordwijk, Netherlands, 2002.

[222] **Limbach, M.**, *Design of a dual-polarized triple stacked patch antenna for broadband SAR applications in P-band*, German Radar Symposium (GRS), Bonn, Germany, 2002.

[223] **Limbach, M**., *Design of an Airborne Dual-Polarized Triple Stacked Patch Antenna for Broadband SAR Applications in P-Band*, European Conference on Synthetic Aperture Radar (EUSAR), pp. 311 - 314, Cologne, Germany, 2002.

[224] **Limbach, M**., *Design of a dual-polarized triple stacked patch antenna for broadband SAR application in P-band*, Open Symposium on Propagation and Remote Sensing, Garmisch-Partenkirchen, Germany, 2002.

[225] **Limbach, M., Gabler, B., Horn, R., Scheiber, R.**, *Fine Resolution, fully Polarimetric P-band Subsystem for E-SAR - Technique and Results*, European Conference on Synthetic Aperture Radar (EUSAR), pp. 275 - 278, Ulm, Germany, 2004.

[226] **Liseno, A.**, Pierri, R., *Which model for inversion? The case of voids*, Union Radio-Scientifique Internationale (URSI) Commission B Open Symposium on Propagation and Remote Sensing, Italy, Pisa 2003.

[227] **Liseno, A., Papathanassiou, K., Hajnsek, I., Scheiber, R.**, Cloude, S.R., *Vegetation bias removal and underlying topography estimation using polarimetric SAR interferometry*, European Conference on Synthetic Aperture Radar (EUSAR), Ulm, Germany, May 2004, pp. 263 - 267, 2004.

[228] **Liseno, A., Papathanassiou, K., Moreira, A.,** Pierri, R., *First results of tomographic SAR inversion on "reduced"; flight-track simulated polarimetric data*, European Conference on Synthetic Aperture Radar (EUSAR), Ulm, Germany, May 2004, pp. 79 - 82, 2004.

[229] **Liseno, A., Papathanassiou, K., Moreira, A.**, Pierri, R., *Parameter inversion of "reduced" SAR flight-tracks: first results over forests*, IEEE Geoscience and Remote Sensing Symposium (IGARSS), Anchorage, Alaska, Sep. 2004.

[230] **Liseno, A**., **Papathanassiou, K, Moreira, A.,** Pierri, R., *Analysis of forest-slab height inversion from multibaseline SAR data,* IEEE Geoscience and Remote Sensing Symposium (IGARSS), 25-29 Jul. 2005, Seoul, Korea, 2005.

[231] **Macedo, K.A.C., Scheiber, R.,** *Controlled Experiment for Analysis of Airborne D-InSAR Feasibility*, European Conference on Synthetic Aperture Radar (EUSAR), Ulm, 25-27 May 2004, pp. 761 - 764, 2004.

[232] **Macedo, K.A.C.d., Andres, C., Scheiber, R.**, *On The Requirements of SAR Processing for Airborne Differential Interferometry*, IEEE International Geoscience and Remote Sensing Symposium (IGARSS), Seoul, Korea, 2005.

[233] **Márquez-Martinez, J., Mittermayer, J.**, *Analysis of Range Ambiguity Suppression methods in SAR by using a Novel Range Ambiguity Raw Data Simulator*, European Conference on Synthetic Aperture Radar (EUSAR), Ulm, Germany, May 25-27, 2004, pp. 593 - 596, 2004.

[234] **Márquez-Martinez, J., Mittermayer, J.,** Rodriguez-Cassola, M., *Radiometric Resolution Optimization for Future SAR Systems*, IEEE Geoscience and Remote Sensing Symposium (IGARSS), Anchorage, Alaska, USA, 20-24 Sep. 2004.

[235] Martinez, C.L., **Papathanassiou, K.**, Canovas, X.F., *Polarimetric and Interferometric Noise Modelling*, IEEE Geoscience and Remote Sensing Symposium (IGARSS), Toronto Canada, 24-28 Jun. 2002, pp. 835 - 837, 2002.

[236] Meadows, P.J., **Hounam, D**., Rye, A.J., Rosich, B., **Börner, T.**, Closa, J., Schättler, B., Smith, P.J., **Zink, M.**, *SAR Product Control Software*, Committee on Earth Observation Satellites (CEOS) Working Group on Calibration and Validation Workshop, London, Great Britain, Sep. 24 - 26, 2002.

[237] Merryman Boncori, J.P., **Schwerdt, M., Hounam, D.**, Schiavon, G., *Implementation of a Co/Decoding Method in SAR Processing Based on Time Domain Correlation*, IEEE Geoscience and Remote Sensing Symposium (IGARSS), Seoul, Korea, 2005.

[238] **Mette, T., Papathanassiou, K., Hajnsek, I.,** Zimmermann, R., *Forest Biomass Estimation using Polarimetric SAR Interferometry*, IEEE Geoscience and Remote Sensing Symposium (IGARSS), Toronto Canada, 24-28 Jun. 2002, pp. 817 - 819, 2002.

[239] **Mette, T., Hajnsek, I., Papathanassiou, K**., *Height biomass allometry in temperate forests*, IEEE Geoscience and Remote Sensing Symposium (IGARSS), 21-25 Jul.2003,Toulouse,France,pp.1942-1944,2003.

[240] **Mette, T., Hajnsek, I., Papathanassiou, K.**, Zimmermann, R., *Waldhoehen- und -biomass Bestimmung im Fichtelgebirge unter Verwendung polarimetrischer SAR Interferometrie (PolInSAR)*, DFD-Nutzerseminar - Neustrelitz 2003.

[241] **Mette, T., Papathanassiou, K., Hajnsek, I.,** Zimmermann, R., *Forest biomass estimation using polarimetric SAR interferometry*, International Workshop on Applications of Polarimetry and Polarimetric Interferometry (PolInSAR), Frascatti, Jan. 2003.

[242] **Mette, T., Papathanassiou, K., Hajnsek, I.,** *Biomass estimation from polarimetric SAR interferometry over heterogeneous forest terrain*, IEEE Geoscience and Remote Sensing Symposium (IGARSS), Anchorage, Alaska, Sep. 2004.

[243] **Mette, T., Papathanassiou, K., Hajnsek, I.**, *Estimating forest biomass from Pol-InSAR data and forest allometry - results from the temperate spruce forest test site Traunstein*, IProc. Retrieval of Bio- and Geophysical Parameters from SAR Data for Land Applications, Innsbruck, 16-19 Nov. 2004.

[244] **Mette, T., Papathanassiou, K., Hajnsek, I.,** *Potential of the forest height derived by polarimetric SAR interferometry to estimate forest biomass*, European Conference on Synthetic Aperture Radar (EUSAR), Ulm, May 2004, pp. 241 - 244, 2004.

[245] **Mette, T., Papathanassiou, K., Hajnsek, I.,** Pretzsch, H., Biber, P., *Applying a common allometric equation to convert forest height from Pol-InSAR data to forest biomass*, IEEE Geoscience and Remote Sensing Sympos. (IGARSS), Anchorage, Alaska, Sep. 2004.

[246] **Misra, A.**, **Scheiber, R.**, *Differential Interferometric SAR Pocessing of E-SAR Data*, International Radar Symposium of India (IRSI), Bangalore, 3-5 Dec. 2003, pp. 624 - 633, 2003.

[247] **Mittermayer, J., Moreira, A.,** *A Generic Formulation of the Extended Chirp Scaling Algorithm (ECS) for Phase Preserving ScanSAR and SpotSAR Processing*, IEEE Geoscience and Remote Sensing Symposium (IGARSS), Honolulu, Hawaii, USA, 24-28 Jul. 2000.

[248] **Mittermayer, J., Moreira, A.**, *Interferometric Extended Chirp Scaling Processing for ScanSAR*, German Radar Symposium (GRS), Berlin, Germany, 11-12 Oct. 2000.

[249] **Mittermayer, J., Moreira, A.**, *Interferometric Processing of Spaceborne SAR Data in Advanced SAR Imaging Modes*, Space-Based Observation Technology (SBOT), Samos, Greece, 15-18 Oct. 2000.

[250] **Mittermayer, J., Moreira, A.,** Loffeld, O., *Comparison of Stripmap and Spotlight Interferometric SAR Processing using E-SAR Raw Data*, European Conference on Synthetic Aperture Radar (EUSAR), Munich/Germany, 23-25 May 2000.

[251] **Mittermayer, J., Wendler, M., Krieger**, **G., Moreira, A., Sutor, T**., **Buckreuss, S**., *Data Processing of an Innovative Forward Looking SAR System for Enhanced Vision*, European Conference on Synthetic Aperture Radar (EUSAR), Munich, Germany, 23-25 May 2000.

[252] **Mittermayer, J., Moreira, A**., *The Extended Chirp Scaling Algorithm for ScanSAR Interferometry*, European Conference on Synthetic Aperture Radar (EUSAR), Munich, Germany, 23-25 May 2000.

[253] **Mittermayer, J., Krieger, G., Moreira, A., Wendler, M.,** *Interferometric Performance Estimation for the Interferometric Cartwheel in Combination with a Transmitting SAR-Satellite*, IEEE Geoscience and Remote Sensing Symposium (IGARSS), pp. 2955 - 2957, Sydney, Australia, 2001.

[254] **Mittermayer, J., Krieger, G., Wendler, M., Moreira, A., Zeller, K.-H**., Touvenot, E., Amiot, T., Bamler, R., *Preliminary Interferometric Performance Estimation for the Interferometric Cartwheel in Combination with ENVISAT ASAR*, Committee on Earth Observation Satellites (CEOS) Workshop, Tokyo, Japan, 2001.

[255] **Mittermayer, J., Márquez Martinez, J.**, *Analysis of Range Ambiguity Suppression in SAR by Up and Down Chirp Modulation for Point and Distributed Targets*, IEEE Geoscience and Remote Sensing Symposium (IGARSS), Toulouse, France, 21-25 Jul. 2003.

[256] **Mittermayer, J.,** Runge, H., *Conceptual Studies for Exploiting the TerraSAR-X Dual Receive Antenna*, IEEE Geoscience and Remote Sensing Symposium (IGARSS), Toulouse, France, 21-25 Jul. 2003.

[257] **Mittermayer, J., Alberga, V., Buckreuss, S.,** Riegger, S., *TerraSAR-X: predicted performance*, International Society for Optical Engineering (SPIE), Agia Pelagia, Crete, Greece, 2003.

[258] **Mittermayer, J.**, Lord, R., Börner, E., *Sliding Spotlight SAR Processing for TerraSAR-X using a New Formulation of the Extended Chirp Scaling Algorithm*, IEEE Geoscience and Remote Sensing Symposium (IGARSS), Toulouse, France, 21-25 Jul. 2003.

[259] **Mittermayer, J., Schulze, D., Steinbrecher, U., Márquez-Martinez, J.**, *The System Engineering and Calibration Segment of the TerraSAR-X Ground Segment*, IEEE Geoscience and Remote Sensing Symposium (IGARSS), pp. 4, Seoul, South Korea, 2005.

[260] **Moreira, A., Mittermayer, J., Scheiber, R.,** *Extended Chirp Scaling SAR Data Processing in Stripmap, ScanSAR and Spotlight Imaging Modes*, European Conference on Synthetic Aperture Radar (EUSAR), Munich, Germany, 23-25 May 2000.

[261] **Moreira, A., Krieger, G., Mittermayer, J.**, *Comparison of Several Bistatic SAR Configurations for Spaceborne SAR Interferometry*, IEEE Geoscience and Remote Sensing Symposium (IGARSS), Sydney, Australia, 2001.

[262] **Moreira, A., Krieger, G., Mittermayer, J., Papathanassiou, K**., *Comparison of Several Bistatic SAR Configurations for Spaceborne SAR Interferometry*, Advanced SAR Workshop, Saint-Hubert, Quebec, Canada, 2001.

[263] **Moreira, A**., *Spaceborborne SAR Systems: Future Developments towards Multi-Static Configurations,* International Radar Symposium (IRS), Dresden, 30 Sep. - 2 Oct. 2003.

[264] **Moreira, A**., *TerraSAR-X Upgrade to a Fully Polarimetric Imaging Mode,* International Workshop on Applications of Polarimetry and Polarimetric Interferometry (PolInSAR), ESA/ESRIN, 14-16 Jan. 2003, Frascati, Italy, 2003.

[265] **Moreira, A., Krieger, G., Hajnsek, I., Hounam, D., Werner, M.**, Riegger, S., Settelmeyer, E., *TanDEM-X: A TerraSAR-X Add-On Satellite for Single-Pass SAR Interferometry*, IEEE Geoscience and Remote Sensing Symposium (IGARSS), pp. 1000 - 1003, Anchorage, USA, 2004.

[266] **Moreira, A., Krieger, G., Hajnsek, I., Papathanassiou, K, Fiedler, H., Hounam, D., Werner, M.**, *Feasibility Analysis of Pol-INSAR Applications with a TerraSAR-X Tandem Mission,* International Workshop on Applications of Polarimetry and Polarimetric Interferometry (PolInSAR), Frascati, Italy, 2005.

[267] **Moreira, A., Krieger, G.**, *TanDEM-X: Global Measurement of the Earth Topography from Space with Unprecedented Accuracy,* International Radar Symposium (IRS) DGON, Berlin, Germany, pp. 25-29, 2005.

[268] Moreno, C., **Gomez Otero, D.**, Bara, M., Casas, J., *A New High Efficiency 1-Watt S-Band GaAs HBT Power Amplifier MMIC for the TTC Transponder of the GALILEO Navigation System*, Tracking, Telemetry and Command Systems for Space Applications (TTC), Darmstadt, Germany, 2004.

[269] **Nannini, M., Liseno, A., Aulinger, T., Papathanassiou, K.**, *Vegetation bias removal and underlying topography estimation using Polarimetric SAR Interferometry*, IEEE Geoscience and Remote Sensing Symposium (IGARSS), Anchorage, Alaska, Sep. 2004.

[270] **Osipov, A.,** *Analytical Methods for Analysis of Electromagnetic Field Behaviour at Edges*, Union Radio-Scientifique Internationale (URSI) Commission B Open Symposium on Propagation and Remote Sensing, Odenthal-Altenberg, Germany, 2000.

[271] **Osipov, A.**, Hongo, K., Kobayashi, H., *High-frequency scattering of an obliquely incident plane electromagnetic wave by an impedance cylinder*, Millennium Conference on Antennas and Propagation, pp. 1 - 4, Davos, Switzerland, 2000.

[272] **Osipov, A.**, *Edge Functions and Their Application to Solution of Canonical Problems of Scattering in Wedge-shaped Domains*, Progress in Electromagnetics Research Symposium (PIERS), pp. 260 - 260, Osaka, Japan, 2001.

[273] **Osipov, A**., *An algorithm for generating Meixner's series*, Progress in Electromagnetics Research Symposium (PIERS), pp. 183 - 183, Honolulu, USA, 2003.

[274] **Osipov, A.**, *Simple approximations for diffraction coefficients of an impedance wedge*, Progress in Electromagnetics Research Symposium (PIERS), pp. 192 - 192, Honolulu, USA, 2003.

[275] **Osipov, A.,** Kamel, A., *Applying the Kontorovich-Lebedev transform to the analysis of electromagnetic diffraction by wedges*, Progress in Electromagnetics Research Symposium (PIERS), pp. 1 - 1, Pisa, Italy, 2004.

[276] **Öttl, H.**, Brieß, K., Lorenz, E., Oertel, D., Skrbek, W., Walter, I., Zhukov, B., *The disaster "Fires", its detection and means to improve information*, 53rd International Astronautical Congress, The World Space Congress - 2002, 10-19 Oct. 2002, Houston, Texas, pp. 1 - 8, 2002.

[277] **Papathanassiou, K., Hajnsek, I.,** Cloude, S.R., **Moreira, A.,** *Forest Parameter Estimation Using Passive Polarimetric Microsatellite Concept*, European Conference on Synthetic Aperture Radar (EUSAR), Cologne, Germany, pp. 357 - 360, 04-06 Jun. 2002.

[278] **Papathanassiou, K., Hajnsek, I., Mette, T.**, Cloude, S.R., *Forest Biomass Estimation Using Polarimetric SAR Interferometry*, Recent Advances in Quantitative Remote Sensing (RAIQRS), Valencia Spain, Sep. 16-20, 2002, pp. 731 - 740, 2002.

[279] **Papathanassiou, K., Hajnsek, I., Moreira, A.**, Cloude, S.R., *Forest Parameter Estimation Using A Passive Polarimetric Mircrosatellite Concept*, IEEE Geoscience and Remote Sensing Symposium (IGARSS), Toronto Canada, 24-28 Jun. pp. 826 - 828, 2002.

[280] **Papathanassiou, K., Mette, T.,** Zimmermann, R., Cloude, S.R., *Forest Parameter Estimation Using Polarimetric SAR Interferometry*, Union Radio-Scientifique Internationale (URSI) Commission F Open Symposium on Propagation and Remote Sensing, Garmisch-Partenkirchen Germany, 12-15 Feb. 2002.

[281] **Papathanassiou, K., Moreira, A.**, *A Passive Polarimetric Micro-Satellite Concept for Global Vegetation Biomass*, Polarimetric and Interferometric SAR Workshop (PI-SAR), Tokyo Japan, Aug. 29-30, 2002.

[282] **Papathanassiou, K.**, Cloude, S.R., *The effect of temporal decorrelation on the inversion of forest parameters from Pol-InSAR data*, IEEE Geoscience and Remote Sensing Symposium (IGARSS),Toulouse, Jul. 2003, pp. 1429 - 1431, 2003.

[283] **Papathanassiou, K., Mette, T., Hajnsek, I.,** *Model based forest height estimation from singel-baseline Pol-InSAR data: The Fichtelgebirge Test Case*, Intern. Workshop on Applications of Polarimetry and Polarimetric Interferometry (PolInSAR),Frascati, Jan.'03.

[284] **Papathanassiou, K.**, Cloude, S.R., *Forest Height Estimation using Dual-Pol InSAR Configurations*, European Conference on Synthetic Aperture Radar (EUSAR), Ulm, Germany, May 2004, pp. 93 - 96, 2004.

[285] **Peichl, M., Greiner, M., Süß, H.**, *DLR activities on aperture synthesis radiometry*, International Geoscience and Remote Sensing Symposium (IGARSS), Honolulu, Hawaii, USA, 24-28 Jul. 2000.

[286] **Peichl, M., Kempf, T., Dill, S., Süß, H**., *High resolution processing of low incidence angle ISAR images for target recognition*, Space-based Observation Technology (SBOT), Samos, Greece, 16-18 Oct. 2000.

[287] **Peichl, M., Süß, H., Dill, S., Greiner, M.**, *Today's imaging technologies and applications of microwave radiometry*, German Radar Symposium (GRS), Berlin, 11-12 Oct. 2000.

[288] **Peichl, M., Süß, H.**, Zeiler, M., **Dill, S.,** *Recent advances in the detection and identification of landmines by microwave radiometry*, Joint Workshop "Research on Demining Technologies", JRC Ispra, Italy, 12-14 Jul. 2000, pp. 72 - 73, 2000.

[289] **Peichl, M., Dill, S., Süß, H.**, *Advanced detection of anti-personnel landmines using multi-spectral low-frequency micorwave radiometry techniques*, Progress in Electromagnetics Research Symposium (PIERS), Osaka, 18-22 Jul. 2001, pp. 70 - 70, 2001.

[290] **Peichl, M., Dill, S., Süß, H.**, *Detection of anti-personnel landmines using microwave radiometry techniques*, NATO Advanced Workshop on "Detection of Explosives and Landmines", St. Petersburg, 9-14 Sep. 2001, pp. 195 - 198, 2001.

[291] **Peichl, M., Dill, S., Süß, H., Keydel, W.,** *Detection of Anti-personnel Landmines using Microwaves*, International Workshop on Commercial Radio Sensors and Communication Techniques (CRSCT), Linz, 23 Aug. 2001, pp. 74 - 76, 2001.

[292] **Peichl, M., Greiner, M., Süß, H., Dill, S.,** *Aperture synthesis radiometry*, ONERA-DLR Aerospace Symposium (ODAS), Bonascre, 23-26 Jan. 2001.

[293] **Peichl, M., Süß, H., Dill, S.,** *Passive imaging technologies for reconnaissance, surveillance, and guidance - functioning, benefits and applications*, NATO/RTO SET Symposium on Passive and LPI Radio Frequency Sensors, Warwaw, 23-25 Apr. 2001.

[294] **Peichl, M., Dill, S., Süß, H.,** *Detection of anti-personnel landmines using passive remote sensing techniques*, 11th ITG/GMA-Fachtagung, Ludwigsburg, 11-12 Mar. 2002, pp. 321 - 325, 2002.

[295] **Peichl, M., Süß, H., Dill, S., Greiner, M.**, *Imaging Technologies and Applications of Microwave Radiometry*, Union Radio-Scientifique Internationale (URSI) Forum, Brussels, Belgium, 13 Dec. 2002.

[296] **Peichl, M., Schulteis, S., Dill, S., Süß, H.**, *Application of microwave radiometry for buried landmine detection*, Union Radio-Scientifique Internationale (URSI) Commission F Open Symposium on Propagation and Remote Sensing, Garmisch-Partenkirchen, Germany, 12-15 Feb. 2002.

[297] **Peichl, M., Schulteis, S., Dill, S., Süß, H.**, *Application of microwave radiometry for buried landmine detection*, German Radar Symposium (GRS), Bonn, 3-5 Sep. 2002, pp. 357 - 361, 2002.

[298] **Peichl, M., Dill, S., Süß, H.**, *A microwave radiometer for buried landmine detection*, Progress in Elecromagnetic Research Symposium Progress in Electromagnetics Research Symposium (PIERS), Singapore, 7-10 Jan. 2003.

[299] **Peichl, M., Dill, S., Süß, H.**, *Application of microwave radiometry for buried landmine detection*, International Workshop on Advanced Ground Penetrating Radar, TU Delft, Delft, The Netherlands, 14-16 May 2003.

[300] **Peichl, M., Süß, H., Dill, S.,** *High resolution passive millimetre-wave imaging technologies for reconnaissance and surveillance*, International Society for Optical Engineering (SPIE) Aerosense 2003 - Passive MMW Imaging Technology VII, Orlando, FL, USA, 21-25 Apr. 2003.

[301] **Peichl, M., Süß, H., Dill, S.,** *High resolution passive millimetre-wave imaging using aperture synthesis techniques*, NATO ET-26 Workshop, DLR, Oberpfaffenhofen, Germany, 5-7 Mar. 2003.

[302] **Peichl, M., Dill, S., Süß, H.**, *Buried landmine detection using microwave radiometry*, Progress in Elecromagnetics Research Symposium (PIERS), Pisa, Italy, 28-31 Mar. 2004.

[303] **Peichl, M., Dill, S., Süß, H.**, *Passive millimetre-wave imaging technologies for reconnaissance and surveillance on UAVs*, 6th Joint International Military Sensing Symposium, Dresden, Germany, 18-21 Oct. 2004.

[304] **Peichl, M., Süß, H., Dill, S., Greiner, M., Jirousek, M.**, *Imaging technologies and applications of microwave radiometry*, European Radar Conference (EuRAD), Amsterdam, The Netherlands, 14-15 Oct. 2004.

[305] **Peichl, M., Greiner, M., Wittmann, V.,** *An image reconstruction and calibration approach for the SMOS aperture synthesis radiometer*, 8th Specialist Meeting on MW Radiometry, Rome, 24-27 Feb. 2004.

[306] **Peichl, M., Süß, H**., *Error analysis of sparse passive synthesis radiometers on UAV platforms*, International Society for Optical Engineering (SPIE), Orlando, FL (USA), 2005.

[307] Pierri, R., **Liseno, A.,** Soldovieri, F., Leone, G., *Advances in microwave subsurface imaging*, Tyrrhenian International Workshop on Remote Sensing (TIWRS), pp. 301 - 310, 2003.

[308] Pipia, L., **Alberga, V., Chandra, M.**, Migliaccio, M., **Ben Khadhra, K.,** *Quantitative assessment of the efficiency of supervised classification using coherent and incoherent polarimetric SAR observables*, European Conf.on Synthetic Aperture Radar (EUSAR), Cologne, Germany, 4-6 Jun. 2002, pp. 729 - 732, 2002.

[309] Potsis, A., **Reigber, A, Mittermayer, J., Moreira, A**., Uzunoglou, N., *Improving the Focussing Properties of SAR Processors for Wide-band and Wide-beam Low Frequency Imaging*, IEEE Geoscience and Remote Sensing Symposium (IGARSS), Sydney, 2001.

[310] **Reigber, A., Papathanassiou, K.,** Cloude, S.R., **Moreira, A.,** *SAR Tomography and Interferometry for the Remote Sensing of Forested Terrain*, European Conference on Synthetic Aperture Radar (EUSAR), Munich, Germany, 23-25 May 2000.

[311] **Reigber, A., Papathanassiou, K., Moreira, A.**, Cloude, S.R., *Polarisation Effects in SAR Tomography*, IEEE Geoscience and Remote Sensing Symposium (IGARSS), Honolulu, Hawaii, USA, 24-28 Jul. 2000.

[312] **Rode, G.**, *Detection Probability of a Ground-based Radar*, Open Symposium on Propagation and Remote Sensing, Garmisch-Partenkirchen, Germany, 2002.

[313] **Rodriguez Cassola, M., Krieger, G., Wendler, M.**, *Analysis of Monostatic SAR Processing Techniques to Focus Stationary Bistatic Airborne Data*, International Radar Symposium (IRS), pp. 209 - 212, Berlin, Germany, 2005.

[314] **Rodriguez Cassola, M., Krieger, G., Wendler, M.,** *Azimuth-invariant, bistatic airborne SAR processing strategies based on monostatic algorithms*, IEEE Geoscience and Remote Sensing Symposium (IGARSS), pp. 1047 - 1050, Seoul, South Korea, 2005.

[315] Runge, H., **Werner, M**., Eineder, M., Breit, H., Suchandt, S., Massonnet, D., *Advanced Synthetic Aperture Radar Observations with Clusters of SAR Satellites*, International Society for Photogrammetry and Remote Sensing (ISPRS) Workshop, Hannover, 2001.

[316] **Scheiber, R.,** Robert, P., *Origin and Correction of Phase Errors in Airborne Repeat-Pass SAR Interferometry*, IEEE Geoscience and Remote Sensing Symposium (IGARSS), Sydney, 9-13 Jul. 2001.

[317] **Scheiber, R.**, *DEM Reconstruction and New Techniques using Airborne SAR Data*, European Association of Geoscientists and Engineers (EAGE) Workshop: "New Technologies for Land Monitoring: from Digital Elevation Models to Subsidence Estimation", Florence, Italy, 27 May 2002.

[318] **Scheiber, R., Bothale, V.M.,** *Application of Multi-Look Techniques for Interferometric SAR Data*, European Conference on Synthetic Aperture Radar (EUSAR), Cologne, pp. 77 – 80, 4-6 Jun. 2002.

[319] **Scheiber, R., Bothale, V.M.,** *Interferometric Multi-Look Techniques for SAR Data*, IEEE Geoscience and Remote Sensing Symposium (IGARSS), Toronto, 24-28 Jun. 2002.

[320] **Scheiber, R.,** *A Three-Step Phase Correction Approach for Airborne Repeat-Pass Interferometric SAR Data*, IEEE Geoscience and Remote Sensing Symposium (IGARSS), Toulouse, 21-25 Jul. 2003.

[321] **Scheiber, R., Hajnsek, I., Papathanassiou, K.,** *Analysis of Short Time Interval Decorrelation Effects for Interferometric SAR in X-, C-, and L-band*, European Conference on Synthetic Aperture Radar (EUSAR), Ulm, pp. 767 – 770, 25-27 May 2004.

[322] **Scheiber, R., Fischer, J.,** *Absolute Phase Offset in SAR Interferometry: Estimation by Spectral Diversity and Integration into Processing*, European Conference on Synthetic Aperture Radar (EUSAR), pp. 97 - 97, Ulm, Germany, 2004.

[323] Scheuchl, B., **Hajnsek, I.,** Cumming, I.G., *Model-based Classification of Polarimetric SAR Sea Ice Data*, IEEE Geoscience and Remote Sensing Symposium (IGARSS), Toronto Canada, pp. 1521 – 1523, 24-28 Jun. 2002.

[324] Scheuchl, B., **Hajnsek, I.**, Cumming, I.G., *Sea Ice Classification using Multi-Frequency Polarimetric SAR Data*, IEEE Geoscience and Remote Sensing Symposium (IGARSS), Toronto Canada, pp. 1914 – 1916, 24-28 Jun. 2002.

[325] Scheuchl, B., **Hajnsek, I.**, Cumming, I., *Classification strategies for polarimetric SAR sea ice data*, International Workshop on Applications of Polarimetry and Polarimetric Interferometry (PolInSAR), Frascatti, Jan. 2003.

[326] Scheuchl, B., **Hajnsek, I.**, Cumming, I., *Potential of SAR polarimetry for sea ice discrimination*, Advanced SAR Workshop, Montreal, Canada, Jun. 2003.

[327] **Schröder, R., Neff, T., Jochim, F., Hajnsek, I.**, *MAPSAR: A small L-Band SAR misson for land observation*, 4th IAA Symposium on Small Satellites for Earth Observation, Berlin, 07-10 Apr. 2003.

[328] **Schwerdt, M., Hounam, D.**, *Quality Control and Calibration of Future SAR Systems*, ONERA-DLR Aerospace Symposium (ODAS), Paris, 20-22 Jun. 2001.

[329] **Schwerdt, M., Zink, M., Hounam, D.,** *A Treatment of SAR Radiometric Resolution including Geolocated Ambiguous Energy*, Committee on Earth Observation Satellites (CEOS) SAR Workshop, Tokio, 2-5 Apr. 2001.

[330] **Schwerdt, M., Hounam, D.**, *SAR Product Control Software (SARCON)*, European Conference on Synthetic Aperture Radar (EUSAR), Cologne 2002.

[331] **Schwerdt, M., Hounam, D., Molkenthin, T.**, *Calibration Concepts for Multiple Mode High Resolution SARs like TerraSAR-X*, Advanced SAR Workshop, Montreal, Canada, 25-27 Jun. 2003.

[332] **Schwerdt, M., Hounam, D., Molkenthin, T.**, *Calibration Concepts for Multitude Mode High Resolution SARs like TerraSAR-X*, International Radar Sysmposium (IRS), Dresden, 30 Sep. 2003 – 2 Oct. 2003.

[333] **Schwerdt, M., Hounam, D.**, Stangl, M., *Calibration Concept for the TerraSAR-X Instrument,* IEEE Geoscience and Remote Sensing Symposium (IGARSS), Toulouse, 21-25 Jul. 2003.

[334] **Shishkova, O**., **Hajnsek, I.**, *A Multi-Frequency Polarimetric Scattering Model for*, IEEE Geoscience and Remote Sensing Symposium (IGARSS), Anchorage, Alaska, pp. 2499 – 2502, Sep. 2004.

[335] Singh, D., **Papathanassiou, K., Hajnsek, I.,** *Semi-empirical approach and radar polarimetry for vegetation observations*, International Workshop on Applications of Polarimetry and Polarimetric Interferometry (PolInSAR), ESA/ESRIN, Frascatti, Jan. 2003.

[336] **Speck, R., Hager, M.**, **Garcia, M.**, **Süß, H**., *An End-to-End-Simulator for Spaceborne SAR-Systems*, European Conference on Synthetic Aperture Radar (EUSAR), Cologne, 4-6 Jun. 2002, pp. 237 - 239, 2002.

[337] Spencer, P., **Alberga, V., Chandra, M., Hounam, D., Keydel, W.,** *SAR Polarimetric Parameters for Land Use Classification*, European Conference on Synthetic Aperture Radar (EUSAR), Munich, 23-25 May 2000, pp. 783 - 785, 2000.

[338] **Steinbrecher, U., Márquez-Martinez, J., Mittermayer, J., Metzig, R., Buckreuss, S.**, Gottwald, M., *New Data Take Commanding Concept for TerraSAR-X Instrument*, European Conference on Synthetic Aperture Radar (EUSAR), Ulm, Germany, 2004.

[339] Suchandt, S., Runge, H., Eineder, M., **Scheiber, R.,** *Measurement of River Surface Currents using SAR Techniques*, IEEE International Geoscience and Remote Sensing Symposium (IGARSS), Seoul, South Korea, 2005.

[340] Suchandt, S., Palubinskas, G., Runge, H., Eineder, M., Meyer, F., **Scheiber, R.**, *An Airborne SAR Experiment For Ground Moving Target Identification*, International Society for Photogrammetry and Remote Sensing (ISPRS): High-Resolution Earth Imaging for Geospatial Information, Hannover, Germany, 2005.

[341] **Süß, H., Schröder, R., Peichl, M., Neff, T.**, *Possible Military Requirements and Applications of Active and Passive Imaging Sensors at Micro- and Millimeterwave Frequencies*, IEEE Geoscience and Remote Sensing Symposium (IGARSS), Toronto, 24-28 Jun. 2002.

[342] **Süß, H.,** *Fully polarimetric measurements of brightness temperature distributions with a quasioptical radiometer system at 90GHz*, International Society for Optical Engineering (SPIE), Passive Millimeter-Wave Imaging Technology VI vol. 4719, 2002.

[343] **Ulbricht, A**., **Reigber, A., Horn, R.**, Potsis, A., **Moreira, A.,** *Multi-frequency SAR-interferometry: DEM-generation in L- and P-band and vegetation height estimation in combination with X-band*, European Conference on Synthetic Aperture Radar (EUSAR), Munich/Germany, 23-25 May 2000.

[344] **Vandewal, M., Speck, R., Süß, H.**, *Raw Data Simulation for SAR-Systems on UAV-Platforms*, European Conference on Synthetic Aperture Radar (EUSAR), Ulm, 25-27 May, 2004, pp. 597 - 600, 2004.

[345] **Wendler, M., Buckreuss, S., Mittermayer, J., Moreira, A.**, Sutor, **T**., *Sector Imaging Radar for Enhanced Vision (SIREV): Simulation and Processing Techniques*, AeroSense, Orlando/Florida, 24 - 28 Apr. 2000.

[346] **Wendler, M., Krieger, G., Horn, R., Gabler, B.,** Dubois-Fernandez, P., Vaizan, B., du Plessis, O., *First Results of a Joint Bistatic Airborne SAR Experiment*, International Geoscience and Remote Sensing Symposium (IGARSS), Toulouse, 21-25 Jul. 2003.

[347] **Wendler, M., Krieger, G., Horn, R., Gabler, B.**, Dubois-Fernandez, P., Vaizan, B., du Plessis, O., Cantalloube, H., *Results of a Bistatic Airborne SAR Experiment*, International Radar Symposium (IRS), Dresden, 30 Sep. - 2 Oct., pp. 247 - 253, 2003.

[348] **Wendler, M., Krieger, G., Rodriguez Cassola, M., Horn, R., Gabler, B.**, Dubois-Fernandez, P., Vaizan, B., Ruault du Plessis, O., Cantalloube, H., *Analysis of Bistatic Airborne SAR data*, European Conference on Synthetic Aperture Radar (EUSAR), pp. 571 - 572, Ulm, Germany, 2004.

[349] **Werner, M.,** Werninghaus, R., *The SRTM Project: International Cooperation and Technical Coordination. A German Perspective.*, International Astronautical Federation (IAF) Congress, Rio de Janeiro, 2000.

[350] **Werner, M.,** *Shuttle Radar Topography Mission (SRTM) Mission Overview*, European Conference on Synthetic Aperture Radar (EUSAR), pp. 209 - 212, Munich, 2000.

[351] **Werner, M.,** Eineder, M., Bamler, R., Rabus, B., Breit, H., Suchandt, S., Knöpfle, W., Holzner, J., Adam, N., *SRTM/X-SAR Calibration Status*, Committee on Earth Observation Satellites (CEOS) -SAR Calibration/Validation Workshop, Hamburg, 2001.

[352] **Werner, M.,** Roth, A., Knöpfle, W., Breit, H., Eineder, M., Suchandt, S., *X-SAR/SRTM digital height models: processing status and results*, European Geophysical Society, American Geophysical Union, and European Union of Geosciences (EGS-AGU-EUG) Joint Assembly Symposium, Nice, France, 06 - 11 Apr. 2003.

[353] **Witte, F., Krieger, G., Mittermayer, J., Wendler, M.,** *Results of the First Helicopter Flights With the New Sector Imaging Radar for Enhanced Vision - SIREV*, International Airborne Remote Sensing Conference, San Francisco, USA, 2001.

[354] Woodhouse, I.H., Cloude, S.R., **Papathanassiou, K**., Hope, J., J. Suarez, J., Osborne, P., Wright, G., *Polarimetric Interferometry in the Glen Affric Project: Results & Conclusions*, IEEE Geoscience and Remote Sensing Symposium (IGARSS), Toronto Canada, 24-28 Jun. 2002, pp. 820 - 822, 2002.

[355] **Younis, M., Gebert, N.**, Lenz, R., Schuler, K., Wiesbeck, W., *A Processing Algorithm for Digital Beamforming SAR*, International Radar Symposium (IRS), 6-8 Sep. 2005, pp. 331 - 336, Berlin, 2005.

[356] Yvinec, Y., Borghys, D., **Süß, H., Keller, M.**, Bajic, M., Wolff, E., Vanhuysse, S., Bloch, I., Yu, Y., Damanet, O., *SMART: Space and Airborne Mined Area Reduction Tools - Presentation*, The European Union in Humanitarian Demining (EUDEM) - Society for Ordnance Technology (SCOT), Brüssel, 15-18 Sep. 2003.

[357] **Zandona-Schneider, R., Liseno, A., Papathanassiou, K., Hajnsek, I.**, *Polarimetric SAR interferometry over urban areas: first results*, European Conference on Synthetic Aperture Radar (EUSAR), Ulm, Germany, May 2004, pp. 755 - 758, 2004.

[358] **Zandona Schneider, R.**, Fernandes, D., *Entropy among a sequency of SAR images for change detection*, IEEE Geoscience and Remote Sensing Symposium (IGARSS), Toulouse, Jul. 2003, pp. 2623 - 2625, 2003.

[359] Zetzsche, C., **Krieger, G.**, Röhrbein, F., *Higher-Order Statistics and the Multivariate Probability Density Function of Natural Images*, European Conference on Visual Perception (ECVP), Groningen, Netherlands, 2000.

[360] Zhu, D., **Scheiber, R.**, Zhu, Z., *Impacts of an Efficient Topography Adaptive Filter on Coherence Estimation and Phase Unwrapping*, European Conference on Synthetic Aperture Radar (EUSAR), Munich, 23-25 May, 2000, pp. 319 - 322, 2000.

[361] **Zink, M., Krieger, G.,** Amiot, T., *Interferometric Performance of a Cartwheel Constellation for TerraSAR-L*, Fringe Workshop, Frascati, Italy, 2003.

3.8.4 Conference Proceedings – Invited Talks/Invited Papers

[362] **Alberga**, **V**., Krogager, E., **Chandra**, **M**., Wanielik, G., *Potential of coherent decompositions in SAR polarimetry and interferometry*, IEEE Geoscience and Remote Sensing Symposium (IGARSS), Anchorage, Alaska, USA, 20-24 Sep. 2004.

[363] **Alberga**, **V.**, Staykova, D., Krogager, E., **Danklmayer**, **A., Chandra, M.**, *Comparison of methods for extracting and utilizing radar target characteristic parameters*, IEEE Geoscience and Remote Sensing Symposium (IGARSS), Seoul, Korea, 2005.

[364] **Aulinger, T**., **Mette**, **T., Papathanassiou, K., Hajnsek, I.**, Heurich, M., Krzystek, P., *Validation of Heights Derived from Interferometric SAR and LIDAR over the Temperate Forest Site Nationalpark Bayerischer Wald*, International Workshop on Applications of Polarimetry and Polarimetric Interferometry (PolInSAR), Frascati, Italy, 2005.

[365] **Ben Khadhra, K**., *Microwaves and Radar Institute - Bistatic Measurement Facility at DLR*, Presentation at Ecole nationale supérieure des ingénieurs des études et techniques d'armement (ENSIETA), Brest, France, 2004.

[366] Boerner, W.-M., Cloude, S., **Moreira, A**., *User collision in sharing of electromagnetic spectrum : Frequency allocation, RF interference reduction and RF security threat mitigation in radio propagation and passive and active remote sensing,* Union Radio-Scientifique Internationale (URSI) Commission F Open Symposium on Propagation and Remote Sensing, Garmisch-Patenkirchen, 2002.

[367] Boerner, W.-M., Cloude, S., **Moreira, A**., *User Collision for Joint Utilization of Electromagnetic Frequency Band: Frequency allocation, RF interference reduction and RF security threat mitigation in radio propagation and passive and active remote sensing,* Union Radio-Scientifique Internationale (URSI) General Assmenbly Symposium, The Netherlands, 2002.

[368] Cloude, S., **Krieger, G., Papathanassiou, K**., *A framework for investigating space-borne polarimetric interferometry using the ALOS-PALSAR sensor*, IEEE Geoscience and Remote Sensing Symposium (IGARSS), pp. 3361 - 3364, Seoul, Korea, 2005.

[369] **Danklmayer, A**., *Application of Principal Component Analysis in Radar Polarimetry*, IEEE Geoscience and Remote Sensing Symposium (IGARSS), Seoul (ROK), 2005.

[370] **Danklmayer, A., Chandra, M**., Boerner, W.-M., *Target Decomposition using PCA*, Union Radio-Scientifique Internationale (URSI) Commission F Open Symposium on Propagation and Remote Sensing, Varese, Italy, 2005.

[371] **Fiedler, H**., *Satellitenfernerkundung mit Hilfe von Syntetischem Apertur Radar*, Interdisziplinärer Workshop Astronomie und Astrophysik (IWAA), Gummer, Italy, 2005.

[372] Garestier, F., **Papathanassiou, K., Hajnsek, I.**, Dubois-Fernandez, P., Dupuis, X., *Analysis of forest parameters and agricultural field structure from high resolution PolInSAR X band data*, International Workshop on Applications of Polarimetry and Polarimetric Interferometry (PolInSAR), Frascati, Italy, 2005.

[373] Garestier, F., **Papathanassiou, K., Hajnsek, I.**, Dubois-Fernandez, P., Dupuis, X., *Analysis of Forest Parameters and Agricultural Field Structure from high resolution PolInSAR X-band data*, International Workshop on Applications of Polarimetry and Polarimetric Interferometry (PolInSAR), Frascati, Italy, 2005.

[374] **Hajnsek, I.**, Cloude, S., *Parameter Inversion over Agricultural Vegetation by Means of PolInSAR*, IEEE Geoscience and Remote Sensing Symposium (IGARSS), Seoul, South Korea, 2005.

[375] **Hajnsek, I**., Cloude, S., *Differential Extinction Estimation over Agricultural Vegetation from Pol-InSAR*, International Workshop on Applications of Polarimetry and Polarimetric Interferometry (PolInSAR), Frascati, Italy, 2005.

[376] **Hajnsek, I.**, Eineder, M., *TerraSAR-X: Science Exploration of Polarimetric and Interferometric SAR*, IEEE Geoscience and Remote Sensing Symposium (IGARSS), Seoul, South Korea, 2005.

[377] **Hajnsek, I., Kugler, F., Papathanassiou, K., Scheiber, R., Horn, R., Moreira, A.**, Hoekman, D., Davidson, M., Attema, E., *INDREX II: Indonesian Airborne Radar Experiment Campaign over Tropical Forest*, International Workshop on Applications of Polarimetry and Polarimetric Interferometry (PolInSAR), Frascati, Italy, 2005.

[378] **Hajnsek, I.,** Weber, M., *TanDEM-X: Science and Custom Exploration*, IEEE Geoscience and Remote Sensing Sympos. (IGARSS),Seoul, South Korea, 2005.

[379] **Kempf, T., Peichl, M., Dill, S., Süß, H.,** *Effects and compensation of phase drift in a 3D tower-turntable ISAR imaging system*, International Radar Symposium (IRS), pp. 693 - 699, Berlin, Germany, 2005.

[380] **Kempf, T., Peichl, M., Dill, S., Süß, H.,** *Investigation of the influence of camouflage on the ATR performance for highly resolved ISAR-images of relocatable targets*, Microwave Advanced Target Recognition and Identification Experiment (MATRIX), Oberammergau, Germany, 2005.

[381] **Keydel, W., Werner, M., Hounam, D.**, *X-SAR as Part of SRTM*, IEEE Geoscience and Remote Sensing Symposium (IGARSS), Honolulu, Hawaii USA, 24-28 Jul. 2000.

[382] **Keydel, W.**, *The European Network, Radar Polarimetry. Theory and Applications, Goals, Structure and Results,* International Symposium on Antennas and Propagation (ISAP), Fukuoka, Japan, 21-25 Aug. 2000.

[383] **Keydel, W.**, *Microwave Remote Sensing Technology: Future development expectations with emphasis on Synthetic Aperture Radar (SAR) and the respective Antennas*, Union Radio-Scientifique Internationale (URSI) General Assembly Symposium, Delhi, India, 2005.

[384] Kimura, H., **Papathanassiou, K., Hajnsek, I.**, *Polarization Orientation Effects in Urban Areas on SAR Data*, IEEE Geoscience and Remote Sensing Symposium (IGARSS), Seoul, South Korea, 2005.

[385] **Krieger, G., Mittermayer, J., Moreira, A., Wendler, M., Witte, F., Keydel, W**., *Sector Imaging Radar for Enhanced Vision*, ONERA-DLR Aerospace Symposium (ODAS), Paris, France, 2001.

[386] **Krieger, G., Fiedler, H., Hounam, D., Moreira, A.**, *Analysis of System Concepts for Bi-and Multistatic SAR Missions*, IEEE Geoscience and Remote Sensing Symposium (IGARSS), pp. 770 - 772, Toulouse, France, 2003.

[387] **Krieger, G., Moreira, A**., *Potentials of Digital Beamforming in Bi- and Multistatic SAR*, IEEE Geoscience and Remote Sensing Symposium (IGARSS), pp. 527 - 529, Toulouse, France, 2003.

[388] **Krieger, G., Fiedler, H., Moreira, A.**, *Bi- and Multistatic SAR: Potentials and Challenges*, European Conference on Synthetic Aperture Radar (EUSAR), pp. 365 - 369, Ulm, Germany, 2004.

[389] **Krieger, G.**, *Spaceborne Bistatic SAR*, National Korean Radar SAR Workshop, Seoul, Korea, 2005.

[390] **Krieger, G., Fiedler, H., Hajnsek, I.,** Eineder, M., **Werner, M., Moreira, A.**, *TanDEM-X: Mission Concept and Performance Analysis*, IEEE International Geoscience and Remote Sensing Symposium (IGARSS), pp. 4890 - 4893, Seoul, Korea, 2005.

[391] **Krieger, G., Moreira, A.**, *Multistatic SAR Satellite Formations: Potentials and Challenges*, IEEE Geoscience and Remote Sensing Symposium (IGARSS), pp. 2680 - 2684, Seoul, Korea, 2005.

[392] **Kugler, F., Hajnsek, I., Papathanassiou, K., Horn, R., Scheiber, R., Moreira, A.,** Hoekman, D., Davidson, M., *INDREX II - Indonesian Airborne Radar Experiment Campaign over Tropical Forest in L- and P-band: First results*, IEEE Geoscience and Remote Sensing Symposium (IGARSS), Seoul, South Korea, 2005.

[393] **Kugler, F., Mette, T., Hajnsek, I., Papathanassiou, K.,** *Forest Biomass from Pol-InSAR - Inversion of Forest height with Pol-InSAR and Subsequent Conversion to Biomass with Allometry Conclusions from three Temperate Test Sites*, IEEE Geoscience and Remote Sensing Sympos. (IGARSS), Seoul, South Korea, 2005.

[394] Lee, H.-W., Chen, K.-S., Lee, J.-S., Shi, J.C., Wu, T.-D., **Hajnsek, I.**, *A Comparisons of Model based and Image based Surface Parameters Estimation from Polarimetric SAR*, IEEE Geoscience and Remote Sensing Symposium (IGARSS), Seoul, South Korea, 2005.

[395] Lee, J.-S., **Papathanassiou, K., Hajnsek, I., Mette, T.,** Grunes, M., Ainsworth, T., Ferro-Famil, L., *Applying Polarimetric SAR Interferometric Data for Forest Classification*, IEEE Geoscience and Remote Sensing Symposium (IGARSS), Seoul, South Korea, 2005.

[396] **Moreira, A., Papathanassiou, K., Krieger, G.,** *Polarimetric SAR Interferometry with a Passive Polarimetric Micro-Satellite Concept,* Union Radio-Scientifique Internationale (URSI) General Assembly Symposium, The Netherlands, 2002.

[397] **Osipov, A.,** *Improving the Physical Optics Approximation*, International Workshop on Advanced Electromagnetics (IWAE), Korakuen Campus, Chuo University, Tokyo, Japan, 2001.

[398] **Osipov, A.,** *Analysis of electromagnetic diffraction by wedges with the method of edge functions*, Union Radio-Scientifique Internationale (URSI) General Assembly Symposium, pp. 1 - 4, Maastricht, the Netherlands, 2002.

[399] **Osipov, A.**, *A hybrid technique for the analysis of scattering by impedance wedges*, Union Radio-Scientifique Internationale (URSI) Commission B Open Symposium on Propagation and Remote Sensing, pp. 1140 - 1142, Pisa, Italy, 2004.

[400] **Osipov, A.,** Senior, T., *Electromagnetic diffraction by an impedance wedge of arbitrary angle*, Union Radio-Scientifique Internationale (URSI) General Assembly Symposium, pp. 1 - 4, New Delhi, India, 2005.

[401] **Öttl, H., Keydel, W.**, *Shuttle Radar Topography Mission*, International Symposium on Space Technology and Science, Morioka, Japan,28 May–04 Jun.'00.

[402] **Papathanassiou, K., Mette, T., Hajnsek, I., Krieger, G., Moreira, A.,** *A Passive Polarimetric Micro-Satellite Concept for Global Biomass Mapping*, Polarimetric and Interferometric SAR Workshop (PI-SAR), Tokyo, Japan, 2002.

[403] **Peichl, M., Süß, H., Dill, S., Greiner, M.,** *Imaging Technologies and Applications of Microwave Radiometry*, Union Radio-Scientifique Internationale (URSI), Radar and Radiometry Session, Brussels, Belgium. 13 Dec. 2002.

[404] **Peichl, M., Süß, H., Dill, S.**, *Imaging Technologies and Applications of Microwave Radiometry*, Electrical and Electronic Engineering for Communication (EEEf-COM) Workshop, Ulm, Germany, 2005.

[405] Potsis, A., **Reigber, A., Moreira, A.,** Ferro-Famil, L., Uzunoglou, N., *Comparison of Chirp Scaling and Wavenumber Domain Algorithms for Airborne Low Frequency SAR Data Processing,* European Conference on Synthetic Aperture Radar (EUSAR), Cologne, Germany, 2002.

[406] Pottier, E., Ferro-Famil L., Cloude, S., **Hajnsek, I., Papathanassiou, K**., Pearson, T., Desnos, Y., *Pol-SARpro v2.0: The Polarimetric SAR Data Processing and Educational Toolbox*, IEEE Geoscience and Remote Sensing Symposium (IGARSS), Seoul, S.outh Korea, 2005.

[407] **Schneider, R.Z., Papathanassiou, K., Liseno, A., Hajnsek, I.,** *The Effect of Polarisation on Coherent Scatterers in Urban Areas*, BioGeoSAR2004, Innsbruck, Austria, 2004.

[408] **Schneider, R.Z., Papathanassiou, K., Hajnsek, I., Moreira, A.,** *Coherent Scatterers in Urban Areas: Characterisation and Information Extraction*, Fringe Workshop, Frascati, Italy, 2005.

[409] **Schneider, R.Z., Papathanassiou, K., Hajnsek, I., Moreira, A.**, *Polarimetric Interferometry over Urban Areas: Information Extraction using Coherent Scatters*, IEEE Geoscience and Remote Sensing Symposium (IGARSS), Seoul, South Korea, 2005.

[410] **Schneider, R.Z., Papathanassiou, K., Hajnsek, I., Moreira, A.,** *Analysis of coherent scatterers over urban areas*, International Workshop on Applications of Polarimetry and Polarimetric Interferometry (PolIn-SAR), Frascati, Italy, 2005.

[411] **Schröder, R.,** *First Results of the SRTM-Mission*, SAR/SLAR Steering Committee Meeting, Berlin, 11-13 Sep. 2000.

[412] **Schröder, R., Klein, K.B**., **Süß, H.,** *Performance Analysis for the SRTM-Mission*, Space-Based Observation Technology (SBOT), 16-18 Oct. 2000, Samos, Greece, pp. 35-1 - 35-5, 2000.

[413] **Schröder, R., Süß, H.**, *Performance Prediction and Simulation for Future Low Cost SAR-Systems*, ONERA-DLR Aerospace Sympos. (ODAS), Paris, 20-22 Jun.'01.

[414] **Schröder, R., Zeller, K.H., Neff, T., Süß, H.,** *Potentials of Reflector Antenna Technology for a Fully Polarimetric L-band Spaceborne SAR Instrument Targeting Land Applications*, European Conference on Synthetic Aperture Radar (EUSAR), Cologne, 4-6 Jun. 2002, pp. 41 - 44, 2002.

[415] **Schröder, R.,** Puls, J., **Hajnsek, I., Jochim, F.**, Quintino, M., Paradella, W., Chamon, M., *The MAPSAR Mission: Objectives, Design and Status*, Simposio Brasileiro de Sensoriamento Remoto (SBSR), Goiania, 16-21 Apr. 2005, pp. 4481 - 4488, 2005.

[416] **Schwerdt, M., Hounam, D., Bräutigam, B.**, **Alvarez Pérez, J.L**., *TerraSAR-X: Calibration Concept of a Multiple Mode High Resolution SAR*, IEEE Geoscience and Remote Sensing Symposium (IGARSS), Seoul, Korea, 2005.

[417] Suchandt, S., Palubinskas, G., **Scheiber, R.,** Meyer, F., Runge, H., Reinartz, P., **Horn, R.**, *Results from an Airborne SAR GMTI Experiment supporting TerraSAR-X Traffic Processor Development*, IEEE Geoscience and Remote Sensing Symposium (IGARSS), Seoul, South Korea, 2005.

[418] **Waegel, K., Hounam, D., Schwerdt, M., Bauer, R.**, *Codierter Radartransponder für wissenschaftliche und kommerzielle Anwendungen*, DGON Jahreshauptversammlung „Mobilität und Sicherheit"; Wolfsburg 23-25 Oct. 2001.

[419] **Werner, M.,** *Shuttle Radar Topography Mission (SRTM) Mission Overview*, European Association for the International Space Year (EURISY) Conference, Varese, Italy, 2000.

[420] **Werner, M.**, *Operating the X-band SAR Interferometer of the SRTM*, IEEE Geoscience and Remote Sensing Symposium (IGARSS), Honolulu, Hawaii USA, 2000.

[421] **Werner, M**., *Mapping the earth from space: first results and applications*, ONERA-DLR Aerospace Symposium (ODAS), Berlin, 2000.

[422] **Werner**, **M.**, **Klein, K.-B., Häusler, M**., *Performance of the Shuttle Radar Topography Mission, X-Band Radar System*, IEEE Geoscience and Remote Sensing Symposium (IGARSS), Honolulu, Hawaii USA, 2000.

[423] **Werner**, **M., Schmullius, C**., Ritter, P., *Shuttle Radar Topography Mission(SRTM): An Overview of the Scientific Experiments in Connection with the X-SAR AO*, IEEE Geoscience and Remote Sensing Symposium (IGARSS), Honolulu, Hawaii USA, 2000.

[424] **Werner**, **M**., *Shuttle Radar Topography Mission (SRTM): Experience with the X-Band SAR Interferometer*, Chinese Institute of Electronics (CIE) International Conference on Radar, pp. 634 - 638, Beijing, China, 2001.

[425] **Werner**, **M.**, *Status of the SRTM data processing: when will the world-wide 30m DTM data be available?* 48. Photogrammetrische Woche, pp. 159 - 165, Stuttgart, 2001.

[426] **Werner**, **M.**, *Disaster Management with SRTM*, United Nations Committee on the Peaceful Uses of Outer Space (UNCOPUOS) Sitzung, Wien, Austria, 2001.

[427] **Werner**, **M**., Eineder, M., *The X-SAR/SRTM Project Calibration Phase*, X-SAR Science Workshop, Firence, Italy, 2001.

[428] **Werner**, **M.**, **Häusler, M.**, *X-SAR/SRTM Instrument Phase Error Calibration*, IEEE Geoscience and Remote Sensing Symposium (IGARSS), Sydney, Australia, 2001.

[429] **Werner**, **M.**, *Digital Height Models from X-SAR/SRTM Single Pass SAR Interferometry*, Tyrrhenian International Workshop on Remote Sensing (TIWRS), Elba Italy, 2003.

[430] **Werner**, **M.**, Roth, A., Eineder, M., *Overview of the X-SAR / SRTM Data Processing and Scientific Investigations*, The Shuttle Radar Topography Mission - Data Validation and Applications Final Workshop, 14-16 Jun. 2005, Reston, Virginia, USA, Reston, Virginia, USA, 2005.

[431] Zetzsche, C., **Krieger, G.**, *Nonlinear image operators, higher-order statistics,and the AND-like combinations of frequency components*, International Symposium Image and Signal Processing and Analysis, pp. 119 - 124, Pula, Croatia, 2001.

[432] Zetzsche, C., **Krieger, G., Mayer, G**., *Nonlinear AND interactions between frequency components and the selective processing of intrinsically two-dimensional signals by cortical neurons*, International Society for Optical Engineering (SPIE) Workshop, pp. 36 - 68, Bellingham, WA (USA), 2001.

3.8.5 Conference Proceedings - Unpublished

[433] **Ben Khadhra, K., Börner, T., Hounam, D., Chandra, M.**, *Bistatic Measurements and Analysis of Surface Scattering*, Kleinheubacher Tagung 2004, Miltenberg, 2004.

[434] **Ben Khadhra, K., Börner, T., Chandra, M., Hounam, D**., *Soil Parameter Estimation And Analysis Of Bistatic X-Band Measurements*, Kleinheubacher Tagung, Miltenberg, Germany, 2005.

[435] **Ben Khadhra, K.**, Nolan, M., **Börner, T., Hounam, D., Chandra, M.**, *Phase Sensitiveness to Soil Moisture in controlled Anechoic Chamber: Measurements and first results*, American Geophysical Union (AGU) 2005, San Francisco, CA, USA, 2005.

[436] **Chandra, M.,** Otto, T., **Danklmayer, A.,** *Interpretation of Co-to-Cross Polar Phases in Weather Radar Measurements*, European Geosciences Union (EGU), General Assembly, Vienna, Austria, 2005.

[437] **Danklmayer, A., Chandra, M.,** *On the Requirements to detect Atmospheric Artefacts in Synthetic Aperture Radar Images*, Union Radio-Scientifique Internationale (URSI) Kleinheu-bacher Tagung, Miltenberg, Germany, 2005.

[438] **Danklmayer, A.,** Galletti, M., **Chandra, M.,** *Potential Application of Principal Component Analysis in Polarimetric weather radar measurements*, European Geosciences Union (EGU), General Assembly, Vienna, 2005.

[439] **De Florio, S., Neff, T., Zehetbauer, T.,** *Analysis of orbits propagation and relative position accuracy of small satellites for SAR interferometry*, IAA Symposium on Small Satellites for Earth Observation, Berlin, Germany, 2005.

[440] **De Florio, S., Neff, T., Zehetbauer, T**., *Operational aspects of orbit determineation with GPS for small satellites with a SAR payload*, IAA Symposium on Small Satellites for Earth Observation, Berlin, Germany, 2005.

[441] **De Florio, S., Zehetbauer, T., Neff, T.**, *Optimal operations planning for SAR satellite constellations in low Earth orbit*, International Symposium on Reducing the Costs of Spacecraft Ground Systems and Operations, ESOC-Darmstadt, Germany, 2005.

[442] **De Florio, S., Zehetbauer, T., Neff, T.**, *Operational Aspects of Orbit Determination with GPS for Small Satellites with SAR Payloads*, IAA Symposium on Small Satellites for Earth Observation, Berlin, Germany, 2005.

[443] **Mittermayer, J., Schulze, D., Steinbrecher, U., Buckreuss, S.**, *SAR Instrument Operation, Calibration and Verification with a Long Term Data Base*, Data Systems in Aerospace (DASIA) Conference, pp. 4, Edinburgh, 2005.

[444] **Mittermayer, J., Schwerdt, M., Steinbrecher, U., Schulze, D., Márquez-Martinez, J.**, *The Instrument Operations and Calibration System for TerraSAR-X*, Advanced SAR Workshop, Saint-Hubert (Longueuil), Quebec, Kanada, 2005.

[445] **Neff, T.**, *Missionssimulator für die weltweite raumgestützte abbildende Aufklärung*, Workshop Nachrichtengewinnung und Aufklärung, Deutsche Gesellschaft für Wehrtechnik (DWT), Cologne, 2005.

[446] **Werner, M.**, Roth, A., Marschalk, U., Eineder, M., Suchandt, S., *Comparison of DEMs derived from SRTM / X- and C-Band*, The Shuttle Radar Topography Mission - Data Validation and Applications Final Workshop, 14-16 Jun. 2005, Reston, Virginia, USA, Reston, Virginia, USA, 2005.

3.8.6 Technical and Project Reports

[447] **Alberga, V.,** *Geometry Calculation,* DLR Project Report TX-SEC-TN-VA01, pp. 8, 2003.

[448] **Alberga, V.,** *Timing Calculation,* DLR Project Report TX-SEC-VA02, pp. 14, 2003.

[449] **Alberga, V.,** *Quantization of the PRF,* DLR Project Report, TX-SEC-TN-VA03, pp. 13, 2003.

[450] **Alberga, V**., *Review,* DLR Project Report TX-SEC-RP-4201, pp. 57, 2004.

[451] **Alberga, V**., *Selection of the PRF,* DLR Project Report TX-SEC-TN-VA04.2, pp. 21, 2004.

[452] **Alberga, V., Wendler, M**., *TerraSAR-X Performance Estimator Design Document*, DLR Project Report TX-IOCS-DD-4402-Vol-07 1.2, pp. 95, 2005.

[453] **Andres, C., Scheiber, R**., *Abschätzung und Korrektur von Restbewegungsfehlern in interferometrischen SAR Daten*, DLR Internal Report DLR-IB-8/2004, pp. 48, 2004.

[454] **Bachmann, M**., *Optimierung eines Phasenschiebers und einer Patchantenne für eine SAR-Anwendung im L-Band*, DLR InternalReport DLR-IB-551-10/2004, pp. 47, 2004.

[455] **Bauer, R., Bräutigam, B., Schwerdt, M.**, *TerraSAR-X Calibration Ground Equipment ITVV Plan*, DLR Project Report TX-IOCS-PL-4322 1.0, pp. 12, 2004.

[456] **Baumgartner, S.,** *SAR Processing and Parameter Estimation of Moving Targets*, DLR Project Report TRAMRAD-DLR-PD-310, pp. 95, 2005.

[457] **Bethke, K.-H., Hounam, D., Klement, D., Kemptner, E., Gabele, M., Baumgartner, S., Krieger, G., Rode, G., Osipov, A., Erxleben, R.,** *TRAMRAD Traffic Monitoring with Radar Phase 1 Summary Report*, DLR Project Report DLR-TRAMRAD-PD-140, pp. 43, 2005.

[458] **Böer, J.,** *Limitations for Calibration Site Planning,* DLR Project Report TX-IOCS-TN-JB01, pp. 10, 2004.

[459] **Böer, J.,** *Ground Segment Conventions and Performance Parameter Definitions*, DLR Project Report TX-GS-DD-4616 1.1, pp. 18, 2005.

[460] **Böer, J**., *TerraSAR-X System Command Generator Design Document*, DLR Project Report TX-IOCS-DD-4402-Vol-05 1.3, pp. 21, 2005.

[461] **Böer, J., Wendler, M.**, *TerraSAR-X Verification Section Volume 01: Data Take Verification Unit Design Document*, DLR Project Report TX-IOCS-DD-4601-Vol-01 1.4, pp. 42, 2005.

[462] **Bothale, V.M., Scheiber, R.**, *Investigations in Application of Multi-Look Processing for SAR Interferometry*, DLR Internal Report DLR-IB-551-1, pp. 107, 2002.

[463] **Bräutigam, B.,** *ICAL Getting Started*, DLR Project Report TX-SEC-TN-BB01 1.1, pp. 9, 2005.

[464] **Bräutigam, B., Hounam, D., Danklmayer, A.,** *Results of trade-offs from Sentinel-1 System Requirements on Calibration and Verification*, DLR Technical Note ES-TN-DLR-SY-0001, Issue 1.1, 2005.

[465] **Bräutigam, B., Hounam, D., Danklmayer, A., Schwerdt, M., Zink, M.,** *Sentinel-1: Input to System Calibration and Verification Concept*, DLR Project Report ES-PL-DLR-SY-0004, Issue 1.0, pp. 89, 2005.

[466] **Bräutigam, B., Hounam, D., Schwerdt, M.,** *TerraSAR-L System Calibration and Verification Concept*, DLR Project Report TS-PL-DLR-SY-0004, Issue 2.2, pp. 98, 2005.

[467] **Bräutigam, B., Schwerdt, M., Bauer, R.**, *TerraSAR-X Calibration Ground Equipment Design Document*, DLR Project Report TX-IOCS-DD-4321 1.2, pp. 11, 2005.

[468] **Buckreuss, S.,** *TerraSAR-L Instrument Calibration Segment ICS Design Specification*, DLR Project Report TS-RS-DLR-GS-04, 2004.

[469] **Buckreuss, S., Mittermayer, J.,** *TerraSAR-X Management Plan*, DLR Project Report TX-SEC-PL-4101 1.0, pp. 32, 2004.

[470] **Buckreuss, S.,** *TerraSAR-X Ground Segment Management Plan*, DLR Project Report TX-GS-PL-0001, 2005.

[471] **Alvarez Pérez, J.L.**, *Antenna Pattern Estimation by a Complex Treatment of Rain Forest Measurements*, DLR Project Report TX-IOCS-TN-AP-4309, Issue 0.1, 2004.

[472] **Alvarez Pérez, J.L.**, *Effects Of Random Amplitude And Phase Errors In The Antenna*, DLR Project Report TX-IOCS-TN-AP-4306, Issue 0.3, 2004.

[473] **Castell-Calderon, M.**, *Development of Requirements for SAR Elevation Phased Array Antenna Pattern Optimization*, DLR Internal Report DLR-IB-551-3/2004, pp. 108, 2004.

[474] **Chiari, M.**, *Untersuchung spektraler radiometrischer Mikrowellensignaturen zur Detektion verborgener Objekte in geschichteten Medien*, pp. 106, 2004.

[475] **Dahme, C.**, *IKT-Konzept 2001*, DLR-IKT-Konzept-2001, DLR Internal Report, Ausgabe 1.0a, 2001.

[476] Dimou, A., **Jäger, G**., *A family of fuzzy edge detectors for SAR images*, DLR Internal Report DLR-IB-551-4/2000, pp. 114, 2000.

[477] **Domke, P.**, *Entwicklung einer Mikrocontroller-Echtzeiterweiterung für die dezentrale Steuerung des flugzeuggetragenen Radarsystems FSAR2000 über CAN-Bus*, DLR Internal Report DLR-IB-551-7/2000, pp. 179, 2000.

[478] **Engwall, M.**, *Evaluation of the Monostatic Radar Signal in the Case of Triple Reflections at Flat Panels*, DLR Project Report DLR-IB-551-5/2001, pp. 70, 2001.

[479] **Erxleben, R., Kemptner, E., Klement, D., Osipov, A., Rode, G.**, *Modelling and RCS Computation of Cars and Background Clutter*, DLR Project Report TRAMRAD-DLR PD-210, pp. 30, 2005.

[480] **Fiedler, H.,** *Analysis of TerraSAR-L Cartwheel Constellations*, Project Report under ESA/ESTEC contract TSLC-OF-DLR-SY-001, pp. 52, 2003.

[481] **Fiedler, H., Krieger, G., Jochim, F.,** *Analysis of TerraSAR-L Cartwheel constellations - Amendment*, Project Report under ESA/ESTEC contract TSLC-OF-DLR-SY-001, pp. 7, 2003.

[482] **Fiedler, H.,** *TerraSAR-X Total Zero Doppler Steering Tables for TerraSAR-X*, DLR Project Report TN-SEC-JM-03 1.2, pp. 14, 2005.

[483] **Fiedler, H., Krieger, G.,** *Polarimetric and Interferometric Mission and Application Study: Mission Assessment*, Project Report under ESA/ESRIN contract 17893/03/I-LG, pp. 21, 2005.

[484] **Fiedler, H.**, *Formation and Coverage Concept.*, DLR Project Report TDX-TN-DLR-1400, pp. 45, 2005.

[485] **Fischer, C.,** *Studie zur Trennung von Volumen und Oberflaechenstreuung mit interferometrischen Multi-Baseline SAR-Daten*, DLR Internal Report DLR-IB-551-1, pp. 93, 2002.

[486] **Gabele, M.,** *SAR-Mehrkanalverfahren zur Detektion bewegter Objekte*, DLR Internal Report DLR-IB-551-6/2004, pp. 114, 2004.

[487] **Gabele, M**., *Multichannel Systems for Ground Moving Target Indication*, DLR Project Report TRAMRAD-DLR-PD-311, pp. 73, 2005.

[488] **Gabler, B.**, *S/C-Chirp: Ein flexibler Radarsignalgenerator für das zukünftige hochauflösende mehrkanalige Flugzeugradar mit synthetischer Apertur F-SAR 2000*, DLR Internal Report DLR-IB-551-6/2000, pp.66, 2000.

[489] **Hajnsek, I.,** *Pilotstudie über Radarbefliegung der Elbauen*, DLR Internal Report DLR-IB-551-1/2001, pp. 93, 2001.

[490] **Hajnsek, I.,** Weber, M., *TanDEM-X User Requirement Document (URD),* DLR Project Report TDX-RD-DLR-1201, 2005.

[491] Hong, W., **Mittermayer, J., Moreira, A.**, *High Squint Airborne SAR Processing - Modeling and Performance Assessment*, DLR Internal Report DLR-IB-551-2/2000, pp. 149, 2000.

[492] **Jochim, F.,** Kirschner, M**., Fiedler, H.,** *Estimation of Fuel Requirement for Bi-static Orbit Configurations*, GSOC DLR Project Report TN-2004-03 (revised 2005), pp. 78, 2005.

[493] **Keller, M.,** *Report on available Satellite Data*, DLR Project Report SMART-1.1, pp. 23, 2003.

[494] **Keller, M.**, *Report on DEM derived from SRTM Data*, DLR Project Report SMART-1.7, pp. 33, 2003.

[495] **Keller, M.**, *Report on Collected and Registered Data, and SAR Coherence Data*, DLR Project Report SMART-2.1, pp. 48, 2003.

[496] **Keller, M**., Maugeri, F., *Report on Zeppelin Measurement Campaigns*, DLR Project Report SMART-1.3, pp. 61, 2003.

[497] **Keller, M.,** Maugeri, F., Müller, R., Amann, V., Fecher, J., Reinartz, P., *Report on Zeppelin Feasibility Study*, DLR Project Report SMART-1.6, pp. 127, 2003.

[498] **Keller, M.**, Vanhuysse, S., Gold, H., Bajic, M., *Report on the Measurement Campaign (Airborne and Ground)*, DLR Project Report SMART-1.2, pp. 171, 2003.

[499] **Keller, M., Dietrich, B.,** Müller, R., Reinartz, P., Datcu, M., *Report on DLR work in SMART*, DLR Project Report SMART-f, pp. 126, 2004.

[500] **Kempf, T., Peichl, M**., *Feinkorrektur von ISAR-Daten aus Turmdrehstandmessungen*, DLR Project Report 1722702000, pp. 37, 2000.

[501] **Krieger, G., Fiedler, H.,** *SAFARI: Multistatic SAR System Concepts*, DLR Project Report SAFARI-TN-DLR-HR 4020, pp. 111, 2002.

[502] **Krieger, G., Wendler, M., Fiedler, H.**, **Werner, M.**, *Preparation of a Bistatic Airborne SAR Experiment DLR/ONERA*, pp. 32, 2002.

[503] **Krieger, G**., *Definition of the TerraSAR-L Cartwheel Constellation: DEM Performance Estimation*, ESA TSLC-TN 3000, 2003.

[504] **Krieger, G., Fiedler, H., Metzig, R.**, *TerraSAR-X Tandem: First Results of Performance and Requirements Analysis*, 2003.

[505] **Krieger, G.**, *TanDEM-X: Mission Analysis and System Performance*, DLR Project Report TDX-TN-DLR-1101, 2005.

[506] **Krieger, G., Fiedler, H.**, *Polarimetric and Interferometric Mission and Application Study: Final Report - Part V: Mission Assessment*, DLR Project Report under ESA/ESRIN contract 17893/03/I-LG, 2005.

[507] **Kugler, F.**, *Temporäre Dekorrelation von Radarfernerkundungsdaten über einen temperaten Mischwald*, DLR Internal Report DLR-IB 551-9/2004, 2004.

[508] **Márquez-Martinez, J.,** *TerraSAR-X PRF Statistical Analysis*, DLR Project Report TX-SEC-TN-MM03 1, pp. 12, 2004.

[509] **Márquez-Martinez, J., Wendler, M., Mittermayer, J., Schröder, R., Dietrich, B., Alberga, V.,** *SNR Enhancement,* DLR Project Report TX-SEC-TN-MM01, pp. 13, 2004.

[510] **Márquez-Martinez, J.**, *Development of a Range Ambiguity Simulator and Investigation of Methods for Range Ambiguity Suppression in SAR*, DLR Internal Report DLR-IB-551-2/2004, pp. 140, 2004.

[511] **Márquez-Martinez, J**., *TERRASAR-X Instrument Table Generator Design Document*, DLR Project Report TX-IOCS-DD-4402-Vol-06 1.3, pp. 68, 2005.

[512] **Márquez-Martinez, J., Mittermayer, J.,** *TerraSAR-X Radar Parameter Generator Design Document, TX-IOCS-DD-4402-Vol-01*, DLR Project Report TX-IOCS-DD-4402-Vol-01 2.3, pp. 126, 2005.

[513] **Metzig, R.,** Mahdi, S., *Vergleich Standard EADS-TRM/TerraSAR-X-TRM Leistungsabgabe/Verlusten,* DLR Project Report TX-SYS-TN-RM01, 04 Nov. 2002, pp. 4, 2002.

[514] **Metzig, R., Mittermayer, J.,** *Preliminary Estimation of Along-Track Gaps between consecutive Data Takes for TerraSAR-X*, DLR Project Report TX-SYS-TN-RM02, pp.3, 2002.

[515] **Metzig, R., Krieger, G., Fiedler., H.,** *Impact of USO Frequency Instability on Instrument Phase Error,* DLR Project Report TX-SEC-TN-RM03, pp. 2, 2003.

[516] **Metzig, R.,** *TerraSAR-X Identification of RF Chain Elements for On-Ground Characterization*, DLR Project Report TX-SEC-TN-4201 1.4, pp. 1, 2004.

[517] **Metzig, R.**, *Impact of RF Chain Elements for On-Ground Characterization*, DLR Project Report TX-SEC-TN-RM07 1.0, 2004.

[518] **Metzig, R.**, *TerraSAR-X Instrument In-Orbit Verification Plan*, DLR Project Report TX-IOCS-PL-4612 1.0, pp. 27, 2004.

[519] **Metzig, R.,** *TerraSAR-X Long-Term System Monitoring Plan*, DLR Project Report TX-IOCS-PL-4615 1.0, pp. 15, 2004.

[520] **Metzig, R**., *Space Segment - IOCS ICD*, DLR Project Report TX-PD-ICD-0002 1.0, pp. 34, 2005.

[521] **Metzig, R.,** *TerraSAR-X Verification Section Volume 02: Instrument Health Monitoring Design Document*, DLR Project Report TX-IOCS-DD-4601-Vol-02 1.2, pp. 19, 2005.

[522] **Misra, A., Scheiber, R**., *Algorithm Development for Differential Interferometric SAR Processing of E-SAR Data*, DLR Internal Report DLR-IB-551-2, pp.76, 2003.

[523] **Mittermayer, J**., **Moreira, A.,** *VGA Drift Droop Effect Investigation,* ESA Technical Report for ASAR System Engeneering Study, DLR Technical Report under ESA/ESTEC Contract and DLR Internal Report, DLR-IB-551-6/2001, 2001.

[524] **Mittermayer, J**., *Timing Strategy,* DLR Project Report TX-SYS-JM02, pp. 5, 2002.

[525] **Mittermayer, J**., *Derivation of Requirements for TerraSAR-X Elevation Beams,* DLR Project Report TX-SEC-TN-JM01, pp. 92, 2004.

[526] **Mittermayer, J.**, *IOCS Technical Validation Plan, Procedures and Report*, DLR Project Report TX-IOCS-PR-4109, pp. 24, 2005.

[527] **Mittermayer, J.,** *IOCS Technical Verification Plan, Procedures and Report,* DLR Project Report TX-IOCS-PR-4108, pp. 39, 2005.

[528] **Mittermayer, J.**, *TerraSAR-X Instrument Operations and Calibration Segment IOCS System Overview*, DLR Project Report TX-IOCS-DD-4106 1.3, pp. 29, 2005.

[529] **Mittermayer, J**., *TerraSAR-X IOCS Integration, Technical Verification And Validation Plan*, DLR Project Report TX-IOCS-PL-4107 2.0, pp. 24, 2005.

[530] **Mittermayer, J.,** *Calibration/Verification Plan*, DLR Project Report TX-GS-PL-4610 1.3, pp. 19, 2005.

[531] **Mittermayer, J.,** *TerraSAR-X Instrument Verification Section Design Document*, DLR Project Report TX-IOCS-DD-4601 1.1, pp. 7, 2005.

[532] **Mittermayer, J.,** *TerraSAR-X Overall Sar System Performance Characterisation/Verification Plan*, DLR Project Report TX-IOCS-PL-4611 1.1, pp. 8, 2005.

[533] **Mittermayer, J.**, *TerraSAR-X Management Plan*, DLR Project Report TX-SEC-PL-4101 1.1, pp. 32, 2005.

[534] **Mittermayer, J.**, Börner, E., *TerraSAR-X Experimental Spotlight Mode Processor Design*, DLR Project Report TX-SEC-DD-4502 1.2, pp. 41, 2005.

[535] **Mittermayer, J., Buckreuss, S.**, *TerraSAR-X IOCS Requirements Specification Document*, DLR Project Report TX-IOCS-RS-4105 1.3, pp. 73, 2005.

[536] **Mittermayer, J., Fiedler, H.**, Börner, E., *TerraSAR-X Total Zero Doppler Steering Tables for TerraSAR-X*, DLR Project Report TN-SEC-JM-03, pp. 14, 2005.

[537] **Moreira, A.**, et al., *TanDEM-X: TerraSAR-X Add-on for Digital Elevation Measurements,* Mission Description Doc., DLR Project Report 2003-3472739, 2003.

[538] **Moreira, A.**, *TanDEM-X: TerraSAR-X Add-On for Digital Observation Mission,* DLR Project Report 2003-3472739, 2005.

[539] **Müller-Sanchez, F.,** *Velocity Estimation of Moving Targets using Along-track SAR Interferometry*, DLR Internal Report DLR-IB-551-7/2004, pp. 99, 2004.

[540] **Osipov, A.,** *Notizenseiten zum Seminarvortrag: High-frequency electromagnetic scattering by non-metallic wedges*, DLR Internal Report DLR-IB-551-2003/1, pp. 40, 2003.

[541] **Papathanassiou, K., Moreira, A.,** *Combined Use of SAR Polarimetry and SAR Interferometry – Critical Review of retrieval algorithms,* DLR Project Report under ESA/ESTEC Contract 15600/01/I-LG, 2002.

[542] P**eichl, M., Dill, S., Kempf, T.**, *Passive Messungen im Mikrowellenbereich an Abbränden von FTS bei Flugkörpern verschiedener Bauart, 3*, 3, DLR Project Report 3471104, pp. 67, 2000.

[543] **Peichl, M., Dill, S.,** *Passive Messungen im Mikrowellenbereich an Abbränden von FTS bei Flugkörpern verschiedener Bauart auf der Schlittenbahn*, Pei1, DLR Project Report 3471111, pp. 35, 2001.

[544] **Peichl, M., Dill, S., Süß, H.,** *HOPE project, Final report - Chapter 7: MWR - Microwave Radiometer*, Pei3, DLR Project Report 3471102, pp. 37, 2002.

[545] **Peichl, M., Greiner, M**., Anterrieu, E., *Assessment of image reconstruction algorithms for aperture synthesis radiometers*, Pei2, DLR Project Report 3471152-1, pp. 41, 2003.

[546] **Peichl, M.,** *Beschreibung des HOPE-Systems für den Technologietransfer*, DLR Technical Note TN-HOPE, pp. 4, 2004.

[547] **Peichl, M.,** *Required Platform Manoeuvres for SMOS Calibration using G Matrix Image Reconstruction Approaches – "Scientific Inputs for the SMOS Level-1 Processor Study"*, DLR Project Report 3471152-2, pp. 23, 2004.

[548] **Peichl, M**., *Verfahren zur Material- bzw. Stoffkonstantenbestimmung*, DLR Technical Note TN-MATMESS-1, pp. 12, 2004.

[549] **Peichl, M., Dill, S.**, *Ergänzende Anmerkungen zum Bericht „Erprobung bildgebender radiometrischer Verfahren"*, DLR Project Report 3471154-2, pp. 16, 2004.

[550] **Peichl, M., Dill, S.**, *Ergänzende Messungen zur Studie „Erprobung bildgebender radiometrischer Verfahren"*, DLR Project Report 3471154-3, pp. 17, 2004.

[551] **Peichl, M., Dill, S.,** *Erprobung bildgebender radiometrischer Verfahren „Radom-Durchblick"*, DLR Project Report 3471154-1, pp. 55, 2004.

[552] **Peichl, M., Greiner, M., Wittmann, V.,** Anterrieu, E., Picard, B., Skou, N., Sobjaerg, S., *Midterm Report: Scientific Inputs for the SMOS Level 1 Processor Development*, DLR Project Report 3471152-3, pp. 78, 2004.

[553] **Peichl, M., Jirousek, M.,** *Image Validation Test using LICEF-1 Receivers*, DLR Project Report 3471151, pp. 61, 2004.

[554] **Peichl, M., Dill, S.**, *Radiometrische Messungen im Millimeterwellen-Bereich von einer künstlichen Deichanlage bei unterschiedlichen Durchnässungszuständen*, DLR Project Report 3471138, pp. 27, 2005.

[555] **Peichl, M., Wittmann, V.,** Anterrieu, E., Picard, B., Skou, N., Sobjaerg, S., *Final Report: Scientific Inputs for the SMOS Level 1 Processor Development - with Emphasis on Image Reconstruction*, DLR Project Report 3471152-4, pp. 126, 2005.

[556] **Planta, K.,** *Simulation einer Clutterstatistik in natürlichem und bebautem Gelände - Konzeption und Ergebnisse*, DLR Internal Report DLR-IB-551-3/2002, pp. 58, 2002.

[557] **Planta, K., Dreher, K.H.**, **Preißner, J.,** *Untersuchung von Auswerteverfahren zur Bestimmung dielektrischer und magnetischer Materialparameter im Mikrowellenbereich mit dem Standard-Hohlleiterverfahren nebst deren experimenteller Verifikation*, DLR Internal Report DLR-IB-551-2/2002, pp. 22, 2002.

[558] **Potsis, A.**, *Experimental Synthetic Aperture Radar (E-SAR) P-band System*, DLR Internal Report DLR-IB-551-8, pp. 62, 2001.

[559] **Potsis, A.**, *Radio Frequency Interference Suppression for Synthetic Aperture Radar*, DLR Internal Report DLR-IB-551-3, pp. 58, 2001.

[560] **Robert, P., Scheiber, R.**, *Airborne Repeat-Pass SAR Interferometry in the Presence of Squint and Baseline Errors*, DLR Internal Report DLR-IB-551-4, pp. 107, 2001.

[561] **Roca-Cusachs** Maennicke, O., *Performance Analysis of Hardware Optimized Block Adaptive Quantizer Algorithm for TerraSAR-X Parameter*, DLR Internal Report DLR-IB-551-4/2004, pp. 101, 2004.

[562] Rocca, F., Hoekman, D., Lucas, R., Lucht, W., Massonnet, D., **Moreira, A.,** Parsons, B., Schmullius, C., Wadge, G., Askne, J., Bamler, R., Bartalev, S., Briole, P., Broquetas, A., Bürgmann, R., Cloude, S., De Grandi, F., Feigl, K., Hallikainen, M., Hensley, S., King, C., Koehl, M., Lanari, R., Law, B., Manninen, T., Milne, T., Nilsson, S., Pampaloni, P., **Papathanassiou, K.,** Pretzsch, H., Rosenquist, A., Salvi, S., Shimada, M., Siqueira, P., Treuhaft, B., Wagner, W., Woodhouse, I., Yamada, H., Zimmermann, R., *HABITAT: Hazard and Biomass Interferometric SAR Observatory,* ESA's Call for Ideas for the Next Earth Explorer Core Missions, pp. 30, 2005-05, 2005.

[563] **Sanz-Marcos, J.,** *TerraSAR-X Experimental Spotlight Mode Processor Design - Azimuth Side-Lobe Suppression for the Sliding-Spotlight Mode*, DLR Internal Report DLR- IB-551-5/2004, pp. 40, 2004.

[564] **Schulze, D.,** *TerraSAR-X IOCS Internal Interface Control Document*, DLR Project Report TX-IOCS-ICD-4110 1.3, pp. 298, 2005.

[565] **Schulze, D.,** *TerraSAR-X LTDB Verification Test Report*, DLR Project Report TX-IOCS-RP-4411 1.0, pp. 76, 2005.

[566] **Schulze, D.,** *TerraSAR-X Long Term Data Base Design Document*, DLR Project Report TX-IOCS-DD-4402-Vol-03 1.1, pp. 4, 2005.

[567] **Schwerdt, M.,** *Internal Calibration Scheme,* DLR Project Report TX-IOCS-TN-IC-4302 1-0, pp. 8, 2003.

[568] **Schwerdt, M.,** *Antenna Pattern Model,* DLR Project Report TX-SEC-TN-AP-4303 0-1, pp. 7, 2003.

[569] **Schwerdt, M, Molkenthin, T.,** *PN-Gating*, DLR Project Report TX-IOCS-TN-PN-4304, pp. 6, 2003.

[570] **Schwerdt, M., Hounam, D., Bräutigam, B.,** *CalVal Tasks of Comissioning Phase,* DLR Project Report TX-IOCS-TN-CP4305, pp. 10, 2004.

[571] **Schwerdt, M.**, *Radiometric Accuracy Budget of TerraSAR-X*, DLR Project Report TX-IOCS-TN-RB-4307, Issue 1.0, 2005.

[572] **Schwerdt, M., Bräutigam, B., Bauer, R.,** *TerraSAR-X Calibration ground equipment requirement specification*, DLR Project Report TX-IOCS-RS-4320 1.2, pp. 12, 2005.

[573] **Schwerdt, M.**, **Alvarez Pérez, J.L**., *Sampling Rate of Reference Antenna Patterns*, DLR Project Report TX-IOCS-TN-AP-4308, Issue 0.1, 2005.

[574] **Schwerdt, M., Hounam, D**., *TerraSAR-X CALIBRATION PLAN*, DLR Project Report TX-IOCS-PL-4301 1.5, pp. 56, 2005.

[575] **Schwerdt, M., Hounam, D., Bachmann, M., Bräutigam, B., Alvarez Pérez, J.,** *TerraSAR-X Instrument Operations and Calibration Segment - Calibration Section - Design Document*, DLR Project Report TX-IOCS-DD-4311 1.3, pp. 126, 2005.

[576] **Steinbrecher, U.,** *Dauer der Kalibrierungssequenzen am Anfang und am Ende eines Data Takes,* DLR Project Report TX-SEC-TN-US01, pp. 2, 2003.

[577] **Steinbrecher, U., Alberga, V.,** *Abschätzung der Variation der Datenrate,* DLR Project Report TX-SEC-TN-US02, pp. 4, 2003.

[578] **Steinbrecher, U.,** *Speicherbedarfabschätzung des LongTerm Parameter Archives,* DLR Project Report TX-SEC-TN-US03, pp. 4, 2003.

[579] **Steinbrecher, U.**, *Konzept des Longterm Data Parameter Archives,* DLR Project Report TX-SEC-TN-US04, pp. 3, 2003.

[580] **Steinbrecher, U.,** LTDB: *Erste Anforderungen an die LTDB,* DLR Project Report TX-SEC-TN-US05, pp. 17, 2003.

[581] **Steinbrecher, U.,** *PN Gating,* DLR Project Report TX-SEC-TN-US06, pp. 2, 2003.

[582] **Steinbrecher, U.,** *Operational-, Pre-operational-, Test-, Offline R2CC,* DLR Project Report TX-SEC-TN-US07, pp. 6, 2003.

[583] **Steinbrecher, U.,** *MPS, R2CC, SARSET und die LTDB Kommunikation und Abläufe,* DLR Project Report TX-SEC-TN-US08, pp. 5, 2003**.**

[584] **Steinbrecher, U.,** *PN Gating High Level Order Interface Parameters,* DLR Project Report TX-SEC-TN-US09, pp. 2, 2003.

[585] **Steinbrecher, U.,** *ICG Output Data Description and System Data Takes,* DLR Project Report TX-SEC-TN-US10, pp. 13, 2003.

[586] **Steinbrecher, U.,** *Operational Aspects of performing DataTakes in the case of GPS unavailability (Longterm)*, DLR Project Report TX-SEC-TN-US11 0.9, pp. 5, 2004.

[587] **Steinbrecher, U**., *GPS Unavailibility Long Term,* DLR Project Report TX-SEC-TN-US11, pp. 5, 2004.

[588] **Steinbrecher, U**., *ICG Configuration,* DLR Project Report TX-SEC-TN-US12, pp. 4, 2004.

[589] **Steinbrecher, U**., *Instrument Configuration Operations,* DLR Project Report TX-SEC-TN-US13, pp.5, 2004.

[590] **Steinbrecher, U**., *MOS Instrument Configuration Table,* DLR Project Report TX-SEC-TN-US14, pp. 4, 2004.

[591] **Steinbrecher, U**., *Requirements from DTV and ICG on Source Packet Evaluation Software (DEU),* DLR Project Report TX-SEC-TN-US15, pp.3, 2004.

[592] **Steinbrecher, U.**, *Requirements from DTV and ICG on Source Packet Evaluation Software (formerly part of DEU)*, DLR Project Report TX-SEC-TN-US15, pp. 5, 2004.

[593] **Steinbrecher, U**., *TerraSAR-X Instrument Operations Section Design DocumenT*, DLR Project Report TX-IOCS-DD-4402 1.3, pp. 6, 2005.

[594] **Steinbrecher, U**., *TSX1 Instrument and Data Take Configuration Change Control*, DLR Project Report TX-SEC-TN-US18 1.5, pp. 21, 2005.

[595] **Steinbrecher, U**., *Annahmen für den ICG*, TX-SEC-TN-US22 1.3, pp. 8, 2005.

[596] **Steinbrecher, U.**, *Allow ICG SwathWidth Degradation*, DLR Project Report TX-SEC-TN-US21 1.0, pp. 4, 2005.

[597] **Steinbrecher,** U., *TerraSAR-X Instrument Command Generator Design Document*, DLR Project Report TX-IOCS-DD-4402-Vol-02 3.1, pp. 105, 2005.

[598] **Steinbrecher, U.,** *TerraSAR-X Long Term Data Base Requirements Specification*, DLR Project Report TX-IOCS-RS-4410 1.2, pp. 7, 2005.

[599] **Vieweg, M**., *Einheitliche Bedienoberfläche für Streufeldsimulationen mit Echtzeitvisualisierung der Objektdrehung und der zugehörigen Radardaten*, DLR Internal Report DLR-IB-551-4/2002, pp. 65, 2002.

[600] **Wendler, M**., *NESZ calculation for TerraSAR-X Performance Analysis,* DLR Project Report TX-NESZcalculation, pp. 4, 2003.

[601] **Wendler, M**., **Márquez-Martinez, J., Mittermayer, J., Schröder, R., Dietrich, B., Alberga, V.,** *SNR Enhancement in Processed SAR Image,* DLR Technical Note TN-finalSNRimage, pp. 10, 2004.

[602] **Wendler, M.,** *TerraSAR-X Instrument Operations and Calibration Segment IOCS Auxiliary Product Specification*, DLR Project Report TX-GS-DD-4111 1.11, pp. 47, 2005.

[603] **Wendler, M., Steinbrecher, U.**, *TerraSAR-X Auxiliary Data Formatter Design Document*, DLR Project Report TS-IOCS-DD-4402-Vol-04 1.4, pp. 17, 2005.

[604] **Werner, M.**, *TanDEM-X Ground Segment Management Plan*, DLR Project Report TDX-DLR-PL-4110, 2005.

[605] **Wittmann, V.,** *Algorithmen*, DLR Technical Note DLR-TN-2020132005, pp. 37, 2004.

[606] **Wittmann, V.,** *Kalibrieren von Radiometern*, DLR Technical Note DLR-TN-2019852005, pp. 44, 2004.

[607] **Zink, M., Buckreuss, S.**, TanDEM-X Mission Concept and Design Overview, DLR Project Report TDX-DD-DLR-1000, 2005.

3.8.7 Patents

[608] **Bauer, R., Waegel, K.-H., Hounam, D.,** *Verfahren zur Umkehr eines Einseitenbands mit einem Träger*, DE 199 06 314, referred on 12 Oct. 2000.

[609] **Bethke, K.-H**., Röde, B., Schroth, A., *Verfahren zum autonomen Führen von Roboterfahrzeugen in Hallen sowie Radarstation zur Durchführung des Verfahrens*, DE 199 10 715 C2, referred on 26 Sep. 2002.

[610] **Brand, B., Zehetbauer, T.,** *Verfahren zur Reduktion des Informationsalters von Bildprodukten von Erdbeobachtungssatelliten*, 10 2005 055 918.2, applied on 22 Nov. 2005.

[611] **Buckreuss, S.**, **Sutor, T**., *Verfahren zur Detektion und Unterdrückung von Störsignalen in SAR-Daten und Einrichtung zur Durchführung des Verfahrens*, DE 198 22 957, US 6,028,549, refereed on 25 May 2000 (DE) and 22 Feb. 2000 (US).

[612] **Fiedler, H**., Börner, E., **Krieger, G., Mittermayer, J.**, *Verfahren zur Verringerung des Dopplerzentroids bei einem kohärenten Impuls-Radarsystem*, DE 103 41 893.9-55 und EP 04 019 660.2 und CA 2,480,752, applied on 09 Sep. 2003.

[613] **Hounam, D., Waegel, K., Dill, S.,** *Verfahren zur Lokalisierung und Identifizierung von Objekten mittels eines codierten Transponders*, DE 196 20 682, referred on 28 Jun. 2001.

[614] **Keydel, W., Süß, H., Schröder, R., Zeller, K.-H.,** *Flugzeug- oder weltraumflugkörpergetragenes Radarsystem mit synthetischer Antennen-apertur*, DE 199 38 592, US 6,388,606, referred on 27 Feb. 2003 (DE) and 14 May 2002 (US).

[615] **Mayer, B.**, *Millimeter Wave Measurement Process*, US 6,255,831, referred on 03 Jul. 2001.

[616] **Moreira, A., Mittermayer, J.,** *Method for azimuth scaling of SAR data and highly accurate processor for two-dimensional processing of scansar data*, EP DE 597 01 960.6-08, referred on 05 Jul. 2000.

[617] **Moreira, A., Mittermayer, J.**, *Method of Processing Spotlight SAR - raw data*, US 6,222,933, referred on 24 Apr. 2001.

[618] **Moreira, A., Fischer, J., Benz, U.,** *Verfahren zur Übertragung von komprimierten Bilddaten eines SAR-Radars*, EP DE 599 00 614.5, referred on 16 Jan. 2002.

[619] **Moreira, A., Mittermayer, J.,** Verfahren zur Verarbeitung von Spot*light SAR-Rohdaten*, EP FR 0 924 534, referred on 08 May 2002.

[620] **Moreira, A., Krieger, G., Mittermayer, J.,** *Satellite Configuration for Interferometric and/or Tomographic Remote Sensing by means of Synthetic Aperture Radar (SAR)*, US 6,677,884, referred on 13 Apr. 2004.

[621] **Moreira, A., Krieger, G., Mittermayer, J.,** *Satellitenkonfiguration zur interferometrischen und/oder tomografischen Abbildung der Erdoberfläche mittels Radar mit Synthetischer Apertur (SAR)*, EP DE 502 01 601.9-08, referred on 24 Nov. 2004.

[622] **Moreira, A., Krieger, G., Mittermayer, J.,** *Satellitenkonfiguration zur interferometrischen und/oder tomografischen Abbildung der Erdoberfläche mittels Radar mit synthetischer Apertur*, FR-GB-NL 1273518 B1, 14 Nov. 2004.

[623] **Reigber, A., Moreira, A.,** *Flugzeug- oder satellitengestütztes tomographisches Radarverfahren mit synthetischer Apertur*, DE 101 60 399 B4, referred on 27 May 2004.

[624] **Reigber, A., Moreira, A.,** *Airborne or Spaceborne Tomographic Synthetic Aperture Radar (SAR) Method*, US 6,894,637, referred on 17 May 2005.

[625] **Sauer, T.,** *Method for generating microwave resolution images of moving objects by inverse Synthetic Aperture Radar*, US 6,023,235, referred on 08 Apr. 2000.

[626] **Sauer, T.,** *Verfahren zur Erzeugung einer im Mikrowellenbereich stattfindenden Abbildung bewegter Objekte mittels Inversen-Synthetic-Aperture-Radars*, GB 2 326 042, referred on 25 Apr. 2001.

[627] **Witte, F., Moreira, A., Keydel, W.,** *Radarantenne*, EP DE 598 00 958.2, referred on 04 Jul. 2001.

[628] **Wittmann, V.,** *Flugkörper in Form eines elektronisch angetriebenen Luft/Raumschiffs*, DE 103 31 740.6-22, applied on 11 Jul. 2003.

3.9 Courses, Lectures and Invited Speeches

3.9.1 Courses and Lectures

[629] **Börner, T.,** *Ermittlung von Materialeigenschaften*, CCG Seminar SE 02.14, Oberpfaffenhofen, 03 Dec. 2002.

[630] **Börner, T.**, *Ermittlung von Materialeigenschaften*, CCG Seminar SE 2.14, Oberpfaffenhofen, 24-28 Nov. 2003.

[631] **Börner**, **T.**, *Ermittlung von Materialeigenschaften*, CCG Seminar SE 2.14, Oberpfaffenhofen, 2005.

[632] **Buckreuß, S.**, *The TerraSAR-X Mission*, CCG Seminar SE 2.06 SAR Principles and Application, Oberpfaffenhofen, 2002.

[633] **Buckreuß, S**., *The TerraSAR-X Mission*, CCG Seminar SE 2.06 SAR Principles and Application, Oberpfaffenhofen, 2003.

[634] **Buckreuß, S.**, *The TerraSAR-X Mission*, CCG Seminar SE 2.06 SAR Principles and Application, Oberpfaffenhofen, 2004.

[635] **Buckreuß, S**., *The TerraSAR-X Mission*, CCG Seminar SE 2.06 SAR Principles and Application, Oberpfaffenhofen, 2005.

[636] **Hajnsek, I.**, *Polarimetric Application of Radar Remote Sensing*', DLR, Oberpfaffenhofen, Germany, 2001.

[637] **Hajnsek, I.**, *Polarimetric Radar Remote Sensing for Land Applications*', University of Jena, Department of Geoinformatik, Germany, 2001.

[638] **Hajnsek, I.**, *SAR Polarimetry' at the Graduiertenkolleg, Synthetic Aperture Radar and Shuttle Radar Topography Mission (SRTM)*' at the Institute of Geology and Geodynamics, Bonn, 2002.

[639] **Hajnsek,I.**, *Polarimetric Radar Remote Sensing for Land Applications',* University of Jena, Department of Geo-Informatik, Germany, 2002.

[640] **Hajnsek, I.**, *SAR Interferometry'*, Summerschool at the Maximilians-University Munich in Munich in the frame of the Münchner Forschungsverbund Fernerkundung mit dem Schwerpunkt Umwelt (MFFU), Germany, 2002.

[641] **Hajnsek, I.,** *SAR Polarimetry and Applications*, CCG Seminar SE 2.02, Oberpfaffenhofen, 2002.

[642] **Hajnsek, I.,** *SAR Polarimetry and Applications*, CCG Seminar SE 2.02, Oberpfaffenhofen, 2003.

[643] **Hajnsek, I.**, *SAR Polarimerty during the 'ENVISAT'*, Summer school at the Ludwig-Maximilians-University Munich in the frame of the Münchner Forschungsverbund Fernerkundung mit dem Schwerpunkt Umwelt (MFFU), Germany, Munich, 2003.

[644] **Hajnsek, I.**, *SAR Polarimetry'*, Summerschool at the Helsinki University Technology, Finland, 2003.

[645] **Hajnsek, I.**, *SAR Polarimetry and Applications*, CCG Seminar SE 2.02, Oberpfaffenhofen, 2004.

[646] **Hajnsek, I.**, *SAR Polarimerty during the 'ENVISAT'*, Summer school at the Ludwig-Maximilians-University Munich in the frame of the Münchner Forschungsverbund Fernerkundung mit dem Schwerpunkt Umwelt (MFFU), Germany, Munich, 2004.

[647] **Hajnsek, I.**, *SAR Polarimetry and Applications*, CCG Seminar SE 2.02, Oberpfaffenhofen, 2005.

[648] **Hajnsek, I.**, *Recent Progress in SAR Polarimetry and SAR Interferometry,* University of Adelaide, South-Australia, Sep. 2005.

[649] **Horn, R.**, *SAR Design*, CCG Seminar SE 2.06 „SAR Principles and Application", Oberpfaffenhofen, 2000.

[650] **Horn, R.**, *DLR Airborne SAR System Design*, CCG Seminar SE 2.06 „SAR Principles and Application", Oberpfaffenhofen, 2000 – 2001.

[651] **Horn, R.**, *DLR Airborne SAR System Design*, CCG Seminar SE 2.02 „SAR Principles and Application", Oberpfaffenhofen, 2002 – 2005.

[652] **Kemptner, E.**, *Beispiele bistatischer Radarquerschnitte*, CCG Seminar SE 2.14, Oberpfaffenh., 2000.

[653] **Kemptner, E.**, *Integralgleichungsmethode und deren Anwendung zur Berechnung von Antennen auf Trägerstrukturen*, CCG Seminar SE2.03, Oberpfaffenhofen, 2000.

[654] **Kemptner, E.**, *Bistatische Radarquerschnitte*, CCG Seminar SE 2.14, Oberpfaffenhofen, 2001.

[655] **Kemptner, E**., *Bistatische Radarquerschnitte*, CCG Seminar SE 2.14, Oberpfaffenhofen, 2-6 Dec. 2002.

[656] **Kemptner, E**., *Integralgleichungsmethode und deren Anwendung zur Berechnung von Antennen auf Trägerstrukturen*, CCG Seminar SE2.03, Oberpfaffenhofen, 25-29 Nov. 2002.

[657] **Kemptner, E**., *Bistatische Radarquerschnitte*, CCG Seminar SE 2.14, Oberpfaffenhofen, 2003.

[658] **Kemptner, E**., *Integralgleichungsmethode und deren Anwendung zur Berechnung von Antennen auf Trägerstrukturen*, CCG Seminar SE2.03, Oberpfaffenhofen, 15-19 Nov. 2004.

[659] **Kemptner, E.**, *Bistatische Radarquerschnitte*, CCG Seminar SE 2.14, Oberpfaffenhofen, 2005.

[660] **Keydel**, **W**., *Mikrowellenfernerkundung mit Flugzeugen und Satelliten,* Vorlesung (24 h) am Institut für Geographie und Fernerkundung der Ludwig-Maximilians-Universität Munich, SS 2001

[661] **Keydel, W.,** *SAR Basics, Peculiarities and Special Modes;* NATO-RTO Seminar on "Advances in Radar Techniques", 6-8 Jun. 2001, Danzig, Polen

[662] **Keydel, W.,** *SAR Systems and their Application Possibilities*, NATO-RTO Seminar on "Advances in Radar Techniques", 6-8 Jun. 2001, Danzig, Polen.

[663] **Keydel, W.,** *„Mikrowellenfernerkundung mit Flugzeugen und Satelliten"*. Vorlesung (24 h) am Institut für Geographie und Fernerkundung, Ludwig-Maximilians-Universität Munich, SS 2001-2004/2005.

[664] **Keydel, W.,** „Radar mit hoher Auflösung für Rundumsicht auf Luftfahrzeugen", CCG Seminar "Intelligente Sensorik", Sep. 2001-2005

[665] **Keydel, W**.,: „Passive Mikrowellen-Sensoren zur Fernerkundung"; CCG Seminar "Intelligente Sensorik" Sep. 2001-2004.

[666] **Keydel, W.**,"*Hochfrequenztechnik"*, Summer Semester Course, Tongji University, Shanghai, China, 2002

[667] **Keydel, W.,** *Introduction to Tutorial "SAR Polarimetry and Interferometry",* EUSAR 2004,Ulm, 24 May 2004.

[668] **Keydel, W.,** *Polarimetric SAR Interferometry;* Tutorial *"SAR Polarimetry and Interferometry",* EUSAR 2004 in Ulm, 24 May 2004.

[669] **Keydel, W.,** *Basics of Normal and Differential SAR Interferometry;* Tutorial *"SAR Polarimetry and Interferometry",* EUSAR 2004 in Ulm, 24 May 2004.

[670] **Keydel, W.,** *„Radar mit hoher Auflösung für Rundumsicht auf Luftfahrzeugen"*, CCG Seminar "*Intelligente Sensorik",* Sep. 2004

[671] **Keydel, W.:** NATO – RTO Lecture Series SET-81, *"Radar Polarimetry and Interferometry"*, 13-23 Oct. 2004 in Brüssel, Washington und Ottawa." published in RTO-EN-SET-081, AC/323(SET-081)TP/47.

[672] **Keydel, W.,** "*Introduction"*, "Normal and Differential SAR Interferometry", "Applications of SAR Interferometry and Polarization", Tutorial at DLR, Oberpfaffenhofen, Germany, 2005.

[673] **Keydel, W.,** "*Fundamentals and Specialities of Synthetic Aperture Radar"; "Normal and Differential SAR Interferometry", "Polarimetry and Interferometry Applications", "Present and Future Airborne and Spaceborne Systems",* NATO-RTO Lecture Series on advanced Radar Techniques, Istanbul Technical University 6-8 Jun. 2005.

[674] **Keydel, W.,** NATO – RTO Lecture Series SET-81 2nd edition, *"Radar Polarimetry and Intererometry"*. 22-23 Mar. 2006, Warsaw Poland, to be published in RTO-EN-SET-081, 2006

[675] **Keydel, W.,** *"Introduction", "Normal and Differential SAR Interferometry", "Applications of SAR Interferometry and Polarization", "Air borne and Spaceborne SAR Systems",* NATO – RTO Lecture Series SET-81, 2nd edition, 2006.

[676] **Klement, D.**, *DLR- Entwurf eines Stealthflugzeugs*, Radar- und Infrarottarnung: Technik und Anwendung, Seminar SE 2.14, Oberpfaffenhofen, 4-8 Dec. 2000.

[677] **Klement, D.**, *DLR- Entwurf eines Stealthflugzeugs*, Radar- und Infrarottarnung: Technik und Anwendung, Seminar SE 2.14, Oberpfaffenhofen, 19-23 Nov. 2001.

[678] **Klement, D.**, *DLR- Entwurf eines Stealthflugzeugs*, Radar- und Infrarottarnung: Technik und Anwendung, Seminar SE 2.14, Oberpfaffenhofen, 2-12 Dec. 2002.

[679] **Klement, D.**, *DLR- Entwurf eines Stealthflugzeugs*, Radar- und Infrarottarnung: Technik und Anwendung, Seminar SE 2.14, Oberpfaffenhofen, 24-28 Nov. 2003.

[680] **Klement, D**., *RCS - Radarmodell SIGMA und Verifikation durch Messungen*, Radar- und Infrarottarnung: Technik und Anwendung, CCG Seminar SE 2.14, Oberpfaffenhofen, 2005.

[681] **Moreira**, **A.,** *Advanced and Future SAR Systems. "SAR Principles and Application",* Wessling, 18 Oct. 2004.

[682] **Moreira, A.,** *SAR Basics. "SAR Principles and Application"*, Wessling, 18 Oct. 2004.

[683] **Moreira, A**., *SAR Theory. "SAR Principles and Application"*, Wessling, 18 Oct. 2004.

[684] **Moreira, A**., *Radar-Fernerkundung mit ASAR*. Münchner Sommerschule 2004, Munich, 26 Jul. 2004.

[685] **Papathanassiou, K.P.**, *Polarimetry SAR Interferometry and Applications*, CCG Seminar SE 2.02, Oberpfaffenhofen, 2002.

[686] **Papathanassiou, K.P.**, *Polarimetry SAR Interferometry and Applications*, CCG Seminar SE 2.02, Oberpfaffenhofen, 2003.

[687] **Papathanassiou, K.P.**, *Polarimetric SAR Interferometry'*, Summerschool at the Helsinki University Technology, Finland, 2003.

[688] **Papathanassiou, K.P.**, *Polarimetry SAR Interferometry and Applications*, CCG Seminar SE 2.02, Oberpfaffenhofen, 2004.

[689] **Papathanassiou, K.P.**, *Polarimetry SAR Interferometry and Applications*, CCG Seminar SE 2.02, Oberpfaffenhofen, 2005.

[690] **Papathanassiou, K.P.**, *Polarimetric SAR Interferometry*, KARI, Soul, Korea, 2005

[691] **Peichl, M., Dill, S.,** *Radiometrie*, CCG Seminar *„Systeme und Verfahren der Aufklärung",* DLR Oberpfaffenhofen, Germany, 13 Sep. 2000.

[692] **Peichl, M.,** *Detektion von Antipersonenminen mit Hilfe von Mikrowellen*, DLR-Kolloquium, Oberpfaffenhofen, Mar. 2002.

[693] **Peichl, M.**, *Imaging Technologies and Applications of Microwave Radiometry*, Union Radio-Scientifique Internationale (URSI) Forum, Royal Military Academy, Radar and Radiometry Session, Brussels, Belgium, 13 Dec. 2002.

[694] **Peichl, M.,** *Imaging technologies and applications of microwave radiometry,* FGAN-Seminar Wachtberg, Schwerpunkttag zur Thematik "Terahertz Imaging", FGAN, Wachtberg, Germany, 12 May 2004.

[695] **Preißner, J.**, *Ermittlung von Materialeigenschaften*, Seminar SE 2.14, Oberpfaffenhofen, 4-8 Dec. 2000, pp. 1 - 17, 2000.

[696] **Preißner, J.**, *Ermittlung von Materialeigenschaften*, Seminar SE 2.14, Oberpfaffenhofen, 19-23 Nov. 2001.

[697] **Rode, G.,** *Landclutter*, CCG Seminar SE 2.14, Oberpfaffenhofen, 2003.

[698] **Rode, G.,** *Landclutter - Rechnersimulation von monostatischem Radarrückstreuhintergrund*, CCG Seminar SE 2.14, Oberpfaffenhofen, 2005.

[699] **Schwerdt, M.**, *SAR System Calibration and Quality Control*, Exploit European SAR Expertise, Tokio, Japan, 2002.

[700] **Süß, H,** *Microwave Radiometry – New Methods and Applications,* Kolloquium at the Institute for High Frequency Technology of the University of Karlsruhe, 03 Feb. 2000.

[701] **Süß, H**., *Collaborations Work,* Earth Observation Business Network (EOBN), 2002, Mac Donald Dettwiler, Richmond, Canada

[702] **Werner, M**., *Interferometric SAR / SRTM,* Tutorial at the Institute of Electronics, Beijing, China, 19. Oct. 2001.

[703] **Werner, M**., *Interferometric SAR / SRTM,* Tutorial ar the Institute of Radio Measurements, Beijing, China, 22. Oct. 2001.

[704] **Werner, M**., *Spaceborne SAR Systems Course,* Remote Sensing Technology Center (RESTEC), Tokyo, Japan, 21. Oct. 2002.

[705] **Werner, M.**, *Digitale Höhenmodelle der Shuttle Radar Topography Mission (SRTM)*, Radar and Communication (RADCOM), Hamburg, 18 Feb. 2004.

[706] **Werner**, **M.**, *Principles of SAR*, Tutorial at the al Radar Conference, Arlington, VA USA, 2005.

3.9.2 Invited Speeches (Plenary Sessions and Seminars)

[707] **Keydel, W.,** *Spaceborne Radar - The Shuttle Radar Topography Mission (SRTM),* German Radar Symposium (GRS), Berlin, Germany, 11-12 Oct. 2000.

[708] **Keydel, W.**, *Perspectives for Future Reconnaissance and Remote Sensing SAR Systems*, German Radar Symposium (GRS), Bonn, Germany, 23-28 Sep. 2002.

[709] **Keydel, W.,** *Perspectives for future Antenna Development for Airborne and Space borne SAR,* The Signal Processing Advances and Smart Antenna Systems Seminar, Helsinki, Finland, 07-08 Oct. 2003.

[710] **Keydel, W.,** *Perspektiven der Mikrowellenfernerkundung: Systeme und Missionen beim DLR,* Akademische Reden und Kolloquien, Universitätsbibliothek Erlangen-Nürnberg, 2004.

[711] **Keydel, W.**, *Entwicklungstendenzen für zukünftige SAR-Systeme*, Festakt 100 Jahre Radar, FGAN-FHR, Wachtberg Werthofen, 30 Apr. 2004.

[712] **Krieger, G.**, *Hochaufgelöste Fernerkundung mit Radarsatelliten*, Wissenschaftliches Kolloquium, Oberpfaffenhofen, Germany, 7 Mar. 2005.

[713] **Moreira, A.,** *Dreidimensionale Abbildung der Erboberfläche in 11 Tagen*. Invited Speech at the University Karlsruhe, Lehrstuhl für Höchstfrequenztechnik und Elektronik, Jul. 2000.

[714] **Moreira, A**., *Radartomographie: ein neues Verfahren zur dreidimensionalen Erdbeobachtung,* Wissenschaftliches Kolloquium, Oberpfaffenhofen, Germany, 5 Nov. 2001.

[715] **Moreira, A.,** *Interferometric Cartwheel: A New SAR Instrument.* Invited Speech at the University of Zürich, Remote Sensing Laboratories, 11 Nov. 2001.

[716] **Moreira, A.,** *Radar-Fernerkundung: Stand der Technik und Herausforderung für die Zukunft.* Invited Speech at the University Karlsruhe, Dec. 12, 2002.

[717] **Moreira, A.,** *SAR-Tomographie: Eine neue Technik zur Abbildung von Volumenstreuern.* Invited Speech at the University Karlsruhe, 17 Jan. 2002.

[718] **Moreira, A.,** *A New Technique for Radar Remote Sensing of Volume Scatterers*, Plenary Session at the Union Radio-Scientifique Internationale (URSI) Comission F Open Symposium on Propagation and Remote Sensing, Garmisch-Patenkirchen, 2002.

[719] **Moreira, A., Krieger, G.,** *Spaceborne Synthetic Aperture Radar (SAR) Systems: State of the Art and Future Developments*, European Microwave Conference, Munich, Germany, 2003.

[720] **Moreira, A.,** *Spaceborne SAR Systems: Future Developments towards Multi-Static Configurations.* Invited Speech in the Plenary Session of the International Radar Symposium (IRS), 30 Sep. - 02 Oct. 2003, Dresden, Berlin.

[721] **Moreira, A.,** *Spaceborne SAR Systems for Polariemtric and Interferometric Applications.* Invited Speech in the Plenary Session International Workshop on Applications of Polarimetry and Polarimetric Interferometry (PolInSAR), 17-21 Jan. 2005, Frascati, Germany

[722] **Moreira, A.,** *Spaceborne SAR Systems.* Invited speech at the Plenary Session of the National Radar Workshop on Synthetic Aperture Radar in Seoul, 22 Jul. 2005, Seoul, Korea

[723] **Moreira, A.,** *Raumgestützte Radar-Fernerkundung: Stand der Technik und künftige Entwicklungen.* Invited Speech at the Friedrich-Alexander-Universität Erlangen-Nürnberg, 10 Jun. 2005

[724] **Moreira, A., Krieger., G.,** *TanDEM-X: Global Measurement of the Earth Topography from Space with Unprecedented Accuracy.* International Radar Symposium (IRS), 6-8 Sep. 2005, Berlin, Germany

[725] **Peichl, M.,** *Detektion von Anti-Personen-Minen*, Tag der Raumfahrt, Oberpfaffenhofen, 21 Sep. 2001.

[726] **Peichl, M.**, *Detektion von Anti-Personen-Minen mit Hilfe von Mikrowellen,* Wissenschaftliches Kolloquium, Oberpfaffenhofen, Germany, 18 Mar. 2002.

[727] **Peichl, M.**, *Imaging technologies and applications of microwave radiometry*, Eingeladener Vortrag zum FGAN-Seminar Wachtberg, Schwerpunkttag zur Thematik „Terahertz Imaging", FGAN, Wachtberg, Germany, 12 May 2004.

[728] **Peichl, M., Süß, H.,** *Entwicklungen und Möglichkeiten passiver Mikrowellentechniken im Sicherheitsbereich*, OBe Seminar, Wildbad-Kreuth, Germany, 2005.

[729] **Schwerdt, M.,** *Mit geschärftem Blick aus dem All - Kalibrierung von abbildenden Radarsystemen,* Wissenschaftliches Kolloquium, Oberpfaffenhofen, Germany, 18 Dec. 2003.

[730] **Süß, H.,** *Raumgestützte Aufklärung mit SAR-Sensoren,* Wissenschaftliches Kolloquium, Oberpfaffenhofen, Germany, 8 Mar. 2004.

[731] **Werner, M.,** *Die Shuttle Radar Topographie Mission*, Wissenschaftliches Kolloquium, Oberpfaffenhofen, Germany, 8 May 2000.

[732] **Werner, M.,** *SRTM: Erste Ergebnisee und Anwendungen*, Internationale Luftfahrtausstellung Berlin (ILA) Berlin, 9 Jun. 2000.

[733] **Werner, M.**, *Shuttle Radar Topography Mission (SRTM): Mission Overview,* European Association for the International Space Year (EURISY), Varese, Italy, 19-20 Sep. 2000.

[734] **Werner, M.**, *Die Shuttle Radar Topography Mission SRTM,* Tag der offenen Tür, Oberpfaffenhofen, 23 Sep. 2000.

[735] **Werner, M.,** *Disaster Management with SRTM,* United Nations Committee on the Peaceful Uses of Outer Space (UNCOPUOS), Wien, Austria, 14 Feb. 2001.

[736] **Werner, M.,** *Hat SRTM das hochgesteckte Ziel erreicht?,* Wissenschaftliches Kolloquium, Oberpfaffenhofen, Germany, 6 Dec. 2004.

4 Acronyms and Abbreviations

Abbreviation	Explanation
ADC	Analogue/Digital Conversion
ADEN	ALOS Data European Node, eopi.esa.int/aden
ADS	Advanced Design System, Agilent, www.agilent.com
ALOS	Advanced Land Observing Satellite, JAXA, Japan
AMA	Antenna Measurement Range
AODA	Attitude and Orbit Determination Avionics
ASAR	Advanced Synthetic Aperture Radar on-board ENVISAT
ASCII	American Standard for Information Interchange
ATI	Along-track inteferometry
ATKIS	Amtliches Topographisch-Kartographisches Informationssystem, www.atkis.de
ATR	Automatic Target Recognition
AWI	Alfred Wegener Research Institute, Germany, www.awi-bremerhaven.de
BISTRO	Simulation program for monostatic and bistatic RCS based on Physical Optics (PO)
BNSC	British National Space Centre, UK, www.bnsc.gov.uk
BSI	Bundesamt für Sicherheit in der Informationstechnik, Germany, www.bsi.de
CAD	Computer Aided Design
CAF	Applied Remote Sensing Cluster, www.dlr.de/caf
CAN	Controller Area Network bus
CAT	Coverage Analysis Tool
CCNS	Computer Controlled Navigation System from IGI
CDEM	Customised Digital Elevation Model
CEOS	Committee on Earth Observation Satellites, www.ceos.org
CFRS	Carbon Fibre Reinforced Silicone
CNES	Centre National d'Études Spatiales, France, www.cnes.fr
CORINE	COoRdination of INformation on the Environment, www.corine.dfd.dlr.de
COTS	Commercial of the Shelf
CR	Corner Reflector
Cryosat	ESA Earth Explorer Mission dedicated to the study the ice caps, launch 2009
DBF	Digital Beamforming
dBZ	Power ratio [decibels x mm^6m^{-3}] for scattering volume containing spherical particles
DDRE	Danish Defence Research Establishment
DEM	Digital Elevation Model
DFD	German Remote Sensing Data Center, www.dlr.de/caf
DGM5	Digitales Geländemodell 5 (Digital Surface Model with a scale1:5000)
D-GPS	Differential Global Postioning System (GPS)
DIMS	Data Information and Management System for Earth Observation
D-InSAR	Differential Interferometric SAR
DLR	German Aerospace Center, www.dlr.de
DO228	Dornier DO228-212 aircraft used for the E-SAR system
DORTE	Detection of Objects in Realistic Terrain
DPC	Displaced Phase Center
DRA	Dual Receive Antenna Mode
dual-pol	Radar operation mode with two polarisations (e.g. HH and HV)
EC	European Commission
ECS	Extended Chirp Scaling algorithm
EEA	European Environment Agency
EM	Electro-Magnetic

ENVISAT	Environmental Satellite, ESA
EOL	End of life
EOWEB	User Interface for Earth Observation on the WEB, eoweb.dlr.de
ERS-1/2	European Remote Sensing Satellites, ESA
ESA	European Space Agency, www.esa.int
ESA/ESRIN	ESA's European Space Research Institute
ESA/ESTEC	ESA's European Space Research and Technology Center
E-SAR	Experimental airborne SAR system of DLR
EUCLID	EUropean Co-operation for the Long term In Defence
FCD	Floating Car Data
FFT	Fast Fourier Transform
FIFO	First-in first-out
FIR	Finite Impulse Response
FLAR	Forward Looking Radar
F-SAR	New airborne SAR system being developed at the HR Institute of DLR
GB	Giga Byte
GEO	Geostationary Earth Orbit
GFZ	Geoforschungszentrum Potsdam, Germany, www.gfz-potsdam.de
GMES	Global Monitoring for Environment and Security, www.gmes.info
GMTI	Ground moving target indication
GPS	Global Positioning System
GSOC	German Space Operation Center, www.gsoc.dlr.de
GTC	Geocoded Terrain Corrected
GUI	Graphical User Interface
HABITAT	Hazard & Biomass Interferometric SAR Observatory
HaFK	Hochagile Flugkörper (High Agile Missile) – DLR project, 2001 - 2004
HDDC	High density digital cassette
HFSS	High Frequency Structure Simulator
HOPE	Handheld Operational Demining System
HR	Microwaves and Radar Institute, www.dlr.de/HR
HRTI	High Resolution Terrain Information
HRWS	High Resolution Wide Swath SAR
HUMINT	Human Intelligence
I/Q	Inphase/Quadrature Phase Detector
IEM	Integral Equation Method
IGI	Ingenieur-Gesellschaft fuer Interfaces, www.igi-systems.com
IHE	Institut für Hochstfrequenztechnik und Elektronik, University of Karlsruhe
IMINT	Image Intelligence
INDREX	E-SAR campaign in Indonesia, 2004
INPE	Instituto National de Pesquisas Espaciais, Brazil, www.inpe.br
INS	Inertial Navigation System
InSAR	Interferometric SAR
IOCS	Instrument Operations and Calibration Segment (as part of TerraSAR-X Ground Segment)
IR	Infrared
IRF	Impulse response function
ISAR	Inverse SAR
ISLR	Integrated Side Lobe Ratio
ISRO	Indian Space Research Organisation; www.isro.org
ISRO/SAC	Indian Space Research Organisation - Space Applications Center
ITU	International Telecommunication Union, www.itu.int
JAXA	Japan Aerospace Exploration Agency, www.jaxa.jp

JERS-1	Japanese Earth Resources Satellite 1
JPL	Jet Propulsion Laboratory, www.jpl.nasa.gov
K&C	JAXA's Kyoto and Carbon Initiative
KM	Kirchhoff Model
LAI	Leaf Area Index
LEO	Low Earth Orbit
LIDAR	Light Detection and Ranging
L-SAR	TerraSAR-L's L-band Synthetic Aperture Radar
LTDB	Long Term Data Base
MAPSAR	Multi-Application Purpose SAR
MEO	Medium Earth Orbit
MMP	INPE's Multi-Mission Platform
MOTHESIM	Modélisation Optimisation Théorie Simulation Mathématique (Institute)
MTI	Moving Target Indication
NASA	National Aeronautics and Space Administration, www.nasa.gov
NESZ	Noise Equivalent Sigma Zero
NGA	National Geospatial-Intelligence Agency (former NIMA)
NORAD	North American Aerospace Defense Command, www.norad.mil
NWA	Network Analyser
ONERA	Office National d'Études et de Recherches Aérospatiales, France, www.onera.fr
PALSAR	Phased Array L-band Synthetic Aperture Radar
PCC	Pulse Coded Calibration
PDR	Preliminary Design Review
PN	Pseudo Noise
PO	Physical Optics
POLDIRAD	Polarisation Diversity Radar - DLR's coherent fully polarimetric C-band weather radar
Pol-InSAR	Polarimetric SAR Interferometry
PPS	Pulse per second
PRF	Pulse Repetition Frequency
PRI	Pulse Repetition Interval
PSLR	Peak to Side Lobe Ratio
PTA	Precise Topography and Aperture algorithm for airborne motion compensation
quad-pol	fully polarimetric radar operation mode (HH, HV, VV, VH)
R&D	Research and Development
Radarsat-2	Second Canadian SAR Satellite, www.radarsat2.info
RAMSES	airborne high resolution SAR system from ONERA
RCS	Radar Cross-Section
RDP	Radar Data Product (TanDEM-X)
RF	Radio frequency
RFID	Radio Frequency Identification
RGI	Radar Geometry Image
rms	Root Mean Square
RP	Repeat-pass
RVoG	Random Volume over Ground
SAR	Synthetic Aperture Radar
SARCON	SAR Product Control Software
SAR-Lupe	Constellation of 5 high resolution SAR satellites in X-band
SCIFT	Scaled Inverse Fourier Transform
Sentinel-1	C-band SAR satellite being developed by ESA in the scope of the GMES program
SETES	SAR End-To-End Simulator
SIGINT	Signal Intelligence

SIGMA	Simulation program for monostatic RCS based on Physical Optics (PO)
SIGRAY	Simulation program for monostatic and bistatic RCS based on Shooting & Bouncing Rays Method
SIR-C	Shuttle Imaging Radar - C
SIREV	Sector Imaging Radar for Enhanced Vision
SLC	Single Look Complex
SME	Small and Medium-Sized Enterprise
SMOS	ESA's Soil Moisture and Ocean Salinity mission
SNR	Signal-to-noise ratio
SPECAN	Spectral Analysis
SPM	Small Pertubation Model
SRTM	Shuttle Radar Topography Mission
SSMM	Solid State Mass Memory
STAP	Space-Time Adaptive Processing
Stdv	Standard Deviation
STK	Satellite Tool Kit
SVA	Spatial Variant Apodisation
SVALEX	E-SAR campaign over sea and land ice over Svalbard, 2005
TanDEM-X	TerraSAR-X add-on for Digital Elevation Measurements, www.dlr.de/HR/tdmx
TDX	TanDEM-X Spacecraft
TEC	Total Electron Content
TerraSAR-L	ESA's L-band SAR Mission, phase B completed
TerraSAR-X	German high resolution X-band radar satellite to be launched in 2006
TEWS	Tsunami Early Warning System
TRAMRAD	Traffic Monitoring with Radar
TRM	Transmit/Receive Module
TSX -1	First TerraSAR-X Satellite
TSXX	TerraSAR-X Exploitation Infrastructure
TWT	Travelling Wave Tube
UAV	Unmanned Aerial Vehicle
UCAV	Unmanned Combat Aerial Vehicle
USO	Ultra Stable Oscillator
UTM	Universal Transverse Mercator
VSWR	Voltage Standing Wave Ratio
WGS	World Geodetic System
X-SAR	X-band Synthetic Aperture Radar
XTI	Across-Track Interferometry

5 Acknowledgement

A large team of Institute's members contributed to this report and their names are recognized below:

Christian Andres
Stefan Baumgartner
Karl-Heinz Bethke
Thomas Börner
Benjamin Bräutigam
Stefan Buckreuß
Andreas Danklmayer
Stephan Dill
Hauke Fiedler
Martina Gabele
Gabriele Hager
Irena Hajnsek
Ralf Horn
David Hounam
Timo Kempf
Erich Kemptner
Wolfgang Keydel
Juliane Klämke
Gerhard Krieger
Christopher Laux
Markus Limbach
Nico Marquardt
Josef Mittermayer
Thomas Neff
Anton Nottensteiner
Konstantinos Papathanassiou
Markus Peichl
Sybille Radzuweit
Rolf Scheiber
Christian Schmidt
Reinhard Schröder
Marco Schwerdt
Jayanti Sharma
Rainer Speck
Helmut Süß
Renate Weist
Marian Werner
Marwan Younis
Tino Zehetbauer
Manfred Zink

The complete list of Institute's members is given in the second volume of this report.

I would like to thank the entire Institute's staff for their valuable work and outstanding research results achieved in the last 5 years.

Alberto Moreira

DLR at a glance

DLR is Germany´s national research center for aeronautics and space. Its extensive research and development work is integrated into national and international cooperative ventures. As Germany´s space agency, DLR has been given responsibility for the forward planning and the implementation of the German space program by the German federal government as well as for the international representation of German interests.

Approximately 5,100 people are employed in DLR´s 31 institutes and facilities at eight locations in Germany: Cologne-Porz (headquarters), Berlin-Adlershof, Bonn-Oberkassel, Braunschweig, Göttingen, Lampoldshausen, Oberpfaffenhofen, and Stuttgart.

DLR also operates offices in Brussels, Paris, and Washington.

DLR's mission comprises the exploration of the Earth and the Universe, research for protecting the environment, for environmentally-compatible technologies, and for promoting mobility, communi-cation, and security. DLR's research portfolio ranges from basic research to innovative applications and products of tomorrow. In that way DLR contributes the scientific and technical know-how that it has gained to enhancing Germany's industrial and technological reputation. DLR operates large-scale research facilities for DLR's own projects and as a service provider for its clients and partners. It also promotes the next generation of scientists, provides competent advisory services to government, and is a driving force in the local regions of its field centers.

Microwaves and Radar Institute – Status Report 2000 - 2005-E-04/06

Deutsches Zentrum für Luft- und Raumfahrt e.V.
in der Helmholtz-Gemeinschaft

German Aerospace Center

Microwaves and Radar Institute
Prof. Dr.-Ing. Alberto Moreira
PO Box 1116
D-82230 Weßling
Telephone: 08153 28-2305
Telefax: 08153 28-1135
E-Mail: alberto.moreira@dlr.de

www.DLR.de/hr